Differential induction and spread of tau pathology in young PS19 tau transgenic mice following intracerebral injections of pathological tau from Alzheimer's disease or corticobasal degeneration brains

Susana Boluda Casas

Ph.D. thesis presented by
SUSANA BOLUDA CASAS
For the degree of Doctor at the
University of Barcelona

DIFFERENTIAL INDUCTION AND SPREAD OF TAU PATHOLOGY IN YOUNG PS19 TAU TRANSGENIC MICE FOLLOWING INTRACEREBRAL INJECTIONS OF PATHOLOGICAL TAU FROM ALZHEIMER'S DISEASE OR CORTICOBASAL DEGENERATION BRAINS

UNIVERSITAT DE BARCELONA-FACULTAT DE MEDICINA
DOCTORATE IN MEDICINE AND TRANSLATIONAL RESEARCH PROGRAMME
2016

Work performed under the direction of Dr. John Q. Trojanowski, at the Center for Neurodegenerative Disease Research (CNDR), Perelman School of Medicine, University of Pennsylvania

Dr. John Q. Trojanowski
Director

Prof. Isidre Ferrer Abizanda
Tutor

Susana Boluda Casas
Ph.D. Student candidate

To my family, friends and colleagues who have given me support along the way.

ABBREVIATIONS

^{11}C-PIB	[^{11}C]-labeled Pittsburgh compound B
3R	Three repeat isoforms of tau
4R	Four repeat isoforms of tau
5-HT	5-Hydroxytryptamine
Ab	Antibody
AD	Alzheimer's disease
AD-Tau	Tau enriched extracts obtained from Alzheimer's disease affected brain tissue
AGD	Argyrophilic grain disease
ALS	Amyotrophic lateral sclerosis
AMPK	5'-adenosine-monophosphate activated protein kinase
ANOVA	Analysis of variance
APP	Amyloid precursor protein
APS	Ammonium persulfate
Aβ	Amyloid-β
BCA	Bicinchoninic colorimetric assay
bvFTD-FTLD	Behavioral variant of fronto-temporal dementia
CA1	Region 1 of hippocampus (Cornus ammonis 1)
CA2/3	Region 2/3 of hippocampus (Cornus ammonis 2/3)
CaMK II	Calcium/calmodulin-dependent protein kinase II
CBD	Corticobasal degeneration
CBD-Tau	Tau enriched extracts obtained from corticobasal degeneration diseased brain tissue
CBS	Corticobasal syndrome
Cdk5	Cyclin-dependent kinase 5
cDNA	Complementary deoxyribonucleic acid
CERAD	Consortium to Establish a Registry for Alzheimer's Disease
CK	Casein kinase
CNDR	Center for Neurodegenerative Disease Research
CNS	Central nervous system
CSF	Cerebral spinal fluid

CTRL-Tau	Tau enriched extract obtained from non diseased brain tissue (control)
DAB	3-3'-Diaminobenzidine
DD	Duration of disease
ddH_2O	Double distilled water
DG	Dentate gyrus
DS	Down syndrome
DSAD	Down syndrome subject with Alzheimer's disease histopathological changes
DSAD-Tau	Tau enriched extracts obtained from Down syndrome patient with Alzheimer's disease affected brain tissue
DTT	Dithiothreitol
DYRK1A	Tyrosin-phosphorylation-regulated kinase 1A
EC	Entorhinal cortex
EDTA	Ethylenediaminetetraacetic acid
ELISA	Enzyme-linked immunosorbent assay
EM	Electron microscopy
EthOH	Ethanol
FA	Formic acid
FBS	Frontal behavioral-spatial syndrome
FBS	Fetal bovine serum
FDA	Food and Drug Administration
FDG	[^{18}F]-fluorodeoxyglucose
FTLD-TDP	Frontotemporal lobar degeneration TDP43-positive
FTLDP-17	Frontotemporal lobar dementia with parkinsonism linked to chromosome 17
FW	Formula weight
GABA	Gamma-aminobutyric acid
GSK-3β	Glycogen synthase kinase 3β
HD	Huntington's disease
HRP	Horse radish peroxidase
HS-RAB	High-salt reassembly buffer
hTau	Human Tau

IHC	Immunohistochemistry
IR1/2	Inter-repeat region between R1 and R2
LC	Locus coeruleus
mAb	Monoclonal antibody
MAPK	Mitogen activated protein kinase
MAPT	Microtubule-associated protein tau gene
MARK	Microtubule affinity-regulating kinase
MES	2-(N-morpholino)ethanesulfonic acid
mo	Months
MoM	Mouse on mouse
MoPrP	Murine prion protein
MRI	Magnetic resonance imaging
mRNA	Messenger ribonucleic acid
mTau	Mouse tau
MTBR	Microtubule-binding repeat region
MTs	Microtubules
MW	Microwave
NA	Not available
naPPA	Nonfluent/agrammatic variant of primary progressive aphasia
NFT	Neurofibrillary tangles
NIA	National Institute on Aging
NIA-AA	National Institute on Aging-Alzheimer's Association
NMDA	N-methyl-D-aspartate
Non-PDPK	Non-proline directed protein kinases
NP Dx	Neuropathological diagnosis
NSAID	Nonsteroidal anti-inflammatory drug
NT	Neuropil threads
p-Ser	Phosphorylated Serine
p-tau	Phosphorylated tau protein
pAb	Polyclonal antibody
PBS	Phosphate-buffered saline
PD	Parkinson's disease
PDPK	Proline directed protein kinases
PES	Polyethersulfone

PET	Positron emission tomography
PFFs	Preformed fibrils
PHF	Paired helical filaments
PHF-EB	Paired helical filament extraction buffer
PiD	Pick's disease
PK-A/B/C/N	Cyclic-AMP-dependent protein kinase (A/B/C/N)
PLC-γ	Phospholipase C-γ
PMD	Postmortem delay
PP2	Protein phosphatase
PPA	Primary progressive aphasia
Pro	Proline
PSP	Progressive supranuclear palsy
PSPS	Progressive supranuclear palsy syndrome
R1	First repeat of tau protein
R2	Second repeat of tau protein
RAB	Reassembly buffer
RS	Richardson syndrome
RT	Room temperature
SAPK	Stress-activated protein kinase
SDS	Sodium dodecyl sulfate
SDS-PAGE	Sodium dodecyl sulfate polyacrylamide gel electrophoresis
Ser	Serine
SF	Straight filaments
SOD1	Superoxide dismutase 1
t-tau	Total tau
T34	Tau protein isoform with 412 amino acid residues
T40	Tau protein isoform with 441 amino acid residues
TBI	Traumatic brain injury
TDP-43	Transactive response DNA binding protein 43 kDa
TEMED	Tetramethylethylenediamine
Tg	Transgenic
Thr	Threonine
ThS	Thioflavin S

TPK	Tyrosin protein kinases
TRIS	Tris(hydroxymethyl)aminomethane
TTBK	Tau tubulin kinase
Tyr	Tyrosine
vols	Volumes
WB	Western Blot
WGA	Wheat germ agglutinin
WT	Wild type
α-syn	α-synuclein

RESUM GLOBAL

INTRODUCCIÓ

1. PROTEÏNA TAU

La proteïna tau és una proteïna amb propietats hidròfiles, altament soluble que es troba majoritàriament als axons neuronals. La funció principal de tau és l'acoblament i l'estabilització dels microtúbuls (MTs).

Basant-se en l'escisió amb quimotripsina, la proteïna tau es divideix en dos dominis: el domini de projecció i el domini d'unió als MTs. El domini de projecció està format per l'extrem N-terminal, que es projecta des de la superfície dels MTs i conté una gran proporció d'aminoàcids (aa) acídics, i la regió rica en prolina, que conté regions d'unió a proteïnes amb domini SH3. El domini d'unió a MTs està format per la regió d'unió a MTs (MTBR), que comprèn 3 o 4 regions de repetició, i l'extrem C-terminal, que és acídic. Les regions de repetició són seqüències de 31 o 32 aa que contenen 18 residus repetits i quasi idèntics i que es troben separats per una seqüència de 13 o 14 aa. Els fragments de 18 aa repetits són els que contenen la seqüència mínima que té capacitat d'unió a la tubulina i és a través d'aquesta regió que tau s'uneix als MTs.

El gen *MAPT* codifica la proteïna tau i es localitza al braç llarg del cromosoma 17 a la posició 17q21.31. El gen *MAPT* conté 16 exons i d'aquests, els exons 2, 3 i 10 estan sotmesos a *splicing* alternatiu que donarà lloc a l'expressió de 6 isoformes diferents de tau (0N4R, 1N4R, 2N4R, 0N3R, 1N3R, 2N3R). Les isoformes contenen entre 352 i 441 aa i varien entre elles per la presència de 3 o 4 regions de repetició a la MTBR i la presència o absència d'insercions de 28 aa o 58 aa a l'extrem N-terminal. Quan l'exó 10 es tradueix les isoformes contenen 4 repeticions (4R) al MTBR mentre que quan l'exó 10 no es tradueix les isoformes només contenen 3 fragments de repetició (3R). La traducció de l'exó 2 i la traducció conjunta de l'exó 2 i 3 donaran lloc a la inserció de 29 aa o de 58 aa i correspondran a les isoformes 1N i 2N respectivament. La isoforma 0N apareix quan hi ha absència de traducció tant de l'exó 2 com del 3.

Les isoformes 3R i 4R s'expressen en la mateixa proporció (1:1) al cervell normal i als individus amb malaltia d'Alzheimer (AD). En canvi, a d'altres taupaties com la paràlisi supranuclear progressiva (PSP), la degeneració corticobasal (CBD) o la malaltia de grans argiròfils (AGD), hi ha un predomini d'isoformes 4R. En el cas de la malaltia de Pick (PiD), per contra, s'observa un predomini d'isoformes 3R.

La principal funció de la proteïna tau és l'acoblament i l'estabilització dels MTs. Aquesta funció s'exerceix mitjançant la unió de tau a la tubulina que induiria la polimerització dels MTs. La forma com la proteïna tau s'uneix als MTs es desconeix, però, s'ha proposat un model on les regions contigües a la MTBR s'unirien fortament als MT i permetrien que la proteïna tau es posicionés sobre la superfície dels MTs, mentre que les regions de repetició a la MTBR s'unirien de forma més dèbil, a través de càrregues electròniques, i serien les responsables d'exercir la funció d'acoblament dels MTs. Aquesta funció es realitzaria a través de seqüències específiques de tau que es troben tant en les regions de repetició com a les regions contigües a aquestes.

La funció d'acoblament i estabilització dels MTs no és l'única funció de tau i es pensa que, a través d'altres dominis de la proteïna, tau exerceix altres funcions com el manteniment de la distància entre fibres de MTs. És més, tau es pot unir a altres proteïnes del citoesquelet com l'actina i d'aquesta manera és capaç de restringir la flexibilitat de les xarxes de MTs. A més a més, tau està involucrada en vies de transducció de senyals i modula l'activitat de les cinases de la família Src. Així mateix, se sap que tau pot unir-se a altres organel·les del citoplasma com els mitocondris.

La proteïna tau presenta modificacions postraduccionals que inclouen la fosforilació, glicosilació, ubiqüitinització, glicació, poliaminació, sumoilació, acetilació i proteòlisi, i es pensa que aquestes modificacions juguen un paper important en la unió de tau als MTs i en la formació d'agregats patològics. La fosforilació és la modificació postraduccional més estudiada i fins ara, a la literatura, s'han descrit 48 aa fosforilats dels 85 aa amb possibilitat de fosforilació que hi ha a la isoforma més llarga de tau (2N4R). Els residus que es fosforilen amb més freqüència són els anomenats motius Ser/Thr-Pro que consisteixen en Ser o Thr seguides per una Pro. Però aquests no són els únics aa amb capacitat de fosforilació, s'ha trobat que les

Tyr també es poden fosforilar. La fosforilació de tau es regula per l'acció de cinases i fosfatases específiques. Les cinases fosforilen tau i es classifiquen en tres grups: cinases dirigides a prolines (PDPK), cinases no dirigides a prolines (non-PDPK) i cinases específiques de Tyr (TPK). Del grup de les PDPK destaca la cinasa glicogen sintasa 3β (GSK-3β) que, també té una funció important en la fosforilació d'Aβ. Les fosfatases, per contra, defosforilen la proteïna tau i entre elles la PP2A té un paper destacat ja que s'ha vist que és responsable del 70% de l'activitat de defosforilació de tau. En condicions fisiològiques hi ha un equilibri entre l'activitat de fosforilació de les cinases i la de desfosforilació de les fosfatases, quan aquest equilibri es perd pot donar lloc a la hiperfosforilació patològica de tau.

En condicions normals tau es troba soluble al citoplasma neuronal, però en situacions patològiques la proteïna tau pot formar agregats insolubles. Es desconeix què provoca la formació dels agregats i es pensa que podria tractar-se d'un procés de múltiples passos on intervindrien modificacions postraduccionals de la proteïna. En un primer pas, la hiperfosforilació anormal de la proteïna donaria lloc a la separació de tau dels MTs i provocaria un augment de tau lliure al citoplasma fent-la més susceptible a l'agregació. La proteïna podria estar sotmesa a canvis de conformació, possiblement per la presència de més canvis postraduccionals, que facilitarien la formació de dímers i oligòmers que evolucionarien en agregats més grans i més estructurats, els quals adoptarien una estructura de fulla plegada β i acabarien formant els cabdells neurofibril·lars (NFT) propis de l'AD.

Entre el 1994 i el 1997 es va descobrir que algunes formes familiars de demència frontotemporal, que actualment coneixem com demència frontotemporal lobar amb parkinsonisme associada al cromosoma 17 (FTLDP-17), eren causades per mutacions de *MAPT*. La FTLDP-17 es caracteritza per presentar inclusions de tau al citoplasma de les neurones i les cèl.lules glials en diferents regions cerebrals i que s'acompanya d'una important pèrdua neuronal. A més, destaca l'absència d'agregats d'Aβ. Aquesta troballa va posar en evidència que la proteïna tau era capaç de causar malaltia sense la necessitat que Aβ hi fos present. Actualment hi ha descrites més de 50 mutacions del gen *MAPT*, que afecten tant els introns com els exons, i que donen lloc a diferents fenotips de la malaltia. Les mutacions exòniques es troben

majoritàriament entre els exons 9 i 13, que codifiquen les regions de repetició de tau, i són mutacions de canvi de sentit, delecions i mutacions silents mentre que les mutacions intròniques s'agrupen a l'intró localitzat immediatament després de l'exó 10. Les mutacions poden tenir un efecte a nivell proteic, de manera que la pèrdua o canvi d'un aa disminueix la capacitat de tau d'adherir-se als MTs o incrementa la seva capacitat de formació d'agregats. Les mutacions també poden tenir un efecte a nivell del RNA que donaria lloc a un increment del *splicing* alternatiu de l'exó 10 i conseqüentment variaria la proporció d'isoformes 3R/4R que promouria la capacitat d'agregació de la proteïna tau.

2. TAUPATIES

Les taupaties són un grup de malalties neurodegeneratives que es caracteritzen per la presència d'agregats intracel·lulars de protenïa tau. Cadascuna d'aquestes malalties presenten una simptomatologia clínica, una distribució topogràfica dels agregats i una afectació cel·lular específica.

La malaltia d'Alzheimer (AD) és la malaltia neurodegenerativa més freqüent i la causa més freqüent de demència. Clínicament cursa amb pèrdua de memòria i histològicament s'associa a agregats extracel·lulars de plaques d'amiloide (Aβ) i a agregats intracel·lulars de proteïna tau (NFT). A l'estudi macroscòpic dels cervells afectats per AD es pot observar atròfia cerebral de predomini a regions temporals i que és molt prominent a l'hipocamp. Habitualment, l'atròfia cerebral va associada a una marcada dilatació dels ventricles. A l'examen microscòpic predominen els agregats d'Aβ que formen plaques de diversa morfologia, incloses les plaques neurítiques, i agregats intracel·lulars de proteïna tau que formen estructures filamentoses anomenades cabdells neurofibril·lars (NFT) al citoplasma neuronal. Cal destacar que a l'AD la patologia de tau predomina a la substància gris sense afectació de la substància blanca, al contrari que a la degeneració corticobasal (CBD) on s'afecten tant l'escorça cerebral com la substància blanca subcortical. Bioquímicament, a l'immunoblot, la proteïna tau patològica es presenta, a l'AD, en un patró de 3 bandes de 60, 64 i 68 kDa i una quarta banda de 72 kDa que no sempre hi és present.

S'ha observat com amb l'evolució de l'AD, tant els agregats patològics d'Aβ com els NFT, s'acumulen seguint un patró estereotipat previsible que ha permès la generació de sistemes de classificació en diferents estadis. Actualment, per a la proteïna Aβ, s'utilitzen dos sistemes diferents de classificació: el CERAD i les fases de Thal. A la classificació de CERAD s'associa l'avaluació semiquantitativa de les plaques neurítiques presents al neocòrtex (0: ninguna; A: escasses; B: moderada; C: abundants) amb l'edat del pacient i els signes clínics de demència, i es dóna un nivell de certesa que l'AD sigui la causa de la demència. Les fases de Thal tenen en compte tots els agregats d'Aβ independentment de la morfologia i es divideixen en 5 estadis: Fase 1: agregats d'Aβ al neocòrtex; Fase 2: Fase 1 més agregats a l'al·locòrtex; Fase 3: Fase 2 més dipòsits al diencèfal; Fase 4: Fase 3 més agregats al tronc cerebral; Fase 5: Fase 4 més dipòsits al cerebel. Pel que fa a les inclusions de tau, Braak va descriure 6 estadis: Estadi I: Afectació de regió transentorrinal; Estadi II: Estadi I més afectació de regions entorrinals; Estadi III: Estadi II i lesions al neocòrtex del gir lingual i fusiforme; Estadi IV: Estadi III més progressió neocortical afectant àrees associatives; Estadi V: Estadi IV més patologia al neocòrtex frontal, parietal i occipital fins a la regió periestriada; Estadi VI: Estadi V més desenvolupament de la malaltia a àrees secundàries i primàries de la regió estriada del lòbul occipital. Recentment s'ha creat l'esquema de graus del NIA-AA que integra els tres estadiatges per gradar la patologia d'Aβ i tau: CERAD, fases de Thal i estadis de Braak, per tal de tenir un sistema consensuat pel diagnòstic neuropatològic de l'AD.

La degeneració corticobasal (CBD) és una taupatia que apareix en gent més jove que l'AD, entre els 50 i 70 anys. Clínicament es pot presentar de forma molt diversa per tant, l'avaluació a l'autòpsia és l'única manera d'obtenir un diagnòstic definitiu. Al 2013 es varen consensuar els criteris clínics de les formes més freqüents de presentació de la CBD: la síndrome corticobasal (CBS), la síndrome frontal conductual-espacial (FBS), la variant no fluent o agramàtica de l'afàsia primària progressiva (naPPA) i la síndrome de la paràlisi supranuclear progressiva (PSPS) o síndrome de Richardson (RS). A l'examen macroscòpic, els cervells afectats per CBD es caracteritzen per presentar atròfia del lòbul frontal superior i parietal parasagital, pèrdua de substància blanca, aplanament del nucli caudat i pèrdua de neuromelanina a la substància negra. A l'estudi histològic s'observen inclusions de

tau a cèl·lules glials i neurones amb afectació de la substància gris cortical i ganglis de la base i de la substància blanca subcortical. Als astròcits la proteïna tau s'acumula als processos astrocitaris formant les anomenades plaques astrocitàries, que són patognomòniques de la malaltia. Bioquímicament els agregats de tau donen lloc, a l'immunoblot, a un patró característic de dues bandes de 64 i 68 kDa i a una tercera banda de 72kDa que no sempre es detecta.

Actualment, les taupaties, no tenen un tractament farmacològic que sigui capaç d'aturar o modificar la progressió de la malaltia i el tractament és principalment simptomàtic.

3. PROPAGACIÓ DE LA PATOLOGIA TAU: HIPÒTESI DE LA TRANSMISSIÓ DE CÈL·LULA A CÈL·LULA

Recentment s'ha observat com en diverses malalties neurodegeneratives; incloses l'AD, AGD, la malaltia de Parkinson (PD) o l'esclerosi lateral amiotròfica (ALS); les proteïnes anòmales acumulades es propaguen amb l'evolució de la malaltia per diferents regions cerebrals seguint un patró estereotipat. Així, en estadis inicials de l'AD les inclusions de tau es veuen al locus coeruleus (LC) i a l'escorça entorrinal, més tard es propagaguen cap a regions límbiques i finalment, en estadis més avançats de la malaltia, afecten el neocòrtex. Aquestes observacions varen suggerir que, de forma similar a les malalties priòniques, els agregats de tau es podien propagar mitjançant una transmissió de cèl·lula a cèl·lula seguint les projeccions neuronals.

Estudis *in vitro* han demostrat com els agregats de proteïna tau patològica poden ser alliberats d'una cèl·lula (la cèl·lula donadora) al medi extracel·lular per ser captats per una altre cèl·lula (la cèl·lula receptora) i una vegada internalitzats induïr la formació d'agregats similars als NFT. La proteïna patològica captada induiria un plegament anòmal de la proteïna tau normal soluble de la cèl·lula receptora.

Els estudis *in vivo* donen suport a les troballes observades als cultius cel·lulars. Clavaguera et al. varen demostrar que la proteïna tau anòmala podia propagar-se d'una cèl·lula a una altre amb experiments en ratolins transgènics (Tg). Varen injectar extracte cerebral de ratolins Tg P301S (que formen inclusions de tau en

edats avançades) al cervell de ratolins Tg ALZ17 (que no desenvolupen agregats de tau) i varen veure com s'induïa la formació d'inclusions de tau als ratolins Tg ALZ17. Liu et al. i de Calignon et al. varen demostrar que la propagació de la patologia de tau es produïa a través de connexions interneuronals. Varen generar ratolins Tg que sobreexpressaven tau patològica a l'escorça entorrinal (EC) i hi formaven agregats. S'observava com els agregats es propagaven a regions de l'hipocamp directament connectades a l'EC en envellir els ratolins. Però van ser Iba et al. qui varen determinar que tau era l'única proteïna necessària per desenvolupar i propagar la malaltia en posar de manifest que la injecció al cervell de ratolins Tg PS19 de fibres recombinants preformades (PFFs) de tau eren capaces d'induir la formació d'agregats i la propagació de tau als ratolins PS19. A més, a l'incrementar el temps de postinjecció, la patologia que desenvolupaven els ratolins PS19 injectats augmentava en intensitat i s'estenia a regions allunyades de la zona d'injecció.

El conjunt d'aquests estudis suggereix que els agregats patològics de tau són capaços de propagar-se a cèl·lules normals properes o a cèl·lules que es troben interconnectades per sinapsis. Aquest fenomen de transmissió intercel·lular també s'ha observat en altres proteïnes incloses l'α-syn, Aβ, TDP43, SOD1 i huntingtina amb repeticions polyQ, fet que suggereix que les malalties neurodegeneratives tenen un mecanisme de propagació similar. A més i tal com s'ha observat a les malalties priòniques i a d'altres malalties neurodegeneratives, és possible que diferents soques de la proteïna tau siguin les responsables de les diverses manifestacions fenotípiques de les taupaties.

HIPÒTESI I OBJECTIUS

L'observació que els agregats proteics d'algunes malalties neurodegeneratives, incloses algunes taupaties, presenten una progressió estereotipada amb l'evolució de la malaltia va fer pensar que aquestes proteïnes mal plegades es podrien transmetre d'una cèl·lula a una altre de manera similar al que succeix amb els prions. L'objectiu d'aquest estudi és:

1. Determinar si els ratolins Tg PS19 desenvolupen inclusions de tau després de la injecció amb extractes proteics enriquits amb tau patològica obtinguda de teixit cerebral humà afectat d'AD i CBD.
2. Determinar si hi ha propagació d'aquests agregats patològics a regions allunyades de la zona d'injecció.
3. Caracteritzar la distribució de les inclusions desenvolupades en els ratolins PS19 i les seves propietats histològiques després de la injecció amb extracte obtingut de les diferents taupaties.
4. Determinar si les característiques dels agregats de tau desenvolupats en els ratolins Tg PS19 són similars a les característiques dels agregats que s'observen a les taupaties en els humans.

MATERIALS I MÈTODES

1. EXTRACTES DE TEIXIT CEREBRAL HUMÀ

Es varen generar extractes enriquits amb proteïna tau patològica (CBD-Tau, AD-Tau, DSAD-Tau) a partir de teixit cerebral humà obtingut del banc de cervells del *Center for Neurodegenerative Disease Research* (CNDR). El CBD-Tau es va obtenir a partir de teixit cerebral de dos individus afectats per CBD. Les preparacions d'AD-Tau i DSAD-Tau es varen generar a partir d'un pacient amb AD i d'un individu amb Síndrome de Down (DS) que presentava canvis histològics indistingibles de l'AD, respectivament. Finalment, per preparar els extractes control (CTRL-Tau) es va utilitzar teixit cerebral d'un pacient sense demència que no presentava signes de malaltia neurodegenerativa ni clínicament ni a l'estudi postmortem.

Els extractes de CBD-Tau i CTRL-Tau es varen generar homogeneïtzant 400 mg de substància gris cortical de pacients que s'havien confirmat histològicament com CBD i CTRL en 10% PBS (pes/volum). L'homogeneïtzat es va sonicar breument en un processador líquid ultrasònic i es va centrifugar a 3000 *g* durant 5 min. El sobrenadant resultant es va centrifugar de nou a 100000 *g* durant 30 min seguit d'una homogeneïtzació del precipitat en 1/3 del volum inicial en PBS que es va

sonicar breument i es va centrifugar de nou a 100000 *g* durant 60 min. El precipitat final es va homogeneïtzar en el 50% del volum inicial de PBS, es va sonicar, aliquotar, congelar i es va guardar a -80ºC fins el seu ús.

Els extractes patològics d'AD-Tau i DSAD-Tau es varen processar a partir de casos confirmats d'AD i DSAD seguint un protocol modificat de gradient de sucrosa per a la purificació de PHF d'AD. En resum, es varen dissecar 50g de teixit de substància gris cortical que es varen homogeneïtzar en 4 volums de la solució amortidora HS-RAB, a continuació, es va incubar l'homogenat durant 30 min en gel per despolimeritzar els MTs i finalment es va centrifugar a 126000 *g* durant 45 min per eliminar la proteïna tau soluble. El precipitat resultant es va utilitzar per generar AD-Tau mitjançant centrifugació diferencial, extracció amb Sarkosyl i ebullició per eliminar contaminants, seguit de fraccionació amb un gradient de sucrosa de 7 passos per enriquir per AD-Tau o DSAD-Tau patològic. Després de la centrifugació del gradient de sucrosa es va veure que l'AD-Tau i DSAD-Tau estaven més enriquits a la interfase entre 1.75 i 2.00 M. D'aquesta fracció es va obtenir l'extracte final que es va aliquotar, congelar i guardar a -80ºC fins el seu ús.

La puresa dels extractes enriquits de CBD-Tau, AD-Tau i DSAD-Tau, i l'absència de tau patològic a les preparacions de CTRL-Tau es va confirmar: amb la realització de SDS-PAGE, tenyint els gels amb blau Coomassie, i analitzant l'immunoblot amb els anticossos anti-tau 17025 i PHF-1. Per determinar la concentració de tau total a les preparacions es va utilitzar el *sandwich* ELISA amb Tau 5 com a anticòs de captura i una barreja dels anticossos antitau HT7/BT2 com a anticossos informadors. La prova d'àcid bicinconínic per determinar la concentració de proteïna total als extractes es va realitzar seguint les instruccions del fabricant.

2. ANIMALS UTILITZATS A L'ESTUDI

Per a aquest estudi es va utilitzar la línia de ratolins transgènics per a la proteïna tau PS19 criats en fons B6C3. Aquests ratolins sobreexpressen la forma humana de la isoforma T34 de tau (1N4R) amb la mutació P301S de *MAPT*. Està descrit que la mutació P301S de *MAPT* dóna lloc a una forma d'inici primerenc de FTDP-17 que és ràpidament letal. Amb l'edat, els ratolins PS19 desenvolupen

agregats de tau a la medul·la espinal, el tronc cerebral, l'escorça i l'hipocamp. A més, també s'observa atròfia cerebral. Clínicament, els ratolins presenten retracció de les potes del darrere quan s'aixequen per la cua, feblesa de les extremitats i amb l'edat progressen a paràlisi associada a esquena geperuda i incapacitat per alimentar-se.

Els diferents extractes (CBD-Tau, AD-Tau, DSAD-Tau, CTRL-Tau) es varen injectar a l'hipocamp i l'escorça de ratolins PS19 amb edats compreses entre 2 i 5 mesos utilitzant coordenades predeterminades: per l'hipocamp (Bregma -2.5 mm, lateral +2 mm, i profunditat -2 mm de la superfície cerebral) i per l'escorça cerebral (Bregma -2.5 mm, lateral +2 mm, i profunditat -0.8 mm de la superfície cerebral). El volum total injectat va ser de 5 μl (2.5 μl/punt injecció). Tots els experiments es varen fer segons els protocols aprovats per la Institutional *Animal Care and Use Committee of the University of Pennsylvania*.

3. ANÀLISI DEL TEIXIT CEREBRAL DELS RATOLINS INJECTATS

Els ratolins es varen sacrificar 1 mes, 3 mesos i 6 mesos després de la injecció; el cervell i la medul·la espinal es varen processar pel seu estudi histològic. En una de cada 20 seccions histològiques obtingudes es va realitzar una tinció d'immunohistoquímica utilitzant dos anticossos anti-tau (AT8 i MC1). A més, es va fer tinció immunohistoquímica amb altres anticossos antitau, amb anticossos contra altres agregats protèics com l'α-syn, Aβ o TDP-43, i anticossos per detectar cèl·lules inflamatòries microglials i astroglials. Finalment, es va fer doble tinció per immunofluorescència per identificar agregats de tau en oligodendròcits i astròcits, així com tincions de Tioflavina S (ThS) per identificar agregats amb estructura amiloide.

La quantificació de l'extensió dels agregats desenvolupats als ratolins PS19 després de les injeccions de CBD-Tau es va fer de manera semiquantitativa (0: niguna; 1+: escassos; 2+: moderats; 3+: abundants). La patologia tau que desenvoluparen els ratolins injectats amb AD-Tau i DSAD-Tau és molt similar entre ella i es va avaluar conjuntament en un sol grup (AD/DSAD-Tau) també de forma semiquantitativa (0: ningun; 1+: escassos; 2+: moderats; 3+: abundants). Per valorar la patologia que es va desenvolupar als ratolins Tg PS19 amb les injeccions de

dilucions seriades de tau es va utilitzar el mateix criteri. La distribució topogràfica de les lesions que es varen observar es va representar mitjançant mapes de calor.

Per valorar la pèrdua neuronal es varen definir unes regions determinades de CA3 i CA1 que eren similars en cada un dels casos. Les seccions es van tenyir amb hematoxilina-eosina (H&E) i es varen prendre imatges a 20x de les regions d'interès. El nombre de neurones es va comptar manualment a partir de les imatges utilitzant el software d'ImageJ (*National Institutes of Health*). Per determinar diferències estadístiques entre els grups es va utilitzar el test de one-way ANOVA i el test de comparació múltiple de Tukey.

RESULTATS

1. LES INJECCIONS DE CBD-Tau i AD-Tau INDUEIXEN EL DESENVOLUPAMENT DE PATOLOGIA TAU ALS RATOLINS Tg PS19

Per investigar si l'extracte de teixit cerebral humà afectat amb diferents taupaties podia induir patología tau als ratolins Tg PS19 i determinar si aquesta patologia presentava característiques similars a les malalties humanes es van generar extractes de CBD-Tau, AD-Tau o DSAD-Tau enriquits amb tau patològic obtinguts a partir de teixit cerebral de 4 pacients afectats amb aquestes taupaties i també d'un individu control. Els extractes es varen injectar a l'hipocamp i l'escorça cerebral de l'hemisferi dret del cervell de ratolins Tg PS19 de 2 a 5 mesos d'edat. Es va examinar la patologia tau resultant 1, 3 i 6 mesos després de la injecció. Els ratolins injectats tant amb CBD-Tau com amb AD-Tau i DSAD-Tau varen desenvolupar patologia tau passat el primer mes després de la injecció.

Els ratolins PS19 injectats amb CBD-Tau varen desenvolupar agregats de tau predominantment a la glia, als tractes de substància blanca, i a l'hipocamp a prop del lloc de la injecció. Passat el primer mes després de la injecció es van observar inclusions tau immunoreactives per AT8 als oligodendròcits de la fímbria de l'hipocamp (4/6; 66% dels ratolins), així com a l'alveus/càpsula externa a prop de la

zona d'injecció (3/6; 50% dels ratolins). L'origen oligodendroglial de les inclusions es va confirmar amb tècniques de doble tinció per immunofluorescència. També es varen desenvolupar algunes inclusions de tau al citoplasma neuronal de les regions de l'hipocamp CA1, CA3, gir dentat i subiculum, però eren escasses en comparació amb el nombre d'oligodendròcits amb inclusions de tau de la fímbria. Les inclusions de tau oligodendroglials també es varen observar en regions rostrals i caudals del cervell a certa distància de la injecció. Passat el primer mes després de la injecció, la patologia tau es va limitar al costat del lloc de la injecció i no es va observar cap agregat patològic a l'escorça cerebral. La injecció d'un segon extracte de CBD-Tau obtingut d'un altre cas amb un diagnòstic neuropatològic confirmat de CDB i que es va injectar en una altra cohort de ratolins va donar lloc a resultats similars.

Els ratolins transgènics PS19 injectats amb extractes enriquits amb tau patològica d'AD-Tau i DSAD-Tau també van desenvolupar patologia tau remarcable passat el primer mes després de la injecció. Atès que la distribució de la patologia tau en els ratolins injectats amb AD-Tau i DSAD-Tau va ser molt similar, i que la intensitat de la patologia en ambdós cervells va ser semblant, les dades generades amb aquests extractes es van considerar junts com el grup AD/DSAD. Aquest grup AD/DSAD-Tau, en contrast amb els ratolins injectats amb CBD-Tau, van desenvolupar patologia tau principalment al soma i als processos neuronals de l'hipocamp. El mapatge de la propagació de tau patològica des del lloc d'injecció de l'hipocamp dels ratolins injectats amb AD/DSAD-Tau va posar de manifest que les inclusions de tau s'estenien a regions rostrals i caudals del cervell ja passat el primer mes postinjecció. A les zones rostrals els nuclis septals laterals estaven involucrats de forma bilateral. Les regions caudals del cervell, com ara el subículum, l'escorça entorrinal (EC), locus coeruleus (LC) i nuclis del rafe, també presentaven agregats neuronals immunoreactius per AT8. A més, es van observar inclusions intracitoplasmàtiques de tau hiperfosforilada als nuclis supramamil·lars (5/8; 63% dels ratolins) i al neocòrtex (4/8; 50% dels ratolins). A més a més, la patologia neuronal també es va desenvolupar a l'hemisferi contralateral on es va limitar principalment a les neurones de l'hipocamp, amb predomini d'inclusions a CA3, i unes quantes neurones immunoreactives per AT8 a l'EC. Cal destacar que després de les injeccions amb AD/DSAD-Tau no es va observar patologia tau als oligodendròcits

passat el primer mes després de la injecció, com tampoc, a la fímbria ni a la substància blanca/càpsula externa subcortical.

Com a control de l'inici de la patologia es varen injectar quatre ratolins PS19 d'entre 2 i 3 mesos d'edat amb CTRL-Tau a l'hipocamp i a l'escorça cerebral. Aquests ratolins no varen desenvolupar patologia tau ni tan sols als 6 mesos postinjecció.

Finalment, en cap dels ratolins PS19 injectats amb CBD-Tau o AD/DSAD-Tau hi havia evidència d'agregats d'α-syn, TDP-43 o patologia Aβ, tot i que aquestes patologies es poden donar al mateix temps que l'AD.

2. LA PATOLOGIA TAU INDUÏDA PER LES INJECCIONS DE CDB-Tau I AD/DSAD-Tau A RATOLINS PS19 JOVES ES DIFON PEL CERVELL I AUGMENTA D'INTENSITAT AMB EL TEMPS

Es va avaluar la progressió de la patologia tau amb l'augment del temps de supervivència en ratolins PS19 després de les injeccions intracerebrals de CBD-Tau i d'AD/DSAD-Tau. La patologia tau oligodendroglial que es veia passat el primer mes després de la injecció als ratolins injectats amb CBD-Tau va augmentar a la fímbria, tant en regions properes com distals, al lloc d'injecció als 3 mesos, i més encara als 6 mesos després de la injecció. Tot i la variabilitat en la quantitat de la patologia tau oligodendroglial que s'observava, els ratolins presentaven un clar increment en la patologia tau als oligodendròcits amb el temps postinjecció. A més, la patologia tau oligodendroglial es va estendre a la fímbria contralateral, encara que no era tan abundant com al costat ipsilateral. Sis mesos després de la injecció, també es va observar l'aparició de plaques astrocitàries a l'estrat radiat de l'hipocamp amb característiques similars a les que s'observen als cervells humans amb CBD.

De la mateixa manera, els ratolins Tg PS19 injectats amb AD/DSAD-Tau van presentar un augment en la intensitat de la patologia tau neuronal, així com una propagació a regions bastant distals del lloc d'injecció amb l'augment del temps de supervivència després de la injecció. Aquest patró de propagació neuronal difereix dràsticament de la forma de propagació de la patologia de tau patològica observat

després de les injeccions de CBD-Tau. Als ratolins injectats amb CBD-Tau la propagació és predominantment glial fet que suggereix una manera diferent de transmissió de tau a CBD que no depèn de les connexions aferents i eferents axonals dels llocs d'injecció com passa a les injeccions d'AD/DSAD-Tau. Tres mesos després de la injecció amb AD/DSAD-Tau es va observar un augment de la intensitat de la patologia a les regions que ja estaven afectades el primer mes després de la injecció. Al costat ipsilateral, el gir dentat (DG) presentava un augment de la patologia tau neuronal als 3 mesos que semblava no variar als 6 mesos. A la regió CA1, en un inici es va veure variabilitat en la quantitat d'inclusions intraneuronals de tau superat el primer mes després de la injecció, però més tard, als 3 i 6 mesos postinjecció la intensitat de la patologia va disminuir. A CA3 la tau patològica també es va reduir notablement entre el primer mes i els 6 mesos després de la injecció. A l'hemisferi contralateral, on les inclusions de tau a l'hipocamp eren menys nombroses, es va veure un augment d'aquestes inclusions amb el temps a DG i CA1, mentre que hi va haver una reducció de la patologia tau a la regió CA3. A més, d'acord amb la interpretació que la propagació de la patologia tau induïda pels extractes d'AD/DSAD-Tau es produeix a través del transport intra-axonal, la patologia tau es va desenvolupar en regions que tenen connexions neuronals amb l'hipocamp i que no estaven involucrades durant el primer mes postinjecció, com el tàlem, nuclis mamil·lars i altres nuclis hipotalàmics. Sis mesos després de la injecció es va observar una disminució de NFT en algunes de les zones afectades dels ratolins injectats amb AD/DSAD-Tau.

3. LA PATOLOGIA TAU INDUÏDA PER LES INJECCIONS D'AD/DSAD-Tau PERÒ NO PER LES INJECCIONS DE CBD-Tau A RATOLINS PS19 DÓNA LLOC A LA PÈRDUA DE NEURONES

Per determinar si la disminució de patologia NFT observada a l'hipocamp en ratolins PS19 injectats amb AD/DSAD-Tau es podia explicar per una pèrdua de neuronal, es va quantificar el nombre de neurones a CA3 al costat contralateral al punt d'injecció utilitzant micrografia digital. Així, es va observar una disminució en el nombre de neurones a CA3 durant el període de temps comprès entre el primer i el tercer mes després de la injecció en comparació amb els controls, però aquesta pèrdua de neurones no va progressar i es va estabilitzar als 6 mesos. En contrapartida, no hi

va haver pèrdua neuronal en ratolins Tg PS19 després de la injecció de CBD-Tau i CTRL-Tau. La pèrdua neuronal s'acompanyava d'astrogliosi entre els 3 i 6 mesos després de la injecció, però la microgliosi va ser lleu i només es va observar als 3 mesos postinjecció.

4. LA INTENSITAT I LA DISTRIBUCIÓ DE LA PATOLOGIA TAU INDUÏDA DESPRÉS DE LA INJECCIÓ DE DSAD-Tau ÉS DOSI DEPENENT

En estudis anteriors s'havia vist com l'abundància d'inclusions neuronals de tau induïdes en ratolins PS19 amb injeccions de fibres preformades (PFF) de tau recombinant no només era depenent del temps, sinó que la patologia induïda després d'injeccions de quantitats creixents de PFF de T40/PS (isoforma de tau 2N4R amb mutació P301S) augmentava amb l'increment de la dosi administrada. Es va investigar aquesta possible dependència a la dosi mitjançant la injecció de diferents dilucions de DSAD-Tau a l'hipocamp i al neocòrtex dels ratolins PS19. Es varen analitzar els resultats 1 mes després de la injecció i es va veure que en totes les concentracions els ratolins varen desenvolupar patologia. Tant al lloc d'injecció com a regions rostrals i caudals de l'hipocamp del costat ipsilateral a la injecció i a totes les concentracions de tau es varen observar inclusions immunoreactives per AT8 al soma de les neurones del gir dentat, CA3 i CA1. Però curiosament es va veure com la intensitat de la patologia a l'hipocamp augmentava amb l'increment de la concentració de tau injectada, i a més, es va veure com les inclusions s'estenien a altres regions del cervell que no estaven involucrades en concentracions més baixes. Així, les inclusions a l'hemisferi contralateral només es veien amb les injeccions de concentracions més altes de tau. Curiosament, a cap de les concentracions injectades de DSAD-Tau no es va desenvolupar patologia als oligodendròcits ni als tractes de substància blanca, contràriament al que s'observava a les injeccions de CDB-Tau.

5. LA PATOLOGIA TAU INDUÏDA PER LES INJECCIONS DE CBD-Tau I AD/DSAD-Tau ADQUIREIX LES CARACTERÍSTIQUES TÍPIQUES DE LA MALALTIA ALS HUMANS

Es va caracteritzar, encara més, la naturalesa de la patologia tau desenvolupada com a conseqüència de les injeccions d'extractes de CBD-Tau i

AD/DSAD-Tau als ratolins PS19 realitzant immunohistoquímica (IHC) amb anticossos monoclonals anti-tau que detecten la proteïna tau humana patològica de CDB i AD. La IHC amb MC1 i TG3 va posar de manifest que les inclusions tau induïdes per CBD-Tau eren modestament positives per a tots dos anticossos monoclonals passat el primer mes després de la injecció, però als 3 mesos i de forma més notable als 6 mesos aquests anticossos detectaren la patologia tau amb més intensitat i en més quantitat. Per contra, les injeccions d'AD/DSAD-Tau varen induir una patologia intensament immunoreactiva per a tots dos anticossos, MC1 i TG3, el primer mes després de la injecció. Notablement, els anticossos antitau específics per a la tau humana (T14) i la tau de ratolí (T49) van tenyir tots els agregats que es varen desenvolupar als ratolins tant oligodendroglials com neuronals. També es va demostrar que només la patologia tau desenvolupada després de les injeccions amb AD/DSAD-Tau era positiva per Tioflavina S (ThS) però en canvi, no es va observar aquesta positivitat a les lesions desenvolupades en ratolins després de la injecció amb CBD-Tau ni als 6 mesos després de la injecció.

DISCUSSIÓ

La malaltia d'Alzheimer (AD), la degeneració corticobasal (CBD), la paràlisi supranuclear progressiva (PSP), la malaltia de grans argiròfils (AGD) i la malaltia de Pick (PiD) són malalties classificades com taupaties que es caracteritzen per presentar agregats intracel·lulars de proteïna tau. Tot i que aquestes malalties tenen en comú l'acumulació de proteïna tau anòmala, clínicament es manifesten de diferent manera, tenen una distribució topogràfica de la patologia determinada i una afectació del tipus cel.lular específica per a cada malaltia. Així trobem que els agregats de tau es poden desenvolupar a neurones o cèl.lules glials; la patologia pot afectar la substància gris solament o afectar la substància blanca i la substància gris alhora; o bé involucrar les regions corticals predominantment o involucrar el tronc cerebral i els nuclis subcorticals al mateix temps.

A l'AD les inclusions de tau s'acumulen de forma jerarquitzada seguint un patró estereotipat de manera que la patologia comença al LC i a l'escorça entorrinal,

seguidament s'afecta l'hipocamp i les regions límbiques, i finalment acaba per involucrar l'escorça cerebral. L'observació d'aquesta disseminació seqüencial de la malaltia juntament amb l'observació que la malaltia afectava regions del cervell interconnectades mitjançant sinapsis van suggerir que la progressió de la malaltia es duia a terme mitjançant la transmissió de la proteïna tau patològica d'una cèl·lula a una altre. Aquest fenomen es va poder demostrar inicialment *in vitro* al veure que extractes de teixit d'AD induïen la formació de PHFs en neurones fetals en cultiu. Més endavant amb l'ús de fibres preformades (PFFs) de tau recombinant es va veure com aquestes eren capaces d'induir la conversió de tau intracel·lular soluble a tau fibril·lar a cèl·lules en cultiu. Estudis *in vivo* varen desmostrar que la inoculació d'homogenats cerebrals de ratolins transgènics que formen NFTs al cervell de ratolins que sobreexpressen tau WT (ALZ17) i que no formen inclusions, induïen la formació d'inclusions de tau a aquests últims. Iba et al. varen posar de manifest que les PFFs de tau injectades a ratolins PS19 eren suficients per induir patologia i que aquesta patologia era capaç de propagar-se pel cervell del ratolí tal i com ho fa l'AD. En conjunt, es va establir que les espècies de tau fibril·lars eren capaces de reclutar i convertir tau endògena soluble en agregats patològics a les neurones i processos neuronals *in vivo* i que aquests agregats patològics es podien transmetre d'una cèl·lula a una altre donant lloc al desenvolupament i progressió de la malaltia.

L'objectiu del meu estudi va ser investigar si els exractes enriquits amb tau patològic obtinguts de cervells humans amb canvis de CBD o AD i DSAD eren capaços d'induir patologia als ratolins PS19 i si aquesta patologia desenvolupada seria similar a la patologia que es desenvolupa als humans amb CBD i AD respectivament. Per això, es varen injectar extractes enriquits amb tau patològic (CBD-Tau, AD-Tau o DSAD-Tau) a l'escorça i l'hipocamp de ratolins Tg PS19 que sobreexpressen la mutació P301S de la isoforma 1N4R de la tau humana, i es va avaluar la patologia resultant en diferents moments (1 mes, 3 mesos i 6 mesos). Cal destacar que els ratolins PS19 varen desenvolupar patologia tau molt ràpidament i es podien observar inclusions de tau passat el primer mes després de la injecció a tots els ratolins. Els agregats es varen notar tant a la zona d'injecció com a regions cerebrals allunyades del punt d'injecció. Amb aquestes troballes vàrem corroborar els resultats dels estudis de Clavaguera et al. demostrant que no tan sols les PFFs i les formes mutades de tau obtingudes de ratolins Tg poden induir patologia tau, sinó que extractes de

teixit humà patològic també poden donar lloc a malaltia en models de ratolins Tg. Notablement, la patologia tau es va desenvolupar en ratolins Tg en els dos estudis tot i que els models de ratolins eren diferents. Clavaguera et al. van basar els seus estudis en un model de ratolí, l'ALZ17, que sobreexpressa la forma WT de la isoforma més llarga de tau humana (2N4R) mentre que el model murí que vaig utilitzar per a aquest estudi, el PS19, sobrexpressa una forma mutada de la isoforma 1N4R de tau. Cal destacar que hi va haver diferències en el temps que els animals varen tardar en desenvolupar la patologia i en el model PS19 utilitzat per aquest estudi la patologia es va desenvolupar de forma considerablement més ràpida. Això es podria explicar per la naturalesa de la proteïna tau sobrexpressada al model murí PS19, ja que se sap que la isoforma mutada P301S té més tendència a agregar-se que la forma de tau humana WT.

En analitzar la distribució anatòmica i el tipus cel·lular on es localitzaven els agregats de tau patològics, es va observar que els ratolins PS19 injectats amb CBD-Tau havien desenvolupat inclusions de tau intracel·lulars de predomini als oligodendròcits en comparació amb els ratolins injectats amb AD-Tau i DSAD-Tau que varen desenvolupar les inclusions al citoplasma neuronal. De seguida, al primer mes després de la injecció, el 66% dels ratolins injectats amb CBD-Tau havien desenvolupat patologia a la fímbria de l'hipocamp a prop de la zona d'injecció i la meitat dels casos injectats varen desenvolupar patologia a l'alveus/càpsula externa. La patologia, a més, s'estenia a les regions caudals i rostrals de la fímbria i l'alveus allunyades de la zona d'injecció. A algunes neurones de l'hipocamp també es varen desenvolupar inclusions citoplasmàtiques, però la quantitat de patologia detectada, comparada amb la de la fímbria, era molt petita. D'altra banda, els ratolins injectats amb AD-Tau i DSAD-Tau varen desenvolupar patologia tau sobretot al citoplasma de les neurones de l'hipocamp, tant en les zones properes a la injecció com a zones allunyades de la zona d'injecció incloent regions caudals com el subículum, EC, LC i fins i tot, l'hipocamp contralateral. Curiosament aquesta distribució de la patologia desenvolupada amb les injeccions de CBD-Tau i AD/DSAD-Tau es corresponia al tipus de patologia que es desenvolupa als humans on, en el cas de CBD l'estudi histològic del cervell posa de manifest una abundància de patologia a la substància blanca, mentre que als casos d'AD la patologia que s'hi desenvolupa predomina a la substància gris amb preservació de la substància blanca. Aquests resultats

suggereixen que hi ha diferents soques de proteïna tau que serien les responsables del diferent desenvolupament dels agregats tant en la distribució del tipus cel·lular afectat en cada cas com en la distribució topogràfica de la patologia, un fenòmen que s'ha descrit a les malaltes priòniques. A les malalties priòniques la proteïna PrP^{sc} és capaç d'adquirir diferents conformacions que li confereixen propietats diferents de manera que cada conformació es caracteritzarà per desenvolupar diferents fenotips de la malaltia en termes de temps d'incubació, regions afectades per la malaltia i patrons d'agregats de PrP^{sc}. La PrP no és l'única proteïna en la qual s'ha observat aquest fenomen i l'existència de diferents soques també s'ha demostrat per l'α-syn, Aβ, i més recentment, per tau.

Aquest estudi ha demostrat que hi ha un increment d'intensitat de la malaltia i que la patologia desenvolupada en ratolins PS19 s'esten a regions distals a la zona d'injecció en relació a l'augment del temps postinjecció. En ratolins injectats amb CBD-Tau es va veure un increment de la patologia de la fímbria entre el primer i el tercer mes després de la injecció, que es va fer més evident al sisè mes postinjecció, moment en que la patologia es podia veure a la fimbria de l'hipocamp contralateral. La propagació de la patologia de tau també es va veure en ratolins injectats amb AD/DSAD-Tau amb l'increment del temps postinjecció. Als 3 mesos es varen observar regions afectades pels agregats on prèviament no n'hi havia, i per altra banda, regions que ja estaven afectades passat el primer mes després de la injecció presentaven un increment de la intensitat de la patologia. Aquestes troballes estan en concordança amb estudis previs on s'hi ha observat increment de patologia tau amb l'augment del temps postinjecció després de la injecció amb extractes de ratolí Tg, o després de la injecció de PFFs de tau recombinant. En diversos estudis s'ha posat de manifest que la transmissió dels agregats de tau es porta a terme entre regions connectades per sinapsis. A l'estudi que vaig portar a terme, als ratolins injectats amb AD/DSAD-Tau s'observava una progressió de la malaltia seguint connexions interneuronals ja que totes les regions afectades en aquests ratolins tenen connexions sinàptiques amb l'hipocamp. En canvi, els ratolins injectats amb CBD-Tau també presentaven evolució de la patologia però, en aquest cas, la progressió no seguia les connexions neuronals esperades i el mecanisme de progressió es desconeix. En un estudi amb ratolins Tg on s'induïa l'expressió d'α-syn als oligodendròcits dels

ratolins, també s'hi observava patologia als axons suggerint que podia haver una transferència de la proteïna patològica dels oligodendròcits als axons. Aquest fenomen, però, no es va observar en un altre estudi amb ratolins Tg amb sobreexpressió de tau als olidogdendròcits. Aquests ratolins, tot i que es van observar signes de neurodegeneració, només presentaven inclusions de tau als oligodendròcits. Als ratolins Tg PS19 utilitzats al meu estudi i injectats amb CBD-Tau s'observaven agregats de tau al neuròpil, fet que fa pensar que en el cas de CBD la transferència de tau dels oligodendròcits als axons i viceversa seria un mecanisme plausible de progressió de la malaltia.

Per descartar que proteïnes diferents de la tau patològica o altres elements en el contingut dels extractes injectats fossin els responsables de la inducció de la patologia tau als ratolins PS19 es va injectar extracte d'un individu control (CTRL-Tau) al còrtex i l'hipocamp. Com era d'esperar, els ratolins PS19 injectats amb CTRL-Tau no presentaven signes de patologia en forma d'inclusions de tau a les zones d'injecció ni a altres regions, ni tan sols 6 mesos després de la injecció. Aquests resultats donen suport a estudis previs que indiquen que és la tau patològica i no la tau normal la responsable de la inducció de la transmissió i propagació de la patologia tau tant *in vivo* com *in vitro*.

De la mateixa manera com en ratolins PS19 injectats amb PFFs de tau recombinant es va veure que el nombre de neurones immunoreactives per MC1 augmentaven a l'incrementar la concentració total de tau als extractes, al meu estudi també es va observar una dependència a la dosi de tau injectada, complementant d'aquesta manera la informació a l'estudi inicial de Clavaguera et al. Per determinar la quantitat mínima de proteïna patològica necessària per a la formació d'agregats als ratolins PS19 es va fer un estudi amb concentracions creixents de tau continguda a l'extracte de DSAD-Tau injectat. Es va veure que fins i tot a les concentracions més baixes els ratolins PS19 desenvolupaven agregats de tau posant de manifest que la patologia es pot induir amb concentracions mínimes de proteïna. A més, amb l'increment de la concentració de tau a l'extracte, la patologia que es desenvolupava era més intensa i implicava més regions cerebrals afectant-se, fins i tot, amb les concentracions més elevades el costat contralateral. Curiosament, ni amb les injeccions a les concentracions més baixes de proteïna tau als extractes de DSAD-Tau

es va desenvolupar patologia als oligodendròcits, demostrant que aquest fenomen molt probablement depèn del tipus de tau injectat i no de la concentració de la proteïna tau present a l'extracte.

La patologia tau desenvolupada als ratolins PS19 després de la injecció amb AD/DSAD-Tau era variable i a CA3 es va observar una disminució important dels agregats tant al costat ipsilateral de la injecció com al contralateral. Aquesta disminució en el nombre d'agregats es va poder explicar per una pèrdua neuronal que ja era significativa als 3 mesos després de la injecció. El mecanisme de toxicitat dels agregats de tau és desconegut, i els resultats als estudis són contradictoris de manera que no queda clar què causa la pèrdua neuronal a l'AD. Hi ha estudis que relacionen la presència de NFT a la pèrdua neuronal però hi ha altres estudis que demostren alteracions sinàptiques, de comportament i de pèrdua neuronal en absència de NFT. Publicacions més recents han posat en el punt de mira els oligòmers solubles de tau com a responsables principals de mort neuronal. La toxicitat podria ser deguda a l'efecte de les diferents soques de tau que afectarien específicament a neurones o, també, podria ser dosi depenent com sugereix un estudi on la injecció d'altes concentracions de PFFs de tau recombinant estan associades a pèrdua neuronal a CA1. La pèrdua neuronal observada en el meu estudi es trobava associada a astrogliòsi i lleugera microgliòsi que són signes de neurodegeneració.

Finalment, a l'estudi s'observa com les característiques histològiques de CBD i AD es reprodueixen als animals injectats amb CBD-Tau i AD/DSAD-Tau respectivament. D'una banda, les inclusions induïdes per CBD-Tau es desenvolupen predominantment als oligodendròcits de forma similar a com ocorre a la CBD i les inclusions de tau als ratolins injectats amb AD/DSAD-Tau es formen sobretot a les neurones com s'observa a l'AD. D'altra banda, l'absència de positivitat per ThS als agregats oligodendroglials als ratolins injectats amb CBD-Tau, fins i tot després de 6 mesos postinjecció, i la positivitat dels agregats neuronals per aquesta tinció histoquímica als animals injectats amb AD/DSAD-Tau donen suport a la versemblança amb les malalties de CBD i AD respectivament.

Actualment, no hi ha cap tractament per l'AD ni per altres taupaties que millorin o aturin la malaltia. Estudis previs suggereixen que la disminució dels

agregats de tau seria beneficiós pels malalts amb AD ja que la intensitat de patologia de NFT es correlaciona millor amb el grau de demència que els agregats d'Aβ. Això ha fet que en els últims anys les investigacions s'hagin focalitzat cap a la proteïna tau. A més, el descobriment en aquest i altres estudis que la proteïna tau patològica es transmet d'una cèl·lula a una altra suggereix que la immunoteràpia podria ser beneficiosa per aquestes malalties obrint possibilitats per a la generació de noves dianes terapèutiques que modifiquin el curs de la malaltia. La injecció d'anticossos o vacunes actives que interferissin amb la proteïna que s'allibera al medi extracel·lular seria un possible mecanisme per aturar la propagació de la malaltia. Recentment, s'han realitzat un nombre d'estudis en animals, tant amb immunoteràpia passiva com amb vacunes, que han donat bons resultats. Així doncs, l'observació en aquest i altres estudis que donen suport a l'existència de diferents soques de la proteïna obre noves possibilitats per generar anticossos que es dirigeixin específicament cap a aquestes soques fent que el tractament sigui més selectiu i d'aquesta manera evitar possibles efectes secundaris. En aquest projecte s'ha generat un model animal que reprodueix la patologia amb les característiques similars als humans i serà un model útil per l'estudi del desenvolupament de noves dianes terapèutiques pel tractament de les taupaties.

CONCLUSIONS

1. Presento models animals similars a CBD i AD que ràpidament desenvolupen inclusions intracel·lulars a glia i a neurones després de la injecció d'extracte proteic enriquit amb tau patològica obtingut de cervells humans amb CBD o AD/DSAD respectivament. La patologia desenvolupada progressa ràpidament i amb un patró estereotipat similar al que s'observa en AD i en altres malalties neurodegeneratives.
2. Els ratolins injectats amb CBD-Tau desenvolupen patologia tau sobretot a oligodendròcits i substància blanca al contrari que els injectats amb AD/DSAD-Tau que desenvolupen inclusions patològiques al soma neuronal. Aquesta distribució és similar a la observada a les malalties de CBD i AD respectivament.

3. La patologia desenvolupada als ratolins PS19 després de la injecció amb CBD-Tau i AD/DSAD-Tau progressa amb el temps i, en el cas de DSAD-Tau, també és dosi depenent. La progressió d'AD/DSAD-Tau segueix les connexions neuronals del lloc d'injecció mentre que la progressió de CBD-Tau és més limitada i no es troba relacionada amb les connexions sinàptiques de la zona d'injecció.

4. En ratolins PS19 s'observa mort neuronal a CA3 de l'hipocamp després de la injecció d'AD/DSAS-Tau però no després de la injecció de CBD-Tau o CTRL-Tau.

5. Aquests experiments aporten evidència addicional per la hipòtesi que la progressió de la malaltia és prion-like i suggereixen que la proteïna tau desenvolupada *in vivo* és depenent de la patologia tau a la preparació indicant que modificacions postraduccionals o diferents soques de la proteïna són responsables de la diversitat entre malalties.

6. Aquests models animals proporcionen sistemes informatius per l'estudi de la transmissió de patologia tau, de degeneració neuronal i glial secundària a tau, i pel desenvolupament de noves teràpies modificadores de malaltia pel tractament de CBD i AD, en particular d'immunoteràpia dirigida a diferents soques de la proteïna tau.

INTRODUCTION

1. TAU PROTEIN

In 1975, Weingarten et al (1) discovered a salt dissociable factor that conferred the ability of tubulin to associate into microtubules and named it tau. Tau is a highly soluble protein that is widely expressed in the central and peripheral nervous system. It is mainly found in axons (2,3) and, at very low concentration, can also be seen in astrocytes and oligodendrocytes (4,5).

1.1 THE STRUCTURE OF TAU PROTEIN

Tau protein has hydrophilic properties, which confer to the protein its high solubility, and is also heat and acid stable (1,6,7). Tau appears as a random coiled protein with a beta structure in the second and third microtubule binding repeats (8–11). Tau protein is considered a dipole and, traditionally the structure has been divided into two large domains based on chymotrypsin cleavage (12): a projection domain and a microtubule-binding domain (Figure 1). The projection domain contains the N-terminal half of the molecule, which is further subdivided in the N-terminal region and the proline-rich region. The N-terminal region, projects from the microtubule surface and contains a high proportion of acidic residues. The proline-rich region, is located next to the microtubule-binding repeats and contains many prolines which are targets for proline-directed kinases and binding sites for proteins with SH3 domains. The microtubule binding domain is referred to as the C-terminal half of the molecule and contains the basic microtubule-binding region (MTBR), and an acidic C-terminal region (13). The MTBR contains 3 or 4 repeat regions which are 31 or 32 amino acid sequences that contain 18 residues with similar but not identical repetitive sequences that are separated by less conserved 13 or 14 amino acid residues, namely the inter-repeat regions (14–16). The 18 amino acid sequence contains the minimal structure with tubulin binding capacity thereby the repeat regions are one of the major sites through which tau protein binds to microtubules. It has been shown that the sequence with the highest ability to bind to microtubules is that contained within the first repeat (R1), the following inter-repeat region (IR1/2), and the second repeat (R2) (14,17,18).

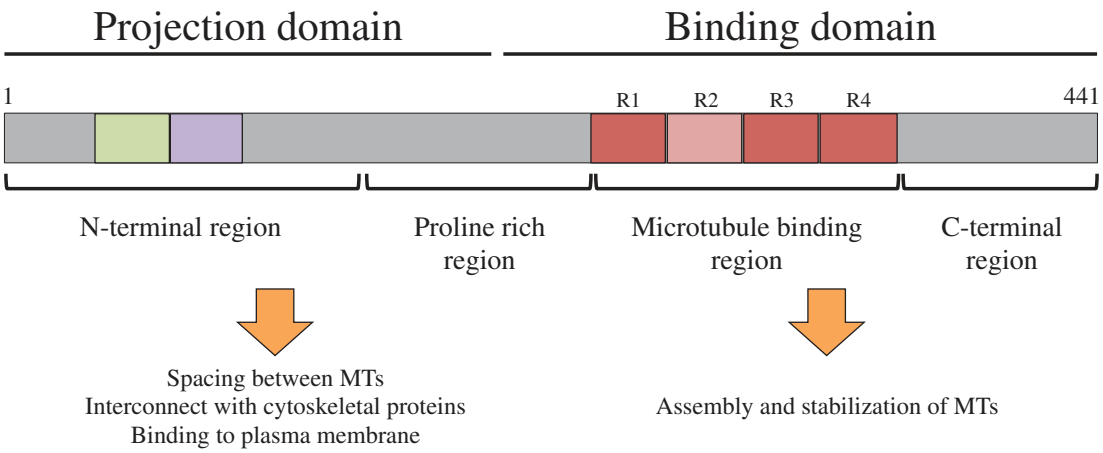

Figure 1. **Structure of tau protein**. Based on chymotrypsin cleavage, tau is divided into two domains: the projection domain and the binding domain. The projection domain includes the N-terminal region and the proline rich region. The binding domain includes the microtubule binding region (MTBR) and the C-terminal region. The MTBR encompasses the repeat regions to which tau protein binds to tubulin. Through the interaction of the domains with other structures of the cell many functions of tau have been described: assembly and stabilization of MTs, spacing between MTs, interconnection with cytoskeletal proteins and binding to plasma membrane.

1.2 THE 6 ISOFORMS OF TAU

Human tau is encoded by the *MAPT* gene that is located in the long arm of chromosome 17 at band position 17q21.31 (19) (Figure 2). *MAPT* gene has 16 exons but only 13 of them are present in the mRNA of the human central nervous system (CNS). Exon -1, 1, 4, 5, 7, 9, 10, 11, 12 and 13 are constitutively present in neuronal mRNA, although exon -1 is not translated. Exons 4A, 6 and 8 are not present in the mRNA of the CNS and exons 2, 3 and 10 are alternatively spliced. This alternative splicing of exons 2, 3 and 10 during the transcription of *MAPT* leads to the expression of 6 isoforms of tau protein. The expression of the isoforms is developmentally regulated, thus in the fetus there is expression of only 0N3R isoforms while in the adult all 6 isoforms are detected (11,20–22).

The isoforms contain between 352 amino acids, the shortest form, and 441 residues, the longest form, and when they are not phosphorylated, the molecular weights range between 45 and 65 kDa (23). The isoforms vary between them by the presence of 3 or 4 tandem repeats in the binding domain at the C-terminal end of the protein and the presence or absence of 29 or 58 amino acid inserts at the N-terminal end of the protein. The inclusion of exon 10, that encodes for a repeat region in the

binding domain, results in 4 repeat isoforms (4R: 0N4R, 1N4R, 2N4R) while its absence, gives rise to 3 repeat isoforms (3R: 0N3R, 1N3R, 2N3R). Exons 2 and 3 encode for 29 amino acid residues each at the N-terminal end of the protein, thus 0N isoforms result from the absence of the transcription of both exons 2 and 3, 1N isoforms in which there is addition of 29 amino acid residues result from the transcription of exon 2, and 2N isoforms which present 58 additional amino acid residues in the N-terminal end of the protein result from the transcription of exons 2 and 3 (21) (Figure 2). Exon 3 is never transcribed independently of exon 2 (24).

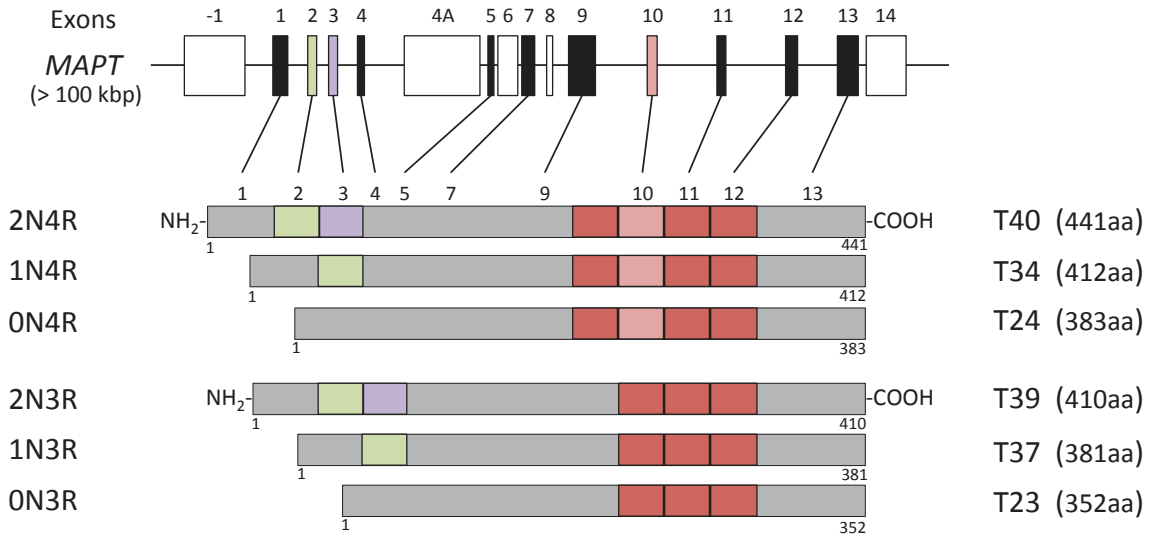

Figure 2. Schematics of the tau gene *MAPT* and the 6 isoforms that result from the alternative splicing of the mRNA.

In the normal adult brain the proportion of 3R and 4R tau isoforms is similar (1:1) however, there is a prevalence of 1N over 0N over 2N isoforms (25,26). In the diseased brain the proportion of the isoforms can be altered causing a predominance of one isoform versus the other. Thus, 4R isoforms predominate in corticobasal degeneration (CBD), progressive supranuclear palsy (PSP) and argyrophilic grain disease (AGD) and 3R isoforms predominate in Pick's disease (PiD) (27). Interestingly, in Alzheimer's disease (AD) the proportion of 3R and 4R isoforms remain similar (Figure 3). Each of these diseases are discussed in Section 2, below.

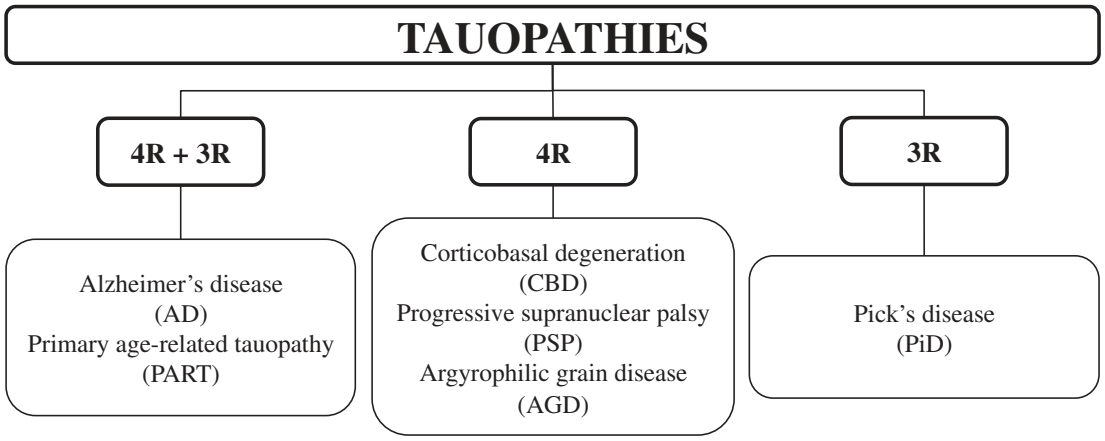

Figure 3. Classification scheme for the most common sporadic tauopathies according to the predominance of 4R or 3R tau isoforms.

Tau protein with 4R isoforms have an increased rate of assembly and also show greater affinity to microtubules compared to tau protein with only three repeat regions at the C-terminal end (28,29).

1.3 BIOCHEMISTRY OF TAUOPATHIES

The analysis of purified tau aggregates from the different tauopathies by sodium dodecyl sulphate-polyacrylamide gel electrophoresis (SDS-PAGE) reveals that tauopathies have a different pattern of bands of insoluble tau as a consequence of the different isoform composition (Figure 4). AD brains show a pattern of 3 major bands at 60, 64 and 68 kDa and a minor band at 72 kDa that resolve in 6 bands when tau is dephosphorylated. The pattern for CBD, PSP and AGD, 4R tauopathies, is similar and resolve in 2 major bands at 64 and 68 kDa and a minor band at 72 kDa that is variably detected. The band pattern remains as three bands after dephosphorylation representing the three 4R isoforms. Finally, PiD, shows a pattern of two major bands at 60 and 64 kDa and a variably detected band at 68 kDa that upon tau dephosphorylation resolves in three bands corresponding to the three 3R isoforms of tau protein (27,30).

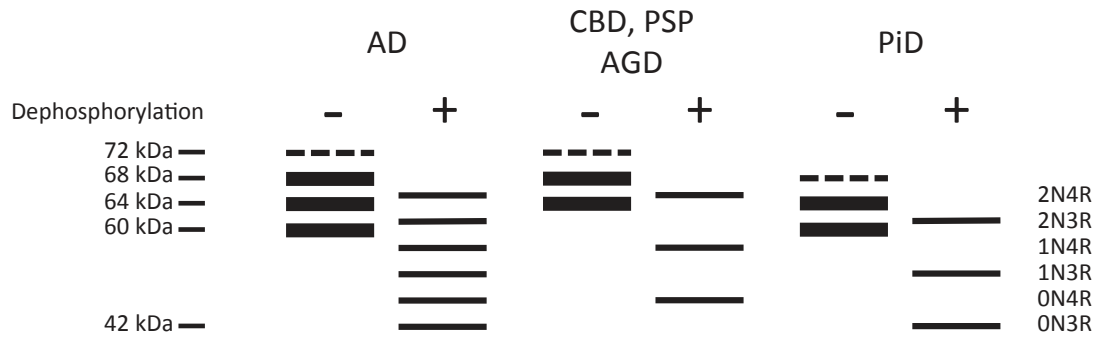

Figure 4. Schematic representation of the Western Blot banding pattern of the sporadic tauopathies (AD, CBD, PSP, AGD and PiD before (-) and after (+) dephosphorylation. (*Modified from* Lee et al., *Annu Rev Neurosci* (2001)24 :1121-159).

1.4 THE FUNCTIONS OF TAU PROTEIN

Tau is a multifunctional protein which tasks are exerted through the binding to microtubules (MTs) and other cellular elements (31,32). The most well known function of tau is the assembly and stabilization of MTs through tubulin polymerization. This function was first described in neuronal cells and also in non-neuronal cells after microinjection of tau protein (9,33–35).

The assembly and stabilization of MTs is done through the binding of tau to the MTs. The way in which tau binds to MTs is not completely understood but it is thought that the repeats of the MTBR of tau protein and the sequences flanking these repeats are involved. A model was proposed whereby the flanking regions, which bind more tightly to MTs, would act as targeting domains being responsible for positioning tau on the MT surface, and the repeat regions, which bind weakly through the interaction of the positive and negative electric charges, would be considered the catalytic domains for MT assembly (12,14,36–40). It has been observed that although the flanking regions bind more tightly to tubulin, only the binding of the repeat regions promote MT assembly (12). Specific sequences have been described both in the repeat regions and the proline-rich regions that are strongly involved in the interaction of tau to MTs. In the case of the microtubule binding repeats, as mentioned above, the R1, R2 and the IR1/2 inter-repeat region ^{275}VQIINK^{280} show

the most efficient binding to MTs, while the bonds through the proline-rich flanking regions include residues ^{225}KVAVVRT^{231} and ^{240}KSRLQTAPV^{248} (16,18,38).

Through the regulation of the stability and dynamics of MT assembly, tau has been involved in establishing neuronal polarity and axonal growth (41,42). Furthermore, tau can interfere with the binding of motor proteins to MTs thus regulating axonal transport (43,44). However, these are not the only roles of tau in neurons, and other functions for tau have been described which are carried out by domains other than the MTBR. For example, the projection domain is thought to be involved in the spacing between axonal microtubules (39,45). Moreover, it has been seen that tau has the ability to interconnect with other cytoskeletal proteins such as neurofilaments through the binding to spectrin and actin filaments which create interactions between actin and MTs restricting the flexibility of the MT latices (46–51). Additionally, tau has been involved in signal transduction pathways and is capable of modulating the activity of Src family kinases (i.e. Fyn, cSrc), through the binding to the SH3 domain of these plasma-membrane-associated proteins (52,53). Furthermore, tau can influence signal transduction processes activated by nerve growth factor (54) and activate phospholipase C-γ (PLC-γ) isozymes (55). Moreover, tau has the ability to interact with cytoplasmic organelles such as mitochondria, which allow a connection between MTs and these organelles (56). Interestingly, the projection domain does not seem to affect microtubule binding affinity or microtubule dynamics (16,57).

1.5 POST-TRANSLATIONAL MODIFICATIONS OF TAU

Tau protein can undergo post-translational changes such as phosphorylation, nitration (58), glycosylation (59,60), ubiquitination (61), glycation (62), polyamination (63), sumoylation (64), acetylation (65,66) and proteolysis or truncation (67,68). It is believed that these changes may play a role in the affinity of tau for MTs and the initiation of tau protein aggregates.

1.5.1 Phosphorylation

Phosphorylation is the most widely studied post-translational change (69). In the normal human brain there are about 1.9 moles of phosphate per mole of tau, whereas in AD brain, tau from NFT carries 6-8 moles of phosphate per mole of tau. This increase in phosphorylation is due to either an increase of phosphorylation in some tau sites that are already phosphorylated in normal brains or to phosphorylation of sites that are only phosphorylated in pathological brains (70).

In the longest isoform of tau there are 85 putative sites that can presumably be phosphorylated. Phosphorylation of 48 of these sites, have already been described in the literature (59,71–77) (Figure 5). The majority of the positions are serine or threonine residues that are immediately followed by proline residues (Ser/Thr-Pro motif) and are most commonly located in the flanking regions of the repeat domains (78). However, these are not the only residues involved in phosphorylation and tyrosine residues can also be phosphorylated.

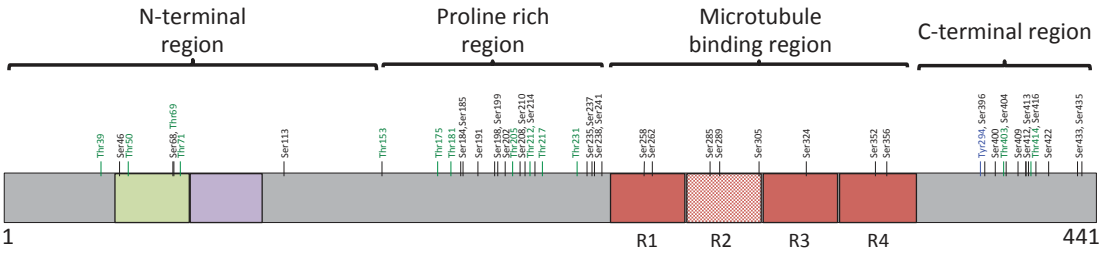

Figure 5. **Phosphorylation sites in tau protein**. Depiction of the forty-eight phosphorylation sites described in the literature of the 85 putative phosphorylation sites of tau protein. The residues most frequently phosphorylated are those located in the regions flanking the MTBR. *Black*: Ser residues, *Green*: Thr residues, *Blue*: Tyr residues.

The phosphorylation status of tau is regulated by the action of specific kinases and phosphatases. Kinases involved in tau phosphorylation have been grouped in three categories according to the residues they phosphorylate: proline directed protein kinases (PDPK), non-proline directed protein kinases (non-PDPK) and protein kinases specific for Tyr (TPK).

The PDPK phosphorylate serine or threonine amino-acid residues that are immediately followed by a proline residue. This group includes glycogen synthase kinase 3β (GSK-3β) (76,79,80), cyclin-dependent kinase 5 (cdk5) (81–83) and mitogen activated protein kinase (MAPK) (84,85). GSK-3β is involved in the phosphorylation of tau and amyloid-β and plays a key role in the pathogenesis of AD (80).

Although not as common, phosphorylation sites in tau protein can be targeted by non-PDPK (86) including cyclic-AMP-dependent kinases A/B/C/N (PKA, PKB/Akt, PKC, PKN) (72,87–89), calcium/calmodulin-dependent protein kinase II (CaMK II) (90), microtubule affinity-regulating kinase (MARK) (91,92), stress-activated protein kinases (SAP: JNK/SAPK1, p38/SAPK2, SAPK3, SAPK4) (93,94), tau tubulin kinases 1/2 (TTBK1/2) (95,96), casein kinases 1α/1δ/1ε/2 (CK1α/1δ/1ε/2) (76,97,98), dual specificity tyrosine-phosphorylation-regulated kinase 1A (DYRK1A) (99) and 5'-adenosine-monophosphate activated protein kinase (AMPK) (100,101).

Finally, the Sr family kinases such as Src, Lck, Syk, Fyn and c-Abl kinase, which belong to the TPK family of kinases, phosphorylate the tyrosine residues present in tau protein (52,53).

Phosphatases are the enzymes responsible for reversing phosphorylation and those that have been related to the dephosphorylation of tau protein include PP2A, PP2B, PP1 and PP5 (102–106). *In vitro*, these enzymes dephosphorylate tau with overlapping specificities, however in human brain tissue PP2A and PP2B dephosphorylate tau in a site-specific manner (27). PP2A accounts for approximately 70% of total brain tau phosphatase activity (103).

An imbalance between kinases and phosphatases can lead to the hyperphosphorylation of tau protein (107). Although increased phosphorylation of tau is seen in physiological situations such as fetal brain development, hibernation, and hypothermia, abnormal hyperphosphorylation occurs in pathological situations and is the base of tauopathies including CBD and AD (74,108–111).

1.6 AGGREGATION OF TAU

The hallmark lesion of tauopathies is the filamentous intracellular aggregates of hyperphosphorylated tau protein in paired helical filaments (PHF) and straight filaments (SF) (112–118). It is not completely understood what causes tau, a highly soluble protein, to aggregate into NFT but it is believed to imply a multi-step process that follows nucleation-elongation dynamics with an initial lag phase of formation of oligomeric intermediates followed by a rapid elongation phase. For this process to take place post-translational modifications and conformational changes of the protein are thought to be involved (59,68,119–122) (Figure 6).

On a first step tau would dissociate from MTs probably due to abnormal hyperphosphorylation causing an increase in the concentration of soluble tau in the cytoplasm (83,123–128). Unbound tau could experience conformational changes by mediation of further post-translational modifications adopting an aggregation-competent conformation that would lead to the formation of oligomers. These oligomers would be capable of adding more monomers, continuing the aggregation process to form subunits of filaments or protomers that would adopt the parallel, in-register cross-β-sheet structure of amyloid aggregates, which then would further organize to finally form NFT (129).

Additionally, the dissociation of tau from the MTs would hamper tau's function of assembly and stability of the MTs causing MTs to disassemble and hence lead to dysfunction of MTs (123,130,131) (Figure 6). It is this process that is thought to contribute to tau-mediated neurodegeneration.

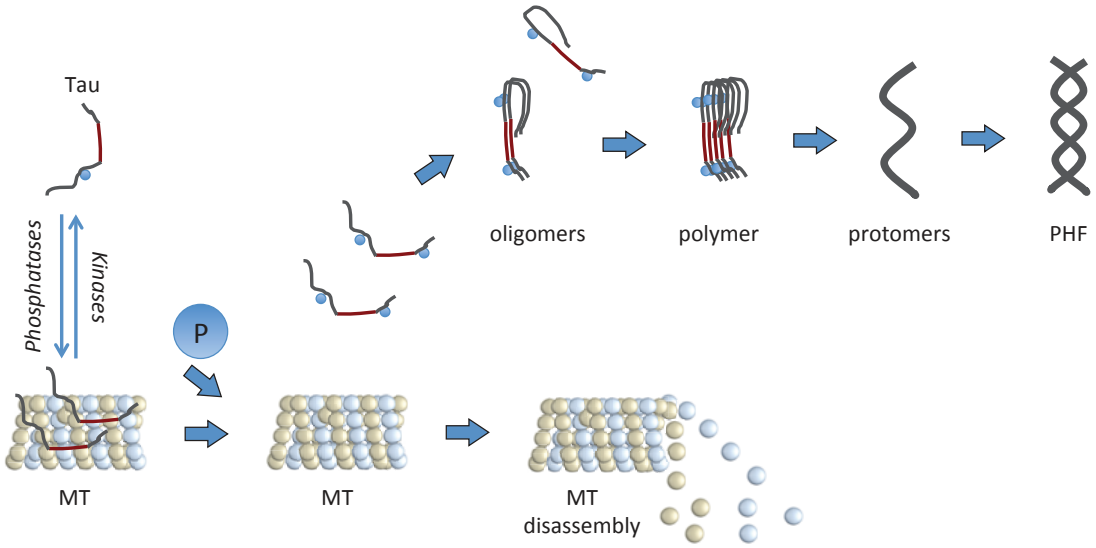

Figure 6. Diagrammatic representation of tau aggregation and disassembly of microtubules (MTs). The action of specific kinases and phosphatases regulate the phosphorylation state of tau thus, the binding of tau to MTs. When tau is hyperphosphorylated it detaches from the MTs, it can experience conformational changes and can aggregate into oligomers, polymers and protomers to finally form the more structured PHFs. The dissociation of tau from MTs induces the disassembly of MTs.

1.7 TAU MUTATIONS

Between 1994 and 1997, it was demonstrated that mutations of the *MAPT* gene were responsible for familial forms of frontotemporal dementia, now known as frontotemporal lobar dementia with parkinsonism linked to chromosome 17 (FTLDP-17) (132–137). The cases were characterized by the presence of aggregates of hyperphosphorylated tau in neuronal and glial cells in the brain accompanied by extensive neuronal loss, but without evidence of Aβ deposits (138). With this finding it was determined that tau alone is sufficient to cause neurodegeneration.

At present, more than 50 disease-causing mutations of the *MAPT* gene have been identified in both exons and introns (139). All exonic mutations except for two are located in exons 9-13, thus most of these mutations involve exons that encode for the repeat regions, and are missense mutations, deletions or silent mutations. The intronic mutations tend to be clustered in the intron immediately following exon 10.

Mutations can be divided into two groups: those with a primary effect at the protein level and those that affect the alternative splicing of tau pre-mRNA (140). Mutations with a primary effect at the protein level are most frequently missense, whereby the change or deletion of a single amino acid decreases the ability of tau to interact with microtubules or promote the assembly of tau into filaments (141). On the other hand, mutations at the introns or coding regions of exon 10 typically have an effect on the RNA by increasing the alternative splicing of exon 10 (135,136). This generally results in an increased production of 4R over 3R tau isoforms creating an imbalance between the isoforms that could increase tau aggregation (140).

The P301S *MAPT* mutation is one of the missense mutations involving the coding region of exon 10. This mutation was first described by Bugiani et al. (142) following the identification of the mutation in two members of a family. Patients with the P301S tau mutation develop a rapidly progressive disease that is characterized by widespread neuronal loss and fibrillar aggregates of tau involving predominantly the neocortex. Tau aggregates of neurons and glial cells, astrocytes (tufted astrocytes) and oligodendrocytes (coiled bodies), can also be seen in subcortical nuclei, brain stem, cerebellar dentate nucleus and subcortical white matter. Tau transgenic mice have been developed with the P301S mutation which recapitulate some of the molecular and cellular features of tauopathies (143,144).

2. TAUOPATHIES

Tauopathies are a group of neurodegenerative diseases of which the hallmark lesion is the presence of intracellular tau aggregates. Similarly to all neurodegenerative diseases, tauopathies are characterized by a loss of specific populations of neurons that involve related functional systems. Tauopathies are progressive diseases and have an onset during middle to late years of life (145,146).

There is a wide range of disorders in which tau aggregates have been described (Table 1) (140). Each of these diseases have a distinct topographical distribution of tau aggregates and specific clinical symptoms (147–155).

Table 1. **Tauopathies**. Diseases that present with tau inclusions during their development (140).

Alzheimer's disease (AD)
Corticobasal degeneration (CBD)
Progressive supranuclear palsy (PSP)
Argyrohpilic grain disease (AGD)
Pick's disease (PiD)
Tangle-only dementia (TOD)
Frontotemporal dementia and parkinsonism linked to chromosome 17 (FTLDP-17)
White matter tauopathy with globular glial inclusions
Down's syndrome (DS)
Amyotrophic lateral sclerosis and parkinsonism-dementia complex
Chronic traumatic encephalopathy (CTE)
Diffuse neurofibrillary tangles with calcification
Familial British dementia
Familial Danish dementia
Gerstmann-Sträussler-Scheinker disease
Guadeloupean parkinsonism
Myotonic dystrophy
Neurodegeneration with brain iron accumulation
Niemman-Pick disease, type C
Non-Guamanian motor neuron disease with neurofibrillary tangles
Postencephalitic parkinsonism
Prion protein cerebral amyloid angiopathy
Progressive subcortical gliosis
SLC9A6-related mental retardation
Subacute sclerosing panencephalitis
Frontotemporal lobar degeneration (some cases caused by C9ORF72 mutations)

Additionally, and depending on the disease, intracellular tau aggregates involve different cell types including neurons, astrocytes and oligodendrocytes in which they acquire diverse morphology (Figure 7) (156,157). Thus, in the

somatodendritic compartment of neurons tau aggregates can be seen as pretangles, neurofibrillary tangles (NFT), globose inclusions or have a spherical morphology known as Pick bodies, whereas when the aggregates are in neuronal cell processes they present with an elongated structure and are named neuropil threads (NT). In oligodendrocytes, tau aggregates in the cytoplasm acquire a comma shape-like morphology known as coiled bodies. In the astrocytes, tau inclusions are commonly located in the processes and aggregates adopt different shapes such as tufted astrocytes, thorn-shaped astrocytes or astrocytic plaques (157).

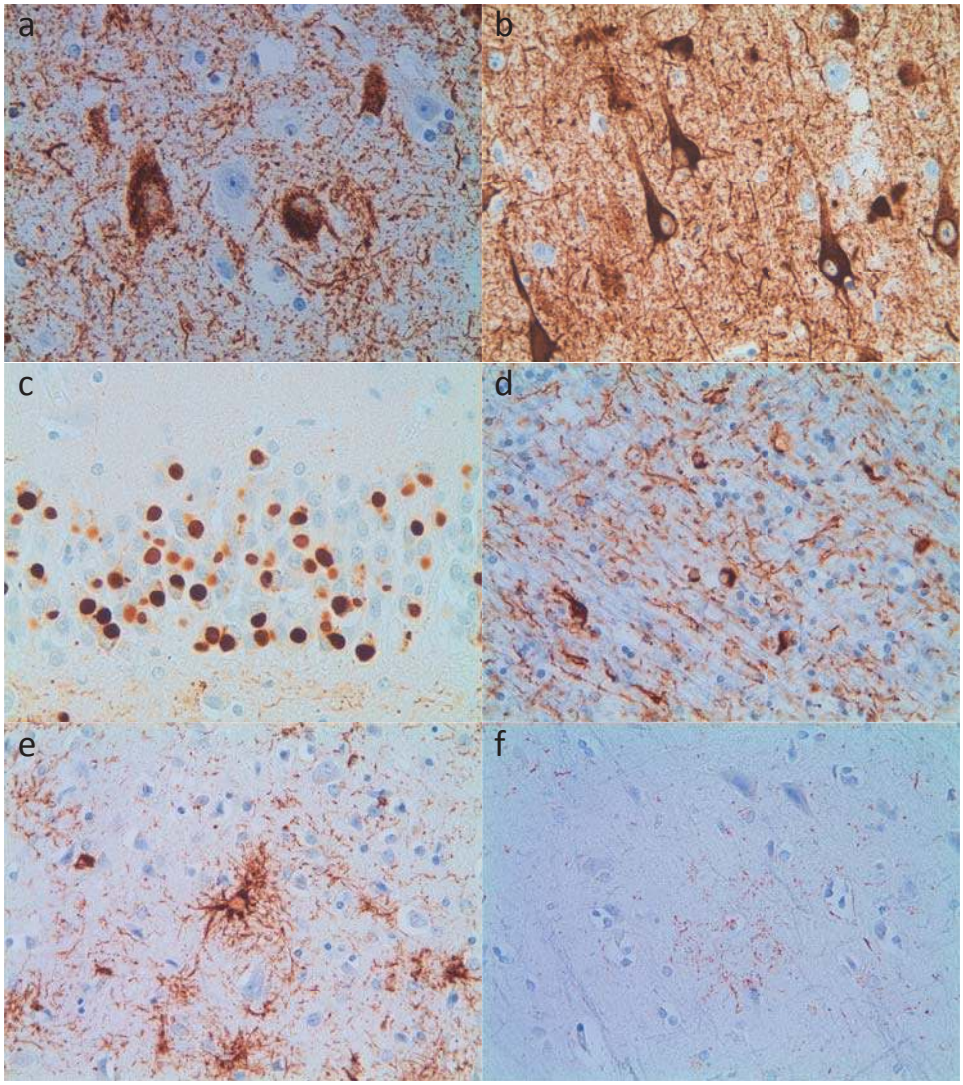

Figure 7. **Different morphology of tau aggregates**. Tau aggregates can involve different cell types including neurons (a, b, c), oligodendrocytes (d) and astrocytes (e, f) acquiring different morphologies within each cell type. In neurons, tau aggregates can be seen as *pretangles* (a), *neurofibrillary tangles (NFT)* (b) or *Pick bodies* (c). In oligodendrocytes, tau accumulates in the cytoplasm in a comma shape morphology and is known as *coiled bodies* (d). In astrocytes tau can accumulate as *tufted astrocytes* (e) and *astrocytic plaques* (f). (a, b) Alzheimer's disease (AD); (c) Pick's disease (PiD); (d, f) Corticobasal degeneration (CBD); (e) Progressive supranuclear palsy (PSP).

2.1 ALZHEIMER'S DISEASE

2.1.1 Epidemiology

Alzheimer's disease (AD) was first described in 1907 by Alois Alzheimer as a disease that presented clinically with loss of memory and was associated, histologically, to β-amyloid plaques and tau neurofibrillary tangles (158,159). AD is the most frequent neurodegenerative disease and the most frequent cause of dementia (160).

It is estimated that in 2015 the prevalence of Americans of all ages suffering from AD was of 5.3 million (161). The calculated annual incidence of AD appears to rise exponentially with age, thus it is expected 2 new cases per 1,000 people age 65 to 74, 13 new cases per 1,000 people age 75 to 84, and 39 new cases per 1,000 people age 85 and older and because of the progressive aging of the population the annual incidence of AD is expected to double by 2050 (161). Additionally, the average annual medical cost per-person of an individual 65 years or older with AD is of approximately $50,000, thus AD represents a substantial health, social and economical burden (161).

According to age of onset AD can be classified as either late onset AD (LOAD) when the clinical symptoms develop in patients 65 years or older, and early onset AD (EOAD), when the clinical symptoms appear in people younger than 65 years of age, in this case symptoms commonly manifest at 45-55 years old.

With the exception of the rare cases of AD caused by genetic mutations, as in many other chronic diseases multiple factors are involved in the development of AD. The greatest risk factor for AD is age >65 years old. Other risk factors include apolipoprotein E gene (*APOE*) ε4 genotype, family history of AD, a diagnosis of mild cognitive impairment (MCI), altered cardiovascular disease risk factors and moderate or severe traumatic brain injury (TBI) (162–165).

Apolipoprotein E (Apo-E) regulates lipid homeostasis by the mediation of lipid transport from one cell type to another. In the CNS, Apo-E is produced by astrocytes and its main function is the transport of cholesterol to neurons. Apo-E has an important role in Aβ metabolism and has been seen in senile plaques in the brains of patients with AD. Apo-E is encoded by *APOE* that is located in chromosome 19 and has three alleles (*APOE* ε2, *APOE* ε3, *APOE* ε4). *APOE* ε4 has been related to an increase of risk for AD and a decrease of the mean age of onset of the disease (162). It has been shown that deposition of senile plaques is more abundant in *APOE* ε4 carrieres than in non-carriers (see Liu et al. (166) for review).

2.1.2 Clinical symptoms

The main clinical presentation of AD is memory dysfunction, typically involving recent memory (167), presenting as a deficit of new learning and encoding of information. With the progression of disease there is language deficits and alterations in visuospatial cognition. Additionally, other clinical symptoms appear such as impaired orientation, aphasia, impairment of executive functions and behavioral disturbances where increasing apathy is the most frequent. Impaired judgment, social misbehavior, frontotemporal dementia, primary visual disturbances and expressive language disorder can also appear but are less frequent (167).

2.1.3 Biomarkers

Neuroimaging and CSF assays have been developed in the past years and are useful biomarkers that have been incorporated in the diagnostic criteria for AD to determine Aβ protein deposition and neuronal degeneration or injury in AD patients (168).

Biomarkers for Aβ protein deposition include the presence of low levels of $A\beta_{42}$ in CSF (169) and increased retention of the radioactive tracer [^{11}C]-labeled Pittsburgh compound B (^{11}C-PIB) in positron emission tomography (PET) amyloid imaging (170). Biomarkers for neurodegeneration include increased concentrations of total tau (t-tau) and phosphorylated tau (p-tau) in CSF (171), hypometabolism in

temporo-parietal regions determined by a decrease in [^{18}F]-fluorodeoxyglucose (FDG) uptake measured by PET (172) and atrophy of the medial, basal and temporal lobe and medial parietal cortex on structural MRI (173).

2.1.4 Macroscopic features

At gross examination it is possible to see a decrease in brain weight and brain volume as a consequence of brain atrophy. The medial temporal regions, including the hippocampus, are the most intensely affected regions but atrophy can also be seen in the frontal and parietal regions with sparing of the occipital lobe and primary motor cortex. There is thinning of the cerebral gyri and widening of the sulci. In coronal sections atrophy of the cortical ribbon, reduced volume of the white matter and significant enlargement of the ventricles, especially the temporal horn of the lateral ventricles is seen (Figure 8). Interestingly, the substantia nigra appears normally pigmented however, the locus coeruleus can appear paler than normal (145,156).

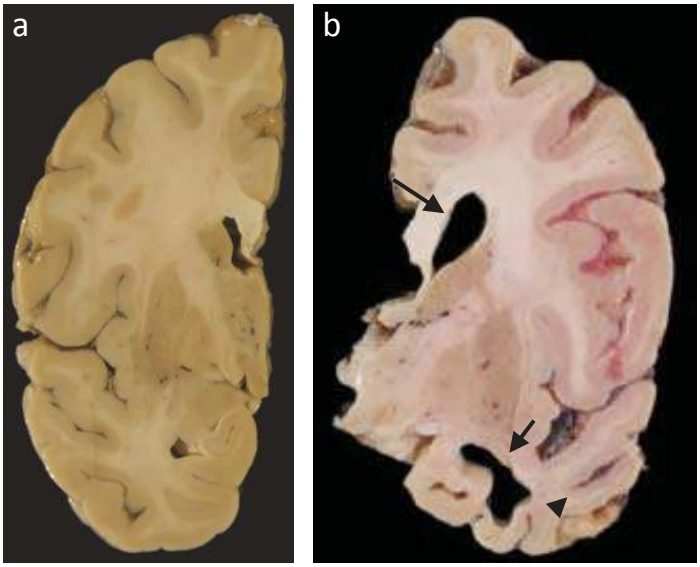

Figure 8. **Macroscopic traits of an Alzheimer's disease (AD) brain**. (a) Normal brain. (b) AD brain with atrophy that presents with dilation of the lateral ventricle (*long arrow*: lateral ventricle; *short arrow*: temporal horn of the lateral ventricle), atrophy of the hippocampus, reduced volume of white matter and thinning of the cortical ribbon (*arrow head*).

2.1.5 Microscopic features

The extracellular accumulation of amyloid-β (Aβ) and the intracellular accumulation of tau protein are the hallmark lesions of AD. Aβ is a cleavage product of the amyloid precursor protein (APP) which in AD accumulates in the extracellular space of the hippocampus and cortex (Figure 9A). Aβ is part of the amyloid plaques and can acquire a range of morphologies: diffuse, primitive, classic and burnt-out (174). Neuritic plaques are commonly associated with dystrophic neurites and inflammatory reaction, astrogliosis and microgliosis, which are commonly seen around plaques.

Tau inclusions are intracellular fibrillar aggregates of hyperphosphorylated tau protein known as neurofibrillary tangles (NFTs) (Figure 9B). In AD they are seen within the somatodendritic compartment of neurons in the hippocampus, limbic regions and, in advanced stages of the disease, in the cortex. Ultrastructurally, the filaments have a dense core with a fuzzy outer coat and have been described as paired helical filaments (PHF) of 20nm of diameter with a 10nm twist every 80nm and straight filaments (SF), which are 15nm in diameter (175).

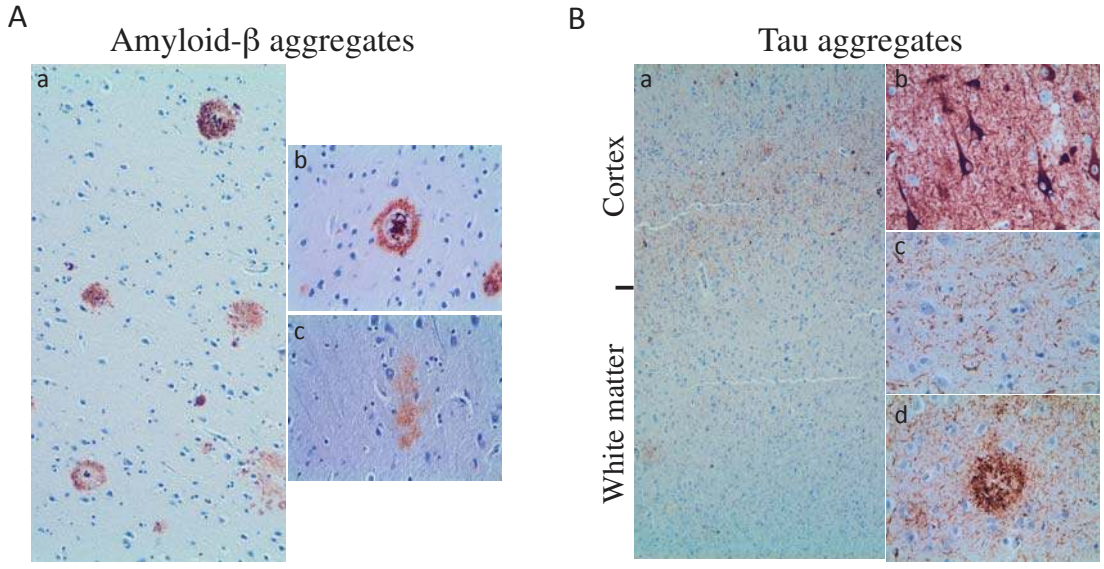

Figure 9. Amyloid-β and tau aggregates are the hallmark lesions of AD. **A** Aβ aggregates are extracellular and can acquire various morphologies (**a-c**): neuritic plaques (**b**) and diffuse plaques (**c**). **B** Tau aggregates are intracellular and in AD are only seen in grey matter while white matter is spared of tau pathology (**a**). Tau aggregates acquire different morphologies: NFT (**b**), neuropil threads (**c**) and dystrophic neurites (**d**).

In advanced disease stages where the cortical layer is involved there can be abundant neuron loss with astrogliosis and when pathology is very intense it results in vacuolation.

In AD, white matter is spare of tau pathology although pallor with myelin stains may be seen (Figure 9B), as opposed to corticobasal degeneration where there is intense white matter pathology. Additionally, in brains of AD patients there is widespread neurotransmitter defects with marked loss of acetylcholine in cerebral cortex and other neurotransmitters such as GABA, 5-HT and noradrenergic neurotransmitters (145).

2.1.6 Histological staging

The pathological aggregates of both the Aβ plaques and NFT accumulate in a predictable hierarchical pattern that has led to the creation of several staging schemes. For Aβ two different staging systems are presently being used for grading, CERAD score and Thal phases, with differences between them, which have been recently reviewed (176). In short, CERAD score (177) associates the semiquantitative assessment of neuritic plaques in the neocortex with the patient's age and clinical signs of dementia and provide a level of certainty for the diagnosis of AD. The semiquantitative asssessment of plaques results in 3 grades: A: sparse plaques; B: moderate amount of plaques; C: frequent amount of plaques. The later developed Thal phase (178) grading scheme appears to be a better predictor of dementia (176). According to this classification there are 5 phases of amyloid deposition in the AD brain: Phase 1: Aβ deposits in the neocortex; Phase 2: phase 1 and Aβ deposits in allocortex; Phase 3: phase 2 and Aβ deposits in diencephalon; Phase 4: phase 3 and Aβ deposits in brain stem; Phase 5: phase 4 and Aβ deposits in cerebellum.

The stereotypical pattern of tau aggregates in NFT in the brain of AD was described by Braak and Braak and resulted in 6 stages (179,180): Stage I: Tau immunoreactive lesions develop in the transentorhinal region; Stage II: Stage I and involvement of entorhinal regions; Stage III: Stage II and lesions in the neocortex of the fusiform and lingual gyri; Stage IV: Stage III and progression into the neocortical

association areas; Stage V: Stage IV and additional tau pathology in the neocortex of frontal, parietal and occipital regions reaching the peristriate region; Stage VI: Stage V and development of pathology in the secondary and primary areas and the striate area in the occipital lobe.

More recently these grading schemes have been revised and consensus guidelines have been provided for the diagnosis of AD: the NIA-AA grading scheme for the neuropathologic diagnosis of AD (181) (Table 2).

Table 2. NIA-AA grading scheme for AD neuropathologic change

NIA-AA score	Thal score	Hierarchical distribution of IHC positive Aβ plaques
A0	0	None
A1	1	Aβ deposits in cortex
	2	Phase 1 and Aβ deposits in allocortex
A2	3	Phase 2 and Aβ deposits in diencephalon
A3	4	Phase 3 and Aβ deposits in brain stem
	5	Phase 4 and Aβ deposits in cerebellum

NIA-AA score	Braak and Braak	Distribution pattern of NFT and NT
B0	0	None
B1	I/II	Transentorhinal and entorhinal regions
B2	III/IV	Limbic allocortex and adjoining neocortex
B3	V/VI	Neocortex, secondary and primary areas

NIA-AA score	CERAD	Semiquantitative assessment of neuritic plaques
C0	0	None
C1	A	Sparse
C2	B	Moderate
C3	C	Frequent

NIA-AA: National Institute on Aging-Alzheimer's Association; IHC: immunohistochemistry; Aβ: amyiloid beta; NFT: neurofibrillary tangles; NT: neuropil threads; CERAD: Consortium to Establish a Registry for Alzheimer's disease

2.1.7 Treatment

There are no current treatments that prevent or modify the course of the disease and the current Food and Drug Administration (FDA) approved treatments for AD are directed to treat the symptoms of the disease by regulating the activity of the neurotransmitters, acetylcholine and glutamate (182). Cholinesterase inhibitors (Donepezil, galantamine and rivastigmine) inhibit acetylcholinesterase resulting in an increase of acetylcholine concentration in the brain. Memantine, a non-competitive antagonist of the glutamatergic receptor NMDA (N-methyl-D-aspartate)

(glutamatergic) acts by regulating the activity of glutamate through the interaction with the receptor avoiding the entrance of calcium into the cell (183).

The effectiveness of these treatments varies across the population. Recent research is focusing on other therapies such as immunotherapy with $A\beta_{42}$, secretase α and β inhibitors, NSAID and statins, insulin regulation, decrease of homocysteine, microtubule stabilizers and anti-tau antibodies (184,185).

2.2 CORTICOBASAL DEGENERATION

2.2.1 Epidemiology

Rebeiz et al (186) first described corticobasal degeneration (CBD) in 1967 and named it "corticodentatonigral degeneration with neuronal achromasia", a descriptive name according to the findings of the cases he studied. Throughout the following years the disease was termed in different ways (187) and in 1989 was finally coined by its current name of corticobasal degeneration (188).

CBD is a sporadic disease with the highest incidence between the fifth to seventh decades of life. Both men and women are equally affected. It is estimated that the prevalence is of 4.9-7.3 cases per 100,000 individuals (189) and the annual incidence rate of 0.02 cases per 100,000 individuals (190).

The only known risk factor for CBD is advanced age. Genetically, and compared to the normal population, CBD patients present with a higher frequency (80%-90%) of the H1/H1 haplotype of *MAPT* (191).

2.2.2 Clinical presentation

CBD has a wide range of clinical presentations including motor, sensory, behavioral and cognitive symptoms. These symptoms are not specific of the disease

making the clinical diagnosis difficult and the evaluation at autopsy is necessary for a definite diagnosis.

In 2013 an international consortium established new consensus diagnostic criteria for CBD by analyzing the most frequent clinical presentations of 209 autopsy confirmed CBD cases from the literature and brain banks with the aim of standardizing diagnostic criteria for research and clinical practice (192). The criteria established four possible clinical syndromes for CBD:

Corticobasal syndrome (CBS): is the most frequent clinical phenotype for CBD accounting for approximately 50% of autopsy-confirmed cases (193). The main features of CBS are levodopa-unresponsive parkinsonism, progressive asymmetric akinesia, and rigidity accompanied by other cortical and basal ganglia dysfunction signs such as limb and oculomotor apraxia, cortical sensory deficits, dystonic posturing of a limb, myoclonus and alien limb phenomenon. However, this is not a specific syndrome for CBD and other pathologies can present with CBS including AD, PSP and FTLD-TDP (194).

Frontal behavioral-spatial syndrome (FBS): is characterized by executive dysfunction, behavioral and personality changes and visuospatial deficits.

Nonfluent/agrammatic variant of primary progressive aphasia (naPPA): includes errors in language production with agrammatic speech and grammatical simplification, speech production is typically strained or halting, with speech-sound errors occurring as a result of cognitive motor speech problems, apraxia of speech.

Progressive supranuclear palsy syndrome (PSPS) or Richardson syndrome (RS): although PSPS is the most frequent clinical presentation in PSP (195) some CBD cases can also present with the clinical symptoms that characterize this syndrome. The main features seen are postural instability, vertical supranuclear gaze palsy, dysarthria, dysphagia and frontal cognitive disturbances.

2.2.3 Biomarkers

Unlike in AD, at present there are no established biomarkers that can aid in the diagnosis of CBD. In MRI studies, in a voxel-based morphometry study of autopsy confirmed CBD patients, it was shown that there was grey matter loss in the posterior lateral and medial frontal lobe regardless the clinical presentation of CBD (196). However, tau levels in CSF assays have been inconclusive, some of them reporting increased levels of t-tau in CBD patients while others showed no differences with healthy controls (197,198).

2.2.4 Macroscopic features

At gross examination an asymmetrical cortical atrophy of the superior frontal and parietal parasagittal areas is characteristic of the disease. Temporal and occipital lobes are often spared except in cases presenting with dementia. The brainstem and cerebellum are usually of normal size. The white matter is often attenuated and may have gray discoloration (Figure 10). There can be flattening of the caudate nucleus, atrophy of anterior and medial thalamus and red-brown discoloration of the globus-pallidus. There is consistent loss of neuromelanin pigment in the substantia nigra (199).

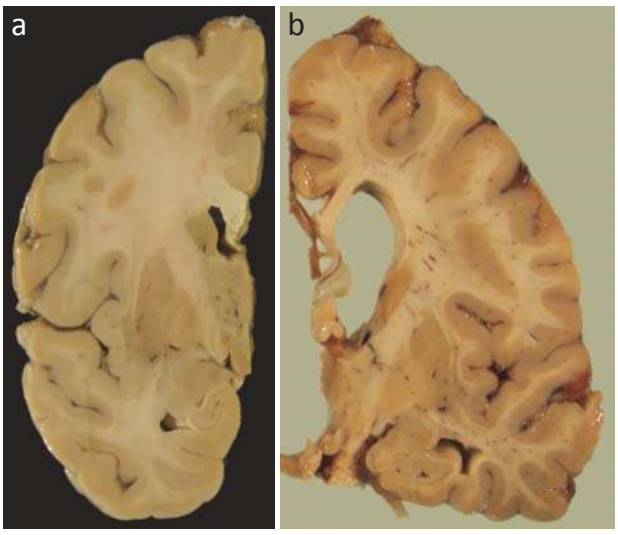

Figure 10. **Macroscopic features of human brain with CBD**. (**a**) Normal brain. (**b**) Section of a CBD brain hemisphere with marked dilation of lateral ventricle and marked loss of white matter.

2.2.5 Microscopic features

The main microscopic findings seen in CBD are the intracellular tau aggregates in neurons and glial cells involving both grey and white matter (Figure 11) (199). The neuronal lesions can be detected by either tau immunohistochemistry or Gallyas silver stain and can adopt various morphologies resembling small NFT, pre-tangles and globose NFT. However, the most characteristic lesions of CBD are those that involve glial cells. Tau aggregates in the astrocytic processes result in astrocytic plaques, which is a very characteristic lesion of the disease and are mainly seen in the cortex although they can also appear in the striatum and putamen. Hyperphosphorylated tau also aggregates in the cytoplasm of oligodendrocytes as coiled bodies.

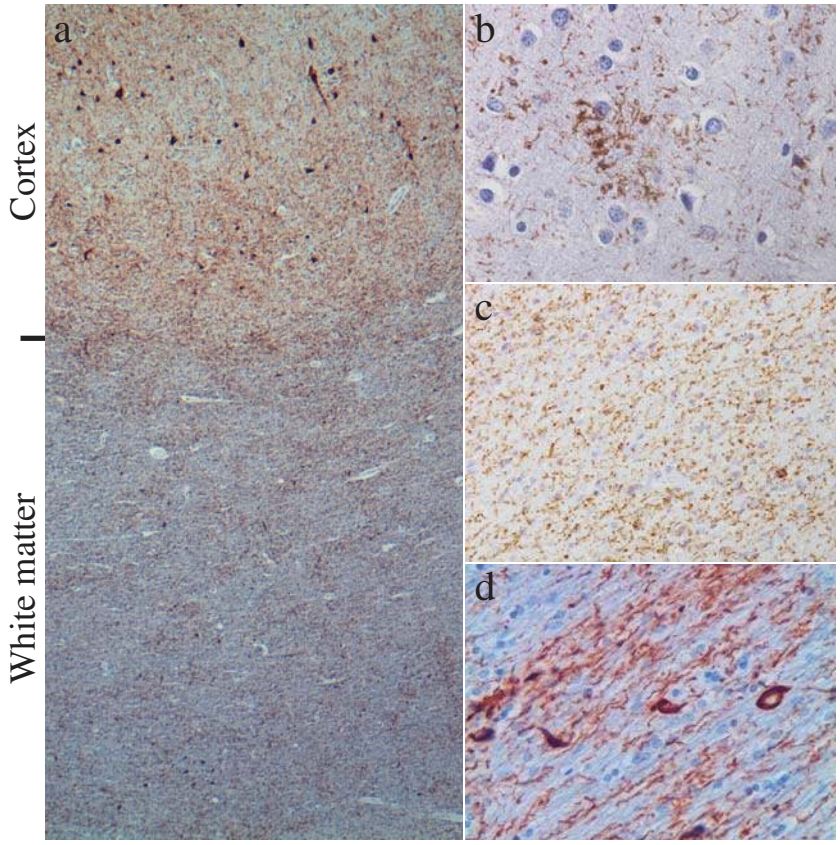

Figure 11. Microscopic findings in CBD brain. (**a-d**) In CBD tau pathology involves grey and white matter. Tau aggregates can be seen in astrocytes (*astocytic plaques*) (**b**) in white matter as neuropil threads (**c**); and in oligodendrocytes (*coiled bodies*) (**d**). AT8 immunohistochemistry.

Ballooned neurons, a form of reactive neurons which are swelled, eosinophilic and immunoreactive to α-B-crystallin, within the 3rd, 5th and 6th cortical layers of the cortex can also be seen in CBD. Marked neuronal loss and gliosis are noted in atrophic cortical areas and myelin loss is also common in white matter of patients with CBD.

As shown by electron microscopy, tau aggregates are formed of straight filaments of 18-20 nm in diameter (200).

2.2.6 Treatment

No disease modifying treatment is currently known for corticobasal degeneration and similarly to AD, the treatment is symptomatic. The treatment focuses to the most prevalent symptoms in the patient, the movement disorders, thus levodopa/carbidopa is used for the parkinsonian symptoms, botulinum toxin for the limb dystonia, clonazepam and levetiractam for the myoclonus. General supportive care to the patient, family and caregiver is important (201).

2.3 OTHER TAUOPATHIES

2.3.1 Progressive supranuclear palsy (PSP)

PSP is a sporadic disease clinically characterized by movement disorders including postural instability, parkinsonism, supranuclear gaze palsy and mild dementia (202). Histologically it presents with neuronal loss, astrocytosis and tau aggregates in neurons and glial cells of subcortical nuclei, brain stem and also in dentate nucleus of the cerebellum. Tufted astrocytes, is the characteristic morphology of astrocytes in grey matter in this disease. Similarly to CBD, the isoforms that predominate in PSP are the 4R tau isoforms.

2.3.2 Argyrophilic grain disease (AGD)

Is an entity first described by Braak and Braak, which occur in elderly people with and without dementia (203). Histologically, AGD is characterized by the presence of tau aggregates located mainly in the medial temporal lobe. The hallmark lesions of this entity are the grains. They are argyrophilic aggregates located in the branching points of apical dendrites that are tau immunoreactive. Other accompanying lesions are ramified astrocytes and oligodendroglial coiled bodies. Similarly to PSP, 4R tau isoforms are the predominant isoforms present in the intracellular aggregates of the disease (204).

2.3.3 Pick's disease (PiD)

PiD is a rare sporadic tauopathy that clinically presents with progressive dementia and personality deterioration. Histopathologically, it is characterized by the presence of tau aggregates, Pick bodies, in the cytoplasm of neurons of the cortex and dentate gyrus of the hippocampus. As opposed to the other tauopathies, in PiD 3R isoforms of tau predominate in the aggregates (205).

3. SPREADING OF TAU PATHOLOGY: CELL-TO-CELL TRANSMISSION HYPOTHESIS

In the 1980's it was observed that the populations of neurons lost in neurodegenerative diseases were anatomically interconnected. Saper et al (206) suggested that this loss of neurons could be explained by a transneuronal spread of a toxic or infectious agent. However, it hasn't been up to now that a more clear understanding of the mechanism of disease progression has been elucidated. Recently, it has been seen how misfolded protein aggregates in various neurodegenerative diseases including AD, AGD, Parkinson's disease (PD) and amyotrophic lateral sclerosis (ALS) accumulated in a stereotypical pattern throughout the progression of the disease (179,204,207–210). The following sections will describe the details of the spreading hypothesis in detail.

In AD tau aggregates are first seen in the locus coeruleus (LC) to later spread to the entorhinal cortex (EC) and other limbic regions to finally, in later stages, involve the neocortex (179,211). In AGD tau pathological inclusions appear in the ambient gyrus first and from there, tau pathology extends to temporal lobe, septum, insular cortex and the cortex of anterior cingulate gyrus to finally involve, in the most advanced stages, the neocortex (204,207).

These observations suggested that tau protein could be transmitted from cell-to-cell in a "prion-like" self-propagating mechanism along defined neuronal projections as opposed to previous thoughts in which these diseases evolved in a cell-autonomous manner in selectively vulnerable brain regions (212). This cell-to-cell transmission concept has been supported by many recent *in vivo* and *in vitro* studies.

3.1 *IN VITRO* TRANSMISSION STUDIES

In recent years, several studies have shown that pathological tau can be taken up by cells to seed aggregation of endogenous tau to form AD-like PHFs or NFTs

(213–215). Frost et al. (214) provided a plausible cellular mechanism of cell-to-cell transfer of misfolded tau protein in a cell culture model. They described how C17.2 neuronal precursor cells could internalize tau aggregates and how these internalized aggregates were able to induce misfolding of endogenous soluble full-length tau. The uptake of tau aggregates was probably achieved through endocytic pathways as the aggregates co-localized with dextran, a marker which is taken up by fluid-phase endocytosis, and not with cholera toxin B, which upon uptake colocalises with lipid rafts. Moreover, these studies determined that the intracellular tau aggregates could transfer between co-cultured cells.

Guo et al. (215) established a cellular system that developed robust NFT-like tau aggregates. The transduction of very small quantities of tau-preformed fibrils (PFFs) into a culture of tau-expressing cells, which expressed the longest isoform of tau (2N4R), induced the aggregation of the soluble tau into inclusions resembling NFT. They also observed that the spontaneous uptake of fibrils transduced in the cell medium was mediated by endocytosis as determined by the reduction in the percentage of cells with inclusions upon incubation with PFFs at 4ºC and by an increase of aggregates after incubation in the presence of WGA, a plant lectin that is internalized by cells via adsorptive endocytosis. Furthermore, tau PFFs were able to recruit normal soluble tau into NFT-like aggregates in primary hippocampal neurons (216).

Kfoury et al. (217) went further and demonstrated that tau fibrils can be released into the cell medium to later be taken up by co-cultured cells and induce fibrillization of soluble tau via direct protein-protein interaction.

In summary, these experiments demonstrate a plausible "prion-like" mechanism of disease progression through transfer of misfolded tau protein from one cell to another, whereby there would be a release of fibrillar tau to the extracellular space by a "donor" cell, this extracellular fibrillar tau would be uptaken by another cell, the "receptor" cell, that would further trigger the formation of new aggregates by templated misfolding of soluble endogenous tau.

The presence of tau in the extracellular medium could be explained by a passive release of tau during cell death. However, there is increasing evidence that tau can be secreted in physiological and non-physiological situations by viable cells through exosomes, in a free non-vesicular form or, more recently described, through ectosomes, a type of extracellular vesicle that originates from the plasma membrane (218–222). On the other hand the uptake of fibrillar tau protein has been seen to occur through fluid-phase endocytosis and receptor-mediated endocytosis (214,215,223,224). Other suggested potential mechanisms of internalization of pathological tau aggregates would be through direct penetration of the plasma membrane of the recipient neuron or through direct intercellular transfer via nanotubes connecting the cytoplasm of the two cells (225).

3.2 *IN VIVO* MODELS OF TRANSMISSION

At the same time that studies *in vitro* suggested a cell-to-cell transfer of tau protein aggregates, investigation in animals was also showing a trans-cellular spread of tau. One of the first *in vivo* studies to observe transmission of tau pathology was that from Clavaguera et al. (226) after injecting brain extracts obtained from P301S mice, a Tg mouse model that expresses the 0N4R human tau isoform with the P301S mutation, which develops abundant filamentous tau inclusions, into the brains of ALZ17 Tg mice. The ALZ17 line expresses a WT 2N4R human tau isoform and does not develop filamentous tau aggregates. Interestingly, the injection of brain homogenates from P301S tau transgenic mice into the brains of ALZ17 mice induced filamentous tau pathology in the latter. Tau pathological aggregates appeared close to the injection site but also in regions away from the injection site demonstrating that there could be transmission of tau pathology.

Liu et al. (227) and de Calignon et al. (228) demonstrated that propagation of tau pathology occurred through synaptic pathways along an anatomically linked network. They developed similar mouse models, a bigenic mouse line that expresses a human mutant form of tau almost exclusively in the superficial layers of the entorhinal cortex (EC). They showed how the pathology originating in the EC

evolved to propagate to DG granule cells, CA3/2 and CA1 regions of the hippocampus, which are regions known to be synaptically connected to the EC. Additionally, de Calignon et al. observed degeneration of synapsis, axons and soma of neurons associated with accumulation of misfolded tau.

But it was Iba et al. (229) who established that recombinant tau PFFs alone were sufficient to induce NFT-like aggregates and spread tau pathology in a Tg mouse model. PS19 tau transgenic mice, which overexpress the P301S mutant human tau of the 1N4R isoform, developed tau aggregates early, before the onset of tau pathology induced by the transgene, after the injection of recombinant tau PFFs into the cerebrum. The pathology increased in intensity and developed in regions away from the injection site in a dose- and time-dependent manner. Additionally, they observed distinct pattern of spreading depending on whether the injection site was the hippocampus alone or the striatum together with the overlaying cortex.

These and other studies suggest that pathological tau propagates to neighboring normal cells or those that are synaptically interconnected (230–235). Thus, it is believed that neurodegenerative diseases share a common mechanism of pathogenesis as similar observations of cell-to-cell transmission have been observed for other misfolded proteins including α-syn related to PD (236), Aβ related to AD (237–239), TDP-43 (240,241) and SOD1 (242) related to ALS, and huntingtin with polyQ repeats related to Huntington's disease (HD) (243).

Additionally, it has been seen that distinct tau strains may underlie diverse manifestations of neurodegenerative tauopathies (233,234). In neurodegenerative diseases, the term strain was first defined for prion disease to refer to the different varieties or isolates of prions that were responsible for producing specific phenotypes of prion disease (244). Thus, prion disease varies in the length of incubation time, the pattern of distribution of PrP^{sc} deposits and the topographic distribution and severity of histopathological changes in relation to different strains. Furthermore, these characteristics are recapitulated upon serial passage within the same host genotype. The properties of the strains are thought to be intimately related to the conformation of the pathological protein PrP^{sc}, whereby a protein with the same primary structure is

able to acquire different conformations, and it is this variability in conformation that leads to the different phenotype of the disease (245,246). Similarly to prion diseases, α-syn (247) in synucleinopathies and Aβ in AD also show different strain properties due to protein conformation, as has been demonstrated in several studies (237,248,249). Therefore, the study of tau strains and cell-to-cell transmission is of relevance not only to tauopathies, but may also provide mechanistic insight to other neurodegenerative diseases, with implications for future therapeutic development.

HYPOTHESIS AND AIMS

Intracellular tau inclusions are the hallmark lesions of tauopathies, which include Alzheimer's disease (AD), corticobasal degeneration (CBD), progressive supranuclear palsy (PSP), argyrophilic grain disease (AGD) and Pick's disease (PiD). The observation that some tauopathies such as AD and AGD evolve following a stereotypical pattern suggests that tau can be taken up by cells and seed aggregation of endogenous tau to form AD-like paired helical filaments (PHFs) or neurofibrillary tangles (NFTs).

Recent *in vitro* studies have determined that tau can be taken up by cells and seed aggregation of endogenous tau to form AD-like PHFs or NFT. Further, injections of brain extracts from mutant human tau Tg mice harboring NFTs into the brains of Tg mice overexpressing wild type human tau (ALZ17 line) induced tau inclusions, while injections of synthetic preformed tau fibrils (PFFs) into PS19 mice overexpressing mutant human tau induced similar tau pathology indicating that tau PFFs alone are sufficient to transmit tau pathology. These and other studies suggest that pathological tau propagates to neighboring normal cells or those that are synaptically interconnected, therefore a cell-to-cell transmission of pathological tau protein is a plausible mechanism of progression for these diseases.

Furthermore, tauopathies show distinct topographic and cell type-specific distribution of tau and recent studies suggest that different strains could account for the diverse manifestations of tauopathies.

The aims of the study were:

1. Determine if PS19 tau transgenic mice develop tau aggregates after the injection of pathological tau-enriched extracts from human brain tissue obtained from cases of different tauopathies.

2. Determine if there is propagation of the tau aggregates within brain regions away from the injection site in these transgenic mice.

3. Characterize the distribution and the histological properties of the aggregates developed in the PS19 mice from the different tauopathies.

4. Determine if the tau aggregates that develop in the PS19 mice have similar characteristics as the aggregates seen in the corresponding human diseases.

Thus, the hypothesis driving these experiments is that the different characteristics of various tauopathies is driven by the intrinsic properties of the tau isoforms involved in forming each hallmark pathology, and that these characteristics are transmissible through the brain via spreading and conversion of endogenous tau to the pathological form in a 'prion-like' mechanism of disease spread *in vivo*.

MATERIALS AND METHODS

1. HUMAN BRAIN TISSUE EXTRACTS

1.1 HUMAN CASES USED FOR THE STUDY

Pathological tau enriched extracts (CBD-Tau, AD-Tau, DSAD-Tau) were prepared from human brain tissue obtained from the *Center for Neurodegenerative Disease Research* (CNDR) brain bank (250). CBD-Tau was obtained from tissue of two CBD subjects that had been longitudinally followed and confirmed at autopsy. Similarly, AD-Tau and DSAD-Tau preparations were obtained from one AD patient and one elderly individual with Down syndrome (DS) respectively (115). The brain of the individual with DS contained abundant NFTs indistinguishable from AD so we refer to this here as DSAD. Brain extracts from a non-demented patient who showed no signs of neurodegenerative disease and no AD neuropathologic change at postmortem histological examination was used to generate normal or control tau (CTRL-Tau) preparations (Table 3).

Table 3. Cases from the CNDR brain bank used to obtain pathological tau extract

ID	NP Dx	NIA score	Age at death (years)	Sex	Brain weight (g)	PMD (hours)	DD (years)	Clinical Diagnositc	ApoE genotype	Other diseases
1	AD	A3;B3;C3	47	Female	864	10	4	AD, probable	ε3/ ε3	DS
2	AD	A3;B3;C3	77	Male	1100	4	8	bvFTD-FTLD	ε3/ ε4	
3	CBD	NA	56	Female	1149	19,5	NA	PPA	ε3/ ε3	
4	CBD	NA	66	Female	906	4	8	PPA	ε2/ ε3	
5	Normal	A0;B0;C0	62	Male	1420	8,5	0	Normal	NA	

AD: Alzheimer's disease; bvFTD-FTLD: behavioral variant of fronto-temporal dementia; CBD: Corticobasal degeneration; DD: duration of disease; DS: Down's syndrome; NA: not available; NIA: National Institute on Aging; NP Dx: Neuropathological diagnosis; PMD: postmortem delay; PPA: primary progressive aphasia

1.2 GENERATION OF ENRICHED PATHOLOGICAL TAU EXTRACTS

To investigate the transmission of tau protein from human brain with a neuropathological diagnosis of AD or CBD we generated pathological tau enriched extracts. When possible we used purchased sterile items and autoclaved material to maintain conditions during extraction the more sterile possible. Additionally, Milli-

Q® water was used for the preparation of buffers which were further filtered sterile in Vacuum Filtration Flasks with a PES membrane of 0.22 µm.

1.2.1 PBS HOMOGENATES

1.2.1.1 REAGENTS

1.2.1.1.1 *PBS*

Ready-made Dulbeco's Phosphate Saline Buffer without calcium and magnesium (Life Technologies) was used for the experiments.

1.2.1.2 APPLIANCES

The appliances used for the preparation of the PBS homogenates are listed in Table 4.

Table 4. Appliances used for the preparation of 10% PBS homogenates

Procedure	**Appliances and Material**	**Brand**
Homogenization	Battery-powered tissue grinder, PELLET PESTLE® Cordless Motor	Sigma-Aldrich
	Disposable PELLET PESTLE® for 1.5ml tubes	
Sonication	Microson™ XL-2000, Ultrasonic liquid processor	Qsonica, LLC
Centrifugation	Optima™ MAS Ultracentrifuge Tabletop	Beckman Coulter
	TLA55 Rotor	
H_2O purification systems	Milli-Q® Integral Water Purification System	EMD Millipore

1.2.1.3 PROTOCOL

CBD-Tau and CTRL-Tau were prepared from human brain tissue obtained from temporal cortex, parietal cortex or striatum of CBD and CTRL cases from the brain bank at CNDR. The following procedure was followed:

1. **Brain tissue dissection:** 400 mg of frozen tissue from parietal cortex, temporal cortex or striatum of CBD or CTRL brains were thawed and dissected clean of meninges and blood vessels.
2. **Homogenization:** The tissue was homogenized in 10 vols PBS and sonicated. The tissue was equally separated in 4 tubes of 1.5 ml each (100 mg of tissue/tube) and homogenized in 500 ml of PBS using the disposable PELLET PESTLES®. Then, the tissue was sonicated for 10 pulses (0.5s/pulse) at setting 2 and 500 ml PBS/tube were added and mixed with the pipette tip 5 times.
3. **Centrifugation of homogenate:** The homogenate was centrifuged with a TLA55 rotor at 3000 *g* for 5 min at 4ºC.
4. **Centrifugation of supernatant:** The resulting pellet was discarded and the supernatant was centrifuged in a TLA55 rotor at 100,000 *g* for 30 min at 4ºC.
5. **Homogenization:** The resulting supernatant was discarded and the pellet was homogenized in 3 vols of PBS (300 µl), which were added to each tube, and further sonicated for 20 pulses (0.5s/pulse) at setting 2. Finally, the homogenates were pooled together in two 1.5 ml tubes.
6. **Centrifugation of pellet homogenate:** The homogenates were centrifuged in a TLA55 rotor at 100,000 *g* for 60 min at 4ºC.
7. **CBD-Tau and CTRL-Tau extracts**: The supernatant was discarded and the pellet was resuspended in 600 µl of PBS, sonicated 20 pulses (0.5s/pulse) at setting 2, aliquoted and stored at -80ºC. The extracts obtained from CBD cases were labeled as CBD-Tau and the extracts obtained from CTRL cases were labeled as CTRL-Tau. These extracts were further used for the injections.

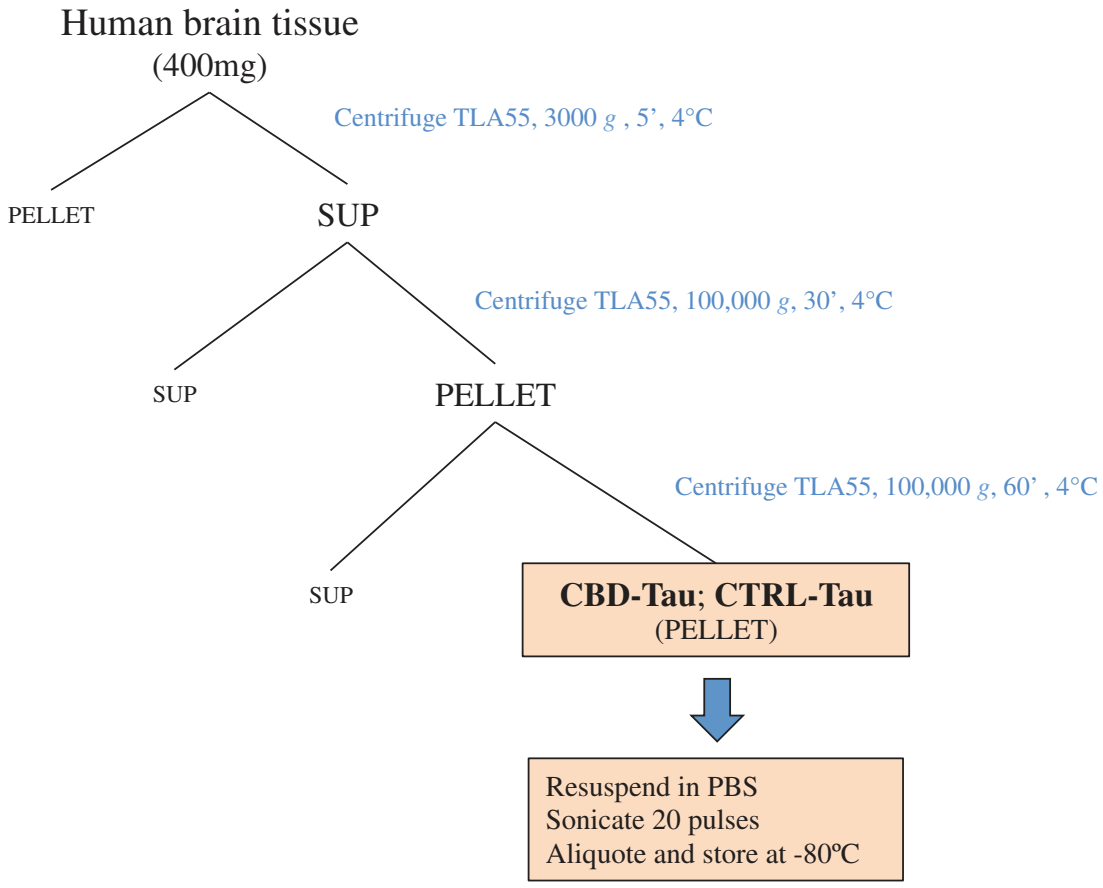

Figure 12. Schematics of the protocol for obtaining CBD-Tau and CTRL-Tau, tau enriched extracts from CBD and CTRL subjects respectively.

1.2.2 PHF-ENRICHED EXTRACTS

1.2.2.1 REAGENTS

1.2.2.1.1 *PBS*

Ready-made Dulbeco's Phosphate Saline Buffer without calcium and magnesium (Life Technologies) was used for the experiments.

1.2.2.1.2 *RAB*

A reassembly buffer (RAB) was employed to prepare the sucrose gradient used for the purification of pathological tau from the human brain tissue and to prepare a high salt reassembly buffer (HS-RAB).

The reagents to prepare the RAB buffer are detailed in Table 5. The solution was brought to pH 6.8 and filtered sterile.

Table 5. Reagents used to prepare 250 ml of RAB buffer

Reagent	Formula weight (g/mol)	Weight (g)
100 mM MES	195.24	4.880
1 mM EDTA	292.25	0.073
0.05 mM $MgSO_4$	120.37	0.015
2 mM DTT		

1.2.2.1.3 *HS-RAB*

High salt reassembly buffer (HS-RAB) for the lysis of mammalian cells and extraction of soluble proteins was prepared by adding NaCl (Fw 58.44 g/mol) up to 750 mM to the RAB buffer.

To prepare 250 ml of 750 mM HS-RAB, 10.96 g of NaCl (Fw: 58.44 g/mol) were added to RAB buffer at pH 6.8 and filtered sterile.

1.2.2.1.4 *PHF-EB*

Paired helical filament extraction buffer (PHF-EB) is a high salt and high sucrose buffer used for the extraction of soluble or small particles of PHF tau. The reagents used to prepare PHF-EB are detailed in Table 6. The solution was brought to pH 7.4 and filtered sterile.

Table 6. Reagents used to prepare 500 ml of PHF-EB buffer

Reagent	Formula weight (g/mol)	Weight (g)
10 mM TRIS	121.14	0.605
10% sucrose	50 ml Milli-Q® water	50
800 mM NaCl	58.44	23.37
1 mM EDTA	292.25	0.146

1.2.2.1.5 *SARKOSYL*

Sodium lauroyl sarcosinate or Sarkosyl is used to break down membrane components in the preparation.

To prepare 50 ml of 25% Sarkosyl stock, 12.5 g of Sarkosyl (FW: 293.38 g/mol) were dissolved in Milli-Q® water and brought to 50 ml.

1.2.2.1.6 *SUCROSE GRADIENT*

A seven phase (1.00 M, 1.25 M, 1.50 M, 1.75 M, 2.00 M, 2.25M and 2.50 M) sucrose gradient was prepared by dissolving sucrose in RAB buffer as shown below (Table 7). The gradient separates proteins by size and density.

Table 7. Scheme used to prepare the sucrose solutions with different molarities

2.50 M sucrose	25.65 g sucrose (MW: 342 g/mol) in 30 ml RAB buffer
2.25 M sucrose	22.5 ml of 2.50 M sucrose + 2.5 ml RAB
2.00 M sucrose	20 ml of 2.25 M sucrose + 2.5 ml RAB
1.75 M sucrose	17.5 ml of 2.00 M sucrose + 2.5 ml RAB
1.50 M sucrose	15 ml of 1.75 M sucrose + 2.5 ml RAB
1.25 M sucrose	12.5 ml of 1.50 M sucrose + 2.5 ml RAB
1.00 M sucrose	10 ml of 1.25 M sucrose + 2.5 ml RAB

1.2.2.1.7 *PHOSPHATE BUFFER (PB)*

40 mM Monosodium phosphate (NaH_2PO_4; FW: 119,98 g/mol) at pH 7.4 was used in one of the last steps of the procedure.

To prepare 100 ml of NaH_2PO_4, 0,48g of NaH_2PO_4 was dissolved in Milli-Q® water and brought to 100 ml.

1.2.2.2 APPLIANCES

The appliances and materials used for the preparation of PHF enriched extracts are listed in Table 8.

Table 8. Appliances and materials used for the preparation of PHF enriched extracts

Procedure	Appliances and materials	Brand
Homogenization	Kontes® Dounce Tissue Grinder 100ml	Kimble Chase
	Pestles Dounce A and Dounce B	
Sonication	Microson™ XL-2000, Ultrasonic liquid processor	Qsonica, LLC
Centrifugation	Optima™ XE Ultracentrifuge	Beckman Coulter
	Type 45 Ti Rotor	
	Type SW55 Ti Rotor	
Lyophilisation	FreeZone 4.5l Benchtop Freeze Dry System	Labconco
H_2O purification systems	Milli-Q® Integral Water Purification System	EMD Millipore

1.2.2.3 PROTOCOL

Paired helical filaments (PHF) are the major structural components of the neurofibrillary tangles (NFTs). While normal human tau is a highly soluble protein that is heat and acid stable, PHF forms filamentous structures of tau that are only soluble in strong detergents or denaturants such as sodium dodecyl sulfate (SDS) and guanidine isothiocyanate, and are buoy in 10% sucrose. This three-day purification procedure takes advantage of these characteristics of normal human tau and PHF and was used for the preparation of AD-Tau and DSAD-Tau extracts.

DAY 1:

1. **Dissection:** Frozen brain tissue from AD and DSAD cases were thawed and dissected clean of meninges and blood vessels and 50 g of gray matter were separated from white matter.
2. **Homogenization of the tissue with HS-RAB:** The 50 g of gray matter were homogenized in 3 vols of cold HS-RAB buffer that contained a protease inhibitor cocktail and a phosphatase inhibitor cocktail using a Dounce A homogenizer first (10 strokes) and a Dounce B homogenizer later (20 strokes). Next, the homogenizer was rinsed with 1 vol HS-RAB buffer and combined with the first homogenate. Finally, the homogenate was incubated at 4ºC for 20 min to depolymerize the microtubules.
3. **Centrifugation of the homogenate:** The homogenate was centrifuged in a Type 45Ti rotor at 126,000 *g* for 45 min at 4°C.

4. **Homogenization of the pellet with PHF-EB:** The supernatant, which contained primarily soluble normal tau, was discarded and the pellet was homogenized in 10 vols of PHF-EB that contained a protease inhibitor and phosphatase inhibitor cocktail using a Dounce B homogenizer (20 strokes).
5. **Centrifugation of the PHF-EB homogenate:** The homogenate was centrifuged in a Type 45Ti rotor at 13,000 *g* for 30 min at 4° C. In the presence of 10% sucrose and at low centrifugal forces, isolated PHF or small PHF aggregates remain in the supernatant whereas larger or intact PHF aggregates are pelleted.
6. **Combining supernatants**: The resulting supernatant was filtered through two moist Kimwipes to remove the floating myelin and saved. The pellet was re-extracted as in steps #4-6. The two filtered supernatants resulting from the two extractions were combined.
7. **Addition of Sarkosyl to the combined supernatants and nutation:** Sarkosyl stock (25%) was added to the supernatnats to 1% and was nutated overnight at 4ºC. This removed the membranous material, therefore enriching the preparation for PHF.

DAY 2

8. **Centrifugation of the extract:** The extract was centrifuged in a Type 45Ti rotor at 125,000 *g* for 60 min at 4ºC. The resulting pellets contained crude PHF.

From this point on, protease inhibitors were not added because they were not very water soluble, but the phosphatase inhibitors continued to be added

9. **Homogenization of the pellet in RAB buffer:** The supernatant was discarded and the pellet was homogenized in RAB buffer in a proportion of approximately 1 ml RAB/20 g of gray matter thus, for 50 g grey matter the pellet was resuspended in 2.5 ml of RAB. Then, the homogenate was sonicated until smooth (70 pulses (0.5s/pulse) at setting 2), boiled for 5 min at 100ºC and let it to cool down. Finally, the homogenate was sonicated for a second time for 20 pulses (0.5s/pulse) at setting 2.

10. **Sucrose gradient:** The sonicated homogenate was loaded onto a step-wise discontinuous sucrose gradient (Table 8) in a proportion of 6 centrifuge tubes for every 50 g of gray matter prepared as follows: i) 500 µl of 2.50 M sucrose were pipetted at the bottom of the tube; ii) 500 µl of 2.25 M sucrose were gently layered on top; iii) 500 µl 2.00 M sucrose were layered on top; iv) 500 µl 1.75 M sucrose were layered on top; v) 500 µl 1.50 M sucrose were layered on top; vi) 500 µl 1.25 M sucrose were layered on top; vii) 500 µl 1.00 M sucrose were layered on top. Finally, no more than 600 µl of crude PHF preparation were layered on top of the sucrose gradient in each tube.
11. **Centrifugation of the sucrose gradient:** The preparation was centrifuged in a SW55Ti swinging rotor at 190,000 *g* for 16 h at 4 °C.

DAY 3

12. **Collection of the "lower band":** After centrifugation two medium- to light-brown bands were seen in each tube (Figure 13). The resulting band at the 1.75M-2.00M interface (LOWER BAND), which contained the highest concentration of PHF-tau proteins, was collected and put in bigger centrifuge tubes.

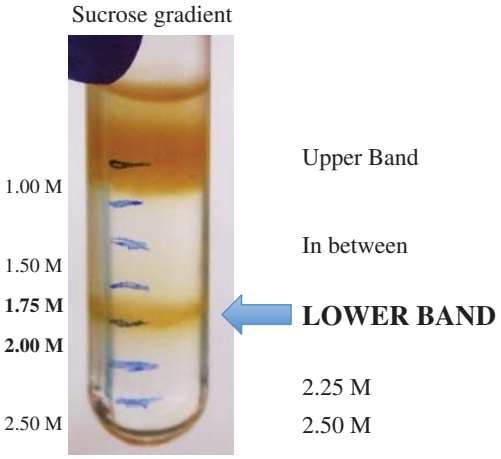

Figure 13. Sucrose gradient. Two brown bands appear after the preparation is centrifuged overnight through a seven-step sucrose gradient. An upper band is seen at the 1.00M interface and a *lower band* (blue arrow) at the 1.75M-2.00M interface. It was in the lower band where the highest concentration of tau protein was obtaine

13. **Water extraction:** The crude PHF was water extracted. First, the LOWER BAND preparations were put in clean centrifuge tubes and then 35 ml of RAB buffer were added. The preparations were centrifuged in a Type 45Ti rotor at 85,000 *g* for 1h 30 min at 4ºC to wash the sucrose. The resulting supernatants were discarded and the pellets were resuspended in 1ml PB buffer, sonicated until homogenized (25 pulses (0.5s/pulse) at setting 2) and 4 ml Milli-Q® H_2O were added to each tube. They were lightly sonicated for 10 pulses (0.5s/pulse) at setting 2 following which another 20 ml of Milli-Q® water was added to each preparation. Then, the preparation was boiled in a boiling water bath for 10 min, was taken out of the stove and to stop the boil, another 10 ml of Milli-Q® water was added to each tube. Finally, the preparation was let stand to cool down for 30 min at room temperature and was centrifuged in a Type 45Ti rotor at 85,000 *g* for 45 min at 4ºC.
14. **Freezing of the supernatant:** The pellet was discarded and the supernatant was frozen and stored at -80ºC.

The process was repeated two more times with 50 g of gray matter (50g x 2) until a total of 150 g of gray matter had been processed and the resulting supernatant was shell frozen.

15. **Lyophilization:** The frozen supernatants from the three consecutive extractions were lyophilized using a bench-top freeze dry system for 24-48 hours. This resulted in a white powder that was pooled together in a 2 ml tube and resuspended in 1ml of Milli-Q® water. The preparation was lyophilized overnight for a second time and the resulting white powder was resuspended in 300 µl of PBS without calcium and magnesium and sonicated for 20 pulses (0.5s/pulse) at setting 2. Finally, the preparation was aliquoted in low binding tubes and frozen at -80ºC until use. These extracts were labeled as AD-Tau and DSAD-Tau and were used for further injections into PS19 tau Tg mice.

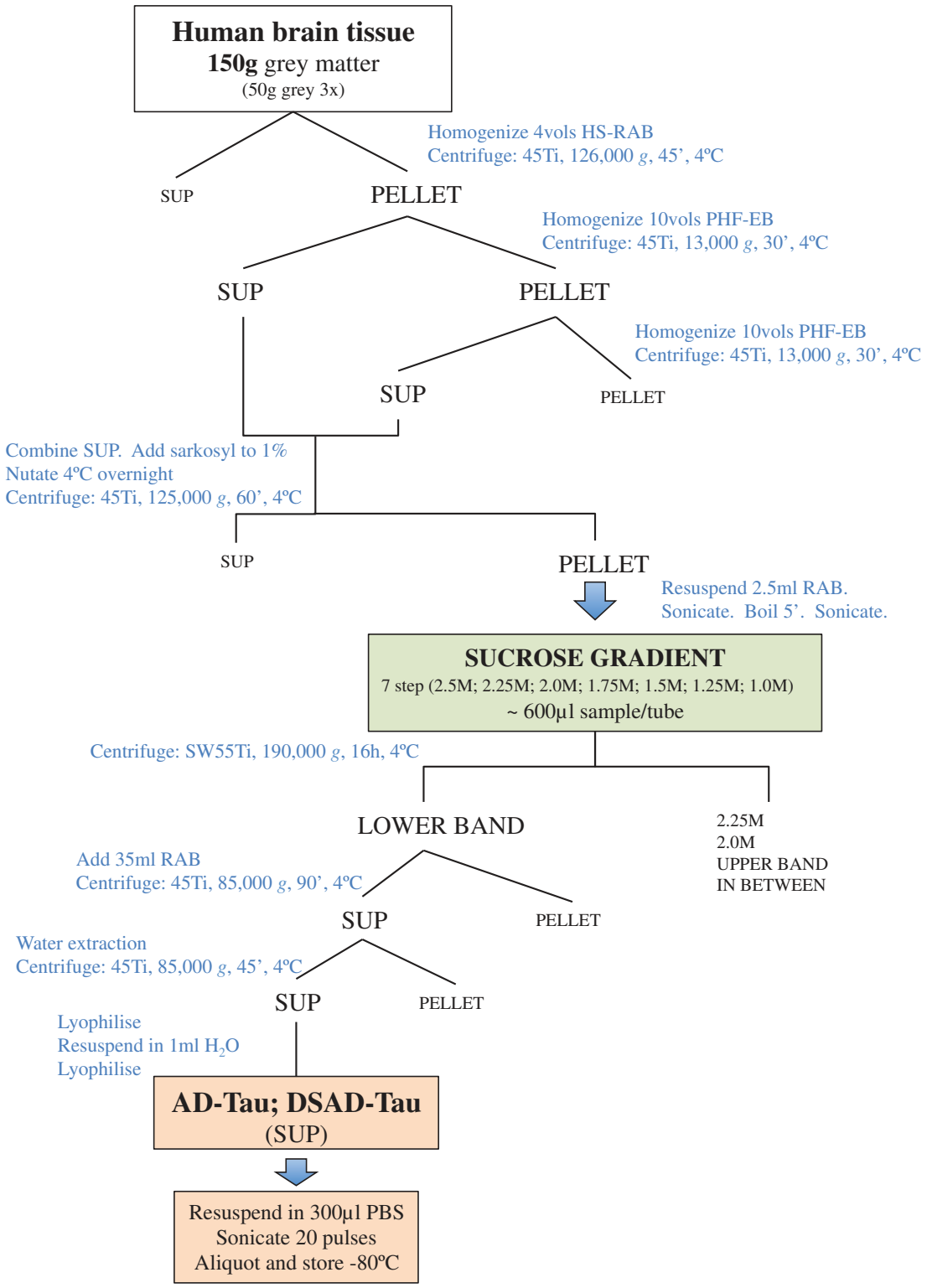

Figure 14. Schematics of the protocol used to obtain AD-Tau and DSAD-Tau, pathological tau enriched extracts from AD and DSAD subjects respectively.

1.3 CHARACTERIZATION OF EXTRACTS

All of the samples were characterized by sodium dodecyl sulfate polyacrylamide gel electrophoresis (SDS-PAGE) and Western Blot (WB) to determine the biochemical properties of the samples (Figure 15), by bicinchoninic colorimetric assay (BCA) to quantify the total amount of protein in the extracts and sandwich enzyme-linked immunosorbent assay (ELISA) to quantify the total amount of tau contained in the samples.

1.3.1 SDS-PAGE AND WESTERN BLOT

1.3.1.1 REAGENTS

The reagents used to load the samples, run the gels, transfer the proteins from the gels to the membrane, stain the gels, and wash the membranes are summarized in Table 9.

Table 9. Summary of the reagents used for SDS-PAGE and immunoblot

Buffer	Content
SAMPLE BUFFER (for 20 ml Laemmil 5x buffer)	Sucrose ……..…10g 0.5M Tris, pH 6.8……..1.85ml 0.1M EDTA…….....1ml 0.1% Bromophenol Blue…1ml 0.05% Pyronine Yellow….1ml DTT 10% SDS……...10ml
RUNNING BUFFER (for 10 l of 10x)	300 g Tris base 1430 g Glycine
TRANSFER BUFFER	10% 10x Running buffer 10% Methanol
COOMASSIE BLUE STAINING SOLUTION	0.1% Coomassie Brilliant Blue 50% Methanol 10% Glacial acetic acid
PONCEAU S STAINING SOLUTION	0.1% Ponceau S 5% Acetic acid
TBS-Tween 20	50 mM Tris-HCl 150 mM NaCl 0.1% Tween 20
5% NON-FAT MILK	50 g Non-fat dry milk 1000 ml TBS

1.3.1.2 GELS: RESOLVING AND STACKING

According to the size of the proteins of interest we used 7.5% resolving polyacrylamide gel and stacking gel to separate the proteins in the extract and be able to analyze the content of tau protein. The reagents used to prepare the gels are listed in Table 10.

Table 10. Reagents used to prepare resolving and stacking gels

Resolving gel (for 4 gels)		**Stacking gel (for 2 gels)**	
Reagent	**Volume**	**Reagent**	**Volume**
ddH2O	21.96 ml	ddH2O	2.9 ml
1.5M tris pH8.8	11.25 ml	0.5M tris pH6.8	1.25ml
30% Acryl/Bis	11.25 ml	30% Acryl/Bis	0.75ml
10% SDS	450 µl	10% SDS	50 µl
10% APS	150 µl	10% APS	25 µl
TEMED	45 µl	TEMED	12.5 µl

1.3.1.3 ANTIBODIES

The primary and secondary antibodies that were used for detection of total tau and phosphorylated tau proteins are detailed in Table 11.

Table 11. Primary and secondary antibodies used for the detection of tau protein in western blots

Primary antibodies						
Antibody	**Type**	**Class**	**Epitope**	**Dilution**	**Source**	**Reference**
PHF1	mAb	IgG1	Tau: p-Ser 394/404	1:1,000	Dr. P. Davis	Otvos et al, 1994 (251)
17025	pAb	IgG	Total tau	1:1,000	CNDR	Yoshiyama et al, 2007 (143)
Secondary antibodies						
Antibody	**Host**	**Reactivity**	**Target Isotype**	**Dilution**	**Source**	
IRDye®680LT goat anti-rabbit IgG (H+L)	goat	rabbit	IgG	1:10,000	Li-Cor	
IRDye®800CW goat anti-mouse IgG (H+L)	goat	mouse	IgG	1:10,000	Li-Cor	

mAb: monoclonal antibody; pAb: policlonal antibody; p-Ser: phosphorylated serine

1.3.1.4 PROTOCOL

1. **SDS-PAGE:** Two 7.5% polyacrylamide gels were prepared and 10 µl of each sample were loaded onto each gel to be run in parallel. For immunoblot DSAD-Tau and AD-Tau were diluted 1:100 and CTRL-Tau and CBD-Tau were loaded without diluting. A constant current of 20 mA (10 mA/gel) was applied for 3 h and 20 min.
2. **Coomassie Blue staining:** One of the gels was stained with Coomassie Blue to allow the visualization of the separated proteins.
3. **Protein transfer:** The proteins from the second gel were transferred onto a 0.45 µm nitrocellulose membrane for 1 h 10 min with a constant voltage of 100 mV. Once done and, to check for the effectiveness of the transfer, the membrane was stained with Ponceau S.
4. **Blocking and detection:** The membrane was blocked with 5% non-fat milk for 1 h at RT to reduce background following which the membrane was incubated with primary antibodies for 1 h at RT. Then, the membrane was washed in TBS-Tween 20 (3 times for 5 min each) and incubated in fluorescent secondary antibodies for 1 h at RT. Finally, the membrane was washed in TBS-Tween 20 (3 times for 5 min each) and viewed in an Odyssey®CLx infrared imaging system.

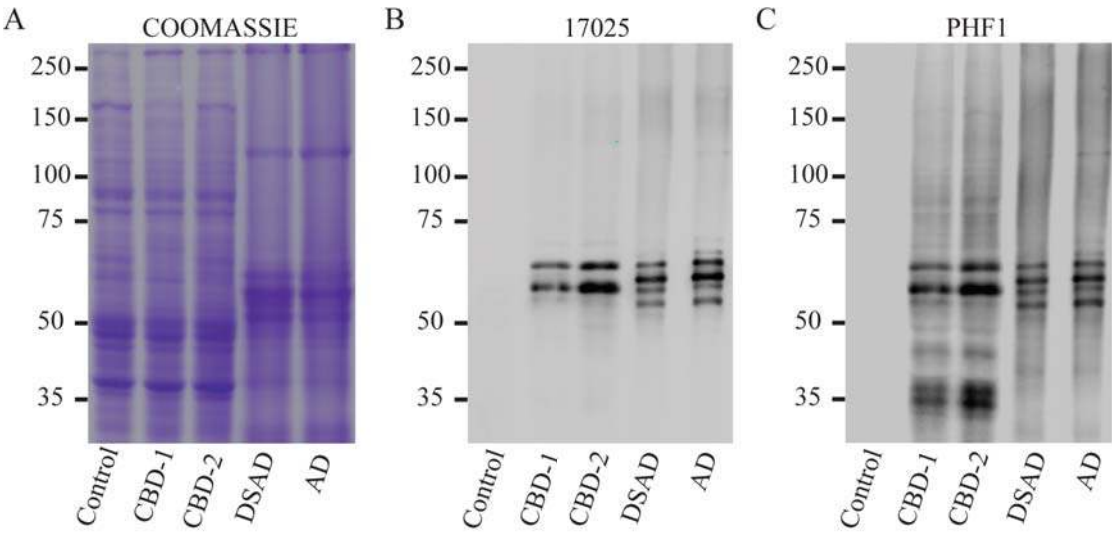

Figure 15 Biochemical analysis of the pathological tau protein enriched extracts obtained from human brains with a neuropathological diagnosis of CBD, AD, DSAD and a non-disease normal control brain used for injection into PS19 Tg mice. **a** SDS gel stained with Coomassie Blue, **b** and **c** Immunoblots stained with 17025 (**b**) and PHF1 (**c**). The total protein loaded was 18 µg for CTRL, 22 µg for CBD-1, 26 µg for CBD-2, 32 µg for DSAD and 26 µg for AD.

1.3.2 BICINCHONINIC ACID ASSAY (BCA)

The colorimetric based bicinchoninic acid assay (Thermo Scientific Pierce™ BCA Protein Assay Kit) was used for detecting and quantifying total proteins in the extracts. This method is based on the color change of the substrate as a result of two reactions, the reduction of Cu^{2+} ions from the copper (II) sulfate to Cu^{+} induced by the proteins and the colorimetric detection of Cu^{+} by a reagent containing bicinchoninic acid. A purple-colored product appears that strongly absorbs light at a wavelength of 562 nm. This is a temperature dependent reaction. The amount of Cu^{2+} reduced is proportional to the amount of protein present in the solution.

The assay was done following the instructions provided by the manufacturer.

1.3.3 SANDWICH ENZYME-LINKED IMMUNOSORBENT ASSAY (ELISA)

A sandwich enzyme-linked immunosorbent assay (ELISA) was performed to measure total tau in the extracts.

1.3.3.1 REAGENTS

The reagents used for the procedure are listed in Table 12.

Table 12. Buffers and reagents used for tau ELISA

Buffer	Reagents
C-BUFFER*	0.02M sodium phosphate buffer pH7.0 (0.1M NaH_2PO + 0.1M Na_2HPO) 2mM EDTA 0.4M NaCl 1% BSA 0.005% thimerosal
PBS	Ready-made Dulbeco's Phosphate Saline Buffer without calcium and magnesium (Life Technologies)
COATING BUFFER (pH 9.6)	0.1M Sodium carbonate ($NaHCO_3$) 0.1M Sodium bicarbonate (Na_2CO_3)
BLOCK ACE SOLUTION*	1% BlockAce Powder 0.05% NaN_3 Diluted in PBS
BSA	Bovine Serum Albumin (Sigma-Aldrich)

*Buffers C and Block Ace were heated at 56ºC for 40 min

1.3.3.2 ANTIBODIES

Human non-phosphorylation dependent tau antibodies were used as coating and detection antibodies to quantify total tau in the human brain tissue extracts (Table 13).

Table 13. Tau antibodies used for quantifying tau protein in the human brain extracts

Antibody	Type	Class	Epitope	Source	Comments
Tau5	mAb (mouse)	IgG1	Tau residues 21 to 230	CNDR	Coating Ab
BT2	mAb (mouse)	IgG1	Tau residues194 to198	Pierce Thermo Scientific	Detection Ab
HT7	mAb (mouse)	IgG1	hTau residues 159 to 163	Pierce Thermo Scientific	Detection Ab

Ab: antibody; hTau: human tau; mAb: monoclonal antibody;

1.3.3.3 PROTOCOL

Day 1. Coating the plate

1. A solution of Tau5-IgG (5mg/ml) in Coating buffer was prepared and a 384-well plate (Nunc®MaxiSorp™ 384-well plate) was coated with 30 ml/well of Tau5.
2. The plates were sealed and centrifuged for 2 min at 1000 *g* at 4ºC. The plate was kept in the refrigerator overnight.

Day 2. Blocking the plate

1. The plate was washed with PBS containing 0.05% Tween-20 in a plate washer (Elx405™ Select Microplate Washer, BioTek) and Block Ace was prepared following the instructions given by the manufacturer.
2. The plates were sealed and centrifuged for 2 min at 1000 *g* at 4ºC and finally kept in the refrigerator for at least 1 week to reduce background.

Day 3. Adding the antigen

1. Aliquots of tau T40 (21) standards (0, 37.5, 75, 150, 300, 600, 1200, 2400pg/ml) diluted in PBS/0.2%BSA were prepared and were loaded onto the plate.
2. Four different dilutions of the samples were prepared and were loaded onto the plate.

3. The plates were sealed and centrifuged for 2 min at 1000 *g* at 4ºC and kept overnight at 4ºC.

Day 4. Adding the reporter

4. The plate was washed and a combination of BT2/HT7 (125 ng/ml) was diluted in C-Buffer and used as reporter.
5. The plate was sealed and centrifuged for 2 min at 1000 *g* at 4ºC and kept overnight at 4ºC.

Day 5. Developing

1. The plate was washed and an HRP-labeled Streptavidin (1:8,000; Thermo, Pierce Pierce High Sensitivity Streptavidin HRP #21130) diluted in C-Buffer was added.
2. The plate was sealed and centrifuged for 2 min at 1000 *g* at 4ºC.
3. The plate was incubated at 25ºC for 1 hour.
4. The plate was washed again and the developing solution made with a combination of Peroxidase substrate and TMB Peroxidase substrate (TMB Microwell Peroxidase Substrate System, KLP) was added to each well.
5. After 10 min of incubation at RT the reaction was quenched by the addition of 30ml of 10% Phosphoric acid to each well.
6. The signal of the wells was measured using the SpectraMax 5M (Molecular Devices) plate reader at 450 nm and the data was analyzed with the Softmax Pro (Molecular Devices) software. The amount of tau in the samples was determined from the T40 standard curve and normalized to the average amount of total tau in the extracts.

2. ANIMALS USED IN THE STUDY

2.1 PS19 MICE

For this study the line PS19 of tau transgenic mice was bred on a mixed background B6C3. These mice were generated using a cDNA encoding the human T34 isoform of tau (1N4R) with the P301S *MAPT* mutation driven by the murine

prion protein promoter (MoPrP) (143). The P301S mutation of *MAPT* is known to cause rapidly lethal and early-onset FTDP-17 (142,252–254). PS19 mice overexpress the mutated human tau isoform by 5-fold over the endogenous mouse tau.

As they age, PS19 tau Tg mice develop tau aggregates in the spinal cord, brain stem, cortex and hippocampus. The mice present with clasping and limb retraction when lifted by the tail followed by limb weakness and brain atrophy. This progresses to paralysis associated with a hunchback posture and an inability to feed. Similarly to tau pathology in AD brains, tau pathology in PS19 mice progresses with time in a hierarchical manner and this progression can be staged (255).

As recently reported (229) and reviewed elsewhere (http://www.alzforum.org/research-models/tau-p301s-line-ps19), the onset of neurodegenerative tauopathy in the PS19 Tg mice at Penn has shifted from 6 to about 12 mo of age thereby allowing a longer time window for the transmission studies described in the study.

2.2 SURGERY PROCEDURE

All experiments were performed in accordance with protocols approved by the Institutional Animal Care and Use Committee of the University of Pennsylvania.

Two to five month old PS19 mice of either gender were deeply anesthetized with a ketamine/xylazine/acepromazine mixture, immobilized in a stereotaxic frame (David Kopf Instruments), following which the different brain extracts were injected stereotaxically into the hippocampus and overlying neocortex using predetermined coordinates for hippocampus (Bregma -2.5 mm, lateral +2 mm, and depth -2 mm from brain surface) and overlying cortex (Bregma -2.5 mm, lateral +2 mm and depth -0.8 mm from brain surface) (Figure 16) with a 10 µl Hamilton syringe under aseptic conditions as described in Iba et al. (229).

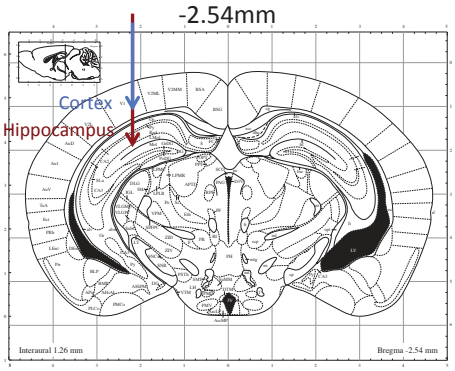

Figure 16. Injection sites. PS19 mice were injected in the hippocampus and overlying cortex of the right hemisphere.

All injected mice were observed during and after surgery. The total volume injected per site was 2.5µl for all mice. The mice used for each experimental condition are summarized in Table 14.

Table 14. PS19 mice used in the study.

Injections of CBD-Tau and Control Brain Extracts

CBD (n=18 mice)

Time postinjection (months)	Number of mice		Total injected tau (µg)
	CBD-1	CBD-2	
1	4	2	0.05
3	4	2	0.05
6	4	2	0.05

CONTROL (n=4 mice)

Time postinjection (months)	Number of mice	Total injected tau (µg)
1	2	0.003
6	2	0.003

Injections of AD-Tau and DSAD-Tau

AD (n=12 mice)/*DSAD* (n=12 mice)

Time postinjection (months)	Number of mice		Total injected tau (µg)	
	AD	DSAD	AD	DSAD
1	4	4	10.5	12.5
3	4	4	10.5	12.5
6	4	4	10.5	12.5

DSAD serial dilutions (n=12 mice)

Time postinjection (months)	Number of mice	Total injected tau (µg)
1	3	0.065
1	3	0.25
1	3	1.5
1	3	12.5

2.2 SACRIFICE

Mice were sacrificed at 1, 3 and 6 mo after injection. Mice were transcardially perfused after anesthesia with 30 ml PBS followed by 15 ml 10 % neutral buffered formaldehyde (NBF). The brain and spinal cord were dissected and fixed by immersion in NBF overnight at 4ºC. The next day they were washed in PBS and predetermined sections of the CNS including cerebrum, brain stem, cerebellum and spinal cord were dehydrated in increasing percentage of alcohol buffers and embedded in paraffin. Tissue blocks were mounted and 6 μm serial histological sections were performed using a Leitz 1512 rotary microtome and saved for further staining with histochemical, immunohistochemical and immunofluorescence techniques.

3. ANALYSIS OF BRAIN TISSUE FROM INJECTED MICE

The tau pathology developed in PS19 tau transgenic mice after the injection of the pathological tau enriched extracts obtained from human brain tissue was characterized with immunohistochemistry, immunofluorescence and histochemical techniques.

3.1 IMMUNOHISTOCHEMISTRY

For immunohistochemistry (IHC) every 20th slide from serially sectioned mouse brains was immunostained with mAb AT8 and MC1. Other antibodies were used as well including additional tau antibodies and markers for other protein aggregates such as α-syn, Aβ, TDP-43 and inflammation and are also listed in Table 15.

3.1.1 ANTIBODIES

The antibodies used in this study encompass antibodies against different epitopes of tau protein (phosphorylation dependent, phosphorylation independent and conformation dependent), antibodies against other proteins that also aggregate in other neurodegenerative diseases and antibodies against glial cells (Table 15).

3.1.2 PROTOCOL

Different immunohistochemical procedures were used depending on the antibody (Table 15). The protocols are detailed below. All of the procedures were done manually.

3.1.2.1 BIOGENEX-HRP

The Biogenex-HRP procedure was the most frequent procedure used for the IHC staining of the histological slides. It uses the Super Sensitive Polymer HRP-Detection system/DAB (BioGenex), which uses a non-biotin polymeric technology that makes use of two major components: Super Enhancer and a Poly-HRP reagent. As the system is not based on the biotin-avidin system there is no background due to endogenous biotin and it is more sensitive for weakly expressed antigens. It is a two-day process.

DAY 1

1. **Deparaffinization and rehydration:** Slides were deparaffinized two times in xylene for 5 min and immersed in descending ethanol series 1 min each (100%, 100%, 95%, 95%, 80%, 70%). Finally, the tissue was hydrated with ddH_2O for 1min.
2. **Formic acid (FA) treatment (if needed):** In the case of pAb 17025 and NAB228, formic acid treatment was needed. For this, after ddH_2O the slides were immersed in 88% FA for 5min and finally rinsed in ddH_2O for 1 min.

Table 15. Antibodies used for the immunohistochemical analyses of the PS19 mice brain tissue

Antibody	Clonality	Isotype		Epitope	IHC protocol	Antigen retrieval	Dilution	Source	Reference
AT8	mAb	IgG1	Tau	p-dependent at p-Ser199/202 and p-Thr205	HRP	None	1:10,000	Thermo Scientific	Mercken et al (256)
MC1	mAb	IgG1	Tau	c-dependent aa 5-15 and 312-322	HRP	None	1:8,000	Dr. P Davies	Jicha et al, (257)
TG3	mAb	IgM	Tau	c-dependent p-Thr231	HRP	None	1:250	Dr. P Davies	Jicha et al (258)
T49	mAb	IgG1	Tau	mTau specific	M.O.M.	None	1:2,000	CNDR	Yoshiyama et al (143)
T14	mAb	IgG1	Tau	hTau specific aa 141-178	M.O.M.	None	1:1,000	CNDR	Kosik et al (259)
RD3	mAb	IgG	Tau	aa 209-224	HRP	FA	1:3,000	Millipore	de Silva et al (260)
RD4	mAb	IgG	Tau	aa 275-291	HRP	FA	1:5,000	Millipore	de Silva et al (260)
17025	pAb	IgG	Tau	Total Tau	HRP	FA	1:1,000	CNDR	Yoshiyama et al (143)
81A	mAb	IgG2a	α-synuclein	p-dependent at p-Ser129	HRP	MW	1:50,000	CNDR	Waxman et al (261)
409/410	mAb	IgG2a	TDP-43	p-dependent at p-409/410	ABC		1:200	CNDR	Neumann et al (262)
NAB228	mAb	IgG2a	β-amyloid	Aβ aa 1-11	ABC	FA	1:60,000	CNDR	Lee et al (263)
Olig2	pAb	IgG	Oligodendrocytes	specific for oligodendrocytes	HRP	MW	1:250	Millipore	
GFAP (clone 2.2B10)	mAb	IgG2a	Astrocytes	specific for astrocytes	HRP	MW	1:1,000	CNDR	Lee et al (264)
Iba-1	pAb	IgG	Microglia	specific for microglia	ABC	FA	1:1,000	Wako Chemicals	

aa: amino acid; c-dependent: conformation dependent; FA: formic acid; HRP: Biogenex-HRP; M.O.M.: Vector®M.O.M.™ immunodetection kit (Vector Laboratories); mAb: monoclonal antibody; MW: microwave; pAb: policlonal antibody; p-dependent: phosphorylation dependent

3. **Blocking of endogenous peroxidases:** Endogenous peroxidase was blocked to avoid background in the tissue. The slides were immersed in a solution of 5% H_2O_2 in methanol for 30 min at RT.
4. **Microwave treatment (MW) (if needed):** If heat antigen retrieval was needed, the deparaffinized slides were immersed in a solution of 1% Vector® Antigen Unmasking Solution Citrate-Based (Vector Laboratories) in ddH_2O and microwaved in a laboratory microwave for 15 min at 99ºC. Once microwaved, the slides were let to cool down for at least 20 min at RT.
5. **Wash**: The slides were then washed in running tap water for 10 min and later immersed in a 0.1M Tris solution for 5 min.
6. **Blocking:** The tissue was immersed in 0.1M Tris/2%FBS for 30 min to block all epitopes in the tissue to prevent the non-specific binding of the secondary antibody that would result in background staining.
7. **Application of antibody:** The slides were wiped and the tissue area was delimited with a hydrophobic barrier pen. Finally, 300 µl of antibody were applied over the tissue and let it incubate at 4ºC overnight, for 16 to 22 hours in a humidified chamber.

DAY 2

1. **Rinse and wash:** The antibody was rinsed off from the tissue with a squirt of 0.1M Tris. Then, the tissue was washed by immersing the slides in 0.1M Tris for 5 min and was followed by a short incubation in 0.1M Tris/2%FBS for 5 min.
2. **Super-Enhancer™ Reagent:** Super-Enhancer™ Reagent (BioGenex) was diluted 1:1 in 0.1M Tris/2%FBS. 300 µl of the solution were applied to the tissue on each slide and was let to incubate for 20 min at room temperature.
3. **Rinse and wash:** The Super-Enhancer™ Reagent was rinsed off from the tissue with a squirt of 0.1M Tris. Then, the tissue was washed by immersing the slides in 0.1M Tris for 5 min and was followed by a short incubation in 0.1M Tris/2%FBS blocking solution for 5 min.
4. **Polymer-HRP Solution:** Polymer-HRP Solution (BioGenex) was diluted 1:1 in 0.1M Tris/2%FBS. 300 µl of the solution were applied to the tissue on each slide and was let to incubate for 30 min at room temperature.

5. **Rinse and wash:** The Polymer-HRP Solution was rinsed off from the tissue with a squirt of 0.1M Tris and then, the tissue was washed by immersing the slides in 0.1M Tris for 5 min. This time, there was no wash in 0.1M Tris/2%FBS.
6. **Substrate Solution (DAB):** 300 μl of Substrate Solution (DAB; BioGenex) prepared following manufacturer's instructions (20ml Stable DAB Substrate Buffer + 20 drops Liquid DAB chromogen; Biogenex) were applied on the tissue slides and was let to incubate for 5-8 min. This step is time sensitive and turned the tissue brown when there was reaction between the primary antibody and the target antigen.
7. **Rinse and wash:** The DAB was rinsed off from the tissue with a squirt of 0.1M Tris and washed by immersing the slides in 0.1M Tris for 5 min.
8. **Counterstain with Hematoxylin:** The slides were counterstained with Myers Hematoxylin for 1 min.
9. **Rinse:** The slides were rinsed in tap running water.
10. **Dehydration and coverslipping:** The stained tissue was dehydrated in descending concentrations of alcohol (1 min each) starting at 70% ethanol (70%, 80%, 95%, 95%, 100%, 100%) and 2 steps of 5 min in xylene. Finally it was coversliped using ThermoScientific™ Richard-Allan Scientific™ Cytoseal™ XLY mounting media.

3.1.2.2 ABC PROCEDURE

For a few antibodies the ABC immunohistochemistry procedure was used (Table 15) as it yielded in better results than the Biogenex-HRP procedure. For this the VECTASTAIN ABC Kit (Vector Laboratories) was used. It is also a 2-day process in which day 1 is the same as the Biogenex-HRP procedure described above.

DAY 2

1. **Rinse and wash:** The antibody was rinsed off from the tissue with a squirt of 0.1M Tris. Then, the tissue was washed by immersing the slides in 0.1M Tris for 1 h followed by another 0.1M Tris wash of 5 min and finally was blocked for 5 min in 0.1M Tris/FBS.

2. **Addition of anti-IgG:** 300 µl of biotinylated anti-mouse IgG or anti-rabbit IgG (Vector Laboratories), depending on the primary antibody, diluted (1:1,000) in 0.1M Tris/2%FBS was applied to the tissue and incubated in a humidified chamber at RT for 1 h.
3. **Rinse and wash:** The IgG was rinsed off from the tissue with a squirt of 0.1M Tris. Then, the tissue was washed by immersing the slides in 0.1M Tris wash of 5 min followed by 5 min blocking in 0.1M Tris/2%FBS
4. **AB Solution:** 300 µl of pre-mixed AB Solution of the VECTASTAIN® ABC Kit (Vector Laboratories) was applied to each section and incubated for 1 h at RT.
5. **Rinse and wash:** The AB solution was rinsed off from the tissue with a squirt of 0.1M Tris and then, the tissue was washed by immersing the slides in a 5 min 0.1M Tris wash.
6. **DAB solution:** 300 µl of DAB solution was applied to the tissue and was let to incubate for 5 min, when a brown signal appeared.
7. **Rinse and wash:** The DAB was rinsed off from the tissue with a squirt of 0.1M Tris. Then, the tissue was washed by immersing the slides in a 5 min 0.1M Tris followed by two washes of ddH_2O of 1 min each.
8. **Heamatoxylin counterstain:** The tissue was counterstained by immersion of the slides in filtered Harris haematoxylin (Nonacidified**,** Shandon**,** Product # 6765001) for 1 minute.
9. **Rinse and wash:** The slides were developed and rinsed in 10-15 min of running tap H_2O.
10. **Dehydration and coverslipping:** The stained tissue was dehydrated in descending concentrations of alcohol (1 min each) starting at 70% ethanol (70%, 80%, 95%, 95%, 100%, 100%) and 2 steps of 5 min in xylene. Finally it was coverslipped using ThermoScientific™ Richard-Allan Scientific™ Cytoseal™ XLY mounting media.

3.2 HISTOCHEMISTRY

3.2.1 HAEMATOXYLIN AND EOSIN

3.2.1.1 STOCK SOLUTIONS

1% stock Eosin: 1 g Eosin Y + 20 ml ddH_2O + 80 ml 95% EtOH

Eosin working solution: 45 ml Eosin (stock) + 135 ml 80% EtOH + 900 ml Glacial Acetic Acid

0.1% Acid Alcohol Solution: 500 ml ddH_2O + 500 ml 100% EthOH + 1 ml HCl

Harris Haematoxylin: Nonacidified**,** Shandon**,** Product # 6765001

3.2.1.2 PROTOCOL

1. **Deparaffinization and rehydration:** Slides were deparaffinized for 5 min twice in xylene and immersed in descending ethanol series 1 min each (100%, 100%, 95%, 95%, 80%, 70%). Finally, the tissue was hydrated with 1 min ddH_2O.
2. **Haematoxylin staining:** The slides were immersed in filtered Harris Haematoxylin for 5 min.
3. **Rinsing:** The sections were rinsed in 2 changes of ddH_2O of 1 min each.
4. **Differentiation:** The slides were immersed in a 0.1% acid alcohol solution for 4 seconds. This step removes the excess dye in the tissue allowing for better visualization of nuclear details.
5. **Rinsing:** The slides were rinsed in tap H_2O for 10-15 min or until sections turn bright blue.
6. **Eosin staining:** The slides were immersed in Eosin for 1 min
7. **Rinsing:** The slides were briefly rinsed in tap H_2O

11. **Dehydration and coverslipping:** The slides were dehydrated in descending concentrations of alcohol (1 min each) starting at 95% ethanol (95%, 95%, 100%, 100%) and 2 steps of 5 min in Xylene. Finally the slides were coverslipped using ThermoScientific™ Richard-Allan Scientific™ Cytoseal™ XLY mounting media.

3.2.2 THIOFLAVIN-S

3.2.2.1 STOCK SOLUTIONS

0.05% $KMnO_4$/PBS: 0.5g $KMnO_4$ + 1000ml PBS

0.2% $K_2S_2O_5$/0.2% oxalic acid/PBS: 2g $K_2S_2O_5$ + 2 g oxalic acid + 1000ml PBS

40% EtOH/60% PBS: 400 ml 100% ethanol + 600 ml PBS

50% EtOH/50% PBS: 500 ml 100% ethanol + 500 ml PBS

0.0125% Thioflavin S: 0.025 g ThioS + 200 ml 40% EthOH/60%PBS

3.2.2.2 PROTOCOL

1. **Deparaffinization and rehydration:** Slides were deparaffinized for 5 min twice in xylene and immersed in descending ethanol series 1min each (100%, 100%, 95%, 95%, 80%, 70%). Finally, the tissue was hydrated with 1min ddH_2O.
2. **Rinsing:** The sections were immersed in PBS for 5 min.
3. **Lipofuscin autofluorescence quenching:** The slides were immersed in 0.05% $KMnO_4$/PBS 20 min.
4. **Rinsing**: The sections where rinsed in PBS for 2min, two times.
5. **Destaining:** The slides were immersed in 0.2% $K_2S_2O_5$/0.2% oxalic acid/PBS until the brown color was removed from sections (1min approx).
6. **Rinsing:** The slides were rinsed in PBS for 2 min, 3 times.
7. **Thioflavin S staining and differentiation:** Slides were immersed in freshly made 0.0125% Thioflavin S for 3 min and was differentiated by immersing the slides in 50% EtOH/50% PBS for 10-15 min.
8. **Rinsing and coverslipping:** The slides were rinsed in PBS for 5 min followed by ddH_2O for 5 min and coverslipped with VECTASHIELD® Mounting Media (Vector Laboratories).

3.3 DOUBLE LABELLING/IMMUNOFLUORESCENCE

To determine the source of tau protein in the aggregates and the precise localization of tau aggregates in white matter double-labelling of predetermined regions of the brain was performed.

3.3.1 ANTIBODIES

Table 16. Primary and secondary antibodies used for the detection of the proteins of interest by immunofluorescence

PRIMARY ANTIBODIES						
Antibody	**Clonality**	**Isotype**	**Epitope**	**Antigen retrieval**	**Dilution**	**Source**
AT8	mAb	IgG1	Tau: p-dependent at p-Ser199/202 and p-Thr205	MW	1:5,000	Thermo Scientific
T49	mAb	IgG1	mTau specific	MW	1:1,000	CNDR
T14	mAb	IgG1	hTau specific aa 141-178	MW	1:500	CNDR
Olig2	pAb	IgG	oligodendrocytes	MW	1:250	Millipore
GFAP (clone 2.2B10)	mAb	IgG2a	astrocytes	MW	1:1,000	CNDR
Iba-1	pAb	IgG	microglia	FA	1:1,000	Wako Chemicals

SECONDARY ANTIBODIES					
Antibody	**Host**	**Reactivity**	**Target Isotype**	**Dilution**	**Source**
Novex™Goat anti-Rabbit IgG (H+L) Secondary Antibody, Alexa Fluor® 594 conjugate	Goat	Rabbit	IgG	1:500	Thermo-Scientific
Novex™Goat anti-Mouse IgG (H+L) Secondary Antibody, Alexa Fluor® 488 conjugate	Goat	Rabbit	IgG	1:500	Thermo-Scientific

FA: formic acid; hTau: human Tau; mAb: monoclonal antibody; mTau: mouse tau; MW: microwave; pAb: policlonal antibody

3.3.2 PROTOCOL

DAY 1

1. **Deparaffinization and hydration:** Slides were deparaffinized for 5 min, twice, in xylene and immersed in descending ethanol series 1 min each (100%, 100%, 95%, 95%, 80%, 70%). Finally, the tissue was hydrated with 1 min ddH_2O.
2. **Microwave pretreatment (if needed):** The deparaffinized slides were immersed in a 1% Vector® Antigen Unmasking Solution Citrate-Based (Vector

Laboratories) in ddH_2O and microwaved in a laboratory microwave for 15 min at 99ºC. Once microwaved, the slides were let to cool down for at least 20min at RT.

3. **Rinsing and blocking:** The slides were rinsed in 10 min tap H_2O immersed in 0.1M Tris for 5 min followed by blocking in 0.1M Tris/2%FBS block for 1 h.
4. **Adding the primary antibody:** 300 μl of primary antibodies diluted as specified in Table 16 in 0.1M Tris/2%FBS buffer were added to the sections and the slides were incubated overnight at 4ºC

DAY 2

1. **Rinsing and washing:** The primary antibody was rinsed from the tissue sections by squirting 0.1M Tris, then the sections were immersed in running tap water for 10 min followed by immersion in 0.1M Tris 5' (3 times). The sections were blocked for 5 minutes in 0.1M Tris/2%FBS.
2. **Secondary antibodies**: 300 μl of fluorescent secondary antibody in a 1:500 dilution in 0.1MTris/2%FBS buffer were added to the tissue sections and incubated at RT for 2 hours.
3. **Rinsing and washing:** The tissue was rinsed from the secondary antibody by squirting 0.1M Tris, then immersed in running tap water for 5 min followed by immersion in 0.1M Tris for 5 min (3 times).
4. **Sudan black treatment:** The tissue sections were treated with Sudan Black for 1 min to quench the autofluorescence of lipofuscin present in tissue cells.
5. **Rinsing and coverslipping:** The slides were rinsed in 0.1M Tris for 5 minutes (3 times) and coverslipped with VECTASHIELD® Mounting Media (Vector Laboratories) with DAPI.

4. QUANTIFICATION AND STATISTICS

4.1 TAU PATHOLOGY

The extent of glial tau pathology was quantified in PS19 mice following injections with CBD-Tau, AD-Tau and DSAS-Tau. For CBD-Tau injected mice,

three coronal CNS levels (bregma -1.22, -2.18 and -2.92 mm) were selected, brain regions were marked according to anatomical/cytoarchitectural patterns (265) and after grading individual brain regions in each mouse, the averaged values of the scores were imported into CNS heat maps using custom-designed heat-map software to create pathology distribution maps. Glial tau pathology was quantified in a semiquantitative manner (0: none; 1+: scant; 2+: moderate; 3+: abundant) where 1+ is rare (at least two tau inclusion bearing oligodendrocytes in a section) to a low burden of glial tau pathology and 3+ represents the presence of at least 25 tau positive oligodendrocytes in a section. The tau pathology spread in the PS19 mice injected with AD-Tau and DSAD-Tau were very similar to each other and thus were evaluated as a single group (AD/DSAD-Tau). In this case tangle and neuritic pathology was evaluated in five coronal planes (bregma 0.98, -1.22, -2.18, -2.92 and -4-48 mm). Tau pathology was more abundant than the CBD-Tau and was also evaluated semiquantitatively (0: none; 1+: scant; 2+: moderate; 3+: abundant). Scant (1+) tau pathology represents the presence of at least two tangle bearing neurons in a particular region of a section and/or low neuritic tau pathology; abundant (3+) represents >50 tau positive neurons in a region of a section and/or abundant neuritic tau pathology. The same criteria were used for the assessment of the serial dilution assay of DSAD-Tau injected mice.

4.2 NEURON LOSS

To evaluate neuron loss, we assessed a defined portion of the CA3 and CA1 region of matched brain sections stained with hematoxylin and eosin (H&E) from PS19 mice injected with AD-Tau or DSAD-Tau (n=7 per time point), CBD-Tau (n=6 per time point) and CTRL-Tau (n=2 per time point) at 1, 3 and 6 mo post-injection using 20x images. Neurons were individually counted using ImageJ software (National Institutes of Health). To determine statistical differences between groups, one-way ANOVA and Tukey's multiple-comparison test was used.

RESULTS

1. INJECTIONS OF CBD-Tau AND AD-Tau INDUCE DISTINCT TAU PATHOLOGY IN PS19 Tg MICE

The generation of tau pathology in mice has been seen with recombinant preformed fibrils (PFFs) and mouse brain homogenates from Tg mice that develop tau aggregates (226,229). The idea was to investigate whether pathological tau from different tauopathy brains induce distinct tau pathologies. For this I generated CBD-Tau, AD-Tau or DSAD-Tau enriched preparations from the brains of 4 patients afflicted with these tauopathies in addition to a CTRL subject. Then, these extracts were injected into the right hippocampus and overlying cortex of PS19 tau Tg mice (2-5 month old) (Table 14). We examined the resulting tau pathology at 1, 3 and 6 mo post-injection intervals. Mice injected with CBD-Tau, AD-Tau and DSAD-Tau developed pathology as early as 1 mo after injection (Figure 17).

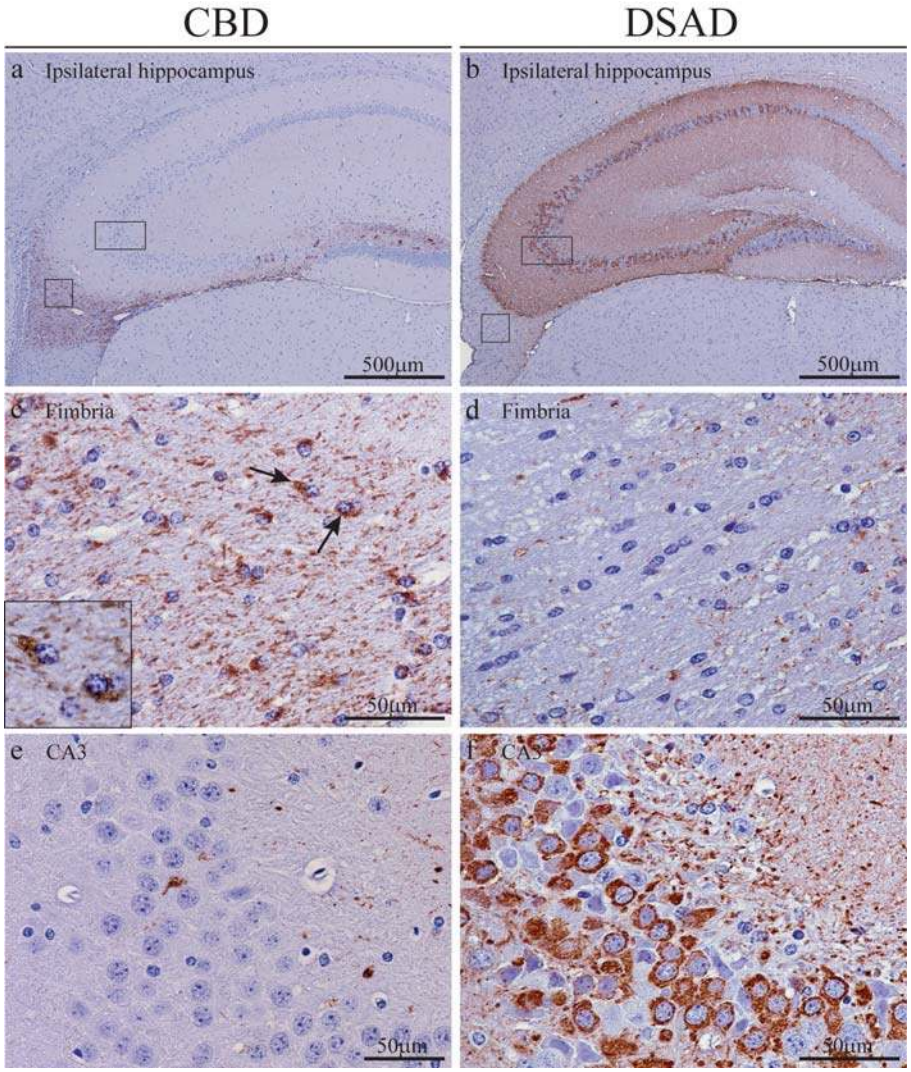

(previous page) **Figure 17**: Development of cell type-specific tau inclusions after injection of CBD-Tau- or DSAD-Tau-enriched protein extracts into the brains of PS19 mice. **a,c,e** AT8-positive oligodendroglial inclusions developed in the fimbria of the hippocampus on the injected side 1 month after the injection of CBD-Tau. **b,d,f** AT8-positive inclusions developed in the perikarya of neurons of the hippocampus of DSAD-Tau-injected mice. **c** A higher magnification of the *square boxed area* in (**a**) is shown in (**c**) demonstrating AT8-positive tau inclusions in many oligodendrocytes of the fimbria. The inset in (**c**) shows a detail of the oligodendrocytes indicated by the black arrows. **d** A higher magnification of the *square boxed area* in (**b**) is shown in (**d**) demonstrating the absence of tau inclusions in the oligodendrocytes of the fimbria which contrasts with the CBD-Tau-injected mice. **e** Higher magnification of the *rectangular boxed area* in (**a**) demonstrating only rare intraneuronal inclusions in the region of the hippocampus (**e**). In **f**, where a higher magnification of the *rectangular boxed area* in (**b**) is depicted, there is abundance of perikaryal AT8 inclusions in CA3 of the hippocampus. Scale bar, upper row 500 mm; middle and bottom rows 50 mm.

1.1 INJECTIONS OF CBD-Tau

PS19 mice injected with CBD-Tau induced predominantly glial tau pathology in white matter tracts and hippocampus close to the injection site at the earliest post-injection time point as detected by mAb AT8 (Figure 17 a, c, e and Figure 18). At 1 mo post-injection, AT8 positive tau inclusions were seen in oligodendrocytes of the adjacent hippocampal fimbria (4/6; 66% of mice) as well as in the alveus/subcortical white matter/external capsule contiguous with the injection site (3/6; 50% of mice) (Figures 18 and 24). Neurons in hippocampal regions CA1, CA3, dentate gyrus and subiculum also showed some perikaryal tau inclusions (Figure 18), but they were scant compared to the oligodendrocytes with tau pathology in the fimbria. They also were infrequent compared to the large numbers of tangle bearing neurons seen in the AD-Tau and DSAD-Tau injected mice described below.

(Following page) **Figure 18**. Tau pathology developed in white matter tracts and, in lesser amount, in hippocampal neurons 1 month after the injection of CBD-Tau. **a,b** AT8-positive aggregates in the hippocampus and adjoining white matter tracts of two CBD-Tau-injected mice. In one of the mice (**a**) tau aggregates appeared in oligodendrocytes of alveus/external capsule (*arrow head*) and, in less amount, in the perikarya of neurons in CA1 (*arrow*). In a second mouse **(b)** the pathology was developed mainly in oligodendrocytes of the fimbria (*arrow*) with scant pathology in neurons of the hippocampus. **c** Higher magnification of the CA1 region in (**a**) (indicated by an arrow) where AT8-positive aggregates can be seen in the neuronal perikarya. **d** Higher magnification of the alveus/external capsule in (**a**) (indicated by an arrow head) where tau aggregates are seen in the cytoplasm of oligodendrocytes. AT8-positive aggregates in oligodendrocytes can also be seen in the fimbria (**e**) where a higher magnification of the region in (**b**) (indicated by an arrow) is seen. Scale bar, *upper row* 500μm; *lower row* (left and right images) 100 μm; *lower row* (central image): 50 μm.

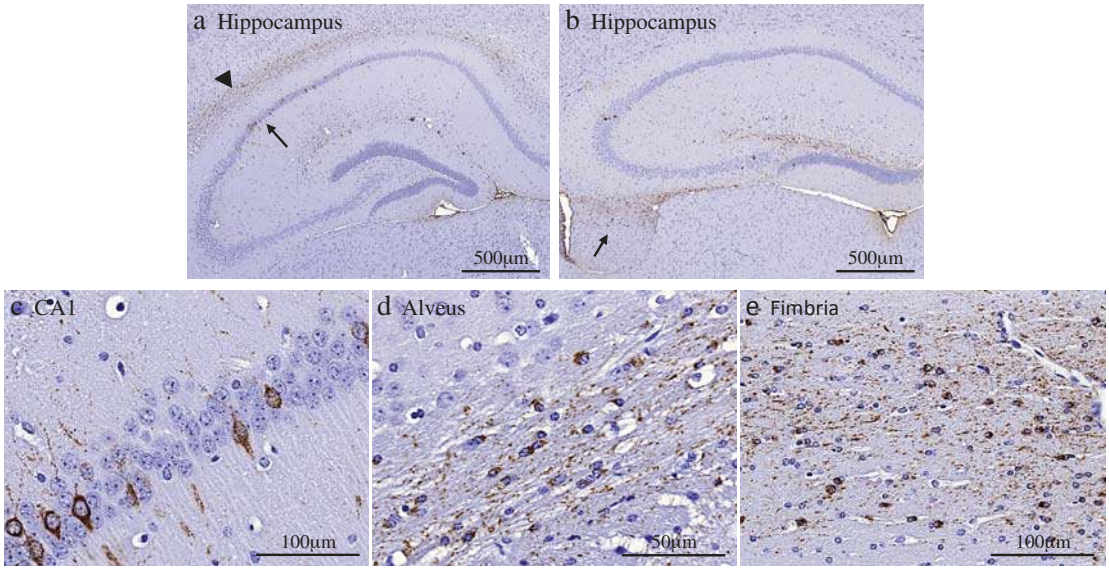

Double labeling with mAb AT8, a phosphorylation dependent tau antibody, and pAb Olig2, an antibody specific for oligodendrocytes, confirmed the oligodendrocytic nature of the tau aggregates developed in the fimbria and alveus/external capsule (Figure 19).

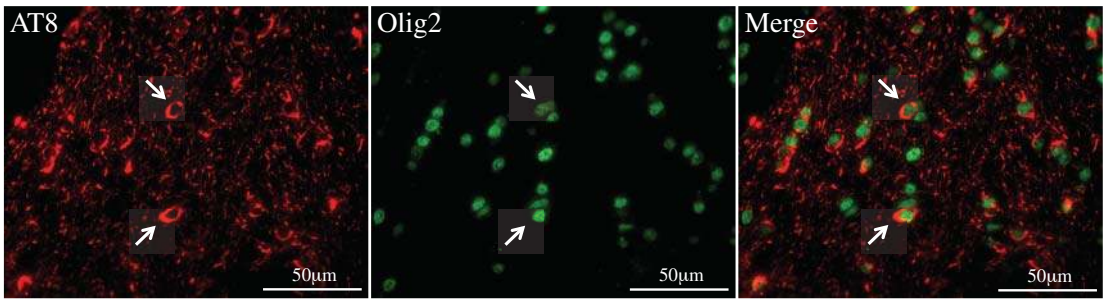

Figure 19. Double labeling of the fimbria confirmed that tau aggregates developed within the cytoplasm of the oligodendrocytes in PS19 Tg mice after the injection of CBD-Tau. mAb AT8 (*red*), specific for phosphorylated tau in Ser202 and Thr203, and pAb Olig2 (*green*), specific for oligodendrocytes. Scale bar, 50µm.

Oligodendroglial tau inclusions extended beyond the injection site to rostral and caudal regions of the brain quite distal from the injection site (Figure 20 and 24b). Infrequent or sparse intraneuronal tau inclusions in the hippocampus were also seen rostral and caudal to the injection site. Additionally, a small number of AT8 immunoreactive neurons were seen in the supramammillary bodies (data not shown). However, at 1 mo post-injection, the tau inclusion pathology was limited to the side

of the injection site (Figure 24b). No tau pathology was seen in the overlying cortex even near the cortical injection site.

a

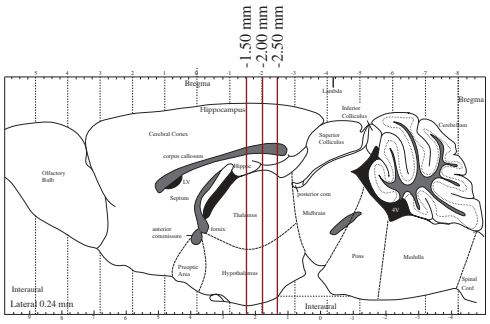

b

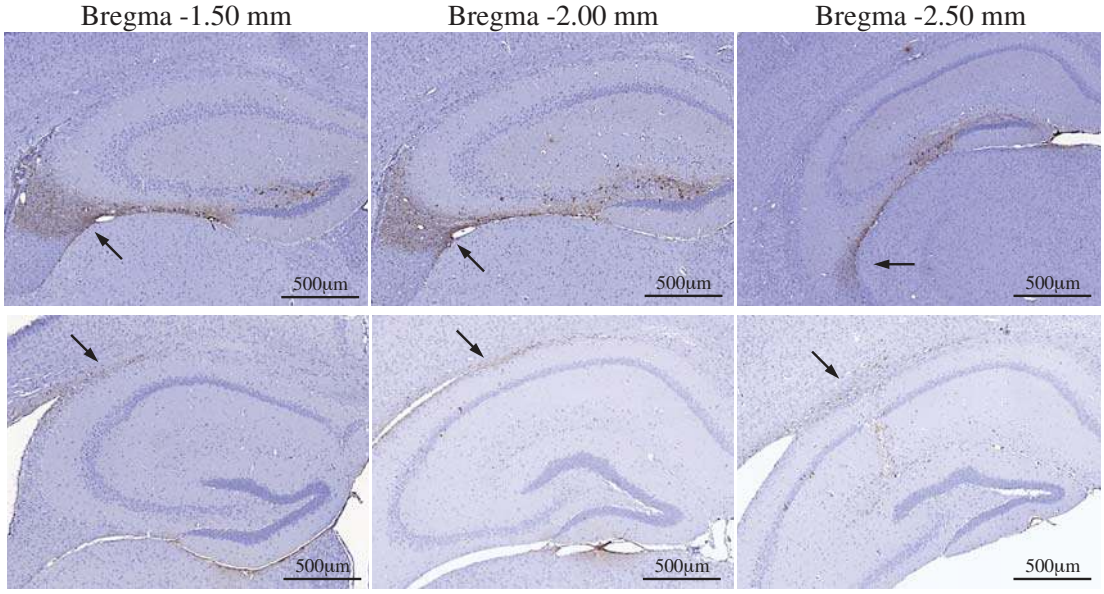

Figure 20. Tau aggregates in oligodendrocytes extended beyond the injection site already at 1 month post-injection. **a** Sagital view of mouse brain indicating the position of the bregma regions depicted in (b) **b** mAb AT8-positive aggregates in oligodendrocytes of white matter at the injection site (Bregma -2.50 mm) and rostral to the injection site (Bregma -2.00 mm and -1.50 mm). *Upper row*, tau pathology in fimbria is indicated by arrows; *lower row*, tau pathology in the alveus/external capsule is indicated by arrows. Scale bar, 500 µm.

Similar results were obtained when CBD-Tau from a second case with a confirmed CBD neuropathological diagnosis was injected in another cohort of mice (Table 14).

1.2 INJECTIONS OF AD-Tau

Next, AD-Tau and DSAD-Tau were injected into the brains of young PS19 mice, which also showed prominent tau pathology at 1 mo post-injection. Since the distribution of tau pathology in mice injected with AD-Tau and DSAD-Tau are very similar and the burden of AD pathology in both brains was similar, the data generated with these extracts were considered together as the AD/DSAD group.

In contrast to the CBD-Tau injected mice, the AD/DSAD-Tau injected mice showed tau pathology mainly in perikarya and processes of hippocampal neurons (Figure 21).

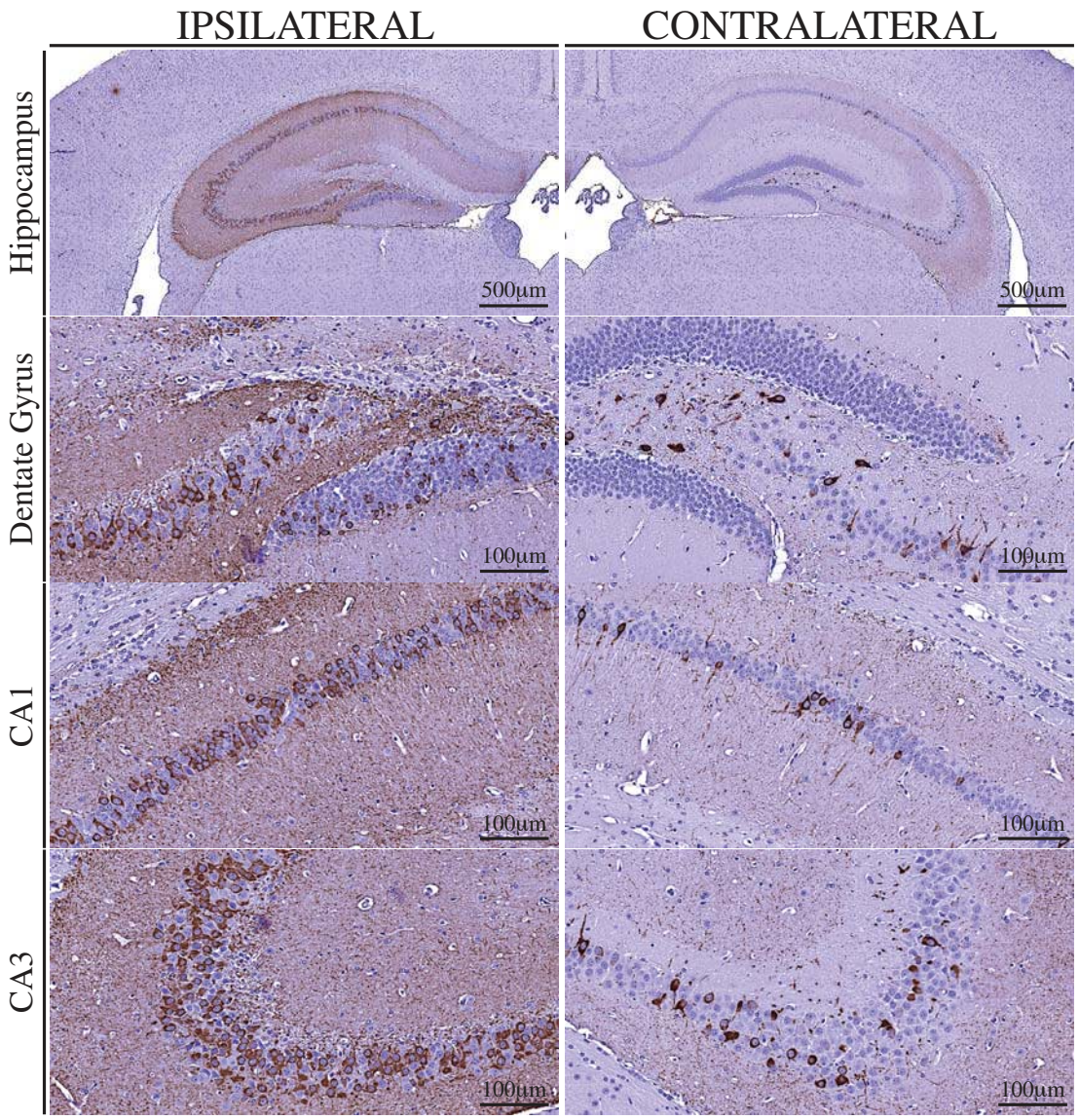

(*Previous page*) **Figure 21.** Tau pathology developed in the perikarya of neurons of the hippocampus of PS19 mice 1mo after the injection of AD/DSAD-Tau. The mice developed tau pathology both in the ipsilateral side of injection (*left column*), where pathology is most abundant, and in the contralateral side of injection (*right column*), where pathology is less profuse. *First row*, low magnification of the hippocampus where abundant tau-positive aggregates can be seen at the side of the injection (left) and, in lesser amount, at the contralateral side of injection (right); *second row*, higher magnification of the dentate gyrus and medial CA3 of ipsilateral side (left) and contralateral side (right); *third row*, higher magnification of CA1 of the ipsilateral side (left) and contralateral side (right); *fourth row*, higher magnification of the CA3 region of the ipsilateral side of the injection (left) and contralateral side (right). AT8 immunostaining. Scale bar, first row 500 μm; second to fourth row, 100 μm.

Mapping the spread of pathological tau from the hippocampal injection site in the AD/DSAD-Tau injected mice demonstrated that the tau pathology extended to rostral and caudal regions of the brain already at 1 mo after injection (Figure 26b). In rostral areas, lateral septal nuclei were involved bilaterally with a moderate burden of tau inclusions in the processes of neurons. In caudal brain regions such as the subiculum, entorhinal cortex (EC), locus coeruleus (LC) and raphe nuclei, there also were AT8 positive neuronal aggregates (Figure 22). Additionally, intracytoplasmic hyperphosphorylated tau inclusions were seen in the supramammillary nuclei (5/8; 63% of mice) and in neocortex (4/8; 50% of mice) (Figure 22).

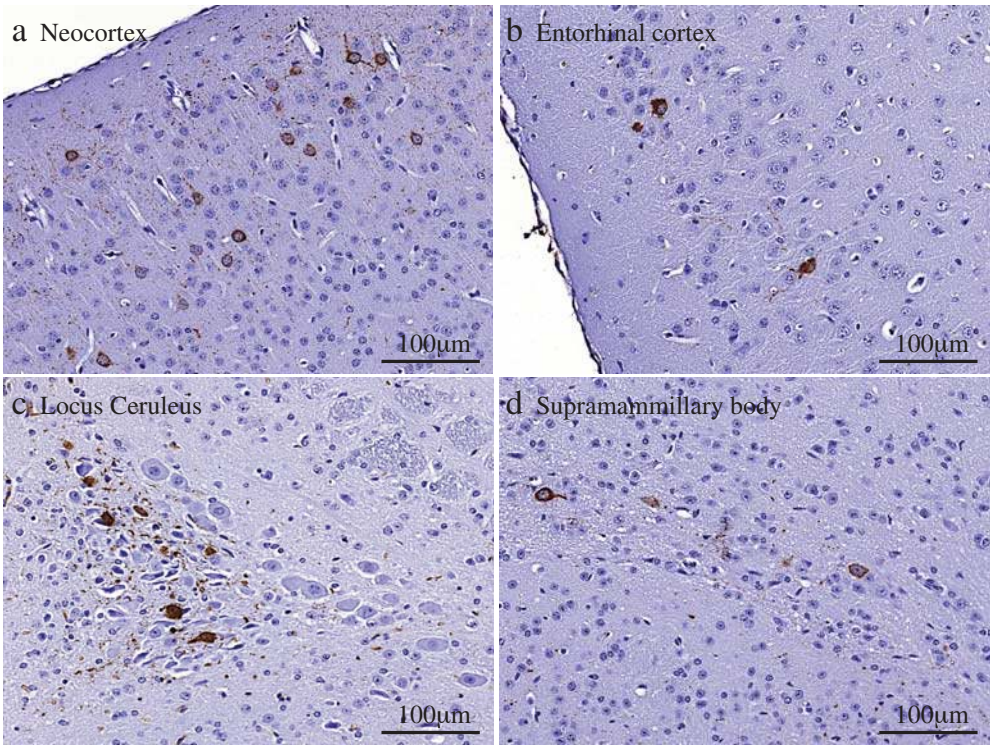

Figure 22. PS19 Tg mice developed AT8-positive neuronal aggregates in the neocortex (**a**) and in regions distant from the injection site including entorhinal cortex (**b**), locus ceruleus (**c**) and supramammillary body (**d**). All of the regions depicted are from the side of the injection. Scale bar, 100 μm

Moreover, neuronal tau inclusion pathology was seen in the contralateral hemisphere where it was mainly limited to hippocampal neurons (Figures 21 and 26b), with a predominance of involvement of CA3 region, and a few AT8 positive neurons in the EC. As in the ipsilateral side, intraneuronal tau pathology of the contralateral side of injection extended to rostral and caudal regions of the brain (Figure 26b).

Notably, no oligodendrocytic tau pathology was seen 1 mo post-injection in the fimbria or the subcortical white matter/external capsule following AD/DSAD-Tau injections.

1.3 INJECTIONS OF CTRL-Tau

As noted above, the non-injected PS19 mice begin to show transgene driven tau pathology at ~12 mo of age (229). To control for this onset of transgene driven tau pathology, four young (2-3 mo old) PS19 mice were injected with CTRL-Tau intracerebrally and these mice did not show any tau pathology at 1 or 6 mo post-injection (Figure 23).

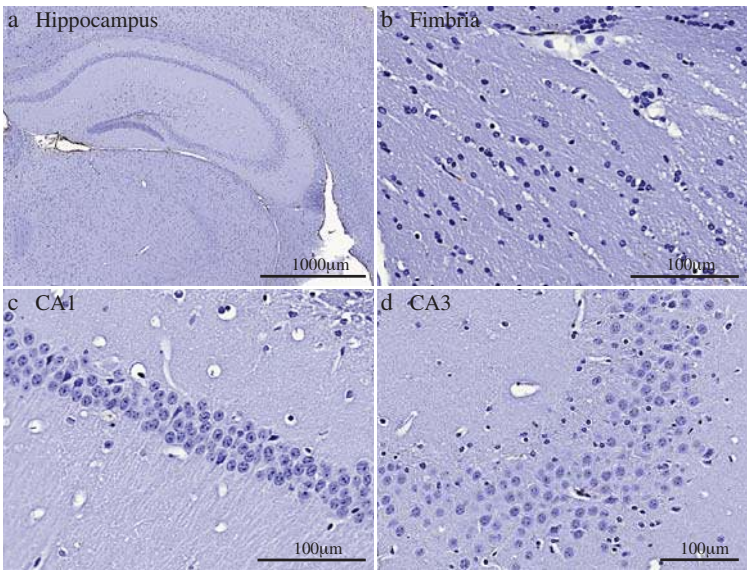

Figure 23. There is absence of pathological tau aggregates in PS19 tau Tg mice injected with CTRL-tau at 6 mo after injection. Microphotographs of histological brain sections showing (**a)** low power view of the hippocampus, **b-c** High power view of **(b)** fimbria, (**c)** CA1 and (**d)** CA3. All of the regions depicted are from the side of injection. AT8 immunostaining. Scale bar, in **a** 1000μm, in **b,c** and **d**, 100 μm.

Finally, none of the CBD-Tau or AD/DSAD-Tau injected PS19 mice showed any evidence of α-synuclein, TDP-43 or β-amyloid pathology despite the fact that these pathologies co-occur in AD/DSAD brains (data not shown) (266–268).

2. TAU PATHOLOGY INDUCED BY CBD-Tau AND AD/DSAD-Tau INJECTIONS INTO YOUNG PS19 MICE SPREAD AND INCREASE WITH TIME

I assessed the progression of transmission of tau pathology with increasing survival times in PS19 tau Tg mice following intracerebral injections of CBD-Tau and AD/DSAD-Tau.

2.1 INJECTIONS OF CBD-Tau

The remarkable oligodendroglial tau pathology seen at 1 mo post-injection in the CBD-Tau injected Tg mice increased in the fimbria near and distal to the injection site at 3 mo, and more so at 6 mo post-injection (Figure 24). Despite the variability in the burden of this oligodendroglial tau pathology, the PS19 mice that survived for 3 and 6 mo post-injection displayed a clear increase in oligodendroglial tau pathology with time.

(*Following page*) **Figure 24**. Tau inclusions that developed in PS19 mice injected with CBD-Tau increased in intensity and spread to regions distal from the injection site with increasing post-injection survival times. **a** Microphotographs of brain sections immunostained with AT8 showing the fimbria, alveus/external capsule and stratum radiatum ipsilateral to the injection site in the PS19 mice at 1, 3, 6 mo post-injection. Scale bar, upper row, 200 μm; middle and lower rows, 100 μm. **b** Heatmaps of coronal sections showing the CBD-Tau induced glial tau pathology at the same time points as in (**a**). Quantification [1 mo (n=6), 3 mo (n=6) and 6 mo (n=6)] was conducted as described in Methods to generate these heatmaps. Each heatmap panel represents pathology distribution in one of the three coronal planes (Bregma, -1.22, -2.18 and -2.92). Left column shows sagittal view of the selected coronal planes indicated by a red line. Blue stars indicate injection site.

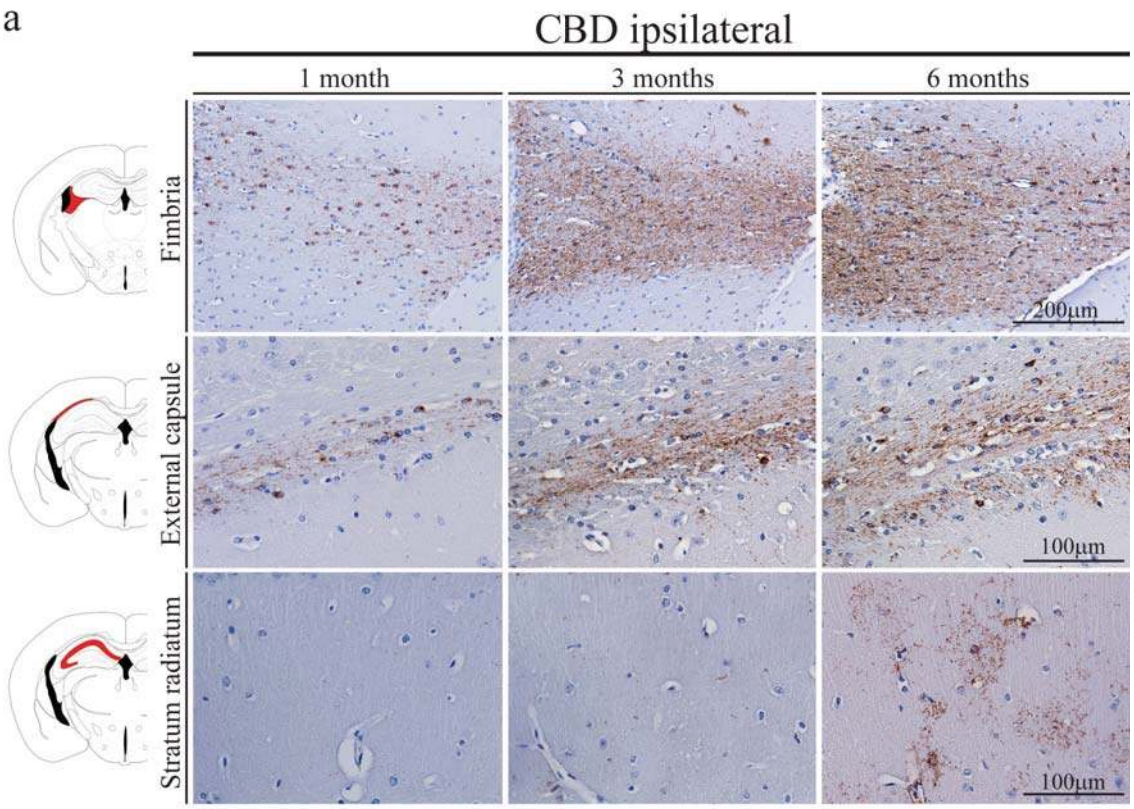
a
CBD ipsilateral
1 month
3 months
6 months
Fimbria
External capsule
Stratum radiatum
200µm
100µm
100µm

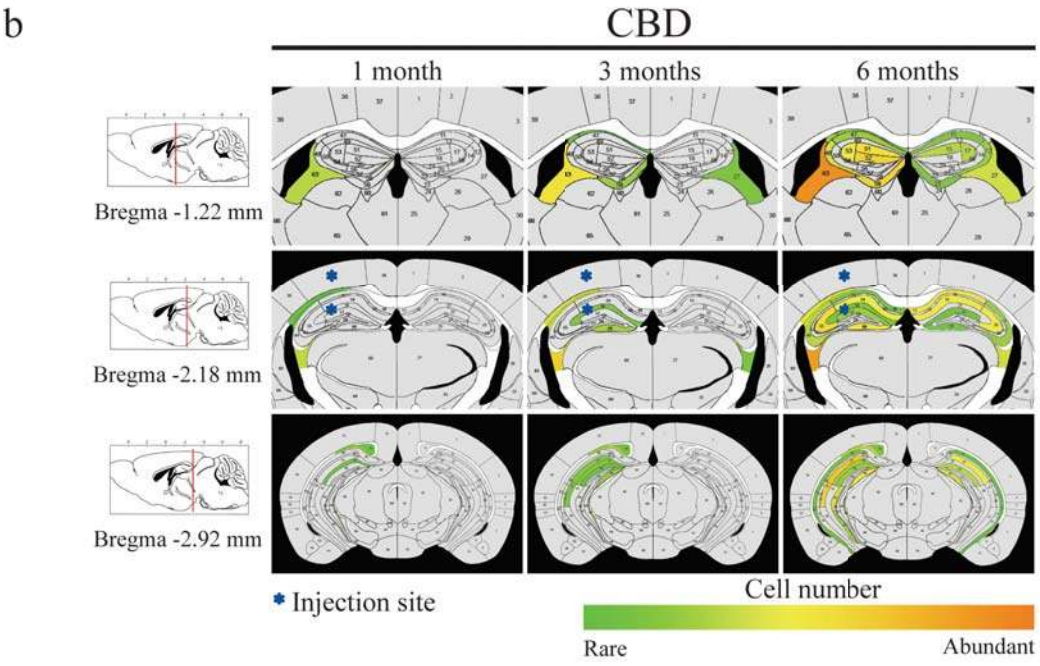
b
CBD
1 month
3 months
6 months
Bregma -1.22 mm
Bregma -2.18 mm
Bregma -2.92 mm
Injection site
Cell number
Rare
Abundant

Additionally, oligodendrocytic tau pathology spread to the contralateral fimbria although it was not as abundant as on the ipsilateral side (Figures 24b and 25). At 6 mo post-injection, astrocytic-like plaques that closely resemble those seen in authentic human CBD brains were prominent in the stratum radiatum of the hippocampus in both hemispheres (Figures 24a and 25)

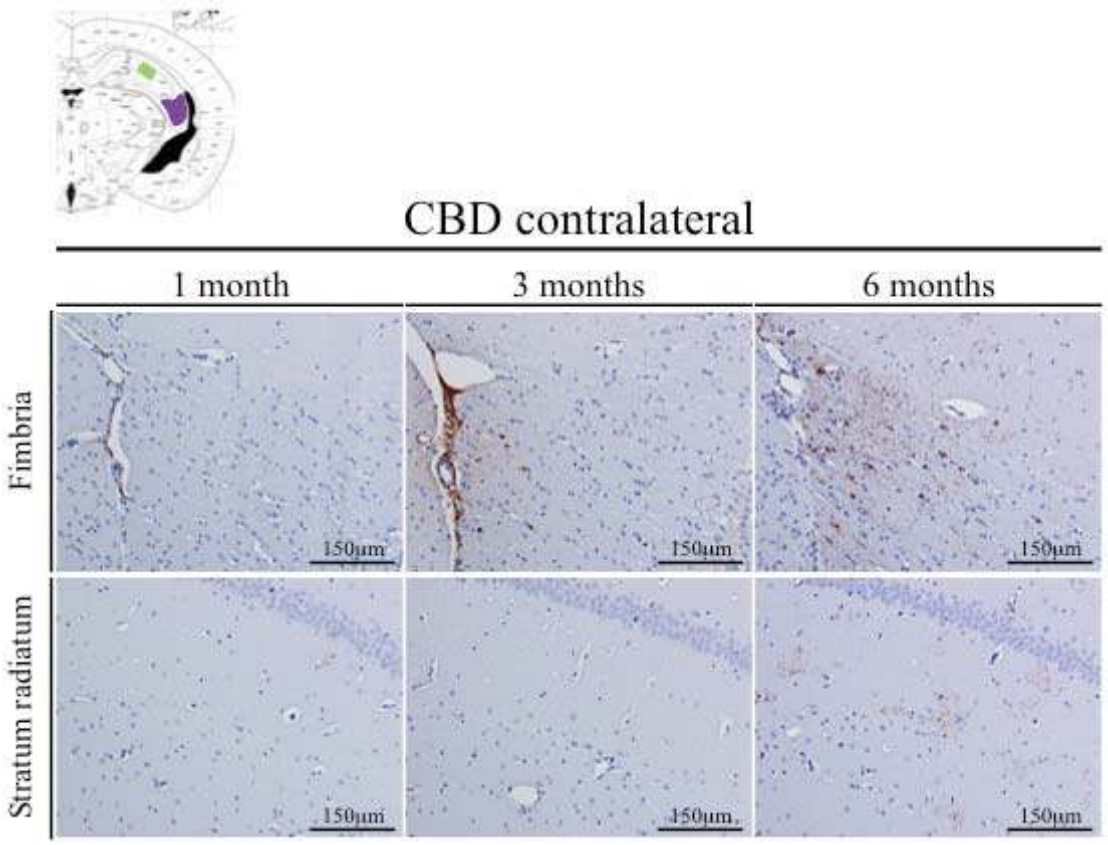

Figure 25. Microphotographs of brain sections immunostained with AT8 showing the fimbria and stratum radiatum of the contralateral hemisphere of the injection side in the PS19 mice at 1, 3 and 6 mo post-injection. Scale bar, 150 μm.

2.2 INJECTIONS OF AD-/DSAD-Tau

Similarly, PS19 tau Tg mice injected with AD/DSAD-Tau showed an increase in the neuronal tau pathology burden as well as prominent spread to regions quite distal from the injection site with increasing post-injection survival times (Figure 26). However, this pattern of neuronal spread, which is consistent with intra-axonal transmission, differed dramatically from the pattern of glial tau pathology spread seen following the CBD-Tau injections, suggestive of a different mode of transmission that

does not depend on the axonal afferents and efferents of the injection sites like the AD/DSAD-Tau injections.

At 3 mo post-injection, there was an increase of the pathology in the regions that were already involved at 1 mo post-injection. In the ipsilateral side, the dentate gyrus (DG) showed an increase in neuronal tau pathology at 3 mo that seemed to plateau at 6 mo. In the CA1 region, there was variability in the burden of intraneuronal tau inclusions at 1 mo post-injection, but there was a decrease of pathology from 3 to 6 mo post-injection. CA3 tau pathology also decreased from 1 to 6 mo post-injection (Figure 26).

In the contralateral hemisphere, hippocampal tau inclusions were less numerous, but they showed an increase in quantity with time in DG and CA1, while a reduction of tau pathology was observed in the CA3 region (Figure 27).

Additionally, in keeping with the interpretation that the spread of AD/DSAD-Tau induced tau pathology occurs through intra-axonal transport, tau pathology was seen in other regions that have neuronal connections with the hippocampus and that were not involved at earlier stages such as the thalamus, mammillary nuclei and other hypothalamic nuclei (Figure 26b).

(*Following page*) **Figure 26.** Neuronal tau inclusions developed in PS19 mice injected with AD-Tau and DSAD-Tau and they increased in abundance, intensity and spread to regions distal from the injected site with increasing post-injection survival times. **a** Microscopic images of brain sections of DSAD-Tau injected mice. The images are representative of the dentate gyrus, CA1 and entorhinal cortex of the side ipsilateral to the injection following IHC with AT8 at 1, 3, 6 mo post-injection. Scale bars, 75μm. **b** Heatmaps of coronal sections of tau pathology seen after injection at the same time points as in (**a**). Semiquantitative analysis of AT8 pathology was performed in AD-Tau and DSAD-Tau injected mice and combined in the heatmap here [1 mo (n=8), 3 mo (n=8) and 6 mo (n=8)]. Each panel represents pathology distribution in one of the five coronal planes (Bregma, 0.98, -1.22 -2.18, -2.92 and -4.48mm) at the different time points after injection. Left column shows sagittal view of the selected coronal planes that are indicated by a red line. Blue stars indicate injection site.

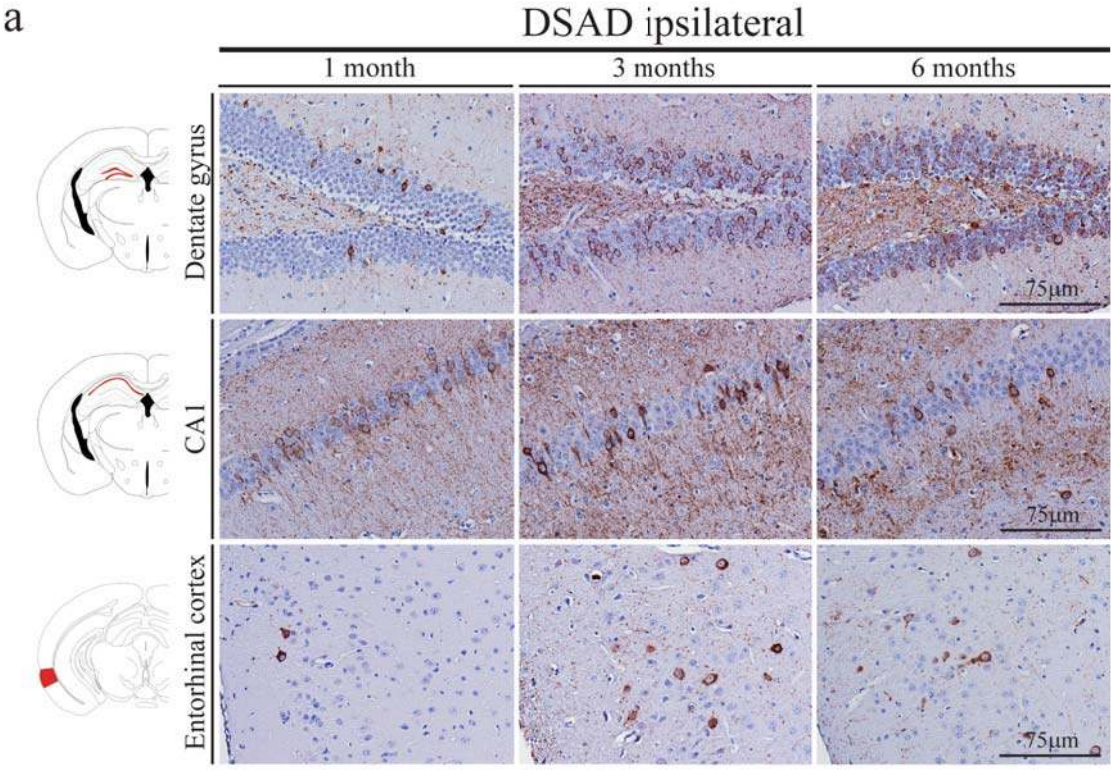
a
DSAD ipsilateral
1 month
3 months
6 months
Dentate gyrus
CA1
Entorhinal cortex
75µm
75µm
75µm

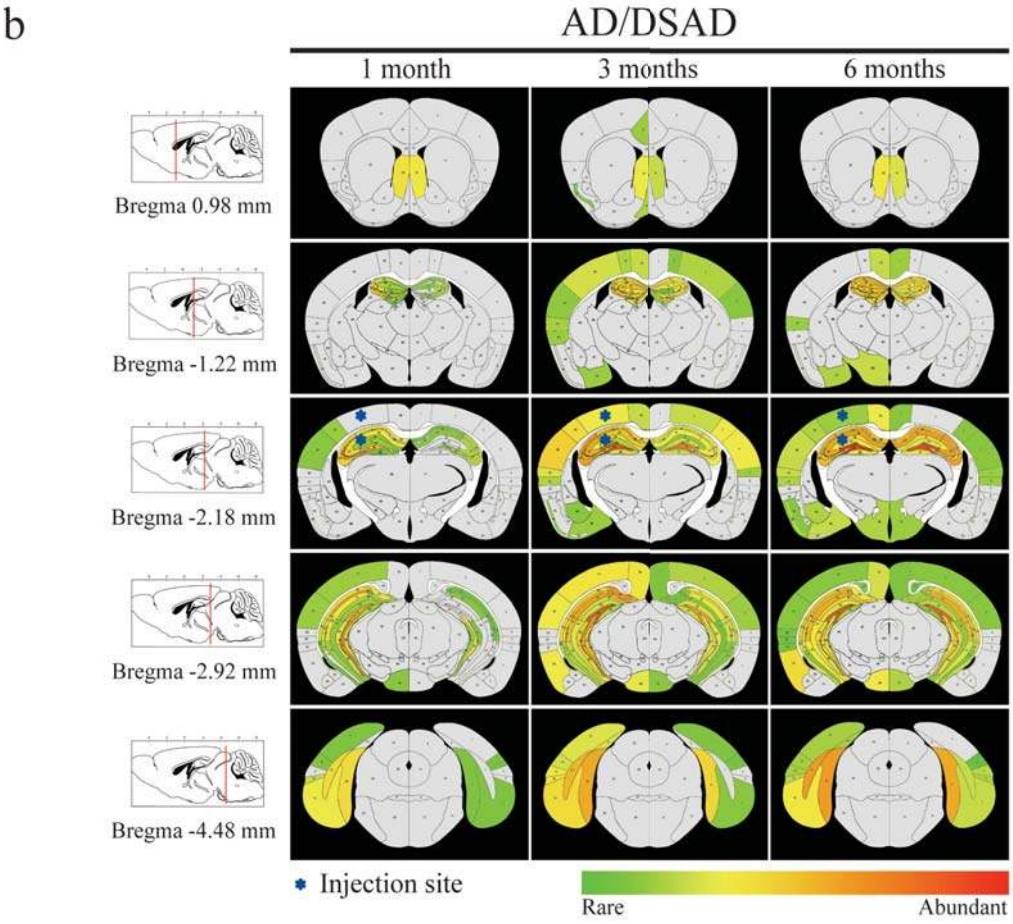
b
AD/DSAD
1 month
3 months
6 months
Bregma 0.98 mm
Bregma -1.22 mm
Bregma -2.18 mm
Bregma -2.92 mm
Bregma -4.48 mm
Injection site
Rare
Abundant

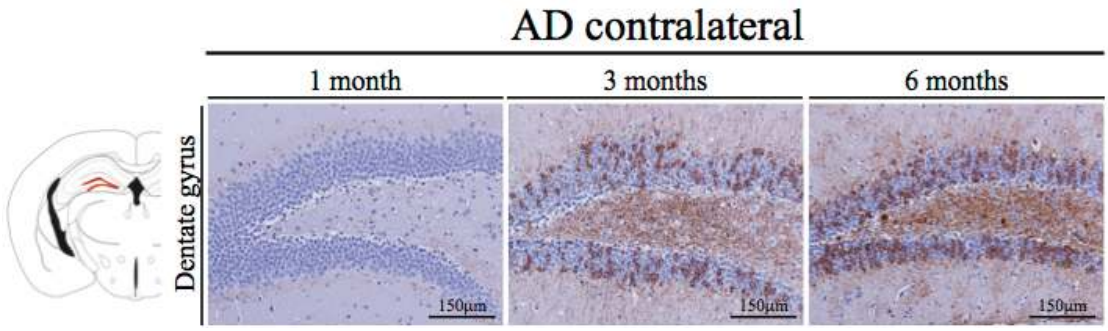

Figure 27. Tau pathology in the contralateral DG after the injection of AD-Tau increases from 1 to 6 mo after injection. Microphotographs of the DG of the contralateral side of the injection site at 1mo, 3mo and 6mo after injection. AT8 immunostaining. Scale bars, 150 μm.

At 3 mo post-injection, neocortical neurons were involved in all of the AD/DSAD-Tau injected mice. Additionally, some tau pathology appeared in white matter tracts with involvement of the fimbria and the dorsal hippocampal commissure at 3 mo, and this pathology increased at 6 mo post-injection where it appeared to be in astrocytes and oligodendroglia, but it never approached the abundance of the glial tau pathology induced by the CBD-Tau injections (data not shown).

At 6 mo post-injection there was a decrease in NFT pathology in many of the affected areas in the AD/DSAD-Tau injected mice.

3. TAU PATHOLOGY INDUCED BY AD/DSAD-Tau, BUT NOT CBD-Tau INJECTIONS INTO YOUNG PS19 MICE RESULTS IN NEURON LOSS WITH TIME

To determine if the decreasing NFT pathology seen in the hippocampal region of AD/DSAD-Tau injected PS19 mice may be due to neuron loss, I quantified the number of CA3 neurons using digital micrography. The quantification was done on the side contralateral to the injection site to avoid possible artifact as a consequence of damage from the injection. As shown in Figure 28, fewer neurons were seen in CA3 at the 1 to 3 mo post-injection time period compared to controls, but this loss of neurons did not progress further as it stabilized at the 6 mo post-injection survival time [138±6 cell, 74±7 neurons and 69±3 neurons at 1, 3 and 6 mo

respectively; p<0.001; (Figure 28b)]. In marked contrast, no neuron loss was seen in mice injected with CBD-Tau (128±5 neurons, 126±5 neurons, 129±9 neurons at 1, 3 and 6 mo respectively) or CTRL-Tau injected mice (129 neurons, 130±9 neurons at 1 and 6 mo respectively). More substantial neuron loss has been reported following injections of very high amounts of tau PFFs (231).

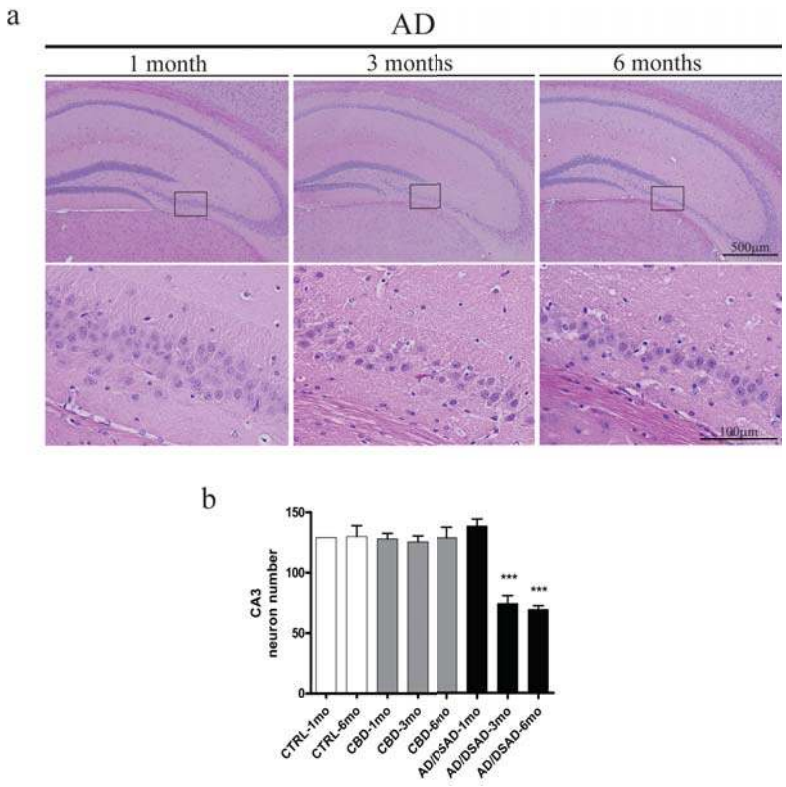

Figure 28. There is neuron loss in the CA3 region of PS19 mice injected with AD-Tau and DSAD-Tau at 3 and 6 mo post-injection. **a** The upper row of images show H&E stained low power microphotographs of the hippocampus contralateral to the AD-Tau injection in PS19 mice at 1, 3, and 6 mo post-injection. The microphotographs in the lower row show higher magnification images of the boxed areas in the upper row. Scale bar, upper row, 500 mm; lower row, 100 mm. **b** Quantification of the neurons in the CA3 region of PS19 mice injected with non-pathological or control (CTRL-Tau) human brain extract versus enriched CBD-Tau or AD-Tau and DSAD-Tau fractions. Error bars indicate SEM; *** p<0.001, as determined by one-way ANOVA and Tukey's multiple-comparison test, with n=2 in CTRL-Tau at 1 mo and 6 mo; n=5 in CBD-Tau at 1 mo and 3 mo; n=6 in CBD-Tau at 6 mo; and n=7 in AD/DSAD-Tau at 1 mo, 3 mo and 6 mo.

I also investigated whether the observed neuron loss was accompanied by inflammatory reaction. For this, I analyzed contiguous sections with immunohistochemistry using an astrocytic specific antibody (GFAP) and a microglial specific antibody (Iba1). There was increase in the number of reactive astrocytes at 3 and 6 moths after the injection of AD/DSAD-Tau in the CA3 region contralateral to

the injection site but not after the injection of CBD-Tau or CTRL-Tau at any time point (Figure 29a). However, the increase of microglial cells was not as obvious and, compared to the CTRL-Tau and CBD-Tau injected mice where no microgliosis was seen at any of the time points, only a slight increase of microglial cells was observed at 3 mo after the injection of AD/DSAD-Tau but not at 1mo or 6mo after the injection (Figure 29b).

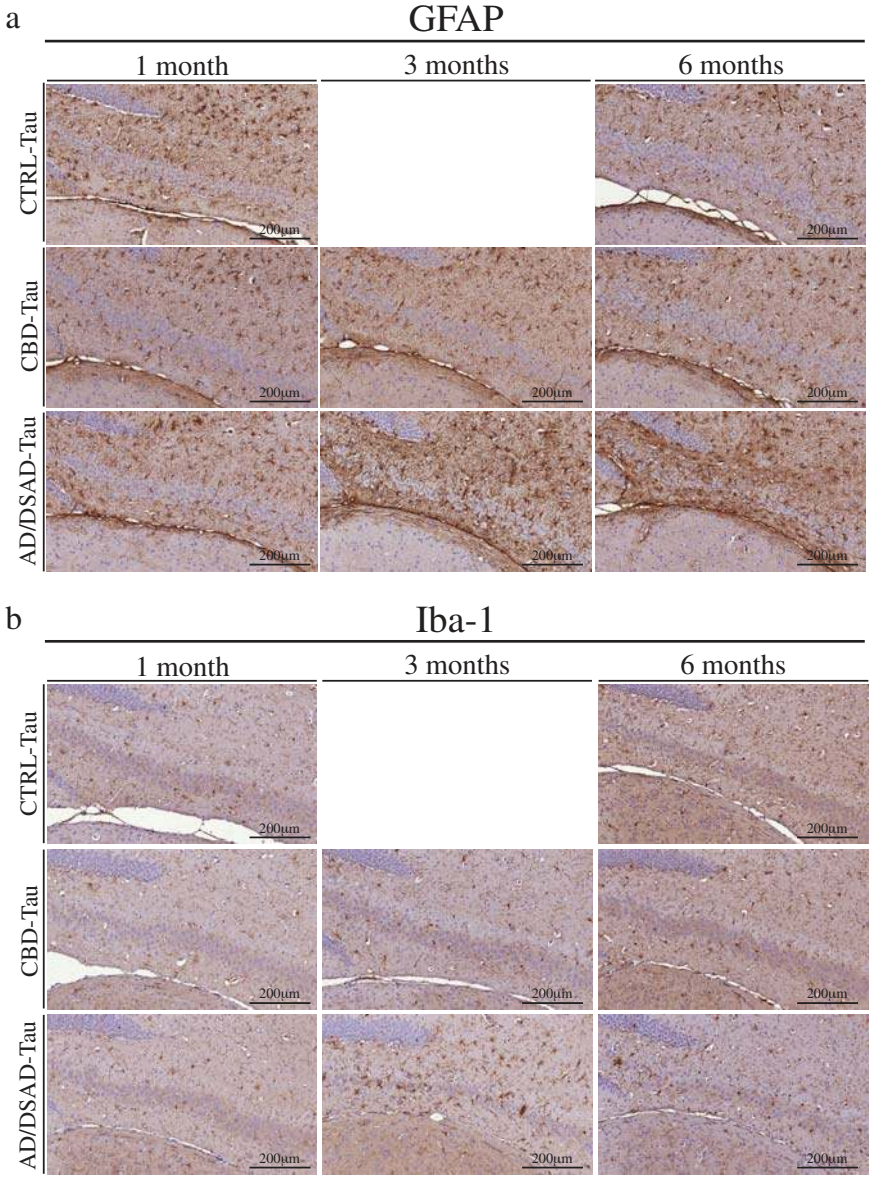

Figure 29. Presence of astrogliosis and slight microgliosis after the injection of AD/DSAD-Tau into PS19 mice but no changes are seen after injection of CBD-Tau or CTRL-Tau. **a** Microphotographs of GFAP immunohistochemistry of the CA3 region at the contralateral side of injection at 1 mo, 3 mo and 6 mo after injection of CTRL-Tau, CBD-Tau and AD/DSAD-Tau. **b** Microphotographs of Iba-1 immunohistochemical staining of the CA3 region at the contralateral side of injection at 1 mo, 3 mo and 6 mo after injection of CTRL-Tau, CBD-Tau and AD/DSAD-Tau. Scale bar, 200 µm.

4. THE BURDEN AND DISTRIBUTION OF DSAD-Tau INDUCED TAU PATHOLOGY IS DOSE DEPENDENT

The abundance of neuronal tau inclusions induced in the PS19 mice with synthetic tau PFFs injections was not only time dependent as described above, but following injections of increasing amounts of recombinant P301S mutant human T40 tau (T40/PS) PFFs, the induced pathology increased in a dose dependent manner as well (229). Thus, I investigated this dose dependency here by injecting serially diluted DSAD-Tau into the hippocampus and overlying neocortex of PS19 mice (Table 3) and analyzing the tau pathology at 1 mo after injection. As shown in Figure 30 (a and c), at the lowest concentration of injected DSAD-Tau, only the ipsilateral hippocampus showed induced tau pathology. AT8 positive inclusions in the perikarya of neurons of dentate gyrus, CA3 and CA1 were seen at the injection site at all injected DSAD-Tau concentrations. The burden of tau pathology in the hippocampus increased with increasing concentrations of injected pathological tau with other regions of the brain becoming involved with increasing DSAD-Tau concentrations (Figure 30). Rostral and caudal regions of the hippocampus of the ipsilateral side were also involved at all injected concentrations and increased in a dose dependent manner, as did the involvement of the contralateral hemisphere. Hence, at the lowest concentrations of DSAD-Tau, there was no tau pathology on the contralateral side of the PS19 injected mice, while higher concentrations of injected pathological tau induced more tau pathology in the contralateral CA3 region (Figure 30c). In sharp contrast to the CBD-Tau injected at 1 mo post-injection, there was no tau pathology in the ipsilateral or contralateral white matter tracts at any concentration of injected DSAD-Tau at 1 mo post-injection.

(*Following page*) **Figure 30.** Dose dependent increase in tau pathology in PS19 mice after the injection of human brain derived DSAD-Tau. At 1 mo after injection, the burden of tau pathology increases and the distribution of pathology is more extensive throughout brain structures following injections of increasing amounts of injected pathological tau. **a** Microphotographs of hippocampus and cortex stained with mAb AT8 after the injection of serial dilutions of DSAD-Tau into PS19 mice. Scale bars, *upper row* 500 μm; *lower row*, 50 μm. **b** Quantification of AT8 immunoreactive neurons in the hippocampus of PS19 mice injected with serial dilutions of DSAD-Tau fractions. Error bars indicate SEM; n=3 for each dose of DSAD-Tau (0.065 μg, 0.25 μg, 1.50 μg. 12.5 μg) **c** Heatmaps of coronal sections of tau pathology after injections of serial dilutions of DSAD-Tau into PS19 mice. Each panel represents pathology distribution in one of the five coronal planes (Bregma, 0.98, -1.22 -2.18, -2.92 and -4.48mm) at 1 mo post-injection (n=3 for each dose of DSAD-Tau). Left column shows sagittal view of the selected coronal planes that are indicated by a red line. Blue stars indicate injection site.

a

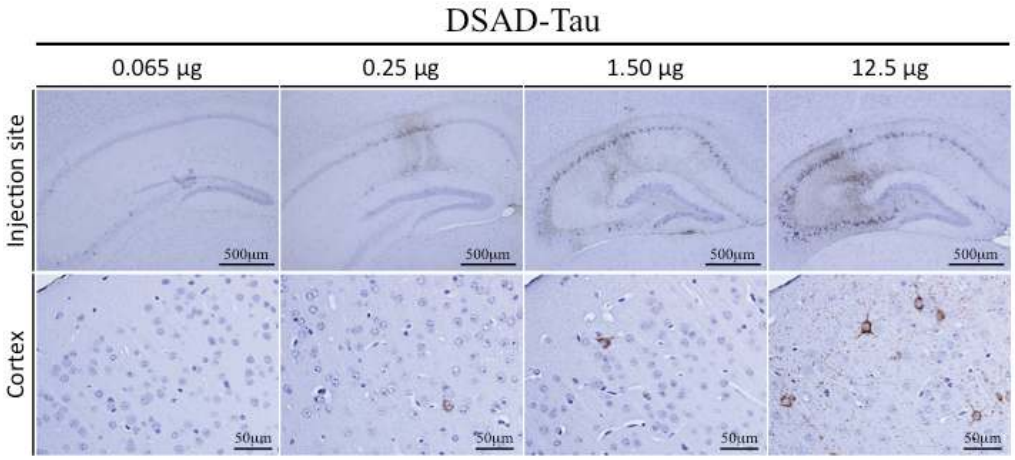
DSAD-Tau
0.065 µg
0.25 µg
1.50 µg
12.5 µg
Injection site
Cortex
500µm
50µm

b

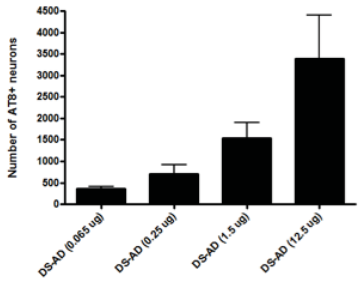
Number of AT8+ neurons
4500
4000
3500
3000
2500
2000
1500
1000
500
0
DS-AD (0.065 ug)
DS-AD (0.25 ug)
DS-AD (1.5 ug)
DS-AD (12.5 ug)

c

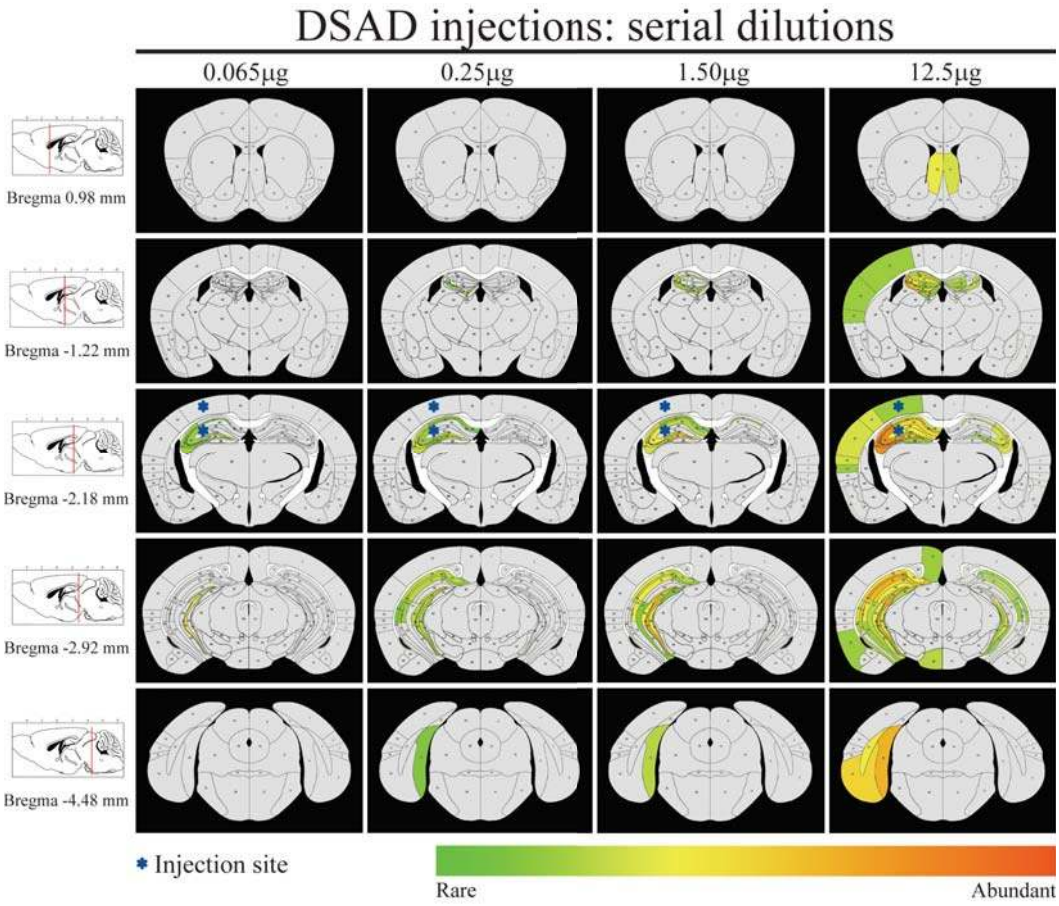
DSAD injections: serial dilutions
0.065µg
0.25µg
1.50µg
12.5µg
Bregma 0.98 mm
Bregma -1.22 mm
Bregma -2.18 mm
Bregma -2.92 mm
Bregma -4.48 mm
Injection site
Rare
Abundant

5. CBD-Tau AND AD/DSAD-Tau INDUCED TAU PATHOLOGY ACQUIRES THE KEY CHARACTERISTICS OF THEIR HUMAN COUNTERPARTS

I further characterized the nature of the CBD-Tau and AD/DSAD-Tau induced tau pathology in PS19 mice by performing IHC using anti-tau mAbs to pathological tau that detect human CBD and AD tau pathology. IHC with MC1 and TG3 showed that tau inclusions induced by CBD-Tau were modestly positive for both mAbs at 1 mo post-injection, but detected more intense and abundant tau pathology at 3 mo which increased further by 6 mo post-injection (Figure 31). By contrast, AD/DSAD-Tau induced tau pathology was intensely immunoreactive for both MC1 and TG3 already at 1 mo post-injection.

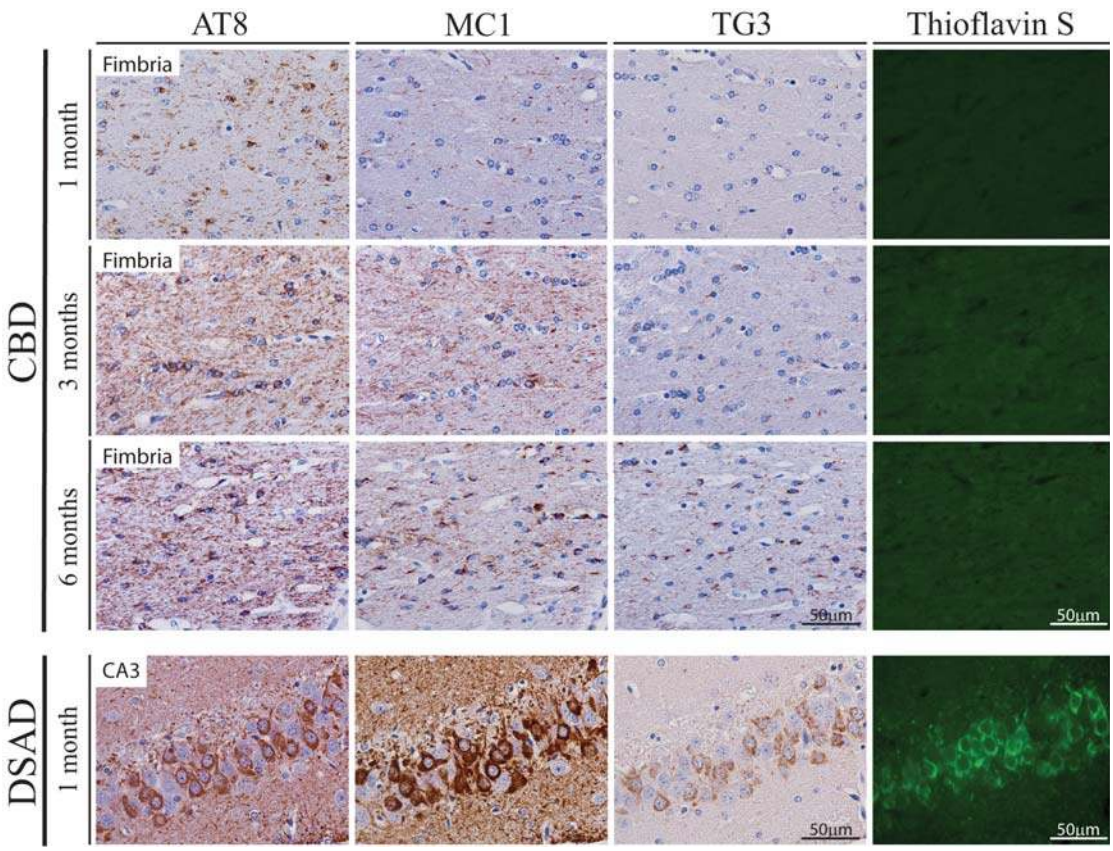

Figure 31. Tau inclusions in PS19 mice after injection of CBD-Tau and DSAD-Tau show properties that recapitulate their human disease counterparts. Microphotographs are of brain sections stained with mAbs AT8, MC1 and TG3 to detect abnormal phosphorylation (AT8) and conformational (MC1, TG3) changes in pathological tau and ThS histochemistry to demonstrate the amyloid properties of the inclusions. Shown here are the fimbria of Tg mice injected with CBD-Tau at 1mo, 3 mo and 6 mo postinjection (upper three rows) and CA3 of Tg mice injected with DSAD-Tau extracts at 1 mo after injection (lower row). Scale bars: 50 μm.

Since AD NFTs are detected by amyloid-binding dyes such as ThS, while tau inclusions in CBD cases are ThS negative (268), I asked if these properties of tau aggregates persisted in our PS19 mice following injections with CBD-Tau and AD/DSAD-Tau. Remarkably, the tau pathology in mice, injected with human-derived CBD-Tau that were AT8 positive, did not show ThS positivity, even at 6 mo after injection, however, tau inclusions appearing only 1 mo post-injection with AD/DSAD-Tau were detected by ThS (Figure 31). Thus, human CBD-Tau and AD/DSAD-Tau templated and propagated tau pathology in the injected PS19 mice that showed compelling immunological and histochemical verisimilitude to their human counterparts.

Further evidence of this verisimilitude came from double immunoflourescence studies showing that the CBD-Tau induced pathology were double labeled with AT8 and Olig2 mAbs confirming the oligodendroglial nature of this oligodendroglial tau pathology while the astrocytic plaques induced by the CBD-Tau showed partial or incomplete co-localization of AT8 and GFAP similar to what is seen in the astrocytic plaques of human CBD (Figure 32) as described (269).

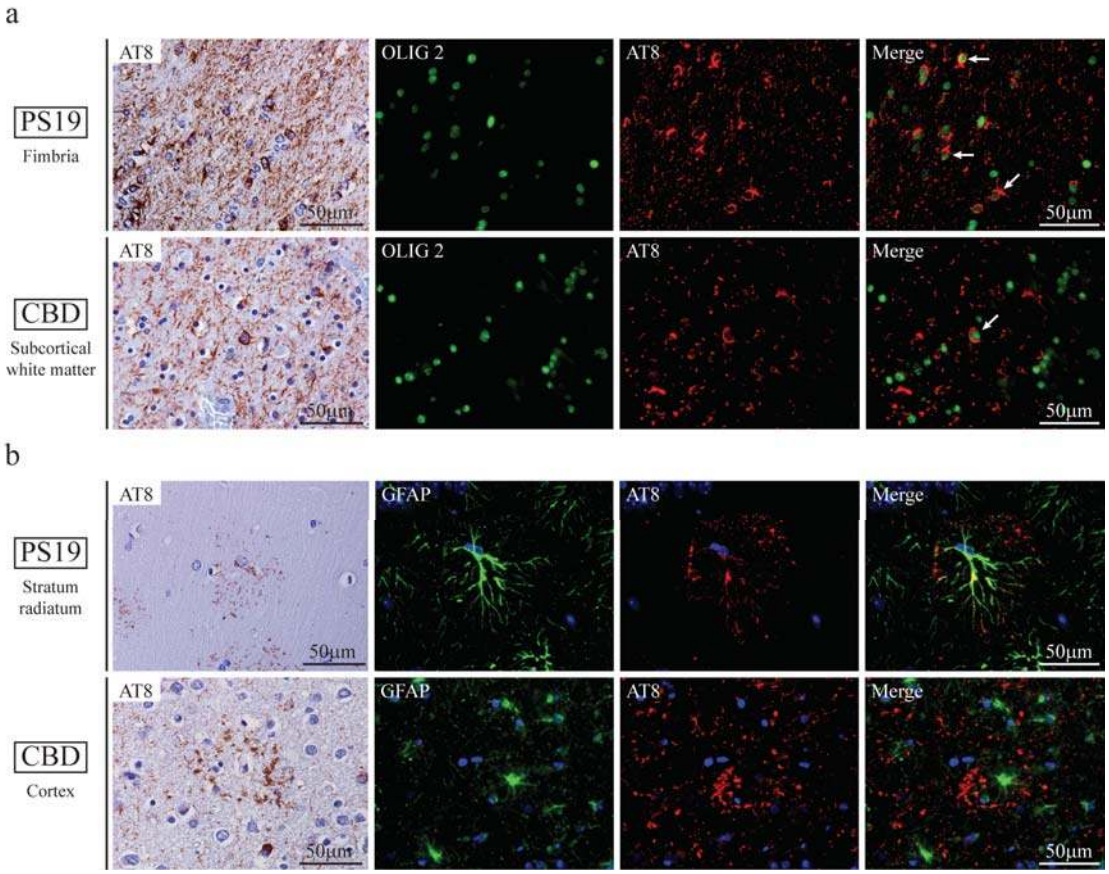

(*Previous page*) **Figure 32.** Accumulation of tau pathology in oligodendrocytes and astrocytes in PS19 mice injected with CBD-Tau parallels pathology of sporadic CBD in humans. **a** Brain sections stained with mAb AT8 in the far left column, while the 3 columns to the right show double immunofluorescence with Olig2 (green), AT8 (red) and merged images in the fimbria of a PS19 mouse 6 mo after injection (upper row) and subcortical white matter of the cingulate gyrus in a sporadic CBD case (lower row). **b** Brain sections stained with mAb AT8 and double immunofluorescence with GFAP (green), AT8 (red) and merged images in the stratum radiatum of the hippocampus of a PS19 mouse 6 mo after injection (upper row) and grey matter of the parietal cortex of a sporadic CBD case (lower row). Scale bar: 50 mm.

I also wanted to evaluate whether the tau-induced pathology was assembled with only the overexpressed human tau of the PS19 Tg mice or endogenous mouse tau was also part of the aggregates that these mice developed. Notably, human (T14) and mouse (T49) specific anti-tau mAbs stained all of the tau pathologies described above (Figure 33) including tau in oligodendrocytes in CBD and tau in neurons in AD/DSAD.

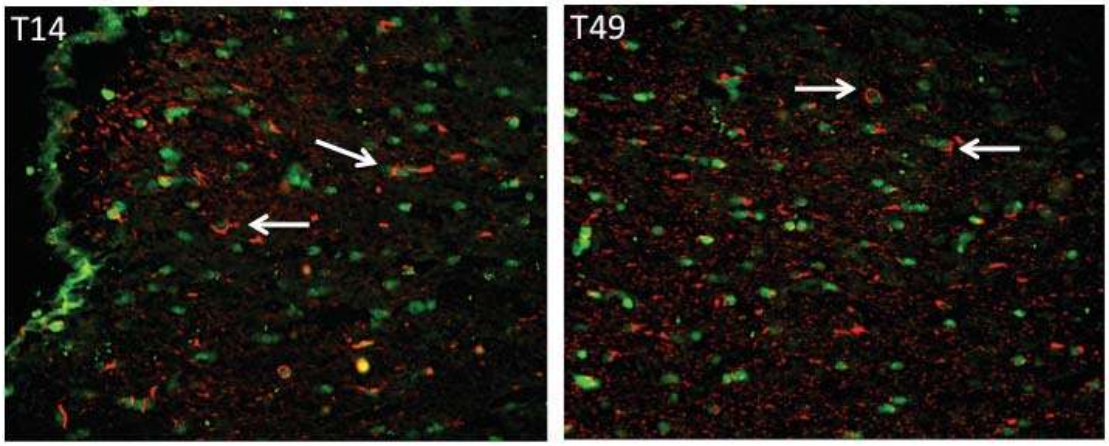

Figure 33. The tau inclusions that developed in PS19 mice after injection of CBD-Tau recruit both the overexpressed human tau and endogenous mouse tau. Microphotographs with double labeling of pAb Olig2 (green) (*left*), specific for oligodendrocytes and mAb T14 (red) (*right*), specific for human tau or mAb T49 (red) specific for mouse tau.

DISCUSSION

Alzheimer's disease (AD), corticobasal degeneration (CBD), progressive supranuclear palsy (PSP), argyrophilic grain disease (AGD) and Pick's disease (PiD) are a group of diseases included in the tauopathies which hallmark lesion is the intracellular aggregates of tau protein. Interestingly, even though these diseases have a common protein as the basis of the disorder each of them manifest with diverse clinical features as well as with distinct topographic and cell type-specific distribution of the pathology (27). Thus tau aggregates can develop in neurons or glial cells, the pathology can affect grey matter only or involve grey and white matter, and be predominant in cortical regions or in brainstem and subcortical nuclei.

In AD, tau aggregates accumulate in a hierarchical stereotypical pattern with pathology first appearing in LC and EC, followed by the hippocampus and limbic areas to finally involve the neocortex (179). This predictable sequential dissemination of the disease together with the observation that pathology involved synaptically interconnected brain regions suggested a cell-to-cell transmission mechanism for disease progression (212). Transmission of tau pathology *in vitro* was demonstrated initially using AD brain extracts that induced formation of PHFs in cultured fetal neurons (213) and later used synthetic tau PFFs to induce the templated conversion of intracellular soluble tau into fibrillar aggregates in cultured cells (214,215). *In vivo* studies showed that inoculation of brain homogenates from mutant tau Tg mice (that form NFTs) into the brains of WT tau expressing ALZ17 mice (that do not form tau inclusions) induced the formation of tau inclusions in the ALZ17 Tg mice (226). Iba et al. (229) demonstrated that synthetic tau fibrils injected into a PS19 tauopathy model is sufficient to induce and propagate AD-like tau pathology. Altogether, it was established that fibrillar species of tau are capable of recruiting and converting endogenous soluble tau into pathological aggregates in neurons and neuronal processes in vivo and that these pathological aggregates could transmit from one cell to the other resulting in development and advancing of pathology.

In this study, I investigated whether extracts enriched with pathological tau obtained from CBD or AD and DSAD human brains induced tau pathology in PS19 mice and whether the developed pathology would be similar to the CBD and AD tau pathology developed in human brains, respectively. For this, brain extracts enriched in CBD-Tau, AD-Tau or DSAD-Tau were injected into the cortex and hippocampus

of a Tg mouse model (line PS19) overexpressing P301S mutant human 1N4R tau and the pathology at different timepoints (1 mo, 3 mo and 6 mo) was evaluated. Interestingly, tau pathology rapidly developed in the mice, already at 1mo after injection intracellular tau aggregates were noted in all injected mice. Tau pathology was observed at the injection site and also distant from the injection site. With these results, the studies of Clavaguera et al. (233) were corroborated demonstrating that not only recombinant PFFs and mutated forms of human tau obtained from a Tg mouse brain can induce tau pathology but also enriched tau extracts from pathological human brain tissue were able to induce tau pathology in Tg mouse models. Interestingly, tau pathology developed in Tg mice in both studies even though the Tg mouse line used for the studies was different as Calvaguera et al. based their research on a mouse model, ALZ17, that overexpresses the longest isoform (2N4R) of WT human tau while the model in this study (PS19) overexpresses a mutated form of tau. However, the model studied here differs in that the time to develop pathology is considerably quicker. This would likely be explained by the nature of tau that is overexpressed in the PS19 mice, it is known that the human mutant P301S isoform is more prone to aggregation than WT human tau (270).

Interestingly, when the anatomical and cell type distribution of pathological tau aggregates was analyzed, it was observed that PS19 mice injected with CBD-Tau developed intracellular tau aggregates mainly in the oligodendrocytes as opposed to the AD-Tau and DSAD-Tau injected mice which developed tau inclusions in the perikarya of neurons. At 1 mo after injection 66% of CBD-Tau injected mice had developed tau pathology in the fimbria of the hippocampus close to the injection site and half of the injected cases had involvement of the alveus/external capsule. The pathology also extended to rostral and caudal regions of the fimbria and alveus farther away from the injection site. Some cytoplasmic neuronal tau aggregates were observed in neurons of the hippocampus but the amount of pathology was very little compared to the burden of pathology seen in the fimbria. On the contrary, AD-Tau and DSAD-Tau injected mice developed tau pathology mainly in the cytoplasm of neurons of the hippocampus near the injected site but also in regions away from the injection site including caudal brain regions such as subiculum, EC and LC and even the contralateral hippocampus. Thus, the cellular distribution of pathology recapitulates the human disease where there is abundance of white matter pathology

in CBD and predominance of involvement of neurons of grey matter with sparing of white matter in AD (27,147). These results suggest that different strains of tau protein would be responsible for the distinct development of pathology both in the topographical distribution and in cell type-specific involvement. In prion disease the different incubation times of disease and deposition patterns of prion protein (PrP^{sc}) are explained by different conformations of the prion protein (245) but the basis of the cell-type preference for the formation of tau inclusions is unknown. A recent study demonstrated *in vitro* and *in vivo* that pathological tau can acquire different conformations, which propagate tau pathology suggesting that these different conformers or strains could result in the different tauopathies (234). Frost et al. were able to propagate different conformers of tau protein in a clonal fashion in cell culture and when these conformers were reintroduced into naïve cells, the cells developed identical clones. The inoculation of two of the strains in mice resulted in two different pathologies that were maintained through three generations. These characteristics have been also shown for α-synuclein where Guo et al. (247) described two distinct strains of α-syn fibrils that showed marked differences in the efficiency of cross-seeding tau aggregation, both *in vitro* and *in vivo*. Aβ, another amyloid forming protein, also showed similar properties (237,248,249). Petkova et al. (248) were able to synthetize two different fibrils from 40-residue Aβ peptides with distinct morphology and molecular structure that were self-propagating and also showed different toxicities in neuronal cell cultures. Additionally, Stöhr et al (249) induced distinct pathologies in Tg mice after the injection of two different strains of Aβ fibrils. Moreover, since tau inclusions in CBD and AD are formed by different tau isoforms (i.e. CBD is predominantly 4R; AD is predominantly 3R and 4R), there is a possibility that this might determine the structure of different tau strains. However, little is known about how different pathological tau isoforms contribute to the heterogeneous phenotypes seen in different tauopathies. That said, we observed that the injection of enriched tau extracts from AD and DSAD brains resulted in similar AD-like neuronal tau pathologies while both of the CBD cases produced distinctly different pathology from the AD/DSAD cases that was remarkably CBD-like. Thus, these findings suggest that the characteristics and distributions of these different tau inclusions are directly related with the nature of the tauopathy.

In this study it was further demonstrated that tau pathology increased in intensity and spread to regions distant to the injection site over time. In CBD-Tau injected mice it was observed that the oligodendroglial pathology seen in fimbria increased in intensity from 1 mo to 3 mo and more so at 6 mo post-injection and it extended to the contralateral hemisphere where at 6 mo after injection tau pathology was easily seen in the fimbria and the hippocampus. Spread of tau pathology in PS19 mice was also seen in AD/DSAD-Tau injected mice with increasing time post-injection in which newly affected regions appeared at 3 mo post-injection and intensity of pathology increased in most areas previously affected by disease including the thalamus, mammillary nuclei and hypothalamic nuclei. These findings were in line with previous reports in which there was an increase of tau pathology after the injection of extracts from Tg mice and also after the injection of recombinant tau PFFs (226,229). Furthermore, it has been established that the pathology progresses through neuron-to-neuron propagation of inter-synaptically connected cells in two elegant experiments in which tau pathology developed in the superficial layers of the EC of Tg mice spread to the hippocampus, a structure synaptically connected to the EC through the perforant pathway, with increasing aging of the mice (227,228). Moreover, a study in which PFFs were injected into P301S Tg mice determined that tau pathology spread was carried out by connectivity and not by proximity, as only regions that were synaptically connected showed pathology regardless of proximity to the injection site (230). Thus, this and other studies suggest that tau transmission occurs along axons that are afferent and efferent to the injection site rather than as a result of the proximity of neurons to the injection site (271). Interestingly, in the study I performed, the AD/DSAD-Tau PS19 injected mice showed a progression of disease following inter-neuronal connections since all of the involved regions are synaptically connected with the hippocampus. However, CBD-Tau injected mice also showed a progression of disease but in this case it didn't follow the expected neuronal connections and the mechanism of progression is unknown. While the AD-like tau pathology spreads in a manner consistent with dissemination through the connectome of the injected brain regions, most likely via intra-axonal transport, the manner in which the CBD glial tau pathology spreads is enigmatic and will require further studies to elucidate. Indeed, while there are staging schemes for AD tau pathology that support the notion of tau pathology spread through inter-connected brain regions (179,212,272), no similar staging exists for CBD tau pathology so it is not clear how

tau pathology might progress and spread in CBD brains. A study in Tg mice overexpressing the WT form of human α-syn specifically in oligodendrocytes also showed pathology in axons which might signify the transfer of α-syn pathology from oligodendrocytes to axons (273). This phenomenon was not seen in another study in which Tg mice developed tau aggregates solely in oligodendrocytes even though the mice showed signs of neurodegeneration (269). However, in the PS19 mice used in my study there were tau aggregates in the white matter resembling neuropil threads thus, even though the mechanism of formation of tau coiled bodies in oligodendrocytes and their propagation is not known it would be plausible to think that the tau aggregates might transfer from oligodendrocytes to axons and vice versa. Thus, future studies are needed to determine if tau is able to shift from oligodendrocytes to axons or another mechanism of transmission is involved in glial tau aggregates.

To control for causes that would lead to the induction of tau pathology in PS19 mice other than the pathological tau protein in the extract, a preparation obtained from non-diseased subject (CTRL-Tau) was injected into the cerebrum of PS19 mice. Similarly to the CBD-Tau and AD/DSAD-Tau these cases were injected in the hippocampus and overlaying cortex. As expected, even at 6 mo after injection PS19 mice injected with CTRL-Tau did not show any sign of tau aggregates at the injection site or in other regions of the brain. The fact that injections of brain extracts from control non-diseased human brains lacking any insoluble pathological tau did not induce tau pathology in age-matched PS19 mice support data from a growing number of studies indicating that pathological tau and not normal tau induce the seeded transmission and spread of pathological tau in vivo and in vitro (for reviews, see (225,274)). In Clavaguera et al. (226) the injection of soluble tau extracts into ALZ17 mice resulted in a much lesser extent of pathology compared to the injection of the insoluble fraction of tau.

In line with Iba et al. findings with PS19 mice injected with PFFs in which they observed a rise in MC1-positive neurons with increasing injected total tau concentrations a similar dose-dependency was seen in my studies adding additional information to the initial report of Clavaguera et al. (233). To determine the

minimum amount of tau protein needed to develop pathology in PS19 mice and to evaluate the effect of tau protein concentration of the extract, serially diluted extracts were injected into PS19 Tg mice. Interestingly, even at the minimum concentration PS19 mice developed tau pathology demonstrating that "seeded" aggregation of tau can occur with minute quantities of pathological tau. The intensity and extent of tau aggregates directly correlated with the concentration of tau protein in the extract. Thus, it was manifest that the burden of pathology increased with increasing tau concentrations and more involvement of rostral and caudal regions was seen. In a similar way, aggregates developed only in the ipsilateral side of injection at lower tau concentrations but the contralateral hippocampus was involved at higher concentrations of pathological tau protein in the extracts. Interestingly, no tau pathology in the white matter was developed in DSAD-Tau injected mice at any of the concentrations tested in sharp contrast to the abundant pathology in the fimbria developed in CBD-Tau injected mice.

Notably, the tau pathology seen in the hippocampus of PS19 tau Tg mice after the injection of AD/DSAD-Tau was variable and appeared to decrease in the CA3 region ipsilateral and contralateral to the injection side. This could be explained by the neuron loss seen in this region that was already significant at 3 mo post-injection (Figure 27). The mechanism of NFT toxicity is unknown, in human studies it was observed that NFTs are seen in brain regions undergoing neurodegeneration, and in AD patients the burden of NFTs correlates well with severity of dementia (275,276). These observations led to think that filamentous tau aggregates are toxic to cells by interfering in cellular processes through mechanisms including a loss of function of tau upon aggregation, synapse recruitment or through gaining of toxicity of tau aggregates through proteasome inhibition (277–279). However, there are studies in which NFT-containing neurons are functionally intact in vivo (280). Furthermore, tau Tg animal models acquire behavioral deficits, synaptic dysfunction, and cell death in the absence of NFTs indicating that other tau species and not NFT are responsible for the neurodegeneration (143,281,282). In this sense, recent literature has involved oligomeric soluble tau as the main responsible species for neuronal cell death (283,284). However, in my study it is noteworthy that the CA3 region in the injected PS19 mice develops neuronal tau inclusions at 1 mo post-injection, and is one of the first regions to show AT8 positive inclusions in the contralateral hippocampus

preceding neuronal death. Thus, it is possible that distinct tau species have a differential effect in the neurons of these mice causing neuronal death and this may occur in a neuron type specific manner or could be dose and time dependent, as might be inferred from a recently published study in which high doses of synthetic tau fibrils caused hippocampal neuron death (231). In this study the injection of high concentration of tau PFFs resulted in the loss of neurons in the CA1 region of the hippocampus. For comparison, I also analyzed neuron loss in the CA1 region of the hippocampus contralateral to the injection site, where tau inclusions were less abundant than in CA3 and no neuron loss was observed. Interestingly, neuron loss in the CA3 region was accompanied by moderate astrogliosis and less conspicuous microgliosis, which is evidence of reactive changes to this neurodegeneration.

Finally, the earlier findings (233) that this tau pathology is largely cell-type specific and recapitulates the specific features of CBD or AD tau pathology following injections of CBD-Tau or AD/DSAD-Tau, respectively, are confirmed. Thus, while the tau inclusions induced by CBD-Tau predominantly developed in oligodendrocytes with some astrocytic plaques, similar to authentic CBD tau pathology, the tau inclusions induced by AD/DSAD-Tau formed mainly in neurons similar to the NFTs in AD and DSAD brains. Other data support the verisimilitude of the CBD-Tau and AD/DSAD-Tau induced tau pathology in the injected PS19 mice to their human counterparts in CBD and AD, respectively. For example, the inclusions resulting in oligodendrocyte pathology in the fimbria after injection of human-derived CBD-Tau were positive for the conformational antibody MC1 while a few inclusions showed TG3 immunoreactivity. Interestingly, ThS was negative even at 6 months after injection, which is a characteristic of tau inclusions in human CBD (268). In contrast, in the AD/DSAD-Tau injected mice there was an intense immunoreactivity for MC1 and TG3 and positivity for ThS staining already at 1 mo after injection, indicating more mature NFT structures analogous to what is seen in AD patients at histological examination.

At present there is no treatment for AD and other related tauopathies that halts or reduces pathology, and in the case of AD therapies offered to patients are limited to neurotransmitter modulators that act on the symptoms but do not target the underlying causes of disesase. Previous work established that the burden of NFT pathology is

better correlated with the degree of dementia than Aβ aggregates and recent work has shown that tau pathology precedes the formation of amyloid plaques in AD suggesting that the reduction of tau pathological aggregates could be more beneficial for AD patients (211,275,276). Thus, the targeting of tau has become a major goal for disease treatment. Furthermore, the demonstration in this and other studies that pathological tau species can transmit from one cell to the next as the main mechanism of progression of disease has opened new possibilities for the discovery of disease-modifying therapies as it suggests that immunotherapy could be of benefit in these diseases. The injection of either therapeutic antibodies or active vaccines that would interfere with the pathological protein by binding to the extracellular tau aggregates while transitioning from cell-to-cell and preventing its spread to neighboring neurons as a means of halting the progression of disease is compelling. A number of studies in animals have already been performed with passive immunotherapy and vaccines targeting phospho-tau, tau oligomers or truncated forms of tau that have yielded good results (285–287). Additionally, the observation in this and other studies that support the existence of different strains of tau protein opens the door to the generation of therapeutic antibodies targetting distinct strains of tau thus making the treatment more selective and specific for pathological conformers of the protein presumably making it more effective and with reduced chances of presenting adverse effects.

In this project a mouse model where tau pathology reproducing the same characteristics as the corresponding AD and CBD human pathology has been generated and it will be useful for the study of the development of new disease-modifying therapies for the treatment of tauopathies.

CONCLUSIONS

1. I present mouse models of CBD-like and AD-like tauopathies that rapidly develop glial and intraneuronal tau inclusions after the injection of pathological tau isolated from CBD or AD/DSAD brains, respectively. The developed pathology progresses rapidly and in a stereotypical pattern similarly to what is observed in AD and other human neurodegenerative diseases.

2. The CBD-Tau injected mice develop pathology preferentially in oligodendrocytes and white matter as opposed to the AD/DSAD-Tau injected mice in which tau pathology appears in the perikarya of neurons. This distribution recapitulates the characteristics of CBD and AD human pathology, respectively.

3. The CBD-Tau and AD/DSAD-Tau injected mice show a progression of tau pathology that is time dependent and, in the case of DSAD-Tau, also dose dependent. The progression of AD/DSAD-Tau follows the connectome of the injection sites however in the CBD-Tau injected mice the progression is more limited and unrelated to the connectome of the injection site.

4. Only tau pathology developed after the injection of AD/DSAD-Tau into PS19 mice but not pathology developed after the injection of CBD-Tau leads to the death of tangle bearing CA3 neurons over time.

5. These experiments provide evidence for the prion-like hypothesis of disease spread and suggest that the tau pathology formed *in vivo* is dependent on the tau pathology in the preparation indicating that there are post-translational modifications or strains of tau protein that are responsible for the variation between diseases.

6. These models will provide informative systems for studies on the transmission of tau pathology, tau mediated neuronal and glial degeneration and the development of disease-modifying therapies for CBD and AD, in particular immunotherapy directed to distinct strains or conformationally modified proteins.

BIBLIOGRAPHY

1. Weingarten MD, Lockwood AH, Hwo S, Kirschner MW. A protein factor essential for microtubule assembly. Proc Natl Acad Sci. 1975;72(5):1858–62.

2. Binder LI, Frankfurter A, Rebhun LI. The distribution of tau in the mammalian central nervous system. J Cell Biol. 1985;101(4):1371–8.

3. Trojanowski JQ, Schuck T, Schmidt ML, Lee VM. Distribution of tau proteins in the normal human central and peripheral nervous system. J Histochem Cytochem. 1989;37(2):209–15.

4. LoPresti P, Szuchet S, Papasozomenos SC, Zinkowski RP, Binder LI. Functional implications for the microtubule-associated protein tau: localization in oligodendrocytes. Proc Natl Acad Sci U S A. 1995;92(22):10369–73.

5. Papasozomenos SC, Binder LI. Phosphorylation determines two distinct species of tau in the central nervous system. Cell Motil Cytoskeleton. 1987;8(3):210–26.

6. Fellous A, Francon J, Lennon A, Nunez J. Microtubule assembly in vitro purification of assembly-promoting factors. Eur J Biochem. 1977;78(1):167–74.

7. Lindwall G, Cole DR. The purification of tau protein and the occurrence of two phosphorylation states of tau in brain. J Biol Chem. 1984;259(19):12241–5.

8. Iqbal K, Gong CX, Liu F. Hyperphosphorylation-induced tau oligomers. Front Neurol. 2013;4:112.

9. Cleveland DW, Hwo SY, Kirschner MW. Physical and chemical properties of purified tau factor and the role of tau in microtubule assembly. J Mol Biol. 1977;116(2):227–47.

10. Schweers O, Schönbrunn-Hanebeck E, Marx A, Mandelkow E. Structural studies of tau protein and Alzheimer paired helical filaments show no evidence for beta-structure. J Biol Chem. 1994;269(39):24290–7.

11. Lee G, Cowan N, Kirschner M. The primary structure and heterogeneity of tau protein from mouse brain. Science. 1988;239(4837):285–8.

12. Gustke N, Trinczek B, Biernat J, Mandelkow EM, Mandelkow E. Domains of tau protein and interactions with microtubules. Biochemistry. 1994;33(32):9511–22.

13. Avila J, Lucas JJ, Perez M, Hernandez F. Role of tau protein in both physiological and pathological conditions. Physiol Rev. 2004;84(2):361–84.

14. Butner KA, Kirschner MW. Tau protein binds to microtubules through a flexible array of distributed weak sites. J Cell Biol. 1991;115(3):717–30.

15. Lee G, Neve RL, Kosik KS. The microtubule binding domain of tau protein. Neuron. 1989;2(6):1615–24.

16. Goode BL, Chau M, Denis PE, Feinstein SC. Structural and functional differences between 3-repeat and 4-repeat tau isoforms: Implications for normal tau function and the onset of neurodegenerative disease. J Biol Chem. 2000;275(49):38182–9.

17. Ennulat DJ, Liem RK, Hashim GA, Shelanski ML. Two separate 18-amino acid domains of tau promote the polymerization of tubulin. J Biol Chem. 1989;264(10):5327–30.

18. Goode BL, Feinstein SC. Identification of a novel microtubule binding and assembly domain in the developmentally regulated inter-repeat region of tau. J Cell Biol. 1994;124(5):769–81.

19. Neve R, Harris P, Kosik K, Kumit D, Donion T, Kurnit D, et al. Identification of cDNA clones for the human microtubule-associated protein tau and chromosomal localization of the genes for tau and microtubule-associated protein 2. Brain Res. 1986;387(3):271–80.

20. Goedert M, Wischik CM, Crowther RA, Walker JE, Klug A. Cloning and sequencing of the cDNA encoding a core protein of the paired helical filament of Alzheimer disease: identification as the microtubule-associated protein tau. Proc Natl Acad Sci U S A. 1988;85(11):4051–5.

21. Goedert M, Spillantini MG, Jakes R, Rutherford D, Crowther RA. Multiple isoforms of human microtubule-associated protein tau: sequences and localization in neurofibrillary tangles of Alzheimer's disease. Neuron. 1989;3(4):519–26.

22. Kosik KS, Orecchio LD, Bakalis S, Neve RL. Developmentally regulated expression of specific tau sequences. Neuron. 1989;2(4):1389–97.

23. Buée L, Bussière T, Buée-Scherrer V, Delacourte A, Hof PR. Tau protein isoforms, phosphorylation and role in neurodegenerative disorders. Brain Res Rev. 2000;33(1):95–130.

24. Andreadis A, Broderick JA, Kosik KS. Relative exon affinities and suboptimal splice site signals lead to non-equivalence of two cassette exons. Nucleic Acids Res. 1995;23(17):3585–93.

25. Liu WK, Dickson DW, Yen SH. Heterogeneity of tau proteins in Alzheimer's disease. Evidence for increased expression of an isoform and preferential distribution of a phosphorylated isoform in neurites. Am J Pathol. 1993;142(2):387–94.

26. Chen S, Townsend K, Goldberg TE, Davies P, Conejero-Goldberg C. MAPT isoforms: differential transcriptional profiles related to 3R and 4R splice variants. J Alzheimer's Dis. 2010;2229(4):1313–29.

27. Lee VM, Goedert M, Trojanowski JQ. Neurodegenerative tauopathies. Annu Rev Neurosci. 2001;24:1121–59.

28. Goedert M, Jakes R. Expression of separate isoforms of human tau protein: correlation with the tau pattern in brain and effects on tubulin polymerization. EMBO J. 1990;9(13):4225–30.

29. Zhong Q, Congdon EE, Nagaraja HN, Kuret J. Tau isoform composition influences rate and extent of filament formation. J Biol Chem. 2012;287(24):20711–9.

30. Zhukareva V, Shah K, Uryu K, Braak H, Del Tredici K, Sundarraj S, et al. Biochemical analysis of tau proteins in argyrophilic grain disease, Alzheimer's

disease, and Pick's disease : a comparative study. Am J Pathol. 2002;161(4):1135–41.

31. Morris M, Maeda S, Vossel K, Mucke L. The many faces of tau. Neuron. 2011;70(3):410–26.

32. Brandt R, Léger J, Lee G. Interaction of tau with the neural plasma membrane mediated by tau's amino-terminal projection domain. J Cell Biol. 1995;131(5):1327–40.

33. Drechsel DN, Hyman AA, Cobb MH, Kirschner MW. Modulation of the dynamic instability of tubulin assembly by the microtubule-associated protein tau. Mol Biol Cell. 1992;3(10):1141–54.

34. Drubin DG, Kirschner MW. Tau protein function in living cells. J Cell Biol. 1986;103(6 Pt 2):2739–46.

35. Lee G, Rook SL. Expression of tau protein in non-neuronal cells: microtubule binding and stabilization. J Cell Sci. 1992 Jun;102 (Pt 2):227–37.

36. Preuss U, Biernat J, Mandelkow EM, Mandelkow E. The "jaws" model of tau-microtubule interaction examined in CHO cells. J Cell Sci. 1997;110 (Pt 6):789–800.

37. Kadavath H, Hofele R V, Biernat J, Kumar S, Tepper K, Urlaub H, et al. Tau stabilizes microtubules by binding at the interface between tubulin heterodimers. Proc Natl Acad Sci. 2015;112(24):7501–6.

38. Mukrasch MD, von Bergen M, Biernat J, Fischer D, Griesinger C, Mandelkow E, et al. The "Jaws" of the tau-microtubule interaction. J Biol Chem. 2007;282(16):12230–9.

39. Frappier TF, Georgieff IS, Brown K, Shelanski ML. Tau regulation of microtubule-microtubule spacing and bundling. J Neurochem. 1994;63(6):2288–94.

40. Jho YS, Zhulina EB, Kim MW, Pincus PA. Monte Carlo simulations of tau proteins: effect of phosphorylation. Biophys J. 2010;99(8):2387–97.

41. Caceres A, Kosik KS. Inhibition of neurite polarity by tau antisense oligonucleotides in primary cerebellar neurons. Nature. 1990;343(6257):461–3.

42. Kosik KS, Caceres A. Tau protein and the establishment of an axonal morphology. J Cell Sci Suppl. 1991;15:69–74.

43. Dixit R, Ross JL, Goldman YE, Holzbaur EL. Differential regulation of dynein and kinesin motor proteins by tau. Science. 2008 Feb 22;319(5866):1086–9.

44. Ebneth A, Godemann R, Stamer K, Illenberger S, Trinczek B, Mandelkow E. Overexpression of tau protein inhibits kinesin-dependent trafficking of vesicles, mitochondria, and endoplasmic reticulum: implications for Alzheimer's disease. J Cell Biol. 1998;143(3):777–94.

45. Chen J, Kanai Y, Cowan NJ, Hirokawa N. Projection domains of MAP2 and tau determine spacings between microtubules in dendrites and axons. Nature. 1992;360(6405):674–7.

46. Carlier MF, Simon C, Cassoly R, Pradel LA. Interaction between microtubule-associated protein tau and spectrin. Biochimie. 1984;66(4):305–11.

47. Correas I, Padilla R, Avila J. The tubulin-binding sequence of brain microtubule-associated proteins, tau and MAP-2, is also involved in actin binding. Biochem J. 1990;269(1):61–4.

48. Griffith LM, Pollard TD. The interaction of actin filaments with microtubules and microtubule- associated proteins. J Biol Chem. 1982;257(15):9143–51.

49. He HJ, Wang XS, Pan R, Wang DL, Liu MN, He RQ. The proline-rich domain of tau plays a role in interactions with actin. BMC Cell Biol. 2009;10:81.

50. Farias GA, Muñoz JP, Garrido J, Maccioni RB. Tubulin, actin, and tau protein interactions and the study of their macromolecular assemblies. J Cell Biochem. 2002;85(2):315–24.

51. Felgner H, Frank R, Biernat J, Mandelkow EM, Mandelkow E, Ludin B, et al. Domains of neuronal microtubule-associated proteins and flexural rigidity of microtubules. J Cell Biol. 1997;138(5):1067–75.

52. Lee G, Newman ST, Gard DL, Band H, Panchamoorthy G. Tau interacts with src-family non-receptor tyrosine kinases. J Cell Sci. 1998;111 (Pt 2):3167–77.

53. Lee G. Tau and src family tyrosine kinases. Biochim Biophys Acta. 2005;1739(2):323–30.

54. Leugers CJ, Lee G. Tau potentiates nerve growth factor-induced mitogen-activated protein kinase signaling and neurite initiation without a requirement for microtubule binding. J Biol Chem. 2010;285(25):19125–34.

55. Hwang SC, Jhon DY, Bae YS, Kim JH, Rhee SG. Activation of phospholipase C-gamma by the concerted action of tau proteins and arachidonic acid. J Biol Chem. 1996;271(31):18342–9.

56. Rendon A, Jung D, Jancsik V. Interaction of microtubules and microtubule-associated proteins (MAPs) with rat brain mitochondria. Biochem J. 1990;269(2):555–6.

57. Levy SF, LeBoeuf AC, Massie MR, Jordan MA, Wilson L, Feinstein SC. Three- and four-repeat tau regulate the dynamic instability of two distinct microtubule subpopulations in qualitatively different manners: Implications for neurodegeneration. J Biol Chem. 2005;280(14):13520–8.

58. Horiguchi T, Uryu K, Giasson BI, Ischiropoulos H, LightFoot R, Bellmann C, et al. Nitration of tau protein is linked to neurodegeneration in tauopathies. Am J Pathol. 2003;163(3):1021–31.

59. Martin L, Latypova X, Terro F. Post-translational modifications of tau protein: Implications for Alzheimer's disease. Neurochem Int. 2011;58(4):458–71.

60. Arnold CS, Johnson GV, Cole RN, Dong DL, Lee M, Hart GW. The microtubule-associated protein tau is extensively modified with O-linked N-acetylglucosamine. J Biol Chem. 1996;271(46):28741–4.

61. Morishima-Kawashima M, Hasegawa M, Takio K, Suzuki M, Titani K, Ihara Y. Ubiquitin is conjugated with amino-terminally processed tau in paired helical filaments. Neuron. 1993;10(6):1151–60.

62. Ledesma MD, Pérez M, Colaco C, Avila J. Tau glycation is involved in aggregation of the protein but not in the formation of filaments. Cell Mol Biol. 1998;44(7):1111–6.

63. Murthy SN, Wilson JH, Lukas TJ, Kuret J, Lorand L. Cross-linking sites of the human tau protein, probed by reactions with human transglutaminase. J Neurochem. 1998;71(6):2607–14.

64. Dorval V, Fraser PE. Small ubiquitin-like modifier (SUMO) modification of natively unfolded proteins tau and α-synuclein. J Biol Chem. 2006;281(15):9919–24.

65. Cohen TJ, Guo JL, Hurtado DE, Kwong LK, Mills IP, Trojanowski JQ, et al. The acetylation of tau inhibits its function and promotes pathological tau aggregation. Nat Commun. 2011;2:252.

66. Irwin DJ, Cohen TJ, Grossman M, Arnold SE, McCarty-Wood E, Van Deerlin VM, et al. Acetylated tau neuropathology in sporadic and hereditary tauopathies. Am J Pathol. 2013;183(2):344–51.

67. Flores-Rodríguez P, Ontiveros-Torres MA, Cárdenas-Aguayo MC, Luna-Arias JP, Meraz-Ríos MA, Viramontes-Pintos A, et al. The relationship between truncation and phosphorylation at the C-terminus of tau protein in the paired helical filaments of Alzheimer's disease. Front Neurosci. 2015;9:33.

68. García-Sierra F, Ghoshal N, Quinn B, Berry RW, Binder LI. Conformational changes and truncation of tau protein during tangle evolution in Alzheimer's disease. J Alzheimers Dis. 2003;5(2):65–77.

69. Lee VM, Otvos L, Carden MJ, Hollosi M, Dietzschold B, Lazzarini RA. Identification of the major multiphosphorylation site in mammalian neurofilaments. Proc Natl Acad Sci U S A. 1988;85(6):1998–2002.

70. Ksiezak-Reding H, Liu WK, Yen SH. Phosphate analysis and dephosphorylation of modified tau associated with paired helical filaments. Brain Res. 1992;597(2):209–19.

71. Vulliet R, Halloran SM, Braun RK, Smith AJ, Lee G. Proline-directed phosphorylation of human tau protein. J Biol Chem. 1992;267(31):22570–4.

72. Correas I, Díaz-Nido J, Avila J. Microtubule-associated protein tau is phosphorylated by protein kinase C on its tubulin binding domain. J Biol Chem. 1992;267(22):15721–8.

73. Biernat J, Mandelkow EM, Schröter C, Lichtenberg-Kraag B, Steiner B, Berling B, et al. The switch of tau protein to an Alzheimer-like state includes the phosphorylation of two serine-proline motifs upstream of the microtubule binding region. EMBO J. 1992;11(4):1593–7.

74. Goedert M, Jakes R, Crowther RA, Six J, Lübke U, Vandermeeren M, et al. The abnormal phosphorylation of tau protein at Ser-202 in Alzheimer disease

recapitulates phosphorylation during development. Proc Natl Acad Sci U S A. 1993;90(11):5066–70.

75. Steiner B, Mandelkow EM, Biernat J, Gustke N, Meyer HE, Schmidt B, et al. Phosphorylation of microtubule-associated protein tau: identification of the site for Ca2(+)-calmodulin dependent kinase and relationship with tau phosphorylation in Alzheimer tangles. EMBO J. 1990;9(11):3539–44.

76. Hanger DP, Byers HL, Wray S, Leung KY, Saxton MJ, Seereeram A, et al. Novel phosphorylation sites in tau from Alzheimer brain support a role for casein kinase 1 in disease pathogenesis. J Biol Chem. 2007;282(32):23645–54.

77. http://cnr.iop.kcl.ac.uk/hagerlab/tautable.

78. Hasegawa M, Morishima-Kawashima M, Takio K, Suzuki M, Titani K, Ihara Y. Protein sequence and mass spectrometric analyses of tau in the Alzheimer's disease brain. J Biol Chem. 1992;267(24):17047–54.

79. Embi N, Rylatt DB, Cohen P. Glycogen synthase kinase-3 from rabbit skeletal muscle. Separation from cyclic-AMP-dependent protein kinase and phosphorylase kinase. Eur J Biochem. 1980;107(2):519–27.

80. Llorens-Martin M, Jurado J, Hernández F, Ávila J. GSK-3β, a pivotal kinase in Alzheimer disease. Front Mol Neurosci. 2014;7:1–11.

81. Kimura T, Ishiguro K, Hisanaga S. Physiological and pathological phosphorylation of tau by Cdk5. Front Mol Neurosci. 2014;7:65.

82. Liu SL, Wang C, Jiang T, Tan L, Xing A, Yu JT. The role of cdk5 in Alzheimer's disease. Mol Neurobiol. 2015 Jul 31;[Epub Ahea.

83. Baumann K, Mandelkow EM, Biernat J, Piwnica-Worms H, Mandelkow E. Abnormal Alzheimer-like phosphorylation of tau-protein by cyclin-dependent kinases cdk2 and cdk5. FEBS Lett. 1993;336(3):417–24.

84. Reynolds CH, Betts JC, Blackstock WP, Nebreda AR, Anderton BH. Phosphorylation sites on tau identified by nanoelectrospray mass spectrometry: differences in vitro between the mitogen-activated protein kinases ERK2, c-Jun N-terminal kinase and P38, and glycogen synthase kinase-3beta. J Neurochem. 2000;74(4):1587–95.

85. Drewes G, Lichtenberg-Kraag B, Döring F, Mandelkow EM, Biernat J, Goris J, et al. Mitogen activated protein (MAP) kinase transforms tau protein into an Alzheimer-like state. EMBO J. 1992;11(6):2131–8.

86. Morishima-Kawashima M, Hasegawa M, Tako K, Suzuki M, Yoshida H, Titani K, et al. Proline-directed and Non-proline directed phosphorylation of PHF-tau. J Biol Chem. 1995;270(2):823–9.

87. Carlyle BC, Nairn AC, Wang M, Yang Y, Jin LE, Simen AA, et al. cAMP-PKA phosphorylation of tau confers risk for degeneration in aging association cortex. Proc Natl Acad Sci U S A. 2014;111(13):5036–41.

88. Jicha GA, O'Donnell A, Weaver C, Angeletti R, Davies P. Hierarchical phosphorylation of recombinant tau by the paired-helical filament-associated protein kinase is dependent on cyclic AMP-dependent protein kinase. J Neurochem. 1999;72(1):214–24.

89. Taniguchi T, Kawamata T, Mukai H, Hasegawa H, Isagawa T, Yasuda M, et al. Phosphorylation of tau is regulated by PKN. J Biol Chem. 2001;276(13):10025–31.

90. Sironi JJ, Yen SH, Gondal JA, Wu Q, Grundke-Iqbal I, Iqbal K. Ser-262 in human recombinant tau protein is a markedly more favorable site for phosphorylation by CaMKII than PKA or PhK. FEBS Lett. 1998;436(3):471–5.

91. Drewes G, Ebneth A, Preuss U, Mandelkow EM, Mandelkow E. MARK, a novel family of protein kinases that phosphorylate microtubule-associated proteins and trigger microtubule disruption. Cell. 1997;89(2):297–308.

92. Lund H, Gustafsson E, Svensson A, Nilsson M, Berg M, Sunnemark D, et al. MARK4 and MARK3 associate with early tau phosphorylation in Alzheimer's disease granulovacuolar degeneration bodies. Acta Neuropathol Commun. 2014 Jan;2:22.

93. Goedert M, Hasegawa M, Jakes R, Lawler S, Cuenda A, Cohen P. Phosphorylation of microtubule-associated protein tau by stress-activated protein kinases. FEBS Lett. 1997;409(1):57–62.

94. Buée-Scherrer V, Goedert M. Phosphorylation of microtubule-associated protein tau by stress-activated protein kinases in intact cells. FEBS Lett. 2002;515(1-3):151–4.

95. Sato S, Cerny RL, Buescher JL, Ikezu T. Tau-tubulin kinase 1 (TTBK1), a neuron-specific tau kinase candidate, is involved in tau phosphorylation and aggregation. J Neurochem. 2006;98(5):1573–84.

96. Ikezu S, Ikezu T. Tau-tubulin kinase. Front Mol Neurosci. 2014 Apr 28;7:33.

97. Li G, Yin H, Kuret J. Casein kinase 1 delta phosphorylates tau and disrupts its binding to microtubules. J Biol Chem. 2004;279(16):15938–45.

98. Knippschild U, Gocht A, Wolff S, Huber N, Löhler J, Stöter M. The casein kinase 1 family: participation in multiple cellular processes in eukaryotes. Cell Signal. 2005;17(6):675–89.

99. Ferrer I, Barrachina M, Puig B, Martínez de Lagrán M, Martí E, Avila J, et al. Constitutive Dyrk1A is abnormally expressed in Alzheimer disease, Down syndrome, Pick disease, and related transgenic models. Neurobiol Dis. 2005;20(2):392–400.

100. Mairet-Coello G, Courchet J, Pieraut S, Courchet V, Maximov A, Polleux F. The CAMKK2-AMPK kinase pathway mediates the synaptotoxic effects of Aβ oligomers through tau phosphorylation. Neuron. 2013;78(1):94–108.

101. Vingtdeux V, Davies P, Dickson DW, Marambaud P. AMPK is abnormally activated in tangle- and pre-tangle-bearing neurons in Alzheimer's disease and other tauopathies. Acta Neuropathol. 2011;121(3):337–49.

102. Trojanowski JQ, Lee VM. Phosphorylation of paired helical filament tau in Alzheimer's disease neurofibrillary lesions: focusing on phosphatases. FASEB J. 1995;9(15):1570–6.

103. Liu F, Grundke-Iqbal I, Iqbal K, Gong CX. Contributions of protein phosphatases PP1, PP2A, PP2B and PP5 to the regulation of tau phosphorylation. Eur J Neurosci. 2005;22(8):1942–50.

104. Gong CX, Liu F, Grundke-Iqbal I, Iqbal K. Post-translational modifications of tau protein in Alzheimer's disease. J Neural Transm. 2005;112(6):813–38.

105. Sontag E, Nunbhakdi-Craig V, Lee G, Bloom GS, Mumby MC. Regulation of the phosphorylation state and microtubule-binding activity of Tau by protein phosphatase 2A. Neuron. 1996;17(6):1201–7.

106. Sontag E, Nunbhakdi-Craig V, Lee G, Brandt R, Kamibayashi C, Kuret J, et al. Molecular interactions among protein phosphatase 2A, tau, and microtubules. Implications for the regulation of tau phosphorylation and the development of tauopathies. J Biol Chem. 1999;274(36):25490–8.

107. Grundke-Iqbal I, Iqbal K, Tung YC, Quinlan M, Wisniewski HM, Binder LI. Abnormal phosphorylation of the microtubule-associated protein tau (tau) in Alzheimer cytoskeletal pathology. Proc Natl Acad Sci U S A. 1986;83(13):4913–7.

108. Arendt T, Stieler J, Strijkstra AM, Hut RA, Rüdiger J, Van der Zee EA, et al. Reversible paired helical filament-like phosphorylation of tau is an adaptive process associated with neuronal plasticity in hibernating animals. J Neurosci. 2003;23(18):6972–81.

109. Planel E, Miyasaka T, Launey T, Chui DH, Tanemura K, Sato S, et al. Alterations in glucose metabolism induce hypothermia leading to tau hyperphosphorylation through differential inhibition of kinase and phosphatase activities: implications for Alzheimer's disease. J Neurosci. 2004;24(10):2401–11.

110. Guillozet-Bongaarts AL, Glajch KE, Libson EG, Cahill ME, Bigio E, Berry RW, et al. Phosphorylation and cleavage of tau in non-AD tauopathies. Acta Neuropathol. 2007;113(5):513–20.

111. Berry RW, Sweet AP, Clark FA, Lagalwar S, Lapin BR, Wang T, et al. Tau epitope display in progressive supranuclear palsy and corticobasal degeneration. J Neurocytol. 2004;33(3):287–95.

112. Kidd M. The history of the paired helical filaments. J Alzheimers Dis. 2006;9(3 Suppl):71–5.

113. Grundke-Iqbal I, Iqbal K, Quinlan M, Tung YC, Zaidi MS, Wisniewski HM. Microtubule-associated protein tau. A component of Alzheimer paired helical filaments. J Biol Chem. 1986;261(13):6084–9.

114. Kosik KS, Joachim CL, Selkoe DJ. Microtubule-associated protein tau (tau) is a major antigenic component of paired helical filaments in Alzheimer disease. Proc Natl Acad Sci U S A. 1986;83(11):4044–8.

115. Lee VM, Balin BJ, Otvos L, Trojanowski JQ. A68: a major subunit of paired helical filaments and derivatized forms of normal Tau. Science. 1991;251(4994):675–8.

116. Wischik CM, Novak M, Edwards PC, Klug A, Tichelaar W, Crowther RA. Structural characterization of the core of the paired helical filament of Alzheimer disease. Proc Natl Acad Sci U S A. 1988;85:4884–8.

117. Ihara Y, Nukina N, Miura R, Ogawara M. Phosphorylated tau protein is integrated into paired helical filaments in Alzheimer's disease. J Biochem. 1986;99(6):1807–10.

118. Brion JP, Couck AM, Passareiro E, Flament-Durand J. Neurofibrillary tangles of Alzheimer's disease: an immunohistochemical study. J Submicrosc Cytol. 1985;17(1):89–96.

119. Friedhoff P, von Bergen M, Mandelkow EM, Davies P, Mandelkow E. A nucleated assembly mechanism of Alzheimer paired helical filaments. Proc Natl Acad Sci U S A. 1998;95(26):15712–7.

120. Congdon EE, Kim S, Bonchak J, Songrug T, Matzavinos A, Kuret J. Nucleation-dependent tau filament formation: the importance of dimerization and an estimation of elementary rate constants. J Biol Chem. 2008;283(20):13806–16.

121. Kuret J, Chirita CN, Congdon EE, Kannanayakal T, Li G, Necula M, et al. Pathways of tau fibrillization. Biochim Biophys Acta. 2005;1739(2-3):167–78.

122. Mondragón-Rodríguez S, Mena R, Binder LI, Smith MA, Perry G, García-Sierra F. Conformational changes and cleavage of tau in Pick bodies parallel the early processing of tau found in Alzheimer pathology. Neuropathol Appl Neurobiol. 2008;34(1):62–75.

123. Alonso AC, Zaidi T, Grundke-Iqbal I, Iqbal K. Role of abnormally phosphorylated tau in the breakdown of microtubules in Alzheimer disease. Proc Natl Acad Sci U S A. 1994;91(12):5562–6.

124. Biernat J, Gustke N, Drewes G, Mandelkow EM, Mandelkow E. Phosphorylation of Ser262 strongly reduces binding of tau to microtubules: distinction between PHF-like immunoreactivity and microtubule binding. Neuron. 1993;11(1):153–63.

125. Mandelkow EM, Biernat J, Drewes G, Gustke N, Trinczek B, Mandelkow E. Tau domains, phosphorylation, and interactions with microtubules. Neurobiol Aging. 1995;16(3):355–62; discussion 362–3.

126. Bramblett GT, Goedert M, Jakes R, Merrick SE, Trojanowski JQ, Lee VM. Abnormal tau phosphorylation at Ser396 in Alzheimer's disease recapitulates development and contributes to reduced microtubule binding. Neuron. 1993;10(6):1089–99.

127. Stoothoff WH, Johnson GVW. Tau phosphorylation: Physiological and pathological consequences. Biochim Biophys Acta. 2005;1739(2):280–97.

128. Köpke E, Tung YC, Shaikh S, Alonso AC, Iqbal K, Grundke-Iqbal I. Microtubule-associated protein tau. Abnormal phosphorylation of a non-paired helical filament pool in Alzheimer disease. J Biol Chem. 1993;268(32):24374–84.

129. Meraz-Ríos MA, Lira-De León KI, Campos-Peña V, De Anda-Hernández MA, Mena-López R. Tau oligomers and aggregation in Alzheimer's disease. J Neurochem. 2010;112(6):1353–67.

130. Li B, Chohan MO, Grundke-Iqbal I, Iqbal K. Disruption of microtubule network by Alzheimer abnormally hyperphosphorylated tau. Acta Neuropathol. 2007;113(5):501–11.

131. Merrick SE, Trojanowski JQ, Lee VM. Selective destruction of stable microtubules and axons by inhibitors of protein serine/threonine phosphatases in cultured human neurons. J Neurosci. 1997;17(15):5726–37.

132. Wilhelmsen KC, Lynch T, Pavlou E, Higgins M, Nygaard TG. Localization of disinhibition-dementia-parkinsonism-amyotrophy complex to 17q21-22. Am J Hum Genet. 1994;55(6):1159–65.

133. Sima AA, Defendini R, Keohane C, D'Amato C, Foster NL, Parchi P, et al. The neuropathology of chromosome 17-linked dementia. Ann Neurol. 1996;39(6):734–43.

134. Foster NL, Wilhelmsen K, Sima AA, Jones MZ, D'Amato CJ, Gilman S. Frontotemporal dementia and parkinsonism linked to chromosome 17: a consensus conference. Conference Participants. Ann Neurol. 1997;41(6):706–15.

135. Spillantini MG, Murrell JR, Goedert M, Farlow MR, Klug A, Ghetti B. Mutation in the tau gene in familial multiple system tauopathy with presenile dementia. Proc Natl Acad Sci U S A. 1998;95(13):7737–41.

136. Hutton M, Lendon CL, Rizzu P, Baker M, Froelich S, Houlden H, et al. Association of missense and 5'-splice-site mutations in tau with the inherited dementia FTDP-17. Nature. 1998;393(6686):702–5.

137. Poorkaj P, Bird TD, Wijsman E, Nemens E, Garruto RM, Anderson L, et al. Tau is a candidate gene for chromosome 17 frontotemporal dementia. Ann Neurol. 1998;43(6):815–25.

138. Spillantini MG, Goedert M, Crowther RA, Murrell JR, Farlow MR, Ghetti B. Familial multiple system tauopathy with presenile dementia: a disease with abundant neuronal and glial tau filaments. Proc Natl Acad Sci U S A. 1997;94(8):4113–8.

139. Ghetti B, Oblak AL, Boeve BF, Johnson KA, Dickerson BC, Goedert M. Invited review: Frontotemporal dementia caused by microtubule-associated protein tau gene (MAPT) mutations: a chameleon for neuropathology and neuroimaging. Neuropathol Appl Neurobiol. 2015;41(1):24–46.

140. Spillantini MG, Goedert M. Tau pathology and neurodegeneration. Lancet Neurol. 2013;12(6):609–22.

141. Hasegawa M, Smith MJ, Goedert M. Tau proteins with FTDP-17 mutations have a reduced ability to promote microtubule assembly. FEBS Lett. 1998;437(3):207–10.

142. Bugiani O, Murrell JR, Giaccone G, Hasegawa M, Ghigo G, Tabaton M, et al. Frontotemporal dementia and corticobasal degeneration in a family with a P301S mutation in tau. J Neuropathol Exp Neurol. 1999;58(6):667–77.

143. Yoshiyama Y, Higuchi M, Zhang B, Huang SM, Iwata N, Saido TC, et al. Synapse loss and microglial activation precede tangles in a P301S tauopathy mouse model. Neuron. 2007;53(3):337–51.

144. Allen B, Ingram E, Takao M, Smith MJ, Jakes R, Virdee K, et al. Abundant tau filaments and nonapoptotic neurodegeneration in transgenic mice expressing human P301S tau protein. J Neurosci. 2002;22(21):9340–51.

145. Dickson D, Weller R, editors. Neurodegeneration. The molecular pathology of dementia and movement disorders. 2nd Editio. West Sussex, UK: Wiley-Blackwell; 2011.

146. Love S, Budka H, Ironside JW, Perry A, editors. Greenfield's Neuropathology. 9th Editio. CRC Press; 2015.

147. Ballatore C, Lee VM, Trojanowski JQ. Tau-mediated neurodegeneration in Alzheimer's disease and related disorders. Nat Rev Neurosci. 2007;8(9):663–72.

148. Hauw JJ, Daniel SE, Dickson D, Horoupian DS, Jellinger K, Lantos PL, et al. Preliminary NINDS neuropathologic criteria for Steele-Richardson-Olszewski syndrome (progressive supranuclear palsy). Neurology. 1994;44(11):2015–9.

149. Braak H, Braak E. Argyrophilic grain disease: Frequency of occurrence in different age categories and neuropathological diagnostic criteria. J Neural Transm. 1998;105(8-9):801–19.

150. Duyckaerts C, Braak H, Brion JP, Buée L, Del Tredici K, Goedert M, et al. PART is part of Alzheimer disease. Acta Neuropathol. 2015;129(5):749–56.

151. Winton MJ, Joyce S, Zhukareva V, Practico D, Perl DP, Galasko D, et al. Characterization of tau pathologies in gray and white matter of Guam parkinsonism-dementia complex. Acta Neuropathol. 2006;111(5):401–12.

152. Ahmed Z, Bigio EH, Budka H, Dickson DW, Ferrer I, Ghetti B, et al. Globular glial tauopathies (GGT): Consensus recommendations. Acta Neuropathol. 2013;126(4):537–44.

153. Dickson DW. Neuropathology of Pick ' s disease. Neurology. 2001;56(11 Suppl 4):S16–20.

154. Alzualde A, Indakoetxea B, Ferrer I, Moreno F, Barandiaran M, Gorostidi A, et al. A novel PRNP Y218N mutation in Gerstmann-Sträussler-Scheinker disease with neurofibrillary degeneration. J Neuropathol Exp Neurol. 2010;69(8):789–800.

155. Vermersch P, Sergeant N, Ruchoux MM, Hofmann-Radvanyi H, Wattez A, Petit H, et al. Specific tau variants in the brains of patients with myotonic dystrophy. Neurology. 1996;47(3):711–7.

156. Ellison D, Love S, Chimelli L, Harding B, Lowe J, Vinters H. Neuropathology. A reference text of CNS pathology. Second Edi. Elsevier Ltd; 2004.

157. Kovacs GG. Invited review: Neuropathology of tauopathies: principles and practice. Neuropathol Appl Neurobiol. 2015;41(1):3–23.

158. Alzheimer A. Über eine eigenartige erkankung der hirnrinde. Allg Zeitschrift für Psychiatr und Phychish-Gerigchtliche Medizin. 1907;64:146–8.

159. Stelzmann RA, Schnitzlein HN, Murtagh FR. An english translation of Alzheimer's 1907 paper , "Über eine eigenartige Erkankung der Hirnrinde." Clin Anat. 1995;8:429–31.

160. Reitz C, Brayne C, Mayeux R. Epidemiology of Alzheimer Disease. Nat Rev Neurol. 2011;7(3):137–52.

161. 2015 Alzheimer's disease facts and figures. Alzheimers Dement. 2015;11(3):332–84.

162. Corder EH, Saunders AM, Strittmatter WJ, Schmechel DE, Gaskell PC, Small GW, et al. Gene dose of apolipoprotein E type 4 allele and the risk of Alzheimer's disease in late onset families. Science. 1993;261(5123):921–3.

163. Roses AD. Apolipoprotein E alleles as risk factors in Alzheimer's disease. Annu Rev Med. 1996;47:387–400.

164. van Dijk EJ, Breteler MM, Schmidt R, Berger K, Nilsson LG, Oudkerk M, et al. The association between blood pressure, hypertension, and cerebral white matter lesions: cardiovascular determinants of dementia study. Hypertension. 2004;44(5):625–30.

165. Russ TC, Hamer M, Stamatakis E, Starr JM, Batty GD, Kivimäki M. Does the Framingham cardiovascular disease risk score also have predictive utility for dementia death? An individual participant meta-analysis of 11,887 men and women. Atherosclerosis. 2013;228(1):256–8.

166. Liu CC, Kanekiyo T, Xu H, Bu G. Apolipoprotein E and Alzheimer disease: risk, mechanisms and therapy. Nat Rev Neurol. 2013;9(2):106-18

167. McKhann GM, Knopman DS, Chertkow H, Hyman BT, Jack CR, Kawas CH, et al. The diagnosis of dementia due to Alzheimer's disease: Recommendations from the National Institute on Aging-Alzheimer's Association workgroups on diagnostic guidelines for Alzheimer's disease. Alzheimer's Dement. 2011;7(3):263–9.

168. Jack CJ, Knopman DS, Jagust WJ, Petersen RC, Weiner MW, Aisen PS, et al. Tracking pathophysiological processes in Alzheimer ' s disease : an updated hypothetical model of dynamic biomarkers. Lancet Neurol. 2013;12(2):207–16.

169. Tapiola T, Alafuzoff I, Herukka SK, Parkkinen L, Hartikainen P, Soininen H, et al. Cerebrospinal fluid {beta}-amyloid 42 and tau proteins as biomarkers of Alzheimer-type pathologic changes in the brain. Arch Neurol. 2009;66(3):382–9.

170. Klunk WE, Engler H, Nordberg A, Wang Y, Blomqvist G, Holt DP, et al. Imaging brain amyloid in Alzheimer's disease with Pittsburgh Compound-B. Ann Neurol. 2004;55(3):306–19.

171. Buerger K, Ewers M, Pirttilä T, Zinkowski R, Alafuzoff I, Teipel SJ, et al. CSF phosphorylated tau protein correlates with neocortical neurofibrillary pathology in Alzheimer's disease. Brain. 2006;129(11):3035–41.

172. Johnson K, Fox N, Sperling R, Klunk W. Brain imaging in Alzheimer disease. Cold Spring Harb Perspect Med. 2012;2(4):1–23.

173. Hampel H, Bürger K, Teipel SJ, Bokde AL, Zetterberg H, Blennow K. Core candidate neurochemical and imaging biomarkers of Alzheimer's disease. Alzheimer's Dement. 2008;4(1):38–48.

174. Thal DR, Walter J, Saido TC, Fändrich M. Neuropathology and biochemistry of Aβ and its aggregates in Alzheimer's disease. Acta Neuropathol. 2014;129(2):167–82.

175. Goedert M. Filamentous nerve cell inclusions in neurodegenerative diseases: tauopathies and alpha-synucleinopathies. Philos Trans R Soc Lond B Biol Sci. 1999;354(1386):1101–18.

176. Boluda S, Toledo JB, Irwin DJ, Raible KM, Byrne MD, Lee EB, et al. A comparison of Aβ amyloid pathology staging systems and correlation with clinical diagnosis. Acta Neuropathol. 2014;128(4):543–50.

177. Mirra SS, Heyman A, McKeel D, Sumi SM, Crain BJ, Brownlee LM, et al. The Consortium to Establish a Registry for Alzheimer's Disease (CERAD). Part II. Standardization of the neuropathologic assessment of Alzheimer's disease. Neurology. 1991;41(4):479–86.

178. Thal DR, Rüb U, Orantes M, Braak H. Phases of A beta-deposition in the human brain and its relevance for the development of AD. Neurology. 2002;58(12):1791–800.

179. Braak H, Braak E. Neuropathological stageing of Alzheimer-related changes. Acta Neuropathol. 1991;82(4):239–59.

180. Braak H, Alafuzoff I, Arzberger T, Kretzschmar H, Tredici K. Staging of Alzheimer disease-associated neurofibrillary pathology using paraffin sections and immunocytochemistry. Acta Neuropathol. 2006;112(4):389–404.

181. Montine TJ, Phelps CH, Beach TG, Bigio EH, Cairns NJ, Dickson DW, et al. National Institute on Aging – Alzheimer's Association guidelines for the neuropathologic assessment of Alzheimer's disease: a practical approach. Alzheimer's Dement. 2012;8(1):1–11.

182. https://www.nia.nih.gov/alzheimers/publication/alzheimers-disease-medications-fact-sheet.

183. Rafii MS, Aisen PS. Advances in Alzheimer's disease drug development. BMC Med. 2015;13(1):62.

184. Luk KC, Song C, O'Brien P, Stieber A, Branch JR, Brunden KR, et al. Exogenous alpha-synuclein fibrils seed the formation of Lewy body-like intracellular inclusions in cultured cells. Proc Natl Acad Sci U S A. 2009;106(47):20051–6.

185. Corbett A, Pickett J, Burns A, Corcoran J, Dunnett SB, Edison P, et al. Drug repositioning for Alzheimer's disease. Nat Rev Drug Discov. 2012 Nov;11(11):833–46.

186. Rebeiz JJ, Kolodny EH, Richardson EP. Corticodentatonigral degeneration with neuronal achromasia: a progressive disorder of late adult life. Trans Am Neurol Assoc. 1967;92:23–6.

187. Riley DE, Lang AE, Lewis A, Resch L, Ashby P, Hornykiewicz O, et al. Cortical-basal ganglionic degeneration. Neurology. 1990;40(8):1203–12.

188. Gibb WR, Luthert PJ, Marsden CD. Corticobasal degeneration. Brain. 1989;112(Pt5):1171–92.

189. Togasaki DM, Tanner CM. Epidemiologic aspects. Adv Neurol. 2000;82:53–9.

190. Winter Y, Bezdolnyy Y, Katunina E, Avakjan G, Reese JP, Klotsche J, et al. Incidence of Parkinson's disease and atypical parkinsonism: Russian population-based study. Mov Disord. 2010;25(3):349–56.

191. Houlden H, Baker M, Morris HR, MacDonald N, Pickering-Brown S, Adamson J, et al. Corticobasal degeneration and progressive supranuclear palsy share a common tau haplotype. Neurology. 2001;56(12):1702–6.

192. Armstrong MJ, Litvan I, Lang AE, Bak TH, Bhatia KP, Borroni B, et al. Criteria for the diagnosis of corticobasal degeneration. Neurology. 2013;80(5):496–503.

193. Kouri N, Whitwell JL, Josephs KA, Rademakers R, Dickson DW. Corticobasal degeneration: a pathologically distinct 4R tauopathy. Nat Rev Neurol. 2011;7(5):263–72.

194. Lee SE, Rabinovici GD, Mayo MC, Wilson SM, Seeley WW, Dearmond SJ, et al. Clinicopathological correlations in corticobasal degeneration. Ann Neurol. 2011;70(2):327–40.

195. Williams DR, Holton JL, Strand C, Pittman A, De Silva R, Lees AJ, et al. Pathological tau burden and distribution distinguishes progressive supranuclear palsy-parkinsonism from Richardson's syndrome. Brain. 2007;130(6):1566–76.

196. Josephs KA, Whitwell JL, Dickson DW, Boeve BF, Knopman DS, Petersen RC, et al. Voxel-based morphometry in autopsy proven PSP and CBD. Neurobiol Aging. 2008;29(2):280–9.

197. Urakami K, Arai H, Wada K, Sasaki H, Kanai M, Shoji M, et al. Diagnostic significance of tau protein in cerebrospinal fluid from patients with corticobasal degeneration or progressive supranuclear palsy. J Neurol Sci. 2001;183(1):95–8.

198. Arai H, Morikawa Y, Higuchi M, Matsui T, Clark CM, Miura M, et al. Cerebrospinal fluid tau levels in neurodegenerative diseases with distinct tau-related pathology. Biochem Biophys Res Commun. 1997;236(2):262–4.

199. Dickson DW, Bergeron C, Chin SS, Duyckaerts C, Horoupian D, Ikeda K, et al. Office of Rare Diseases neuropathologic criteria for corticobasal degeneration. J Neuropathol Exp Neurol. 2002;61(11):935–46.

200. Ksiezak-Reding H, Morgan K, Mattiace LA, Davies P, Liu WK, Yen SH, et al. Ultrastructure and biochemical composition of paired helical filaments in corticobasal degeneration. Am J Pathol. 1994;145(6):1496–508.

201. Armstrong MJ. Diagnosis and treatment of corticobasal degeneration topical collection on movement disorders. Curr Treat Options Neurol. 2014;16(3):282.

202. Steele JC, Richardson JC, Olszewski J. Progressive supranuclear palsy. A heterogeneous degeneration involving the brain stem, basal ganglia and cerebellum with vertical gaze and pseudobulbar palsy, nuchal dystonia and dementia. Arch Neurol. 1964;10:333–59.

203. Braak H, Braak E. Argyrophilic grains: characteristic pathology of cerebral cortex in cases of adult onset dementia without Alzheimer changes. Neurosci Lett. 1987;76(1):124–7.

204. Ferrer I, Santpere G, Van Leeuwen FW. Argyrophilic grain disease. Brain. 2008;131(6):1416–32.

205. Kovacs GG, Rozemuller AJ, van Swieten JC, Gelpi E, Majtenyi K, Al-Sarraj S, et al. Neuropathology of the hippocampus in FTLD-Tau with Pick bodies: a study of the BrainNet Europe Consortium. Neuropathol Appl Neurobiol. 2013;39(2):166–78.

206. Saper CB, Wainer BH, German DC. Axonal and transneuronal transport in the transmission of neurological disease: potential role in system degenerations, including Alzheimer's disease. Neuroscience. 1987;23(2):389–98.

207. Saito Y, Ruberu NN, Sawabe M, Arai T, Tanaka N, Kakuta Y, et al. Staging of argyrophilic grains: an age-associated tauopathy. J Neuropathol Exp Neurol. 2004;63(9):911–8.

208. Braak H, Ghebremedhin E, Rüb U, Bratzke H, Del Tredici K. Stages in the development of Parkinson's disease-related pathology. Cell Tissue Res. 2004;318(1):121–34.

209. Braak H, Del Tredici K, Rüb U, De Vos RA, Jansen Steur EN, Braak E. Staging of brain pathology related to sporadic Parkinson's disease. Neurobiol Aging. 2003;24(2):197–211.

210. Brettschneider J, Del Tredici K, Toledo JB, Robinson JL, Irwin DJ, Grossman M, et al. Stages of pTDP-43 pathology in amyotrophic lateral sclerosis. Ann Neurol. 2013;74(1):20–38.

211. Braak H, Del Tredici K. The pathological process underlying Alzheimer's disease in individuals under thirty. Acta Neuropathol. 2011;121(2):171–81.

212. Braak H, Del Tredici K. Alzheimer's pathogenesis: Is there neuron-to-neuron propagation? Acta Neuropathol. 2011;121(5):589–95.

213. De Boni U, Crapper DR. Paired helical filaments of the Alzheimer type in cultured neurones. Nature. 1978;271(5645):566–8.

214. Frost B, Jacks RL, Diamond MI. Propagation of tau misfolding from the outside to the inside of a cell. J Biol Chem. 2009;284(19):12845–52.

215. Guo JL, Lee VM. Seeding of normal tau by pathological tau conformers drives pathogenesis of Alzheimer-like tangles. J Biol Chem. 2011;286(17):15317–31.

216. Guo JL, Lee VM. Neurofibrillary tangle-like tau pathology induced by synthetic tau fibrils in primary neurons over-expressing mutant tau. FEBS Lett. 2013;587(6):717–23.

217. Kfoury N, Holmes BB, Jiang H, Holtzman DM, Diamond MI. Trans-cellular propagation of tau aggregation by fibrillar species. J Biol Chem. 2012;287(23):19440–51.

218. Cocucci E, Meldolesi J. Ectosomes and exosomes: shedding the confusion between extracellular vesicles. Trends Cell Biol. 2015;25(6):364–72.

219. Saman S, Kim W, Raya M, Visnick Y, Miro S, Saman S, et al. Exosome-associated tau is secreted in tauopathy models and is selectively phosphorylated in cerebrospinal fluid in early Alzheimer disease. J Biol Chem. 2012;287(6):3842–9.

220. Saman S, Lee NC, Inoyo I, Jin J, Li Z, Doyle T, et al. Proteins recruited to exosomes by tau overexpression implicate novel cellular mechanisms linking tau secretion with Alzheimer's disease. J Alzheimer's Dis. 2014;40(Suppl 1):S47–70.

221. Dujardin S, Bégard S, Caillierez R, Lachaud C, Delattre L, Carrier S, et al. Ectosomes: A new mechanism for non-exosomal secretion of tau protein. PLoS One. 2014;9(6):28–31.

222. Chai X, Dage JL, Citron M. Constitutive secretion of tau protein by an unconventional mechanism. Neurobiol Dis. 2012;48(3):356–66.

223. Wu JW, Herman M, Liu L, Simoes S, Acker CM, Figueroa H, et al. Small misfolded tau species are internalized via bulk endocytosis and anterogradely and retrogradely transported in neurons. J Biol Chem. 2013;288(3):1856–70.

224. Holmes BB, DeVos SL, Kfoury N, Li M, Jacks R, Yanamandra K, et al. Heparan sulfate proteoglycans mediate internalization and propagation of specific proteopathic seeds. Proc Natl Acad Sci U S A. 2013;110(33):E3138–47.

225. Guo JL, Lee VM. Cell-to-cell transmission of pathogenic proteins in neurodegenerative diseases. Nat Med. 2014;20(2):130–8.

226. Clavaguera F, Bolmont T, Crowther RA, Abramowski D, Frank S, Probst A, et al. Transmission and spreading of tauopathy in transgenic mouse brain. Nat Cell Biol. 2009;11(7):909–13.

227. Liu L, Drouet V, Wu JW, Witter MP, Small SA, Clelland C, et al. Trans-synaptic spread of tau pathology in vivo. PLoS One. 2012;7(2):1–9.

228. De Calignon A, Polydoro M, Suárez-Calvet M, William C, Adamowicz DH, Kopeikina KJ, et al. Propagation of tau pathology in a model of early Alzheimer's disease. Neuron. 2012;73(4):685–97.

229. Iba M, Guo JL, McBride JD, Zhang B, Trojanowski JQ, Lee VM. Synthetic tau fibrils mediate transmission of neurofibrillary tangles in a transgenic mouse model of Alzheimer's-like tauopathy. J Neurosci. 2013;33(3):1024–37.

230. Ahmed Z, Cooper J, Murray TK, Garn K, McNaughton E, Clarke H, et al. A novel in vivo model of tau propagation with rapid and progressive neurofibrillary tangle pathology: The pattern of spread is determined by connectivity, not proximity. Acta Neuropathol. 2014;127(5):667–83.

231. Peeraer E, Bottelbergs A, Van Kolen K, Stancu IC, Vasconcelos B, Mahieu M, et al. Intracerebral injection of preformed synthetic tau fibrils initiates widespread tauopathy and neuronal loss in the brains of tau transgenic mice. Neurobiol Dis. 2015;73:83–95.

232. Stancu IC, Vasconcelos B, Ris L, Wang P, Villers A, Peeraer E, et al. Templated misfolding of tau by prion-like seeding along neuronal connections impairs neuronal network function and associated behavioral outcomes in tau transgenic mice. Acta Neuropathol. 2015;875–94.

233. Clavaguera F, Akatsu H, Fraser G, Crowther RA, Frank S, Hench J, et al. Brain homogenates from human tauopathies induce tau inclusions in mouse brain. Proc Natl Acad Sci U S A. 2013;110(23):9535–40.

234. Sanders DW, Kaufman SK, Devos SL, Sharma AM, Mirbaha H, Li A, et al. Distinct tau prion strains propagate in cells and mice and define different tauopathies. Neuron. 2014;82(6):1–18.

235. Dujardin S, Lécolle K, Caillierez R, Bégard S, Zommer N, Lachaud C, et al. Neuron-to-neuron wild-type tau protein transfer through a trans-synaptic mechanism: relevance to sporadic tauopathies. Acta Neuropathol Commun. 2014;2(1):14.

236. Luk KC, Kehm V, Carroll J, Zhang B, Brien PO, Trojanowski JQ, et al. Pathological a-Synuclein Transmission in Nontransgenic Mice. Science. 2012;338(6109):949–53.

237. Stohr J, Watts JC, Mensinger ZL, Oehler a., Grillo SK, DeArmond SJ, et al. Purified and synthetic Alzheimer's amyloid beta (A) prions. Proc Natl Acad Sci. 2012;109(27):11025–30.

238. Meyer-Luehmann M, Coomaraswamy J, Bolmont T, Kaeser S, Schaefer C, Kilger E, et al. Exogenous induction of cerebral beta-amyloidogenesis is governed by agent and host. Science. 2006;313(5794):1781–4.

239. Eisele YS, Obermüller U, Heilbronner G, Baumann F, Kaeser SA, Wolburg H, et al. Peripherally applied Abeta-containing inoculates induce cerebral beta-amyloidosis. Science. 2010;330(6006):980–2.

240. Hasegawa M, Nonaka T, Tsuji H, Tamaoka A, Yamashita M, Kametani F, et al. Molecular dissection of TDP-43 proteinopathies. J Mol Neurosci. 2011;45(3):480–5.

241. Chen AK, Lin RY, Hsieh EZ, Tu PH, Chen RP, Liao TY, et al. Induction of amyloid fibrils by the C-terminal fragments of TDP-43 in amyotrophic lateral sclerosis. J Am Chem Soc. 2010;132(4):1186–7.

242. Münch C, O'Brien J, Bertolotti A. Prion-like propagation of mutant superoxide dismutase-1 misfolding in neuronal cells. Proc Natl Acad Sci U S A. 2011;108(9):3548–53.

243. Ren PH, Lauckner JE, Kachirskaia I, Heuser JE, Melki R, Kopito RR. Cytoplasmic penetration and persistent infection of mammalian cells by polyglutamine aggregates. Nat Cell Biol. 2009;11(2):219–25.

244. Bruce ME, McConnell I, Fraser H, Dickinson AG. The disease characteristics of different strains of scrapie in Sinc congenic mouse lines: implications for the nature of the agent and host control of pathogenesis. J Gen Virol. 1991 Mar;72(Pt 3):595–603.

245. Safar J, Wille H, Itri V, Groth D, Serban H, Torchia M, et al. Eight prion strains have PrP(Sc) molecules with different conformations. Nat Med. 1998;4(10):1157–65.

246. Poggiolini I, Saverioni D, Parchi P. Prion protein misfolding, strains, and neurotoxicity: an update from studies on mammalian prions. Int J Cell Biol. 2013;2013:910314.

247. Guo JL, Covell DJ, Daniels JP, Iba M, Stieber A, Zhang B, et al. Distinct α-synuclein strains differentially promote tau inclusions in neurons. Cell. 2013;154(1):103–17.

248. Petkova AT, Leapman RD, Guo Z, Yau WM, Mattson MP, Tycko R. Self-propagating, molecular-level polymorphism in Alzheimer's beta-amyloid fibrils. Science (80-). 2005;307(5707):262–5.

249. Stöhr J, Condello C, Watts JC, Bloch L, Oehler A, Nick M, et al. Distinct synthetic Aβ prion strains producing different amyloid deposits in bigenic mice. Proc Natl Acad Sci U S A. 2014;11(28):10323–8.

250. Toledo JB, Van Deerlin VM, Lee EB, Suh E, Baek Y, Robinson JL, et al. A platform for discovery: The University of Pennsylvania Integrated Neurodegenerative Disease Biobank. Alzheimer's Dement. 2014;10(4):477–84.

251. Otvos L, Feiner L, Lang E, Szendrei GI, Goedert M, Lee VM. Monoclonal antibody PHF-1 recognizes tau protein phosphorylated at serine residues 396 and 404. J Neurosci Res. 1994;39(6):669–73.

252. Sperfeld AD, Collatz MB, Baier H, Palmbach M, Storch A, Schwarz J, et al. FTDP-17: an early-onset phenotype with parkinsonism and epileptic seizures caused by a novel mutation. Ann Neurol. 1999;46(5):708–15.

253. Yasuda M, Yokoyama K, Nakayasu T, Nishimura Y, Matsui M, Yokoyama T, et al. A Japanese patient with frontotemporal dementia and parkinsonism by a tau P301S mutation. Neurology. 2000;55(8):1224–7.

254. Lossos A, Reches A, Gal A, Newman JP, Soffer D, Gomori JM, et al. Frontotemporal dementia and parkinsonism with the P301S tau gene mutation in a Jewish family. J Neurol. 2003 Jun;250(6):733–40.

255. Hurtado DE, Molina-Porcel L, Iba M, Aboagye AK, Paul SM, Trojanowski JQ, et al. A{beta} accelerates the spatiotemporal progression of tau pathology and augments tau amyloidosis in an Alzheimer mouse model. Am J Pathol. 2010;177(4):1977–88.

256. Mercken M, Vandermeeren M, Lübke U, Six J, Boons J, Van de Voorde A, et al. Monoclonal antibodies with selective specificity for Alzheimer tau are directed against phosphatase-sensitive epitopes. Acta Neuropathol. 1992;84(3):265–72.

257. Jicha GA, Bowser R, Kazam IG, Davies P. Alz-50 and MC-1, a new monoclonal antibody raised to paired helical filaments, recognize conformational epitopes on recombinant tau. J Neurosci Res. 1997;48(2):128–32.

258. Jicha GA, Lane E, Vincent I, Otvos L, Hoffmann R, Davies P. A conformation- and phosphorylation-dependent antibody recognizing the paired helical filaments of Alzheimer's disease. J Neurochem. 1997;69(5):2087–95.

259. Kosik KS, Orecchio LD, Binder L, Trojanowski JQ, Lee VM, Lee G. Epitopes that span the tau molecule are shared with paired helical filaments. Neuron. 1988;1(9):817–25.

260. De Silva R, Lashley T, Gibb G, Hanger D, Hope A, Reid A, et al. Pathological inclusion bodies in tauopathies contain distinct complements of tau with three or four microtubule-binding repeat domains as demonstrated by new specific monoclonal antibodies. Neuropathol Appl Neurobiol. 2003;29(3):288–302.

261. Waxman EA, Duda JE, Giasson BI. Characterization of antibodies that selectively detect alpha-synuclein in pathological inclusions. Acta Neuropathol. 2008;116(1):37–46.

262. Neumann M, Kwong LK, Lee EB, Kremmer E, Flatley A, Xu Y, et al. Phosphorylation of S409/410 of TDP-43 is a consistent feature in all sporadic and familial forms of TDP-43 proteinopathies. Acta Neuropathol. 2009;117(2):137–49.

263. Lee EB, Leng LZ, Zhang B, Kwong L, Trojanowski JQ, Abel T, et al. Targeting amyloid-beta peptide (Abeta) oligomers by passive immunization with a conformation-selective monoclonal antibody improves learning and memory in Abeta precursor protein (APP) transgenic mice. J Biol Chem. 2006;281(7):4292–9.

264. Lee VM, Page CD, Wu HL, Schlaepfer WW. Monoclonal antibodies to gel-excised glial filament protein and their reactivities with other intermediate filament proteins. J Neurochem. 1984;42(1):25–32.

265. Paxinos G, Franklin K. The mouse brain in stereotaxic coordinates. 2nd ed. Waltham, MA; 2003.

266. Lippa CF, Fujiwara H, Mann DM, Giasson B, Baba M, Schmidt ML, et al. Lewy bodies contain altered alpha-synuclein in brains of many familial Alzheimer's disease patients with mutations in presenilin and amyloid precursor protein genes. Am J Pathol. 1998 Nov;153(5):1365–70.

267. Lippa CF, Schmidt ML, Lee VM, Trojanowski JQ. Antibodies to alpha-synuclein detect Lewy bodies in many Down's syndrome brains with Alzheimer's disease. Ann Neurol. 1999;45(3):353–7.

268. Schmidt ML, Schuck T, Sheridan S, Kung MP, Kung H, Zhuang ZP, et al. The fluorescent Congo red derivative, (trans, trans)-1-bromo-2,5-bis-(3-

hydroxycarbonyl-4-hydroxy)styrylbenzene (BSB), labels diverse beta-pleated sheet structures in postmortem human neurodegenerative disease brains. Am J Pathol. 2001;159(3):937–43.

269. Higuchi M, Zhang B, Forman MS, Yoshiyama Y, Trojanowski JQ, Lee VM. Axonal degeneration induced by targeted expression of mutant human tau in oligodendrocytes of transgenic mice that model glial tauopathies. J Neurosci. 2005;25(41):9434–43.

270. Goedert M, Jakes R, Crowther RA. Effects of frontotemporal dementia FTDP-17 mutations on heparin-induced assembly of tau filaments. FEBS Lett. 1999;450(3):306–11.

271. Iba M, McBride JD, Guo JL, Zhang B, Trojanowski JQ, Lee VM. Tau pathology spread in PS19 tau transgenic mice following locus coeruleus (LC) injections of synthetic tau fibrils is determined by the LC's afferent and efferent connections. Acta Neuropathol. 2015;130(3):349–62.

272. Braak H, Thal DR, Ghebremedhin E, Del Tredici K. Stages of the pathologic process in Alzheimer disease. J Neuropathol Exp Neurol. 2011;70(11):960–9.

273. Yazawa I, Giasson BI, Sasaki R, Zhang B, Joyce S, Uryu K, et al. Mouse model of multiple system atrophy alpha-synuclein expression in oligodendrocytes causes glial and neuronal degeneration. Neuron. 2005;45(6):847–59.

274. Jucker M, Walker LC. Self-propagation of pathogenic protein aggregates in neurodegenerative diseases. Nature. 2013;501(7465):45–51.

275. Arriagada P, Growdon JH, Hedley-Whyte ET, Hyman BT. Neurofibrillary tangles but not senile plaques parallel duration and severity of Alzheimer's disease. Neurology. 1992;42(3 Pt 1):631–9.

276. Gómez-Isla T, Hollister R, West H, Mui S, Growdon JH, Petersen RC, et al. Neuronal loss correlates with but exceeds neurofibrillary tangles in Alzheimer's disease. Ann Neurol. 1997;41(1):17–24.

277. Trinczek B, Biernat J, Baumann K, Mandelkow EM, Mandelkow E. Domains of tau protein, differential phosphorylation, and dynamic instability of microtubules. Mol Biol Cell. 1995;6(12):1887–902.

278. Ittner LM, Ke YD, Delerue F, Bi M, Gladbach A, van Eersel J, et al. Dendritic function of tau mediates amyloid-beta toxicity in Alzheimer's disease mouse models. Cell. 2010;142(3):387–97.

279. Keck S, Nitsch R, Grune T, Ullrich O. Proteasome inhibition by paired helical filament-tau in brains of patients with Alzheimer's disease. J Neurochem. 2003;85(1):115–22.

280. Kuchibhotla K, Wegmann S, Kopeikina KJ, Hawkes J, Rudinskiy N, Andermann ML, et al. Neurofibrillary tangle-bearing neurons are functionally integrated in cortical circuits in vivo. Proc Natl Acad Sci U S A. 2014;111(1):510–4.

281. Santacruz K, Lewis J, Spires T, Paulson J, Kotilinek L, Ingelsson M, et al. Tau suppression in a neurodegenerative mouse model improves memory function. Science. 2005;309(5733):476–81.

282. Wittmann CW, Wszolek MF, Shulman JM, Salvaterra PM, Lewis J, Hutton M, et al. Tauopathy in Drosophila: neurodegeneration without neurofibrillary tangles. Science. 2001;293(5530):711–4.

283. Kopeikina KJ, Hyman BT, Spires-Jones TL. Soluble forms of tau are toxic in Alzheimer's disease. Transl Neurosci. 2012;3(3):223–33.

284. Lasagna-reeves CA, Castillo-carranza DL, Sengupta U, Sarmiento J, Troncoso J, Jackson GR, et al. Identification of oligomers at early stages of tau aggregation in Alzheimer's disease. FASEB J. 2012;26(5):1946–59.

285. Valera E, Spencer B, Masliah E. Immunotherapeutic approaches targeting amyloid-β, α-synuclein, and tau for the treatment of neurodegenerative disorders. Neurotherapeutics. 2015;

286. Pedersen JT, Sigurdsson EM. Tau immunotherapy for Alzheimer's disease. Trends Mol Med. 2015;21(6):394–402.

287. Wisniewski T, Drummond E. Developing therapeutic vaccines against Alzheimer's disease. Expert Rev Vaccines. 2015;

SUPPLEMENT

Acta Neuropathol
DOI 10.1007/s00401-014-1373-0

ORIGINAL PAPER

Differential induction and spread of tau pathology in young PS19 tau transgenic mice following intracerebral injections of pathological tau from Alzheimer's disease or corticobasal degeneration brains

Susana Boluda · Michiyo Iba · Bin Zhang · Kevin M. Raible · Virginia M-Y. Lee · John Q. Trojanowski

Received: 10 October 2014 / Revised: 4 December 2014 / Accepted: 4 December 2014

Abstract Filamentous tau pathologies are hallmark lesions of several neurodegenerative tauopathies including Alzheimer's disease (AD) and corticobasal degeneration (CBD) which show cell type-specific and topographically distinct tau inclusions. Growing evidence supports templated transmission of tauopathies through functionally interconnected neuroanatomical pathways suggesting that different self-propagating strains of pathological tau could account for the diverse manifestations of neurodegenerative tauopathies. Here, we describe the rapid and distinct cell type-specific spread of pathological tau following intracerebral injections of CBD or AD brain extracts enriched in pathological tau (designated CBD-Tau and AD-Tau, respectively) in young human mutant P301S tau transgenic (Tg) mice (line PS19) ~6–9 months before they show onset of mutant tau transgene-induced tau pathology. At 1 month post-injection of CBD-Tau, tau inclusions developed predominantly in oligodendrocytes of the fimbria and white matter near the injection sites with infrequent intraneuronal tau aggregates. In contrast, injections of AD-Tau in young PS19 mice induced tau pathology predominantly in neuronal perikarya with little or no oligodendrocyte involvement 1 month post-injection. With longer post-injection survival intervals of up to 6 months, CBD-Tau- and AD-Tau-induced tau pathology spread to different brain regions distant from the injection sites while maintaining the cell type-specific pattern noted above. Finally, CA3 neuron loss was detected 3 months post-injection of AD-Tau but not CBD-Tau. Thus, AD-Tau and CBD-Tau represent specific pathological tau strains that spread differentially and may underlie distinct clinical and pathological features of these two tauopathies. Hence, these strains could become targets to develop disease-modifying therapies for CBD and AD.

Keywords Alzheimer's disease · Corticobasal degeneration · Seeded transmission of pathological tau · Frontotemporal degeneration

S. Boluda · M. Iba · B. Zhang · K. M. Raible · V. M.-Y. Lee · J. Q. Trojanowski (✉)
Department of Pathology and Laboratory Medicine, The Center for Neurodegenerative Disease Research, Institute on Aging, University of Pennsylvania, Perelman School of Medicine, 3600 Spruce Street, Philadelphia, PA 19104-4283, USA
e-mail: trojanow@mail.med.upenn.edu

Introduction

Alzheimer's disease (AD), corticobasal degeneration (CBD), progressive supranuclear palsy (PSP), argyrophilic grain disease (AGD) and Pick's disease (PiD) are neurodegenerative tauopathies characterized by different clinical features as well as distinct topographic and cell type-specific tau pathologies [2, 29]. Tau is predominantly an axonal microtubule-associated protein expressed as 6 alternatively spliced isoforms encoded by the tau gene (*MAPT*) with 3 (3R tau) versus 4 (4R tau) microtubule (MT)-binding repeats and 0 (0N), 1 (1N) or 2 (2N) amino terminal inserts resulting in 4R0N, 4R1N, 4R2N, 3R0N, 3R1N and 3R2N tau proteins at a 1:1 ratio of 3R to 4R tau in the adult CNS [2, 29]. Tau promotes MT assembly as well as stability, and while young tau knockout mice appear normal, aged knockout mice show synapse loss and cognitive impairments [36]. In the disease state, tau is hyperphosphorylated [28], nitrated [17], acetylated [8, 20, 21, 38] and glycosylated [26, 37] which may contribute to disease. While all 6 tau isoforms contribute to tau pathology in AD, 4R tau isoforms predominate in CBD, AGD and PSP, and 3R tau isoforms predominate in PiD [11, 39, 54–56].

Published online: 24 December 2014

The identification of >40 *MAPT* mutations pathogenic for familial tauopathies indicates that pathological tau alone is sufficient to cause neurodegeneration [2, 18, 44, 47, 48, 53].

It is known that pathological tau is taken up by cells and seeds aggregation of endogenous tau to form AD-like paired helical filaments (PHFs) or neurofibrillary tangles (NFTs) [9, 12, 14]. Further, injections of brain extracts from mutant human tau Tg mice harboring NFTs into the brains of Tg mice overexpressing wild-type human tau (ALZ17 line) induced tau inclusions [7], while injections of synthetic preformed tau fibrils (PFFs) into PS19 mice overexpressing mutant human tau induced similar tau pathology [19] indicating that tau PFFs alone are sufficient to transmit tau pathology. These and other studies suggest that pathological tau propagates to neighboring normal cells or those that are synaptically interconnected [1, 10, 35].

Since distinct tau strains may underlie diverse manifestations of neurodegenerative tauopathies [6, 45], we characterized the differential topography, cell spreading and consequences of tau pathology induced in the PS19 mice after injections of enriched pathological tau preparations from CBD (CBD-Tau) or AD (AD-Tau) brains and showed that this resulted in striking CBD-like or AD-like tau pathology that we attribute to different specific tau strains in CBD-Tau and AD-Tau.

Materials and methods

Tg Mice

Line PS19 Tg mice overexpressing the T34 isoform of tau (4R1N) encoding the P301S *MAPT* mutation driven by the murine prion protein promoter [52] were used in the studies described here. The PS19 line at Penn was maintained on a B6C3 background, but as recently reported [19] and reviewed elsewhere (http://www.alzforum.org/research-models/tau-p301s-line-ps19), the onset of neurodegenerative tauopathy in the PS19 Tg mice at Penn has shifted from 6 to about 12 months of age thereby allowing a longer time window for the transmission studies described here.

Generation of enriched pathological tau from CBD and AD brains

Brain extracts from two longitudinally followed and autopsy confirmed CBD subjects as well as one AD patient and one elderly individual with Down syndrome (DS) whose brain contained abundant NFTs indistinguishable from AD, so we refer to this here as DSAD [28], were prepared. Brain extracts from a non-demented patient who showed no signs of neurodegenerative disease and no AD neuropathologic change at postmortem histological examination were used to generate normal or control tau (CTRL-Tau) preparations. All procedures were done sterile and at 4 °C.

For the preparation of CBD-Tau and CTRL-Tau, 400 mg of cortical gray matter from histologically confirmed cases of CBD and CTRL subjects were homogenized in 10 % PBS (W/V), briefly sonicated with an ultrasonic liquid processor (QSonica Microson™ XL-2000; 10 pulses; setting 2; 0.5 s/pulse) and centrifuged at 3,000*g* for 5 min (Beckman Coulter Optima™ MAX Ultracentrifuge). The resulting supernatant was centrifuged again at 100,000*g* for 30 min, following which the pellet was re-suspended in PBS in 1/3 of the initial volume, briefly sonicated and centrifuged again at 100,000*g* for 60 min. The resulting pellet was resuspended in PBS at 50 % of the initial volume. The pellet was sonicated, aliquoted, snap-frozen and stored at −80 °C until use.

The pathological AD-Tau- and DSAD-Tau-enriched preparations were processed from histologically confirmed AD and DSAD cases following a modified sucrose gradient protocol for the purification of AD PHFs [31]. Briefly, 50 g of frozen cortical gray matter was dissected, homogenized in 4 volumes of high-salt (H–S) RAB buffer (RAB buffer: 100 mM MES, 1 mM EDTA, 0.5 mM $MgSO_4$, 2 mM DTT, pH 6.8 + 0.75 M NaCl), incubated for 30 min on ice to depolymerize MTs and centrifuged at 126,000*g* for 45 min to remove soluble tau. The resulting pellet was used to generate AD-Tau by differential centrifugation, extraction with Sarkosyl and boiling to remove contaminants, followed by fractionation using a step-wise sucrose gradient to enrich for pathological AD-Tau [31]. AD-Tau was most enriched between the 1.75 and 2.00 M sucrose interface after overnight centrifugation and this material was collected and washed after which its purity was verified (see below).

Western blot analysis

The purity of enriched CBD-Tau and AD-Tau as well as the lack of pathological tau in the normal CTRL-Tau preparations was confirmed using Coomassie blue stained 7.5 % SDS-PAGE gel. The total protein loaded was 18 µg for CTRL, 22 µg for CBD-1, 26 µg for CBD-2, 32 µg for DSAD and 26 µg for AD. The same samples were analyzed by immunoblotting using anti-tau antibodies that recognize a phosphorylation-independent anti-tau polyclonal antibody raised to recombinant tau (17025, 1:2,000; produced in the Penn Center for Neurodegenerative Disease Research (CNDR); [52]) and PHF tau phosphorylated at Ser 396/404 (monoclonal antibody (mAb) PHF-1, 1:1,000; a gift of Peter Davies; [41]) as shown in Fig. 1.

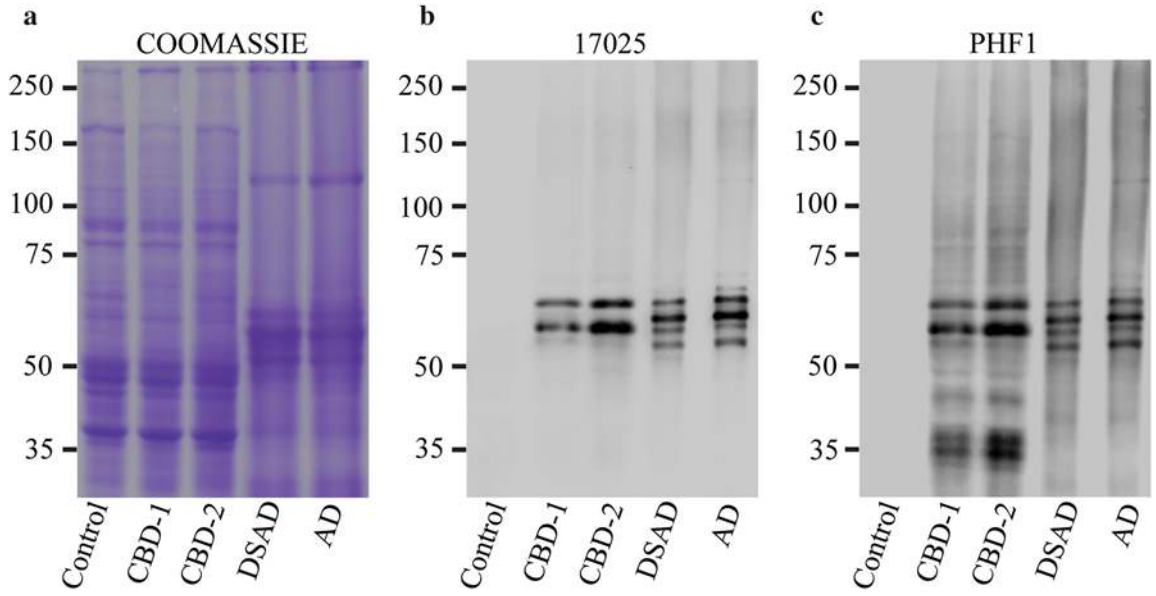

Fig. 1 Biochemical analysis of the pathological tau protein-enriched extracts obtained from human brains with a neuropathological diagnosis of CBD, AD, DSAD and a non-disease normal control brain used for injection into PS19 Tg mice. SDS gel stained with *Coomassie blue* (**a**). Immunoblots stained with 17025 (**b**) and PHF1 (**c**)

Tau enzyme-linked immunosorbent assay (ELISA)

To determine total tau concentration in the fractions enriched in CBD-Tau, AD-Tau, DSAD-Tau and CTRL-Tau, we performed sandwich ELISA with anti-tau mAb Tau 5 as the capturing antibody in combination with mAbs HT7/BT2 (Thermo-Scientific) for the reporter antibodies, as previously described [14].

Stereotaxic surgery

All experiments were performed in accordance with protocols approved by the Institutional Animal Care and Use Committee of the University of Pennsylvania. Briefly, 2 to 5 month old PS19 mice of either gender were deeply anesthetized with a ketamine/xylazine/acepromazine mixture, immobilized in a stereotaxic frame (David Kopf Instruments), following which different brain extracts were injected stereotaxically into the hippocampus and overlying neocortex using predetermined coordinates for hippocampus (Bregma −2.5 mm, lateral +2 mm, and depth −2 mm from brain surface) and overlying cortex (Bregma −2.5 mm, lateral +2 mm and depth −0.8 mm from brain surface) with a 10 µl Hamilton syringe under aseptic conditions as described [19]. All injected mice were observed during and after surgery. The total volume injected per site was 2.5 µl for all mice. The mice used for each experimental condition are summarized in Table 1.

Histology and immunohistochemistry (IHC)

At 1, 3 and 6 months post-injection, mice were sacrificed and their brains were fixed and processed as reported [19]. IHC was conducted on mouse brain sections incubated with primary antibodies followed by a polymer horseradish peroxidase detection system (Biogenex) and counterstained with hematoxylin. For semiquantitative IHC studies, every 20th slide from the serially sectioned mouse brains was immunostained with mAb AT8 (specific for tau phosphorylated at Ser202/Thr205; 1:10,000; Thermo-Scientific) and mAb MC1 (specific for a pathologic conformation of tau; 1:8,000; a gift from Peter Davies; [22]). Other anti-tau antibodies used in this study include: TG3 (specific for a conformation-dependent phosphorylated tau epitope; 1:250; a gift from Peter Davies; [23]), mAb T49, CNDR (specific for mouse tau; 1:2,000; [52]) and mAb T14, CNDR (specific for human tau, amino acids 141–178; 1:1,000; [25]). We also used 3R (RD3 1:2,500-5,000; Millipore, Billerica, MA, USA) and 4R (RD4 1:5,000-10,000; Millipore, Billerica, MA, USA) tau isoform-specific antibodies as described earlier [20]. Other antibodies used include mAb 81A, CNDR (specific for α-synuclein phosphorylated at Ser129; 1:50,000; [51]), mAb 409/410-TDP-43 (phosphorylation dependent at amino acids 409/410; 1:200; [40]), mAb NAB228, CNDR (antibody specific for $A\beta_{1-11}$: 1:60,000 with formic acid pre-treatment; [27]), Olig2 (specific for oligodendrocytes; 1:250, Millipore), a rat anti-glial fibrillary acidic protein (GFAP) mAb, CNDR (specific for

Table 1 PS19 mice used for the experiments

Injections of CBD-Tau and CTRL-Tau				
CBD ($n = 18$ mice)				
Time postinjection (months)	Number of mice		Total injected tau (μg)	
	CBD-1	CBD-2		
1	4	2	0.05	
3	4	2	0.05	
6	4	2	0.05	
CTRL ($n = 4$ mice)				
Time postinjection (months)	Number of mice	Total injected tau (μg)		
1	2	0.003		
6	2	0.003		
Injections of AD-Tau and DSAD-Tau				
AD ($n = 12$ mice)/*DSAD* ($n = 12$ mice)				
Time postinjection (months)	Number of mice		Total injected tau (μg)	
	AD	DSAD	AD	DSAD
1	4	4	10.5	12.5
3	4	4	10.5	12.5
6	4	4	10.5	12.5
DSAD serial dilutions ($n = 12$ mice)				
Time postinjection (months)	Number of mice	Total injected tau (μg)		
1	3	0.065		
1	3	0.25		
1	3	1.5		
1	3	12.5		

All mice were injected at two sites: right hippocampus and overlying cortex. The injected volume for all mice was 5 μl total (2.5 μl/site). CBD1 and CBD2 represent CBD-Tau generated from two different CBD brains. All mice were 2 months old at time of injection except for the group injected with CBD-Tau (CBD-1) that were 5 months old at time of injection. The older mice did not show any differences in the distribution and extent of tau pathology since mice injected with CBD-Tau from CBD1 and CBD2 brains were similar

astrocytes; 1:1,000; clone 2.2B10; [30]) and pAb, Iba-1 (specific to microglia; 1:1,000; Wako Chemicals).

Double-label immunofluorescence studies were used to identify glial cells with tau pathology as described [19]. To assess the amyloid properties of the tau inclusions induced by CBD-Tau, AD-Tau and DSAD-Tau, sections were also stained with the Thioflavin S (ThS) amyloid-binding dye as described [19].

Quantification and statistics

We quantified the extent of glial tau pathology spread following injections with CBD-Tau in PS19 mice in a semi-quantitative manner (0: none; 1+: scant; 2+: moderate; 3+: abundant) where 1+ is rare (at least two tau inclusion bearing oligodendrocytes in a section) to a low burden of glial tau pathology and 3+ represents the presence of at least 25 tau-positive oligodendrocytes in a section. The tau pathology spread in the PS19 mice injected with AD-Tau and DSAD-Tau was more abundant than the CBD-Tau-injected mice, but they were very similar to each other and they were evaluated semiquantitatively (0: none; 1+: scant; 2+: moderate; 3+: abundant) as a single group. Scant (1+) tau pathology represents the presence of at least two tangle-bearing neurons in a particular region of a section and low neuritic tau pathology. Abundant (3+) represents >50 tau-positive neurons in a region of a section or abundant neuritic tau pathology. The same criteria were used for the assessment of the serial dilution assay of DSAD-Tau-injected mice. The topographical distribution of the tau pathology following CBD-Tau and AD-Tau or DSAD-Tau injections was used to generate heatmaps as described [19].

To evaluate neuron loss, we assessed a defined portion of the CA3 and CA1 region of matched brain sections stained with hematoxylin and eosin (H&E) from PS19 mice injected with AD-Tau or DSAD-Tau ($n = 7$ per time point), CBD-Tau ($n = 6$ per time point) and CTRL-Tau ($n = 2$ per time point) at 1, 3 and 6 months post-injection using 20× images. Neurons were individually counted using ImageJ software (National Institutes of Health). To determine statistical differences between groups, one-way ANOVA and Tukey's multiple-comparison test were used.

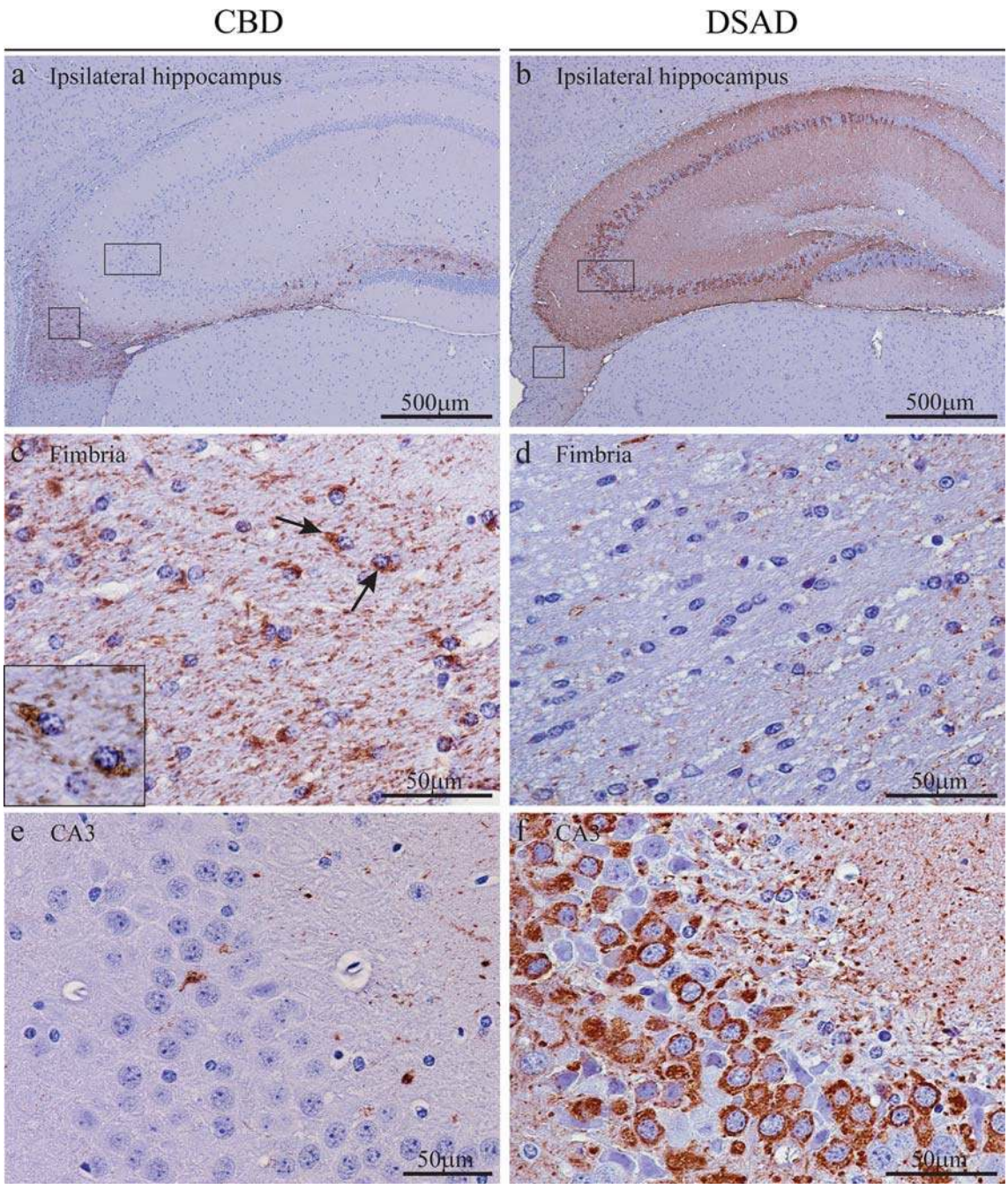

Fig. 2 Development of cell type-specific tau inclusions after injection of CBD-Tau- or DSAD-Tau-enriched protein extracts into the brains of PS19 mice. **a**, **c**, **e** AT8-positive oligodendroglial inclusions developed in the fimbria of the hippocampus on the injected side at 1 month after the injection of CBD-Tau. **b**, **d**, **f** AT8-positive inclusions developed in the perikarya of neurons of the hippocampus of DSAD-Tau-injected mice. **c** A higher magnification of the *square boxed area* in (**a**) is shown in (**c**) demonstrating AT8-positive tau inclusions in many oligodendrocytes of the fimbria (**c**). The *inset* in (**c**) shows a detail of the oligodendrocytes indicated by the *black arrows*. **d** A higher magnification of the *square boxed area* in (**b**) is shown in (**d**) demonstrating the absence of tau inclusions in the oligodendrocytes of the fimbria (**d**) which contrasts with the CBD-Tau-injected mice. **e** Higher magnification of the *rectangular boxed area* in (**a**) demonstrating only rare intraneuronal inclusions in the CA3 region of the hippocampus (**e**). In **f**, where a higher magnification of the *rectangular boxed area* in (**b**) is depicted, there is abundance of perikaryal AT8 inclusions in CA3 of the hippocampus. *Scale bar*, *upper row* 500 μm; *middle* and *bottom rows* 50 μm

Results

Injections of CBD-Tau and AD-Tau induce tau pathology in PS19 Tg mice

To investigate whether pathological tau from different tauopathy brains induce distinct tau pathologies, we generated CTRL-Tau, CBD-Tau, AD-Tau or DSAD-Tau enriched preparations from the brains of a CTRL subject and 4 patients afflicted with these tauopathies, respectively, and then we injected them into the right hippocampus and overlying cortex of PS19 Tg mice (2–5 months old) (Table 1) after which we examined the resulting tau pathology at 1, 3 and 6 months post-injection intervals (Figs. 2, 3, 4). Mice developed pathology as early as 1 month after injection. PS19 mice injected with CBD-Tau induced predominantly glial tau pathology in white matter tracts and hippocampus close to the injection site at the earliest post-injection time point as detected by mAb AT8 (Fig. 2a, c, e). At 1 month post-injection, AT8-positive tau inclusions were seen in oligodendrocytes of the adjacent hippocampal fimbria (4/6; 66 % of mice) as well as in the alveus/subcortical white matter/external capsule contiguous with the injection site (3/6; 50 % of mice) (Fig. 2, 3). Neurons in hippocampal regions CA1, CA3, dentate gyrus and subiculum also showed some perikaryal tau inclusions (Fig. 2e), but they were scant compared to the oligodendrocytes with tau pathology in the fimbria (Fig. 2c). They also were infrequent compared to the large numbers of tangle-bearing neurons seen in the AD-Tau and DSAD-Tau injected mice (Fig. 2b, d, f) described below. Oligodendroglial tau inclusions extended beyond the injection site to rostral and caudal regions of the brain quite distal from the injection site (Fig. 3b). Infrequent or sparse intraneuronal tau inclusions in the hippocampus were also seen rostral and caudal to the injection site. Additionally, a small number of AT8 immunoreactive neurons were seen in the supramammillary bodies (data not shown). At 1 month post-injection, the tau inclusion pathology was limited to the side of the injection site, however, no tau pathology was seen in the overlying cortex even near these cortical injection sites. Finally, similar results were obtained when CBD-Tau from a second case with a confirmed CBD neuropathological diagnosis was injected in another cohort of mice (Table 1).

We next injected AD-Tau and DSAD-Tau into the brains of young PS19 mice which also showed prominent tau pathology at 1 month post-injection. Since the distribution of tau pathology in mice injected with AD-Tau and DSAD-Tau is very similar and the burden of AD pathology in both brains was similar, the data generated with these extracts were considered together as the AD/DSAD group. However, in contrast to the CBD-Tau-injected mice, the AD/DSAD-Tau-injected mice showed tau pathology mainly in perikarya and processes of hippocampal neurons (Fig. 2b, d, f). Mapping the spread of pathological tau from the hippocampal injection site over time post-injection in the AD/DSAD-Tau injected mice demonstrated that the tau pathology extended to rostral and caudal regions of the brain (Fig. 4). In rostral areas, lateral septal nuclei were involved bilaterally with a moderate burden of tau inclusions in the processes of neurons. In caudal brain regions such as the subiculum, entorhinal cortex (EC) (Fig. 4), locus coeruleus (LC) and raphe nuclei, there also were AT8-positive neuronal aggregates (data not shown). Additionally, intracytoplasmic hyperphosphorylated tau inclusions were seen in the supramammillary nuclei (5/8; 63 % of mice) and in neocortex (4/8; 50 % of mice). Moreover, neuronal tau inclusion pathology was seen in the contralateral hemisphere where it was mainly limited to hippocampal neurons, with a predominance of involvement of CA3 region, and a few AT8-positive neurons in the EC. As in the ipsilateral side, intraneuronal tau pathology extended to rostral and caudal regions of the brain. Notably, no oligodendrocytic tau pathology was seen 1 month post-injection in the fimbria or the subcortical white matter/external capsule following AD/DSAD-Tau injections. Finally, the tau pathology detected in these studies was exclusively 4R immunoreactive as would be expected in the PS19 that do not express any 3R tau.

As noted above, our non-injected PS19 mice begin to show transgene-driven tau pathology at ~12 months of age [19]. To control for this onset of transgene-driven tau pathology, we injected four young (2- to 3-month-old) PS19 mice with CTRL-Tau intracerebrally and these mice did not show any tau pathology at 1 or 6 months post-injection (data not shown).

Finally, none of the CBD-Tau- or AD/DSAD-Tau-injected PS19 mice showed any evidence of α-synuclein, TDP-43 or β-amyloid pathology despite the fact that these pathologies co-occur in AD/DSAD brains [32–34].

Fig. 3 Tau inclusions that developed in PS19 mice injected with CBD-Tau increased in intensity and spread to regions distal from the injection site with increasing post-injection survival times. **a** Micrographs of brain sections immunostained with AT8 showing the fimbria, alveus/external capsule and stratum radiatum ipsilateral to the injection site in the PS19 mice at 1, 3, 6 months post-injection. *Scale bar*, *upper row* 200 μm; *middle* and *lower rows* 100 μm. **b** Heatmaps of coronal sections showing the CBD-Tau-induced glial tau pathology at the same time points as in (**a**). Quantification [1 month ($n = 6$), 3 months ($n = 6$) and 6 months ($n = 6$)] was conducted as described in "Materials and methods" to generate these heatmaps. Each heatmap *panel* represents pathology distribution in one of the three coronal planes (Bregma −1.22, −2.18 and −2.92). *Left column* shows sagittal view of the selected coronal planes indicated by a *red line*. *Blue stars* indicate injection site

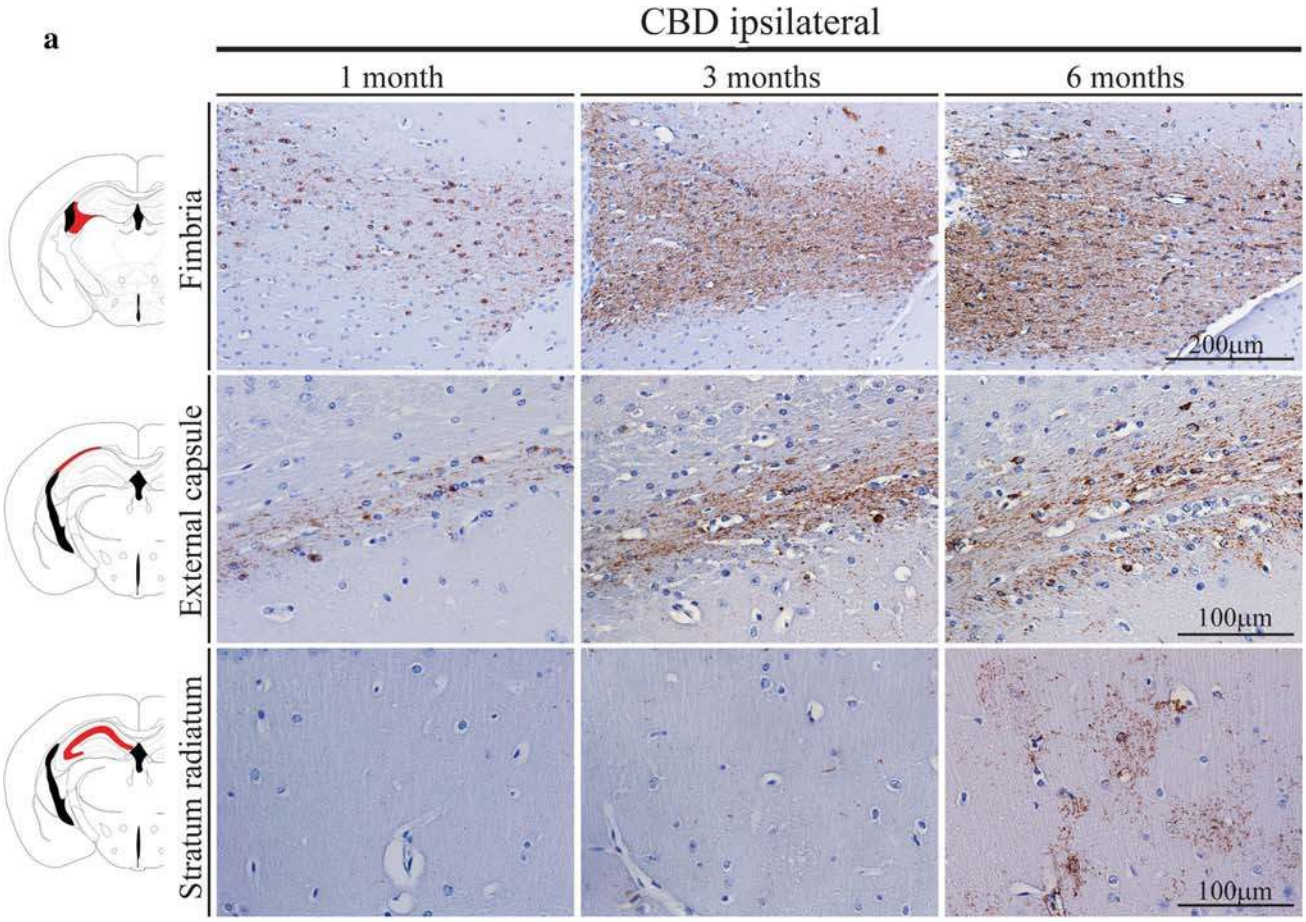
a
CBD ipsilateral
1 month
3 months
6 months
Fimbria
External capsule
Stratum radiatum
200µm
100µm
100µm

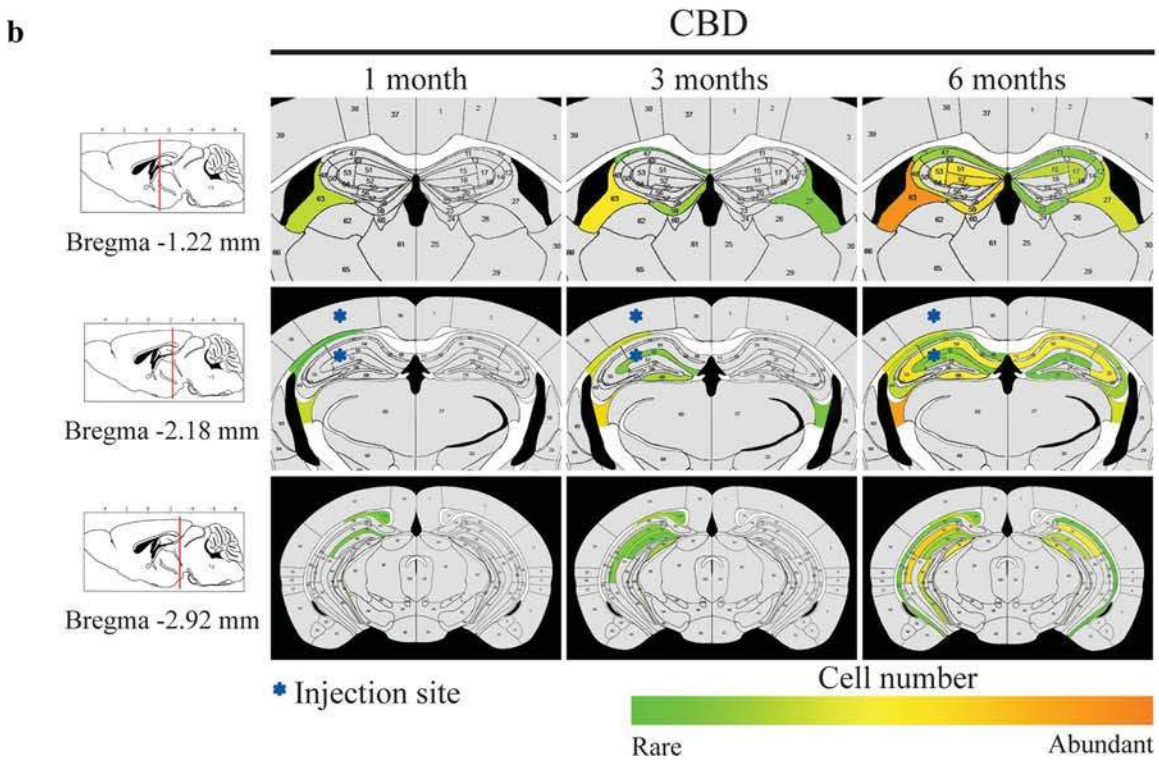
b
CBD
1 month
3 months
6 months
Bregma -1.22 mm
Bregma -2.18 mm
Bregma -2.92 mm
Injection site
Cell number
Rare
Abundant

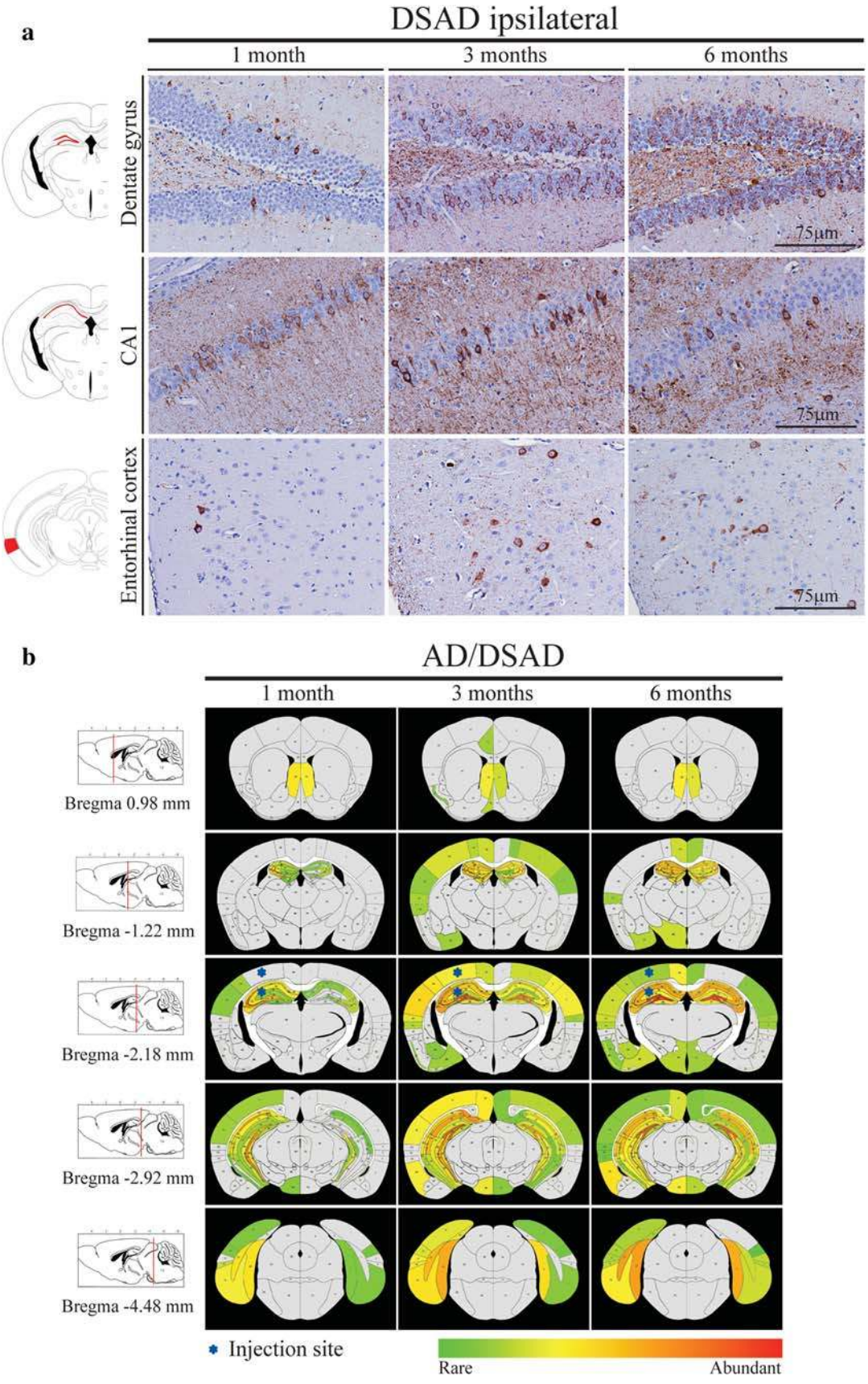
a
DSAD ipsilateral
1 month
3 months
6 months
Dentate gyrus
CA1
Entorhinal cortex
75µm
b
AD/DSAD
1 month
3 months
6 months
Bregma 0.98 mm
Bregma -1.22 mm
Bregma -2.18 mm
Bregma -2.92 mm
Bregma -4.48 mm
Injection site
Rare
Abundant

◀**Fig. 4** Neuronal tau inclusions developed in PS19 mice injected with AD-Tau and DSAD-Tau and they increased in abundance, intensity and spread to regions distal from the injected site with increasing post-injection survival times. **a** Microscopic images of brain sections of DSAD-Tau-injected mice. The images are representative of the dentate gyrus, CA1 and entorhinal cortex of the side ipsilateral to the injection following IHC with AT8 at 1, 3, 6 months post-injection. *Scale bars* 75 μm. **b** Heatmaps of coronal sections of tau pathology seen after injection at the same time points as in (**a**). Semiquantitative analysis of AT8 pathology was performed in AD-Tau- and DSAD-Tau-injected mice and combined in the heatmap here [1 month ($n = 8$), 3 months ($n = 8$) and 6 months ($n = 8$)]. Each *panel* represents pathology distribution in one of the five coronal planes (Bregma 0.98, −1.22 −2.18, −2.92 and −4.48 mm) at different time points after injection. *Left column* shows sagittal view of the selected coronal planes that are indicated by a *red line*. *Blue stars* indicate injection site

Tau pathology induced by CBD-Tau and AD/DSAD-Tau injections into young PS19 mice spread and increase with time

We assessed the progression of transmission of tau pathology with increasing survival times in PS19 mice following intracerebral injections of CBD-Tau and AD/DSAD-Tau. The remarkable oligodendroglial tau pathology seen at 1 month post-injection in the CBD-Tau-injected Tg mice increased in the fimbria near and distal to the injection site at 3 months, and more so at 6 months post-injection (Fig. 3). Despite the variability in the burden of this oligodendroglial tau pathology, the PS19 mice that survived for 3 and 6 months post-injection displayed a clear increase in oligodendroglial tau pathology with time. Additionally, oligodendrocytic tau pathology spread to the contralateral fimbria although it was not as abundant as on the ipsilateral side (Fig. 3b). At 6 months post-injection, astrocytic-like plaques that closely resemble those seen in authentic human CBD brains were prominent in the stratum radiatum of the hippocampus in both hemispheres (Fig. 3a). Similarly, PS19 tau Tg mice injected with AD/DSAD-Tau showed an increase in the neuronal tau pathology burden as well as prominent spread to regions quite distal from the injection site with increasing post-injection survival times (Fig. 4). However, this pattern of neuronal spread, which is consistent with intra-axonal transmission, differed dramatically from the pattern of glial tau pathology spread seen following the CBD-Tau injections, suggestive of a different mode of transmission that does not depend on the axonal afferents and efferents of the injection sites like the AD/DSAD-Tau injections.

At 3 months post-injection, there was an increase of the pathology in the regions that were already involved at 1 month post-injection. In the ipsilateral side, the dentate gyrus (DG) showed an increase in neuronal tau pathology at 3 months that seemed to plateau at 6 months. In the CA1 region, there was variability in the burden of intraneuronal tau inclusions at 1 month post-injection, but there was a decrease of pathology from 3 to 6 months post-injection. CA3 tau pathology also decreased from 1 to 6 months post-injection. In the contralateral hemisphere, hippocampal tau inclusions were less numerous, but they showed an increase in quantity with time in DG and CA1, while a reduction of tau pathology was observed in the CA3 region. Additionally, in keeping with the interpretation that the spread of AD/DSAD-Tau-induced tau pathology occurs through intra-axonal transport, tau pathology was seen in other regions that were not involved at earlier stages such as the thalamus, mammillary nuclei and other hypothalamic nuclei (Fig. 4b). At 3 months post-injection, neocortical neurons were involved in all of the AD/DSAD-Tau-injected mice. Additionally, some tau pathology appeared in white matter tracts with involvement of the fimbria and the dorsal hippocampal commissure at 3 months, and this pathology increased at 6 months post-injection where it appeared to be in astrocytes and oligodendroglia, but it never approached the abundance of the glial tau pathology induced by the CBD-Tau injections (data not shown). However, at 6 months post-injection there was a decrease in NFT pathology in the majority of affected areas in the AD/DSAD-Tau-injected mice.

Tau pathology induced by AD/DSAD-Tau, but not CBD-Tau injections into young PS19 mice results in neuron loss with time

To determine if the decreasing NFT pathology seen in the hippocampal region of AD/DSAD-Tau injected PS19 mice may be due to neuron loss, we quantified the number of CA3 neurons, in the area delimited by the rectangle, on the side contralateral to the injection site using digital micrography. As shown in Fig. 5, fewer neurons were seen in CA3 at the 1–3 months post-injection time period compared to controls, but this loss of neurons did not progress further as it stabilized at the 6 months post-injection survival time [138 ± 6 cell, 74 ± 7 and 69 ± 3 neurons at 1, 3 and 6 months, respectively; $p < 0.001$; (Fig. 5b)]. In marked contrast, no neuron loss was seen in mice injected with CBD-Tau (128 ± 5, 126 ± 5, 129 ± 9 neurons at 1, 3 and 6 months, respectively) or CTRL-Tau injected mice (129, 130 ± 9 neurons at 1 and 6 months, respectively). Additionally, we analyzed the CA1 region of the hippocampus on the contralateral side of the injection site but no neuron loss was observed at any of the post-injection survival time points for mice injected with AD/DSAD-Tau (330 ± 13, 321 ± 36, 318 ± 25 neurons at 1, 3 and

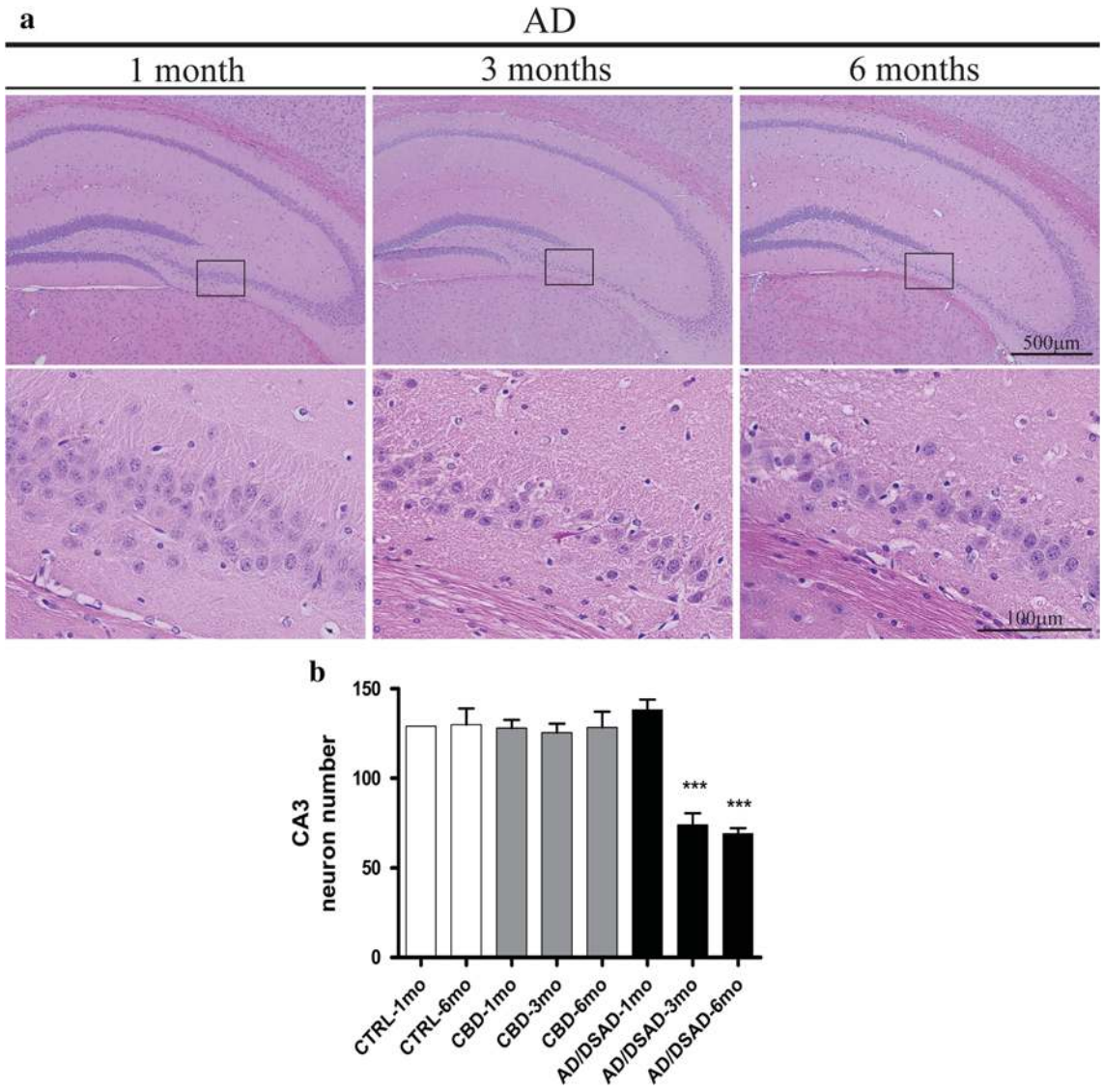

Fig. 5 There is neuron loss in the CA3 region of PS19 mice injected with AD-Tau and DSAD-Tau at 3 and 6 months post-injection. **a** The *upper row* of images show H&E stained low-power microphotographs of the hippocampus contralateral to the AD-Tau injection in PS19 mice at 1, 3, and 6 months post-injection. The microphotographs in the *lower row* show higher magnification images of the *boxed areas* in the *upper row*. *Scale bar*, *upper row* 500 μm; *lower row* 100 μm. **b** Quantification of the neurons in the CA3 region of PS19 mice injected with non-pathological or control (CTRL-Tau) human brain extract versus enriched CBD-Tau or AD-Tau and DSAD-Tau fractions. *Error bars* indicate SEM; $***p < 0.001$, as determined by one-way ANOVA and Tukey's multiple-comparison test, with $n = 2$ in CTRL-Tau at 1 month and 6 months; $n = 5$ in CBD-Tau at 1 month and 3 months; $n = 6$ in CBD-Tau at 6 months; and $n = 7$ in AD/DSAD-Tau at 1, 3 and 6 months

6 months, respectively), CBD-Tau (301 ± 17, 303 ± 32, 325 ± 30 neurons at 1, 3 and 6 months, respectively) or CTRL-Tau (286 ± 13, 330 ± 5 neurons at 1 and 6 months, respectively) (data not shown).

We further studied the association of the neuron loss with reactive changes to neurodegeneration and we observed an increase in astrogliosis in the CA3 region of the hippocampus associated with the loss of neurons, however, microgliosis was less intense.

The burden and distribution of DSAD-Tau-induced tau pathology is dose dependent

The abundance of neuronal tau inclusions induced in the PS19 mice with synthetic tau PFF injections was not only time dependent as described above, but following injections of increasing amounts of recombinant P301S mutant human T40 tau (T40/PS) PFFs, the induced pathology increased in a dose-dependent manner as well [19]. Thus,

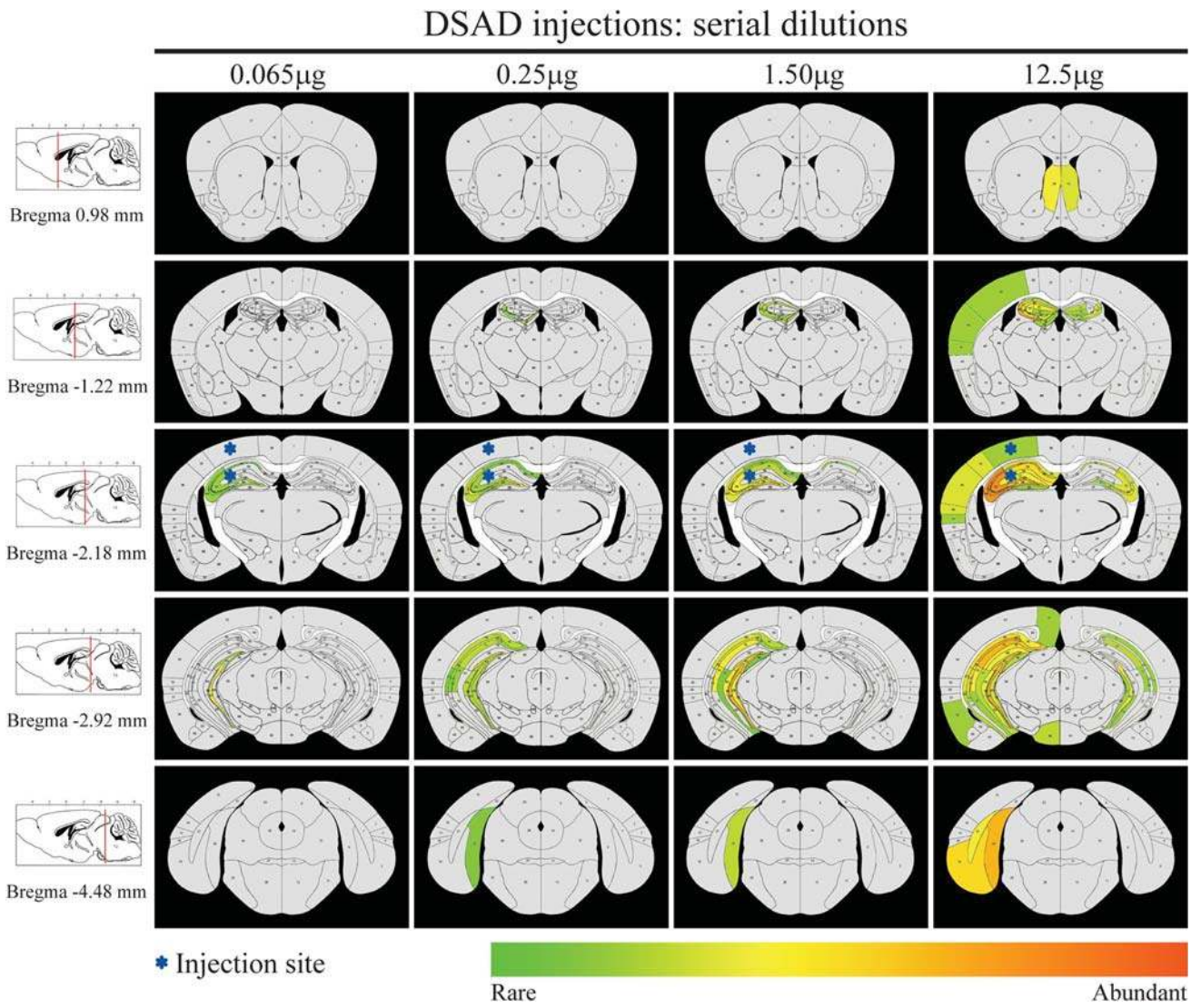

Fig. 6 Dose-dependent increase in tau pathology in PS19 mice after the injection of human brain derived DSAD-Tau. At 1 month after injection, the burden of tau pathology increases and the distribution of pathology is more extensive throughout brain structures following injections of increasing amounts of injected pathological tau. Heatmaps of coronal sections of tau pathology after injections of serial dilutions of DSAD-Tau into PS19 mice. Each *panel* represents pathology distribution in one of the five coronal planes (Bregma 0.98, −1.22 −2.18, −2.92 and −4.48 mm) at 1 month post-injection ($n = 3$ for each dose of DSAD-Tau). *Left column* shows sagittal view of the selected coronal planes that are indicated by a *red line*. *Blue stars* indicate injection site

we investigated this dose dependency here by injecting serially diluted DSAD-Tau into the hippocampus and overlying neocortex of PS19 mice (Table 1) and analyzing the tau pathology at 1 month after injection. As shown schematically in Fig. 6, at the lowest concentration of injected DSAD-Tau, only the ipsilateral hippocampus showed induced tau pathology. AT8-positive inclusions in the perikarya of neurons of dentate gyrus, CA3 and CA1 were seen at the injection site and also in rostral and caudal regions of the hippocampus of the ipsilateral side. The burden of tau pathology in the hippocampus increased with increasing concentrations of injected pathological tau with other regions of the brain becoming involved with increasing DSAD-Tau concentrations (Fig. 6). Inclusions in the contralateral hemisphere also developed in a dose-dependent manner. Hence, at the lowest concentrations of DSAD-Tau, there was no tau pathology on the contralateral side of the PS19-injected mice, while higher concentrations of injected pathological tau induced more tau pathology in the contralateral CA3 region. In sharp contrast to the CBD-Tau injected at 1 month post-injection, there was no tau pathology in the ipsilateral or contralateral white matter tracts at any concentration of injected DSAD-Tau at 1 month post-injection.

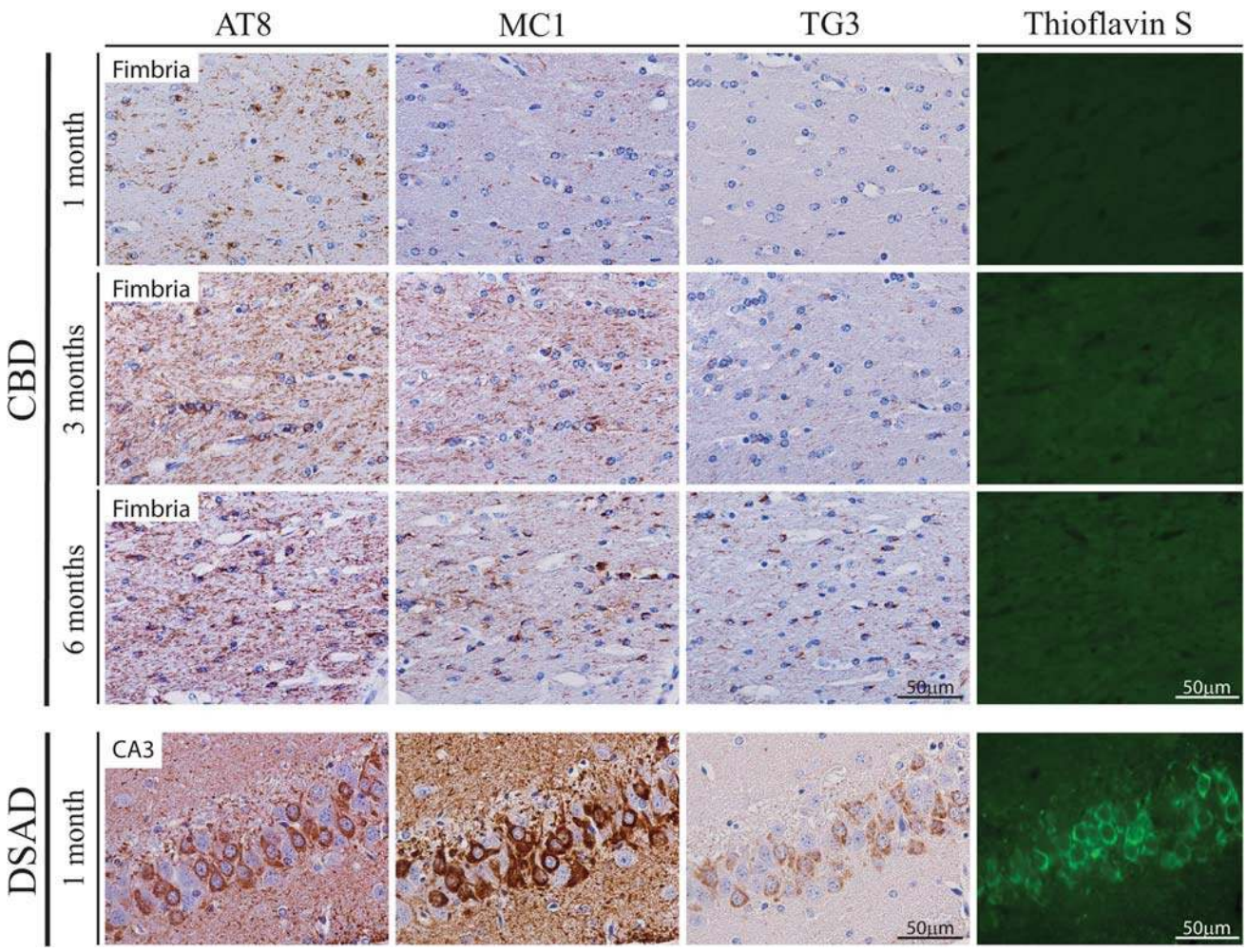

Fig. 7 Tau inclusions in PS19 mice after injection of CBD-Tau and DSAD-Tau show properties that recapitulate their human disease counterparts. Microphotographs are of brain sections stained with mAbs AT8, MC1 and TG3 to detect abnormal phosphorylation (AT8) and conformational (MC1, TG3) changes in pathological tau and ThS histochemistry to demonstrate the amyloid properties of the inclusions. Shown here are the fimbria of Tg mice injected with CBD-Tau at 1 month, 3 and 6 months post-injection (*upper three rows*) and CA3 of Tg mice injected with DSAD-Tau extracts at 1 month after injection (*lower row*). *Scale bars* 50 µm

CBD-Tau- and AD/DSAD-Tau-induced tau pathology acquires the key characteristics of their human counterparts

We further characterized the nature of the CBD-Tau- and AD/DSAD-Tau-induced tau pathology in PS19 mice by performing IHC using anti-tau mAbs to pathological tau that detect human CBD and AD-Tau pathology. IHC with MC1 and TG3 showed that tau inclusions induced by CBD-Tau was modestly positive for both mAbs at 1 month post-injection, but detected more intense and abundant tau pathology at 3 months which increased further by 6 months post-injection (Fig. 7). By contrast, AD/DSAD-Tau-induced tau pathology was intensely immunoreactive for both MC1 and TG3 already at 1 month post-injection. Notably, human (T14) and mouse (T49) specific anti-tau mAbs stained all of the tau pathologies described above although T49 stained oligodendroglial tau pathology very weakly (data not shown).

Since AD NFTs are detected by amyloid-binding dyes such as ThS, while tau inclusions in CBD cases are ThS negative [46], we asked if these properties of tau aggregates persisted in our PS19 mice following injections with CBD-Tau and AD/DSAD-Tau. Remarkably, the tau pathology in mice, injected with human-derived CBD-Tau that were AT8 positive, did not show ThS positivity, even at 6 months after injection, however, tau inclusions appearing only 1 month post-injection with AD/DSAD-Tau were detected by ThS (Fig. 7). Thus, human CBD-Tau and AD/DSAD-Tau templated and propagated tau pathology in the injected PS19 mice that showed compelling immunological and histochemical verisimilitude to their human counterparts.

Further evidence of this verisimilitude came from double immunofluorescence studies showing that the CBD-Tau-induced pathology was double labeled with AT8 and Olig2 mAbs confirming the oligodendroglial nature of this

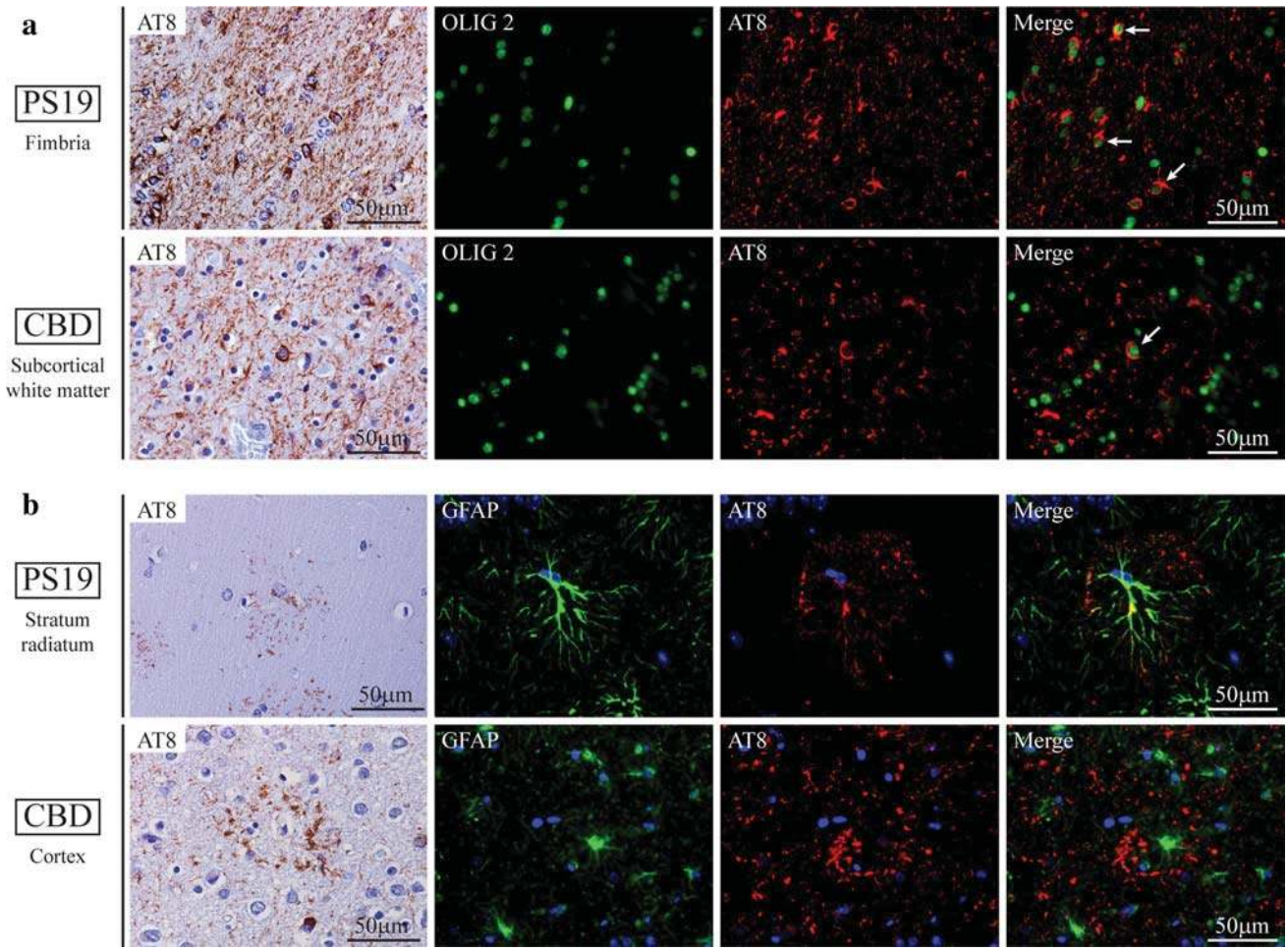

Fig. 8 Accumulation of tau pathology in oligodendrocytes and astrocytes in PS19 mice injected with CBD-Tau parallels pathology of sporadic CBD in humans. **a** Brain sections stained with mAb AT8 in the far *left column*, while the 3 columns to the *right* show double immunofluorescence with Olig2 (*green* in nucleus), AT8 (*red* in cytoplasm and neurites) and merged images in the fimbria of a PS19 mouse 6 months after injection (*upper row*) and subcortical white matter of the cingulate gyrus in a sporadic CBD case (*lower row*). **b** Brain sections stained with mAb AT8 and double immunofluorescence with GFAP (*green*), AT8 (*red*) and merged images in the stratum radiatum of the hippocampus of a PS19 mouse 6 months after injection (*upper row*) and gray matter of the parietal cortex of a sporadic CBD case (lower row). *Scale bar* 50 μm

oligodendroglial tau pathology while the astrocytic plaques induced by the CBD-Tau showed partial or incomplete co-localization of AT8 and GFAP similar to what is seen in the astrocytic plaques of human CBD (Fig. 8) as described [16].

Discussion

Here, we substantially extend the prior studies of Clavaguera et al. [6] by showing that intracellular tau pathology rapidly develops within 4 weeks rather than within several months in a Tg mouse model (line PS19) overexpressing P301S mutant human 4R1N tau after intracerebral injections of brain extracts enriched in CBD-Tau, AD-Tau or DSAD-Tau. We confirm the earlier findings [6] that this tau pathology is largely cell type specific and recapitulates the specific features of CBD or AD Tau pathology following injections of CBD-Tau or AD/DSAD-Tau, respectively. Thus, while the tau inclusions induced by CBD-Tau predominantly developed in oligodendrocytes with some astrocytic plaques, similar to authentic CBD-Tau pathology, the tau inclusions induced by AD/DSAD-Tau formed mainly in neurons similar to the NFTs in AD and DSAD brains. However, we significantly extended the initial report of Clavaguera et al. [6] by biochemically characterizing the pathological tau, we injected in more detail and demonstrating that the induction and spread of this tau pathology is time as well as dose dependent, and in the case of AD/DSAD-Tau, this tau pathology is associated with time-dependent neuron loss in the CA3 region while no similar neuron loss

was seen in the CBD-Tau injected mice. Moreover, we also used antibodies to specific pathological tau conformations as well as ThS staining and double-label immunofluorescence with AT8 and Olig2 and GFAP antibodies to extend the comparison of the human CBD and AD/DSAD pathologies to the tau pathologies induced in the PS19 tau Tg mice injected with CBD-Tau or AD/DSAD-Tau, respectively. Thus, we report novel data indicating that while CBD-Tau and AD/DSAD-Tau induced dramatically different tau pathology in the PS19 mice, CBD-Tau- and AD/DSAD-Tau-induced tau pathology shows remarkable verisimilitude to human CBD and AD-Tau pathology, respectively.

While the AD-like tau pathology spreads in a manner consistent with dissemination through the connectome of the injected brain regions, most likely via intra-axonal transport, the manner in which the CBD glial tau pathology spreads is enigmatic and will require further studies to elucidate. Indeed, while there are staging schemes for AD-Tau pathology that support the notion of tau pathology spread through interconnected brain regions [3–5], no similar staging exists for CBD-Tau pathology so it is not clear how tau pathology might progress and spread in CBD brains. The fact that injections of brain extracts from control non-diseased human brains lacking any insoluble pathological tau did not induce tau pathology in age-matched PS19 mice support data from a growing number of studies indicating that pathological tau and not normal tau induce the seeded transmission and spread of pathological tau in vivo and in vitro (for reviews, see [15, 24]).

Transmission of tau pathology in vitro was demonstrated initially using AD brain extracts that induced formation of PHFs in cultured fetal neurons [9] and later used synthetic tau PFFs to induce the templated conversion of intracellular soluble tau into fibrillar aggregates in cultured cells [12, 14]. In vivo studies showed that inoculation of brain homogenates from mutant tau Tg mice (that form NFTs) into the brains of WT tau expressing ALZ17 mice (that do not form tau inclusions) induced the formation of tau inclusions in the ALZ17 Tg mice [7]. Iba et al. [19] demonstrated that synthetic tau fibrils injected into a PS19 tauopathy model is sufficient to induce and propagate AD-like tau pathology. Altogether, it was established that fibrillar species of tau are capable of recruiting and converting endogenous soluble tau into pathological aggregates in neurons and neuronal processes in vivo. In our present study, we showed that enriched pathological tau extracts obtained from CBD or AD and DSAD brains induce tau pathology in PS19 mice similar to CBD and AD Tau pathology in human brains, respectively. These results support the notion that different tauopathy-specific pathological tau strains may account for the diverse clinical and pathological phenotypes of tauopathy variants. Moreover, our mouse model differs from the initial report of Clavaguera et al. [6] in that the tau pathology in our model developed earlier and showed a striking verisimilitude to key features of CBD or AD Tau pathology following injections of CBD-Tau or AD/DSAD-Tau, respectively.

Some tauopathies characteristically show tau inclusions in glial cells and neurons [2, 29]. The basis of this cell-type preference for the formation of tau inclusions is unknown, but a recent study demonstrated in vitro and in vivo that pathological tau can acquire different conformations which propagate tau pathology suggesting that these different conformers or strains could result in the different tauopathies [45]. These characteristics have been also shown for α-synuclein [13] and Aβ [43, 49, 50]. Moreover, since tau inclusions in CBD and AD are formed by different tau isoforms (i.e. CBD is predominantly 4R; AD is predominantly 3R and 4R), this also might determine the structure of different tau strains. However, little is known about how different pathological tau isoforms contribute to the heterogeneous phenotypes seen in different tauopathies. That said, we observed that the injection of enriched tau extracts from AD and DSAD brains resulted in similar AD-like neuronal tau pathologies while both the CBD cases produced distinctly different pathology from the AD/DSAD cases that was remarkably CBD like. Thus, these findings suggest that the characteristics and distributions of these different tau inclusions are directly related with the nature of the tauopathy.

Notably, the tau pathology seen in the hippocampus of PS19 tau Tg mice after the injection of AD/DSAD-Tau was variable and appeared to decrease in the CA3 region ipsilateral and contralateral to the injection and we showed that this could be explained by the neuron loss seen in this region that was already significant at 3 months post-injection (Fig. 5). It is noteworthy that the CA3 region in the injected PS19 mice develops neuronal tau inclusions at 1 month post-injection, and is one of the first regions to show AT8-positive inclusions in the contralateral hippocampus preceding neuronal death. Thus, it is possible that distinct tau species have a differential effect in the neurons of these mice causing neuronal death and this may occur in a neuron type-specific manner or could be dose and time dependent, as might be inferred from a recently published study in which high doses of synthetic tau fibrils caused hippocampal neuron death [42]. For comparison, we also analyzed neuron loss in the CA1 region of the hippocampus contralateral to the injection site, where tau inclusions were less abundant than in CA3 and no neuron loss was observed. Interestingly, neuron loss in the CA3 region was accompanied by moderate astrogliosis and less conspicuous microgliosis, which is evidence of reactive changes to this neurodegeneration.

Other data support the verisimilitude of the CBD-Tau- and AD/DSAD-Tau-induced tau pathology in the injected PS19 mice to their human counterparts in CBD and AD, respectively. For example, the inclusions resulting in oligodendrocyte pathology in the fimbria after injection of human-derived CBD-Tau were positive for the conformational antibody MC1 while a few inclusions showed TG3 immunoreactivity. Interestingly, ThS was negative even at 6 months after injection which is a characteristic of tau inclusions in human CBD [46]. In contrast, in the AD/DSAD-Tau-injected mice there was an intense immunoreactivity for MC1 and TG3 and positivity for ThS staining already at 1 month after injection, indicating more mature NFT structures analogous to what is seen in AD patients at histological examination.

In conclusion, we present mouse models of CBD-like and AD-like tauopathies that rapidly develop glial and intraneuronal tau inclusions after the injection of pathological tau isolated from CBD or AD/DSAD brains, respectively, and also rapidly progress in a stereotypical pattern. For AD/DSAD-Tau, this progression is both time and dose dependent as well as dependent on the connectome of the injection sites. Notably, this tau pathology leads to the death of tangle-bearing CA3 neurons over time. In sharp contrast, the spread of CBD-Tau-induced tau pathology in glial cells was more limited as well as unrelated to the connectome of the injection site and it did not appear to cause the loss of neurons or glial cells. Thus, we anticipate that these models will provide informative systems for studies on the transmission of tau pathology, tau-mediated neuronal and glial degeneration and the development of disease-modifying therapies for CBD and AD.

Acknowledgments Susana Boluda was supported by Bolsa de Ampliación de Estudios (BA11/00021) from the Spanish government, Instituto de Salud Carlos III, Ministerio de Ciencia e Innovación, Madrid, Spain. This work was supported by the CurePSP Foundation, NIH grant AG17586, the Marian S. Ware Alzheimer Program, the Karen Cohen Segal, the Eleanor Margaret Kurtz Endowed Fund, the Mary Rasmus Endowed Fund for Alzheimer's Research, Mrs. Gloria J. Miller and Arthur Peck, M.D. We thank Theresa Schuck, John Robinson and Jennifer McBride for their technical assistance in immunohistochemistry, Linda Kwong for her technical assistance in biochemistry procedures and reading of this manuscript, Sue Leight for her technical assistance in mouse manipulation, Magdalena Nitla for her technical assistance in mouse injections and Young Baek and Rui Tong for data management.

Conflict of interest The authors declare that they have no conflict of interest.

Ethical standard All applicable international, national, and/or institutional guidelines for the care and use of animals were followed. All procedures performed in studies involving animals were in accordance with the ethical standards of the institution or practice at which the studies were conducted.

References

1. Ahmed Z, Cooper J, Murray TK, Garn K, McNaughton E, Clarke H, Parhizkar S, Ward MA, Cavallini A, Jackson S, Bose S, Clavaguera F, Tolnay M, Lavenir I, Goedert M, Hutton ML, O'Neill MJ (2014) A novel in vivo model of tau propagation with rapid and progressive neurofibrillary tangle pathology: the pattern of spread is determined by connectivity, not proximity. Acta Neuropathol 127(5):667–683
2. Ballatore C, Lee VM, Trojanowski JQ (2007) Tau-mediated neurodegeneration in Alzheimer's disease and related disorders. Nat Rev Neurosci 8(9):663–672. doi:10.1038/nrn2194
3. Braak H, Braak E (1991) Neuropathological stageing of Alzheimer-related changes. Acta Neuropathol 82(4):239–259
4. Braak H, Del Tredici K (2011) Alzheimer's pathogenesis: is there neuron-to-neuron propagation? Acta Neuropathol 121(5):589–595
5. Braak H, Thal DR, Ghebremedhin E, Del Tredici K (2011) Stages of the pathologic process in Alzheimer disease: age categories from 1 to 100 years. J Neuropathol Exp Neurol 70(11):960–969
6. Clavaguera F, Akatsu H, Fraser G, Crowther RA, Frank S, Hench J, Probst A, Winkler DT, Reichwald J, Staufenbiel M, Ghetti B, Goedert M, Tolnay M (2013) Brain homogenates from human tauopathies induce tau inclusions in mouse brain. Proc Natl Acad Sci 110(23):9535–9540
7. Clavaguera F, Bolmont T, Crowther RA, Abramowski D, Frank S, Probst A, Fraser G, Stalder AK, Beibel M, Staufenbiel M, Jucker M, Goedert M, Tolnay M (2009) Transmission and spreading of tauopathy in transgenic mouse brain. Nat Cell Biol 11(7):909–913
8. Cohen TJ, Guo JL, Hurtado DE, Kwong LK, Mills IP, Trojanowski JQ, Lee VM (2011) The acetylation of tau inhibits its function and promotes pathological tau aggregation. Nat Commun 2:252
9. De Boni U, Crapper DR (1978) Paired helical filaments of the Alzheimer type in cultured neurones. Nature 271(5645):566–568
10. de Calignon A, Polydoro M, Suarez-Calvet M, William C, Adamowicz DH, Kopeikina KJ, Pitstick R, Sahara N, Ashe KH, Carlson GA, Spires-Jones TL, Hyman BT (2012) Propagation of tau pathology in a model of early Alzheimer's disease. Neuron 73(4):685–697
11. Forman MS, Zhukareva V, Bergeron C, Chin SSM, Grossman M, Clark C, Lee VMY, Trojanowski JQ (2002) Signature tau neuropathology ingray and white matter of corticobasal degeneration. Am J Pathol 160(6):2045–2053. doi:10.1016/s0002-9440(10)61154-6
12. Frost B, Jacks RL, Diamond MI (2009) Propagation of tau misfolding from the outside to the inside of a cell. J Biol Chem 284(19):12845–12852
13. Guo JL, Covell DJ, Daniels JP, Iba M, Stieber A, Zhang B, Riddle DM, Kwong LK, Xu Y, Trojanowski JQ, Lee VM (2013) Distinct alpha-synuclein strains differentially promote tau inclusions in neurons. Cell 154(1):103–117
14. Guo JL, Lee VM (2011) Seeding of normal tau by pathological tau conformers drives pathogenesis of Alzheimer-like tangles. J Biol Chem 286(17):15317–15331
15. Guo JL, Lee VM (2014) Cell-to-cell transmission of pathogenic proteins in neurodegenerative diseases. Nat Med 20(2):130–138. doi:10.1038/nm.3457
16. Higuchi M, Zhang B, Forman MS, Yoshiyama Y, Trojanowski JQ, Lee VM (2005) Axonal degeneration induced by targeted expression of mutant human tau in oligodendrocytes of transgenic mice that model glial tauopathies. J Neurosci 25(41):9434–9443
17. Horiguchi T, Uryu K, Giasson BI, Ischiropoulos H, LightFoot R, Bellmann C, Richter-Landsberg C, Lee VM, Trojanowski JQ

(2003) Nitration of tau protein is linked to neurodegeneration in tauopathies. Am J Pathol 163(3):1021–1031
18. Hutton M, Lendon CL, Rizzu P, Baker M, Froelich S, Houlden H, Pickering-Brown S, Chakraverty S, Isaacs A, Grover A, Hackett J, Adamson J, Lincoln S, Dickson D, Davies P, Petersen RC, Stevens M, de Graaff E, Wauters E, van Baren J, Hillebrand M, Joosse M, Kwon JM, Nowotny P, Che LK, Norton J, Morris JC, Reed LA, Trojanowski J, Basun H, Lannfelt L, Neystat M, Fahn S, Dark F, Tannenberg T, Dodd PR, Hayward N, Kwok JB, Schofield PR, Andreadis A, Snowden J, Craufurd D, Neary D, Owen F, Oostra BA, Hardy J, Goate A, van Swieten J, Mann D, Lynch T, Heutink P (1998) Association of missense and 5′-splice-site mutations in tau with the inherited dementia FTDP-17. Nature 393(6686):702–705
19. Iba M, Guo JL, McBride JD, Zhang B, Trojanowski JQ, Lee VM (2013) Synthetic tau fibrils mediate transmission of neurofibrillary tangles in a transgenic mouse model of Alzheimer's-like tauopathy. J Neurosci 33(3):1024–1037
20. Irwin DJ, Cohen TJ, Grossman M, Arnold SE, McCarty-Wood E, Van Deerlin VM, Lee VM, Trojanowski JQ (2013) Acetylated tau neuropathology in sporadic and hereditary tauopathies. Am J Pathol 183(2):344–351
21. Irwin DJ, Cohen TJ, Grossman M, Arnold SE, Xie SX, Lee VM, Trojanowski JQ (2012) Acetylated tau, a novel pathological signature in Alzheimer's disease and other tauopathies. Brain 135(Pt 3):807–818
22. Jicha GA, Bowser R, Kazam IG, Davies P (1997) Alz-50 and MC-1, a new monoclonal antibody raised to paired helical filaments, recognize conformational epitopes on recombinant tau. J Neurosci Res 48(2):128–132
23. Jicha GA, Lane E, Vincent I, Otvos L Jr, Hoffmann R, Davies P (1997) A conformation- and phosphorylation-dependent antibody recognizing the paired helical filaments of Alzheimer's disease. J Neurochem 69(5):2087–2095
24. Jucker M, Walker LC (2013) Self-propagation of pathogenic protein aggregates in neurodegenerative diseases. Nature 501(7465):45–51
25. Kosik KS, Orecchio LD, Binder L, Trojanowski JQ, Lee VM, Lee G (1988) Epitopes that span the tau molecule are shared with paired helical filaments. Neuron 1(9):817–825
26. Ledesma MD, Perez M, Colaco C, Avila J (1998) Tau glycation is involved in aggregation of the protein but not in the formation of filaments. Cell Mol Biol 44(7):1111–1116
27. Lee EB, Leng LZ, Zhang B, Kwong L, Trojanowski JQ, Abel T, Lee VM (2006) Targeting amyloid-beta peptide (Abeta) oligomers by passive immunization with a conformation-selective monoclonal antibody improves learning and memory in Abeta precursor protein (APP) transgenic mice. J Biol Chem 281(7):4292–4299
28. Lee VM, Balin BJ, Otvos L Jr, Trojanowski JQ (1991) A68: a major subunit of paired helical filaments and derivatized forms of normal tau. Science 251(4994):675–678
29. Lee VM, Goedert M, Trojanowski JQ (2001) Neurodegenerative tauopathies. Annu Rev Neurosci 24:1121–1159
30. Lee VM, Page CD, Wu HL, Schlaepfer WW (1984) Monoclonal antibodies to gel-excised glial filament protein and their reactivities with other intermediate filament proteins. J Neurochem 42(1):25–32
31. Lee VM, Wang J, Trojanowski JQ (1999) Purification of paired helical filament tau and normal tau from human brain tissue. Methods Enzymol 309:81–89
32. Lippa CF, Fujiwara H, Mann DM, Giasson B, Baba M, Schmidt ML, Nee LE, O'Connell B, Pollen DA, St George-Hyslop P, Ghetti B, Nochlin D, Bird TD, Cairns NJ, Lee VM, Iwatsubo T, Trojanowski JQ (1998) Lewy bodies contain altered alpha-synuclein in brains of many familial Alzheimer's disease patients with mutations in presenilin and amyloid precursor protein genes. Am J Pathol 153(5):1365–1370
33. Lippa CF, Rosso AL, Stutzbach LD, Neumann M, Lee VM, Trojanowski JQ (2009) Transactive response DNA-binding protein 43 burden in familial Alzheimer disease and Down syndrome. Arch Neurol 66(12):1483–1488
34. Lippa CF, Schmidt ML, Lee VM, Trojanowski JQ (1999) Antibodies to alpha-synuclein detect Lewy bodies in many Down's syndrome brains with Alzheimer's disease. Ann Neurol 45(3):353–357
35. Liu L, Drouet V, Wu JW, Witter MP, Small SA, Clelland C, Duff K (2012) Trans-synaptic spread of tau pathology in vivo. PLoS One 7(2):1
36. Ma QL, Zuo X, Yang F, Ubeda OJ, Gant DJ, Alaverdyan M, Kiosea NC, Nazari S, Chen PP, Nothias F, Chan P, Teng E, Frautschy SA, Cole GM (2014) Loss of MAP function leads to hippocampal synapse loss and deficits in the Morris Water Maze with aging. J Neurosci 34(21):7124–7136
37. Martin L, Latypova X, Terro F (2011) Post-translational modifications of tau protein: implications for Alzheimer's disease. Neurochem Int 58(4):458–471
38. Min SW, Cho SH, Zhou Y, Schroeder S, Haroutunian V, Seeley WW, Huang EJ, Shen Y, Masliah E, Mukherjee C, Meyers D, Cole PA, Ott M, Gan L (2010) Acetylation of tau inhibits its degradation and contributes to tauopathy. Neuron 67(6):953–966
39. Mott RT, Dickson DW, Trojanowski JQ, Zhukareva V, Lee VM, Forman M, Van Deerlin V, Ervin JF, Wang DS, Schmechel DE, Hulette CM (2005) Neuropathologic, biochemical, and molecular characterization of the frontotemporal dementias. J Neuropathol Exp Neurol 64(5):420–428
40. Neumann M, Kwong LK, Lee EB, Kremmer E, Flatley A, Xu Y, Forman MS, Troost D, Kretzschmar HA, Trojanowski JQ, Lee VM (2009) Phosphorylation of S409/410 of TDP-43 is a consistent feature in all sporadic and familial forms of TDP-43 proteinopathies. Acta Neuropathol 117(2):137–149
41. Otvos L Jr, Feiner L, Lang E, Szendrei GI, Goedert M, Lee VM (1994) Monoclonal antibody PHF-1 recognizes tau protein phosphorylated at serine residues 396 and 404. J Neurosci Res 39(6):669–673
42. Peeraer E, Bottelbergs A, Van Kolen K, Mahieu M, Duytschaever H, Verdonck L, Torremans A, Andries L, Brunden KR, Trojanowski JQ, Lee VM, Dewachter I, Kemp JA, Moechars D (2014) Intracerebral injection of tau aggregates initiates widespread tauopathy and neuronal loss in transgenic mouse brain. Neurobiol Dis 73C:83–95
43. Petkova AT, Leapman RD, Guo Z, Yau WM, Mattson MP, Tycko R (2005) Self-propagating, molecular-level polymorphism in Alzheimer's beta-amyloid fibrils. Science 307(5707):262–265
44. Poorkaj P, Bird TD, Wijsman E, Nemens E, Garruto RM, Anderson L, Andreadis A, Wiederholt WC, Raskind M, Schellenberg GD (1998) Tau is a candidate gene for chromosome 17 frontotemporal dementia. Ann Neurol 43(6):815–825
45. Sanders DW, Kaufman SK, DeVos SL, Sharma AM, Mirbaha H, Li A, Barker SJ, Foley AC, Thorpe JR, Serpell LC, Miller TM, Grinberg LT, Seeley WW, Diamond MI (2014) Distinct tau prion strains propagate in cells and mice and define different tauopathies. Neuron 82(6):1271–1288
46. Schmidt ML, Schuck T, Sheridan S, Kung MP, Kung H, Zhuang ZP, Bergeron C, Lamarche JS, Skovronsky D, Giasson BI, Lee VM, Trojanowski JQ (2001) The fluorescent Congo red derivative, (trans, trans)-1-bromo-2,5-bis-(3-hydroxycarbonyl-4-hydroxy)styrylbenzene (BSB), labels diverse beta-pleated sheet structures in postmortem human neurodegenerative disease brains. Am J Pathol 159(3):937–943
47. Spillantini MG, Goedert M (2013) Tau pathology and neurodegeneration. Lancet Neurol 12(6):609–622

48. Spillantini MG, Van Swieten JC, Goedert M (2000) Tau gene mutations in frontotemporal dementia and parkinsonism linked to chromosome 17 (FTDP-17). Neurogenetics 2(4):193–205
49. Stohr J, Condello C, Watts JC, Bloch L, Oehler A, Nick M, DeArmond SJ, Giles K, DeGrado WF, Prusiner SB (2014) Distinct synthetic Abeta prion strains producing different amyloid deposits in bigenic mice. Proc Natl Acad Sci 111:10329–10334
50. Stohr J, Watts JC, Mensinger ZL, Oehler A, Grillo SK, DeArmond SJ, Prusiner SB, Giles K (2012) Purified and synthetic Alzheimer's amyloid beta (Abeta) prions. Proc Natl Acad Sci 109(27):11025–11030. doi:10.1073/pnas.1206555109
51. Waxman EA, Giasson BI (2008) Specificity and regulation of casein kinase-mediated phosphorylation of alpha-synuclein. J Neuropathol Exp Neurol 67(5):402–416
52. Yoshiyama Y, Higuchi M, Zhang B, Huang SM, Iwata N, Saido TC, Maeda J, Suhara T, Trojanowski JQ, Lee VM (2007) Synapse loss and microglial activation precede tangles in a P301S tauopathy mouse model. Neuron 53(3):337–351
53. Yoshiyama Y, Lee VM, Trojanowski JQ (2013) Therapeutic strategies for tau mediated neurodegeneration. J Neurol Neurosurg Psychiatry 84(7):784–795
54. Zhukareva V, Joyce S, Schuck T, Van Deerlin V, Hurtig H, Albin R, Gilman S, Chin S, Miller B, Trojanowski JQ, Lee VM (2006) Unexpected abundance of pathological tau in progressive supranuclear palsy white matter. Ann Neurol 60(3):335–345
55. Zhukareva V, Mann D, Pickering-Brown S, Uryu K, Shuck T, Shah K, Grossman M, Miller BL, Hulette CM, Feinstein SC, Trojanowski JQ, Lee VM (2002) Sporadic Pick's disease: a tauopathy characterized by a spectrum of pathological tau isoforms in gray and white matter. Ann Neurol 51(6):730–739
56. Zhukareva V, Shah K, Uryu K, Braak H, Del Tredici K, Sundarraj S, Clark C, Trojanowski JQ, Lee VM (2002) Biochemical analysis of tau proteins in argyrophilic grain disease, Alzheimer's disease, and Pick's disease: a comparative study. Am J Pathol 161(4):1135–1141